

Understanding the role of N6-methyladenosine marked DNA:RNA hybrids and their potential reader HNRNPA2B1

Paige Lowe MRes, BSc

School of Medicine
Division of Cancer and Stem Cells

Thesis submitted to the University of Nottingham for

the Degree of Doctor of Philosophy

November 2021

Abstract

N6-methyladenosine (m^6A) is the most abundant modification found in eukaryotic mRNA with a suggested role in alternative splicing, localisation, translation and mRNA decay. The m^6A modification is modified by m^6A methyltransferases, removed by demethylases and recognised by m^6A-binding proteins such as YTHDF2 and HNRNPA2B1. According to several studies, m^6A RNA methylation can contribute to tumorigenesis, migration, proliferation, and resistance to radio- or chemotherapy of human cancers. Previously, our group has demonstrated that m^6A is present on nucleic acid structures known as R-loops, formed by a DNA:RNA hybrid and an unpaired single-stranded DNA. Our pilot data suggest that m^6A may influence various aspects of R-loop biology, however, the potential involvement of HNRNPA2B1 in R-loop metabolism has not been studied to date.

Utilising a range of techniques including immunocytochemistry, DNA:RNA hybrid immunoprecipitation (DRIP), chromatin immunoprecipitation (ChIP) and siRNA-mediated knockdown of HNRNPA2B1 mRNA, we examined the distribution and function of m^6A-marked DNA:RNA hybrids and their functional interaction with HNRNPA2B1 in human non-tumorigenic and cancer cell lines.

Employing an HNRNPA2B1 knockout semi-haploid HAP1 cell line, we found the levels of m^6A marked DNA:RNA hybrids were elevated or reduced depending upon the location of the corresponding locus in the genome. Loss of YTHDF2 resulted in decreased binding to repetitive and intronic DNA:RNA hybrid-specific loci. Whereas the loss of HNRNPA2B1 resulted in increased binding of YTHDF2 to repetitive and intronic DNA:RNA hybrid regions, specifically where we observed increases in R-loop levels in HNRNPA2B1 KO cells in these repetitive and individual intronic DNA:RNA hybrid-specific loci. In conclusion, we observed interplay between HNRNPA2B1 and YTHDF2, with HNRNPA2B1 dependent on YTHDF2 to interact with m^6A-marked DNA:RNA hybrids.

In both glioblastoma multiforme (GBM) and medulloblastoma (MB) cell lines, we observed very high levels of m^6A-related genes particularly, high levels of HNRNPA2B1 mRNA in MB.

In GBM cell lines, we showed that m^6A marked DNA:RNA hybrid presence varied between GBM cell lines. Whereas, in MB cells, m^6A marked DNA:RNA hybrid presence was observed across the genome in repetitive and in individual m^6A-DNA:RNA hybrid-containing loci of key MB genes. Moreover, the transient knockdown of HNRNPA2B1 caused cell lifting from the growth surface in both GBM and MB cells.

Acknowledgements

I would like to thank my supervisors Dr Alexey Ruzov, Dr Nicholas RF Hannan and Professor David Bates for their time, support, and encouragement over the last four years at University of Nottingham. I am also grateful to the technical and administrative staff of Cancer and Stem cells department who have provided me with invaluable help and support. Also, a special thanks to Dr Robert Marcus for their time, help and expertise in confocal microscopy.

On a more personal note, I would like to thank my amazing husband, Christopher Hallett. Without your constant support, jokes, and encouragement, I would not be where I am today. Thank you for being by my side through the end of undergraduate, my masters and now my PhD. You deserve an honorary PhD! Thanks for always attempting to understand what I am saying about my work and just nodding when you don't. Huge thank you to my all my family for your love, support, and encouragement, particularly my dad, my mum, my step-mum, my brother and sister, my grandparents and in-laws. Shout out to my Nanny Lowe for always keeping me humble and reminding me that I will not be a "proper" doctor at the end of this!

This PhD experience would not have been the same without Dr Lara Lewis, Dr Ashley Ramsawhook, and Dr Maria Eleftheriou. Thank you for always being there to talk through problems, making me laugh, going for coffee and eating cake with. Good friends are hard to find, so I am so lucky to have made three during this time. To the girls in the defunct A54 office, especially Dr Peggy Lo, Dr Kate Vo, Emma Collins and Paulina Durczak, thank you for the long chats, coffee, biscuits and being great laboratory/lunch buddies.

Thanks to Matt Critcher, Luke and Polley Runacres for showing there is a life outside of academia and being my friend since undergraduate! Thanks for always making me smile on my bad days and giving me great stories, and phrases I'll take with me such as "Just wing it". Looking forward to many more years and stories we'll have as friends.

Finally, special thanks to my cats, Duke and Diesel, for keeping me company while writing this thesis.

Publications and Conferences

Publications

Lowe, P., Olinski, R. and Ruzov, A. (2021) 'Evidence for Noncytosine Epigenetic DNA Modifications in Multicellular Eukaryotes: An Overview', in, pp. 15–25. doi: 10.1007/978-1-0716-0876-0_2.

Conferences

Genome Science Annual Meeting, *"Involvement of m^6A modified DNA:RNA hybrids within Glioblastoma and Medulloblastoma",* Nottingham, UK (September 2018).

From Stem Cells to Human Development Meeting, *"Potential involvement of NEIL1 in Base Excision Repair-dependent DNA demethylation during hepatic differentiation"*, Surrey, UK (September 2018).

Cancer Research Nottingham (CRN) Symposium, *"Involvement of m^6A modified DNA:RNA hybrids within Glioblastoma and Medulloblastoma",* Nottingham, UK (September 2018).

MERCIA Stem Cell Alliance, *"Potential involvement of NEIL1 in Base Excision Repair-dependent DNA demethylation during hepatic differentiation"*, Birmingham, UK (September 2018).

Centre of Biomolecular Sciences Summer Symposium, *"Understanding the role of N6-methyladenosine marked R-loops and their potential reader HNRNPA2B1"*, Nottingham, UK (June 2019).

Chromatin and Epigenetics, *"Understanding the role of N6-methyladenosine marked R-loops and their potential reader HNRNPA2B1"*, Essex, UK (September 2019).

Thesis statement and contributions

I hereby declare that this thesis has been composed by myself and has not been submitted for any other degree previously. This project was supervised by Dr Alexey Ruzov, Dr Nicholas RF Hannan, and Professor David Bates. Acknowledgements of specific procedures not performed by myself are stated; otherwise, the work described is my own.

Dr Maria Eleftheriou prepared FB83, LN18, LN229, U251, U87MG and UW228-3 replicates and performed RNA extraction and cDNA synthesis for m^6A gene expression analysis. Dr Lara Lewis prepared and fixed hiPSCs to glass chamber slides for m^6A/Ph-H3 immunostaining as well as verifying sonicated fragments by Agilent Tapestation D5000 screen tapes, ensuring that fragments between 200-1000 base pairs for DRIP and ChIP were generated. All the mass spectrometric analysis of N6mrA marks was performed at Ryszard Olinsky laboratory at Nicolaus Copernicus University, Poland. Flow cytometry cell sorting was carried out by Nicola Croxall and Dr David Onion in the University of Nottingham Flow Cytometry Facility. Dr Alexey Ruzov created the summary figure (Fig. 6.1) as a proposed model of our results.

Covid-19 Impact Statement

In February 2020, I had just over 6 months of experimental work planned. This included second replicate experiments of m^6A DRIP and S9.6 DRIP experiments in Chapters 3, 4 and 5 as well as a second replicate for YTHDF2 ChIP and HNRNPA2B1 ChIP experiments in Chapter 3. This would have allowed us to perform statistics on these experiments and therefore determine the significance of these results. Another scheduled experiment was to continue investigating why in Chapters 4 and 5 the cells lifted after treatment with HNRNPA2B1 siRNA. This would have involved qPCR of HNRNPA2B1 siRNA treated cells compared to the control to evaluate the gene expression of EMT markers and proliferation markers to determine if these were responsible. It was planned to perform flow cytometry experiments to evaluate if the HNRNPA2B1 siRNA treatment was leading to apoptosis and cell death by staining with Annexin V and PI staining. Finally, I began building an *HNRNPA2B1* overexpression plasmid utilising the PiggyBac transposon transfection to determine if the elevated levels of HNRNPA2B1 would reduce the reduces the levels of m^6A marked DNA:RNA hybrids as hypothesised as well as reverse the effects of *HNRNPA2B1* knockdown in GBM and MB cells.

In March 2020, when went into lockdown, experiments were left unfinished with many of the key results only having when we replicate. At that time, in discussion with my supervisors, we decided to adapt my planned experiments and focus on drafting a thesis with the results I had already obtained. By May 2020, it was finalised that I should write up the results I obtained over the last 2.5 years and not return to the laboratory. Therefore, I adapted my chapters to have an overarching theme but to assess different hypotheses.

Table of contents

Abstract i

Acknowledgements iii

Publications and Conferences iv

Thesis statement and contributions v

Covid-19 Impact Statement vi

Table of contents vii

List of Figures xii

List of Tables xvii

Abbreviations xviii

Chapter 1: Introduction 1

1.1 Epitranscriptomics 1

1.1.1 Pseudouridine (Ψ) 2

1.1.2 5-methylcytidine (m^5C) 3

1.1.3 Adenosine to Inosine editing 7

1.1.4 N1-methyladenosine (m^1A) 7

1.1.5 N6, 2'-O-dimethyladenosine (m^6Am) 8

1.2 N6-methyladenosine (m^6A) 9

1.2.1 m^6A writers 9

1.2.2 Erasers of m^6A 12

1.2.3 m^6A readers 12

1.2.4 Relevance of m^6A to cancer 15

1.2.4.1 Acute myeloid leukaemia (AML) 16

1.2.4.2 Breast cancer (BC) 18

1.2.4.3 Glioblastoma multiforme (GBM) 21

1.3 DNA:RNA hybrids 22

1.3.1 Formation and removal of DNA:RNA hybrids 22
1.3.2 Roles and functions of DNA:RNA hybrids 24
1.3.2.1 Class switch recombination 24
1.3.2.2 Telomere modulation 25
1.3.2.3 Gene expression 25
1.3.2.4 DNA repair 26
1.3.2.5 DNA damage 26
1.3.3 DNA:RNA hybrids role in human disease 29
1.3.4 The presence of m^6A on DNA:RNA hybrids within the genome 30
1.4 Hypothesis and Aims 32

Chapter 2: Materials and Methods 37

2.1 Cell culture 37
2.1.1 Cell lines 37
2.1.2 Preparation of media and cell culture 38
2.1.3 Cryopreservation and thawing of cells 39
2.1.4 Sub-culturing of cells 39
2.1.5 Human pluripotent stem cell culture 40
2.2 Cell culture assays 40
2.2.1 siRNA knockdown 40
2.2.1.1 Use of Attachment factor on growth surface 41
2.2.2 Growth curves 41
2.2.3 Flow cytometry cell sorting 41
2.3 Molecular biology 42
2.3.1 RNA extraction 42
2.3.2 Complementary DNA (cDNA) synthesis 42
2.3.3 Gene expression analysis by Real time Quantitative Polymerase Chain Reaction (qPCR) 43
2.3.4 Polymerase Chain Reaction (PCR) 44
2.3.5 Agarose gel electrophoresis 45
2.3.6 Genomic DNA extraction and Sonication 45
2.3.7 DNA:RNA hybrid and m^6A marked DNA:RNA hybrid immunoprecipitation (S9.6 DRIP and m^6A DRIP) 46
2.3.8 Chromatin immunoprecipitation (ChIP) 48
2.3.9 Immunocytochemistry 48
2.3.9.1 m^6A marked DNA:RNA hybrid immunostaining 51

2.4 Confocal microscopy imaging 52
2.5 Stable-isotope dilution ultra-performance liquid chromatography with tandem mass spectrometry (SID-UPLC-MS/MS) 53
2.6 Bioinformatics 53
2.7 Statistical Analysis 53
Chapter 3: Characterisation of HNRNPA2B1 knockout in HAP1 cells. 54
3.1 Introduction 54
3.2 Aims 59
3.3 Results 60
3.3.1 Characterisation of HAP1 HNRNPA2B1 KO cell line. 60
3.3.1.1 Sanger sequencing confirms the insertion of nucleotide which leads to a frameshift mutation in HNRNPA2B1. 61
3.3.1.2 Both isoforms of HNRNPA2B1 are impacted by nucleotide insertion within RRM domains 63
3.3.1.3 Cell proliferation is marginally affected by KO of HNRNPA2B1 in HAP1 cells. 67
3.3.2 Knockout of HNRNPA2B1 impacts the levels of DNA:RNA hybrids dependent upon their location in the genome. 68
3.3.2.1 Depletion of HNRNPA2B1 has a mixed influence on gene expression of m^6A related genes and DNA:RNA hybrid related genes. 69
3.3.2.2 HNRNPA2B1 KO cells display no difference in the levels of DNA:RNA hybrids in immunostaining experiments. 70
3.3.2.3 HNRNPA2B1 KO and WT cells display no significant difference in the levels of immunostaining of DNA damage indicator, γ-H2AX 73
3.3.2.4 Mass spectrometry suggests a decrease in the levels of m^6A on DNA:RNA hybrids within HNRNPA2B1 KO cells. 75
3.3.2.5 DNA:RNA hybrids are enriched within repetitive and specific intronic sequences in HNRNPA2B1 KO cells. 76
3.3.2.6 m^6A-marked DNA:RNA hybrids are reduced within repetitive sequences but increased in specific intronic sequences in HNRNPA2B1 KO cells. 79
3.3.3 Interplay between HNRNPA2B1 and YTHDF2 when interacting with m^6A-marked DNA:RNA hybrids. 81
3.3.3.1 HNRNPA2B1 protein interactome suggests co-expression and interaction with YTHDF2, spliceosome and DNA:RNA hybrid maintenance proteins. 82
3.3.3.2 Immunocytochemistry suggests interplay between YTHDF2 and HNRNPA2B1 localisation within the nucleus. 86
3.3.3.3 YTHDF2 binding to repetitive and intronic sequences increases within HNRNPA2B1 KO cells. 90

3.3.3.4 HNRNPA2B1 binding to repetitive sequences and individual DNA:RNA-containing loci decreases in YTHDF2 KO cells. 92

3.3.4 HNRNPA2B1 differentially interacts with different DNA:RNA hybrid-containing loci in the introns of *WWOX* gene. 93

3.3.4.1 DNA:RNA hybrids and m^{6}A-marked DNA:RNA hybrids found in the introns of WWOX by analysis of m^{6}A-DRIP and S9.6 DRIP next-generation sequencing. 93

3.3.4.2 DNA:RNA hybrids have increased enrichment in *WWOX* Intron 4 and 8 but decrease in *WWOX* Intron 5 in HNRNPA2B1 KO compared to HAP1 WT cells. 97

3.3.4.3 YTHDF2 binding increases to *WWOX* intronic sequences where DNA:RNA hybrids are present in HNRNPA2B1 KO cells. 99

3.3.4.4 HNRNPA2B1 binding differs depending upon the location of the DNA:RNA hybrid within *WWOX* intronic sequences in YTHDF2 KO cells. 101

3.4 Technical Discussion 103

Chapter 4: Investigating the potential role of HNRNPA2B1 in the metabolism of m^{6}A-marked DNA:RNA hybrids in Glioblastoma Multiforme 108

4.1 Introduction 108

4.2 Aims 111

4.3 Results 111

4.3.1 Elevated levels of m^{6}A writers and readers in GBM. 111

4.3.1.1 Expression of m^{6}A related genes show similar pattern in GBM patient samples and GBM continuous cell lines. 111

4.3.1.2 HNRNPA2B1 high expression is not linked to one GBM subgroup but it is prevalent in non-disclosed GBM patients. 113

4.3.1.3 m^{6}A-related genes show similar gene expression pattern in foetal brain cells, LN18, LN229, U251 and U87MG GBM cell lines. 116

4.3.1.4 Primary GBM cells have lower expression of m^{6}A-related genes compared to continuous GBM cell lines. 120

4.3.2 Levels of m^{6}A-marked DNA:RNA hybrids varied between GBM cell lines... 123

4.3.2.1 DNA:RNA hybrids and m^{6}A-DNA:RNA hybrids levels in repetitive sequences are both lower in U251 compared to hiPSCs. 123

4.3.2.2 The levels of m^{6}A on DNA:RNA hybrids in intronic regions of *CDK6*, *RB1* and *NF1* genes are lower in U251 GBM line compared to hiPSCs. 125

4.3.2.3 SID-UPLC-MS/MS demonstrates the levels of m^{6}A on DNA:RNA hybrids in GBM cell lines. 129

4.3.2.4 U251 exhibit the lowest levels of m^{6}A-DNA:RNA hybrids immunostaining compared to hiPSCs, LN18 and SVGA cells. 131

4.3.3 siRNA mediated knockdown of *HNRNPA2B1* in U251 cells leads to elevated m^{6}A content. 132

4.3.3.1 Validation of HNRNPA2B1 knockdown in U251 cells. 133

4.3.3.2 Loss of HNRNPA2B1 in U251 cells significantly increases m^{6}A levels within the nucleus without substantial change in the levels of DNA:RNA hybrids. 134

4.3.4 Investigating the impact of *HNRNPA2B1* depletion in LN18 GBM cells. 139

4.3.4.1 Validation HNRNPA2B1 knockdown in LN18 cells. 139

4.3.4.2 Attachment to growth surface is impaired after knockdown of *HNRNPA2B1* in LN18 cells and is restored with the use of attachment factor. 140

4.3.4.3 Knockdown of HNRNPA2B1 increases expression of m^{6}A-related genes with high levels of YTHDF2 maintained within HNRNPA2B1 depleted LN18 cells. . 141

4.3.4.4 Significant increase in the gene expression of DNA:RNA hybrid related genes and immunocytochemical presence of DNA:RNA hybrids in HNRNPA2B1 depleted LN18 cells. 146

4.4 Technical Discussion 149

Chapter 5: Investigating the potential role of HNRNPA2B1 in the metabolism of m^{6}A-marked DNA:RNA hybrids in Medulloblastoma 154

5.1 Introduction 154

5.2 Aims 158

5.3 Results 159

5.3.1 Elevated levels of *HNRNPA2B1* are found in MB cells. 159

5.3.1.1 MB patients samples are characterised by high levels of *HNRNPA2B1* expression. 159

5.3.1.2 Elevated levels of m^{6}A writers, readers, and erasers in UW228-3 cells. . 162

5.3.1.3 Elevated mRNA expression of DNA:RNA hybrid related genes within UW228-3 cells. 165

5.3.2 m^{6}A-marked DNA:RNA hybrids are present in UW228-3 cells. 166

5.3.2.1 m^{6}A-DNA:RNA hybrids levels in repetitive sequences are lower in UW228-3 compared to hiPSCs. 167

5.3.2.2 Intronic loci in *GLI2*, *CDK6*, *RB1* and *NF1* have lower m^{6}A-marked DNA:RNA hybrid enrichment in UW228-3 compared to hiPSCs. 169

5.3.2.3 SID-UPLC-MS/MS identified the presence of m^{6}A-marked DNA:RNA hybrids in UW228-3 cells. 172

5.3.3 siRNA mediated knockdown of HNRNPA2B1 within UW228-3 leads to elevated DNA:RNA hybrid presence. 173

5.3.3.1 Validation HNRNPA2B1 knockdown in UW228-3 cells. 174

5.3.3.2 Attachment to growth surface is impaired after knockdown of *HNRNPA2B1* in UW228-3 cells and is restored with the use of a commercial attachment factor. 175

5.3.3.3 Knockdown of HNRNPA2B1 significantly increases the levels of DNA:RNA hybrids in UW228-3 cells. 177
5.4 Technical Discussion 180
Chapter 6: Main Discussion 184
6.1 Potential role of HNRNPA2B1 in the metabolism of R-loops. 184
6.1.1 The impact of HNRNPA2B1 depletion on DNA:RNA hybrids is dependent upon their genomic location. 184
6.1.2 HNRNPA2B1 depends on YTHDF2 in its binding to m^{6}A-marked DNA:RNA hybrids. 188
6.1.3 Is the DNA:RNA hybrid presence in WWOX linked to alternative splicing or common fragile sites? 190
6.2 Presence of m^{6}A marked DNA:RNA hybrids are markedly lower in brain tumours compared to hiPSCs, yet gene expression of m^{6}A related genes were elevated in brain tumours. 194
6.3 Depletion of HNRNPA2B1 resulted in increased levels of DNA:RNA hybrids and m^{6}A in brain tumours. 196
6.4 Could HNRNPA2B1 be a potential targeted cancer therapy for brain tumours? 198
6.5 Concluding remarks and future work 199
Appendix – Supplementary figures 203
References 209

List of Figures

Figure 1.1: Selection of abundant modifications observed on RNA. 2
Figure 1.2: The dynamic methylation and demethylation of m^{6}A. 11
Figure 1.3: Types of direct and indirect binding mechanisms for m^{6}A reader proteins. 14
Figure 1.4: Overview of m^{6}A reader proteins impact on mRNA functions. 15
Figure 1.5: Molecular mechanisms involving the m^{6}A modification in breast cancer. 20
Figure 1.6: Structure of DNA:RNA hybrid and their methods of detection. 23
Figure 1.7: DNA:RNA hybrid presence gives rise to DNA damage. 28
Figure 1.8: Dynamics of m^{6}A-marked DNA:RNA hybrids and the interacting m^{6}A readers YTHDF2 and HNRNPA2B1 during the cell cycle. 32

Figure 1.9: Writers and readers of m^{6}A interact with DNA:RNA hybrids in HeLa cells. 34

Figure 1.10: HNRNPA2B1 preferentially binds to m^{6}A marked DNA:RNA hybrids in intronic sequences which can affected by the loss of RNaseH1 or METTL3. 35

Figure 3.1: Main mechanisms of constitutive and alternative splicing. 57

Figure 3.2: PCR analysis of HNRNPA2B1 knockout impacted HNRNPA2B1 gene transcripts within HNRNPA2B1 KO and WT HAP1 cells. 61

Figure 3.3: Nucleotide insertion causes frame shift mutation within HAP1 HNRNPA2B1 KO cell line from Horizon Discovery. 62

Figure 3.4: Nucleotide insertion results in disruption of both RRM1 and RRM2 domains in HAP1 HNRNPA2B1 KO cells. 63

Figure 3.5: Structural differences between HNRNPA2B1 isoforms, HNRNPA2 and HNRNPB1. 65

Figure 3.6: Nucleotide insertion reduces the mRNA transcripts of both HNRNPA2 and HNRNPB1 isoforms. 67

Figure 3.7: Silencing of HNRNPA2B1 has no significant impact on cell proliferation. 68

Figure 3.8: Knockout of HNRNPA2B1 significantly increases expression of DNA:RNA hybrid helicase gene, DHX9. 70

Figure 3.9: High variability of DNA:RNA hybrid staining in HAP1 wild-type and HNRNPA2B1 KO cells. 72

Figure 3.10: No difference in γ-H2AX immunostaining in HNRNPA2B1 KO compared to HAP1 WT cells. 74

Figure 3.11: Knockout of HNRNPA2B1 appears to affect the genomic levels of m^{6}A-marked DNA:RNA hybrids differently compared to m^{6}A modified RNA. 76

Figure 3.12: Knockout of HNRNPA2B1 led to increased enrichment of DNA:RNA hybrids in SINE/Alu elements. 77

Figure 3.13: Knockout of HNRNPA2B1 led to increased enrichment of DNA:RNA hybrids in MYH16 and decreased in HECW1. 78

Figure 3.14: HNRNPA2B1 KO led to decreased levels of m^{6}A-DNA:RNA hybrids within repetitive elements. 80

Figure 3.15: Knockout of HNRNPA2B1 led to increased enrichment of m^{6}A-DNA:RNA hybrids within MYH16 and HECW1..... 81

Figure 3.16: Protein-protein interactome network suggests functional protein interactions between HNRNPA2B1, SRSF3, SRSF10, DHX9 and DDX3X..... 83

Figure 3.17: HNRNPA2B1 and YTHDC1 have the most involvement in mRNA splicing, processing, transport, and export from the nucleus. 85

Figure 3.18: YTHDF2 nuclear immunostaining increases within the nucleus in HNRNPA2B1 KO cells..... 87

Figure 3.19: HNRNPA2B1 immunostaining decreases within the nucleus in YTHDF2 KO cells..... 89

Figure 3.20: YTHDF2 binding in HNRNPA2B1 KO cells increases in both repetitive elements and intronic sequences. 91

Figure 3.21: HNRNPA2B1 binding in YTHDF2 KO cells decreases in both repetitive elements and intronic sequences..... 92

Figure 3.22: m^{6}A-marked DNA:RNA hybrids and DNA:RNA hybrids within intronic regions of WWOX in hiPSCs. 94

Figure 3.23: WWOX canonical gene structure, protein structure and alternative splicing isoforms..... 96

Figure 3.24: Knockout of HNRNPA2B1 leads to decrease of DNA:RNA hybrid enrichment in Intron 5 of WWOX but increase in Intron 4 and 8 of WWOX..... 98

Figure 3.25: YTHDF2 binding increased within WWOX Intron 4, 5 and 8 in HNRNPA2B1 KO cells..... 100

Figure 3.26: HNRNPA2B1 binding decreased in Intron 4 and 8 but increased in Intron 5 of WWOX in YTHDF2 KO cells. 102

Figure 4.1: GBM patient samples and cell lines exhibit similar expression patterns of m^{6}A-related genes. 113

Figure 4.2: HNRNPA2B1 expression is not linked to any known GBM subgroup. 115

Figure 4.3: METTL3, METTL14, YTHDF2 and HNRNPA2B1 gene expression is significantly increased in glioblastoma cell lines compared to hiPSCs. 118

Figure 4.4: LN18, LN229 and U87MG cells have similar expression pattern of m^{6}A related genes. 119

Figure 4.5: Primary glioblastoma cell line have lower expression of m^{6}A-related and DNA:RNA hybrid related genes compared to continuous cell lines. 120

Figure 4.6: Gene expression for m^{6}A-related genes is lower in primary glioblastoma cell lines compared to hiPSCs. 122

Figure 4.7: Levels of m^{6}A marked DNA:RNA hybrids in repetitive elements are lower in U251 compared to hiPSCs. 124

Figure 4.8: Levels of DNA:RNA hybrids in repetitive elements are lower in U251 compared to hiPSCs. 125

Figure 4.9: Enrichment levels of m^{6}A-marked DNA:RNA hybrids within CDK6 introns are lower in U251 compared to hiPSCs. 127

Figure 4.10: Enrichment levels of m^{6}A-marked DNA:RNA hybrids within RB1 introns are lower in U251 compared to hiPSCs. 128

Figure 4.11: Enrichment levels of m^{6}A-marked DNA:RNA hybrids within NF1 introns are lower in U251 compared to hiPSCs. 129

Figure 4.12: SVGA and LN18 cells have lower levels of m^{6}A present on DNA:RNA hybrids compared to hiPSCs. 130

Figure 4.13: m^{6}A DNA:RNA hybrids immunostaining is lower in U251 cells compared to hiPSCs, SVGA and LN18. 132

Figure 4.14: Optimisation of siHNRNPA2B1 knockdown in U251 cells. 134

Figure 4.15: No significant difference in DNA:RNA hybrid levels in U251 siHNRNPA2B1 cells. 136

Figure 4.16: m^{6}A levels significantly increase within the nuclei of siHNRNPA2B1 depleted U251 cells compared with non-treated U251. 137

Figure 4.17: Positive correlation between HNRNPA2B1 loss and increased m^{6}A presence within the nucleus. 138

Figure 4.18: Optimisation of siHNRNPA2B1 knockdown in LN18 cells. 140

Figure 4.19: Increased level of attachment to growth surface with commercial attachment factor present for LN18 siHNRNPA2B1 knockdown cells. 141

Figure 4.20: Increases in gene expression of m^{6}A writers, readers and erasers upon siHNRNPA2B1 knockdown in LN18. ..... *143*

Figure 4.21: No significant increase in YTHDF2 levels in LN18 siHNRNPA2B1 cells. *145*

Figure 4.22: Knockdown of HNRNPA2B1 in LN18 increases gene expression of DHX9 and DDX3X compared to siControl LN18 cells. *146*

Figure 4.23: DNA:RNA hybrids levels increase in LN18 siHNRNPA2B1 cells. *148*

Figure 5.1: Elevated expression of HNRNPA2B1 in the subgroup of MB. *160*

Figure 5.2: HNRNPA2B1 expression and impact on overall survival probability varies upon subgroup. *162*

Figure 5.3: Gene expression of m^{6}A writers, readers and erasers are elevated in UW228-3 cells. *164*

Figure 5.4: HNRNPA2B1 and YTHDF2 gene expression have higher expression in UW228-3 compared to GBM cell lines. *165*

Figure 5.5: Increased expression of DNA:RNA hybrid related genes within UW228-3. ..... *166*

Figure 5.6: Levels of m^{6}A-marked DNA:RNA hybrids within repetitive elements are lower in UW228-3 compared to hiPSCs. *168*

Figure 5.7: Levels of DNA:RNA hybrids within repetitive elements are lower in UW228-3 compared to hiPSCs. *169*

Figure 5.8: Enrichment levels of m^{6}A marked DNA:RNA hybrids within intronic sequences of GLI2 are lower in UW228-3 compared to hiPSCs. *171*

Figure 5.9: Enrichment levels of m^{6}A marked DNA:RNA hybrids within intronic sequences of CDK6 are lower in UW228-3 compared to hiPSCs. *172*

Figure 5.10: UW228-3 cells have lower levels of m^{6}A present on DNA:RNA hybrids compared to hiPSCs. *173*

Figure 5.11: Optimisation of HNRNPA2B1 siRNA within UW228-3 cells. *175*

Figure 5.12: Increased level of cell attachment to growth surface with commercial attachment factor in UW228-3 siHNRNPA2B1 knockdown cells compared to untreated UW228-3 siHNRNPA2B1 knockdown cells. *176*

Figure 5.13: Knockdown of HNRNPA2B1 in UW228-3 increases expression of DNA:RNA hybrid related genes. *177*

Figure 5.14: DNA:RNA hybrids presence increased in UW228-3 siHNRNPA2B1 cells. 179

Figure 6.1: Proposed model of YTHDF2 and HNRNPA2B1 interplay in regulation of DNA:RNA hybrid dynamics in WT, HNRNPA2B1 KO and YTHDF2 KO HAP1 cells. 200

Supplementary figure 1: U251 and UW228-3 have similar cell population counts in the cell cycle phases. 203

Supplementary figure 2: Expression cut off for high and low expression of HNRNPA2B1 in GBM subgroups. 204

Supplementary figure 3: Expression cut off for high and low expression of HNRNPA2B1 in GBM non-disclosed subgroups. 205

Supplementary figure 4: Expression cut off for high and low expression of HNRNPA2B1 in MB subgroups. 206

Supplementary figure 5: Expression cut off for high and low expression of HNRNPA2B1 in MB Group 3 subgroup. 207

Supplementary figure 6: Expression cut off for high and low expression of HNRNPA2B1 in MB SHH subgroup. 208

List of Tables

Table 1.1: Overview of RNA modification sites, roles, and cancer implications. 5

Table 2.1: Cancer cell line characteristics. 37

Table 2.2: Media formulation. 38

Table 2.3: List of qPCR 5' and 3' primers 43

Table 2.4: Phusion PCR 5' and 3' primers 44

Table 2.5: List of DRIP and ChIP primers 47

Table 2.6: The antibodies and other reagents used for immunostaining. 50

Abbreviations

Abbreviations	Description
A	Adenine/Adenosine
ADAR1/2	Adenosine deaminase acting on dsRNA1 and 2
ADH	Alcohol dehydrogenase
AKML	Acute megakaryoblastic leukaemia
Akt	Protein kinase B
ALKBH1	AlkB Homolog 1, Histone H2A Dioxygenase
ALKBH3	AlkB Homolog 3, Alpha-Ketoglutarate Dependent Dioxygenase
ALKBH5	AlkB Homolog 5, RNA Demethylase
ALS	Amyotrophic lateral sclerosis
ALYREF	Aly/REF export factor
AML	Acute myeloid leukaemia
ANG	Angiopoietin
ANOVA	Analysis of variance
AS	Alternative splicing
ASB2	Ankyrin repeat and SOCS box containing 2
ATAR	All-trans-retinoic acid
ATM	Ataxia telangiectasia mutated
ATR	Serine/Threonine-specific protein kinase
BC	Breast cancer
BCL2	BCL2 apoptosis regulator
BER	Base excision repair
BNIP3	BCL2 interacting protein 3
BRCA	Breast cancer susceptibility gene
C	Cytosine/Cytidine
C9orf72	Chromosome 9 open reading frame 72
CASP	Caspases/cysteine-aspartic proteases
CAT	Catalase
CBLL1/HAKAI	Casitas B-lineage lymphoma-transforming sequence-like protein 1
CCR4-NOT	Carbon catabolite repression 4 — Negative on TATA-less
CDH1	E-cadherin
CDH2	N-cadherin
CDK1	Cyclin dependent kinase 1
CDK6	Cyclin dependent kinase 6
CDKN2A	Cyclin Dependent Kinase Inhibitor 2A
CDS	Coding sequence
CEBPA	CCAAT enhancer-binding protein alpha
CEBPZ	CCAAT enhancer binding protein zeta
CFS	Common fragile site
ChIP	Chromatin immunoprecipitation
ChrRNA-seq	Chromatin associated RNA sequencing
CML	Chronic myelogenous leukaemia

c-MYC	MYC Proto-Oncogene
CNS	Central nervous system
COX2/PTGS2	Prostaglandin-endoperoxide synthase 2
CRISPR	Clustered regularly interspaced short palindromic repeats
CSR	Class switch recombination
CT	Computerised tomography
CTDNEP1	CTD Nuclear Envelope Phosphatase 1
CTNNB1	Catenin Beta 1
CXCR4	C-X-C motif chemokine receptor 4
CYP1B1	Cytochrome P450 family 1 subfamily B member 1
DAPI	4′,6-diamidino-2-phenylindole
DCP2	miRNA-mediated mRNA degradation and MRNA 2
DDX3X	DEAD-Box Helicase 3 X-Linked
DGCR8	DiGeorge syndrome critical region 8
DHX	DExH-Box Helicase
DKC1	Dyskerin pseudouridine synthase 1
DMEM	Dulbecco’s Modified Eagles Medium
DMSO	Dimethyl sulfoxide
DNA	Deoxyribonucleic acid
DNMT	DNA methyltransferase-like
DRBP	DNA and RNA binding proteins
DRIP	DNA:RNA hybrid immunoprecipitation
DROSHA	Drosha Ribonuclease III
DSB	Double-stranded breaks
DTT	Dithiothreitol
EGFR	Epidermal growth factor receptor
eIF3	Eukaryotic initiation factor 3
EMT	Epithelial-to-mesenchymal transition
EPIs	Enhancer-promoter interactions
ER	Oestrogen receptor
ERK	Extracellular signal-regulated protein kinase
eRNAs	Enhancer-associated RNAs
ESE	Exonic splicing enhancers
ESS	Exonic splicing silencers
FADD	Fas Associated Via Death Domain
FBS	Foetal bovine serum
FC	Fold change
FLT3	Fms related receptor tyrosine kinase 3
FMR1	Fragile X mental retardation 1
FOXM1	Forkhead box protein M1
FTO	FTO Alpha-Ketoglutarate Dependent Dioxygenase
FXN	Frataxin
G	Guanine/Guanosine
G phase	Growth phase
GABRA1	Gamma-Aminobutyric Acid Type A Receptor Subunit Alpha 1
GAPDH	Glyceraldhyde 3- phospate dehydrogenase

GBM	Glioblastoma multiforme
GFI	Growth Factor Independent Transcriptional Repressor
GFP	Green fluorescent protein
GIN	Glioblastoma Invasive
GLI	GLI family zinc finger
GO	Gene ontology
GSC	Glioblastoma stem cells
H2AX	H2A histone family member X
hAID	Human activation-induced cytidine deaminase
HAP	Haploid
HBXIP	Hepatitis B X-interacting protein
HCl	Hydrochloric acid
HECW1	HECT, C2 And WW Domain Containing E3 Ubiquitin Protein Ligase 1
hiPSCs	Human induced pluripotent stem cells
hm5C	5-hydroxylmethylcytidine
HNC	Head and neck cancer
HNRNP	Heterogeneous Nuclear Ribonucleoprotein
HR	Homologous recombination
HSPC	Haematopoietic stem and progenitor cell
I	Inosine
IDH1	Isocitrate dehydrogenase (NADP(+)) 1
IDH1	Isocitrate Dehydrogenase (NADP(+)) 1
IGF2BP	Insulin-like growth factor-2 mRNA-binding protein
IgG	Immunoglobulin G
IGV	Integrative Genomics Viewer
ISE	Intronic splicing enhancers
ISS	Intronic splicing silencers
ITCH	E3 ubiquitin-protein ligase itchy homologue
ITD	Internal tandem duplication
KBTBD4	Kelch Repeat and BTB Domain Containing 4
KDM6A	Lysine Demethylase 6A
KH	K homology
KLF4	Kruppel-like factor 4
KMT2C	Lysine Methyltransferase 2C
KMT2D	Lysine Methyltransferase 2D
KO	Knockout
lincRNA	Long non-coding RNA
LINE1	Long interspersed nuclear element-1
LINEs	Long interspersed nuclear elements
LPA	Lipoprotein (A)
M phase	Mitosis phase
m^1A	N1-methyladenosine
m^5C	5-methylcytidine
m^6A	N6-methyladenosine
m^6Am	N6, 2'-O-dimethyladenosine
MAD1L1	Mitotic Arrest Deficient 1 Like 1

MALAT1	Metastasis associated lung adenocarcinoma transcript 1
MAN2B2	Mannosidase Alpha Class 2B Member 2
MAT2A	Methionine adenosyltransferase 2A
MB	Medulloblastoma
MET	Mesenchymal-to-epithelial transition
METTL	Methyltransferase Like
MGMT	O-6-Methylguanine-DNA Methyltransferase
MINT-seq	Methylation-inscribed nascent transcript sequencing
miRNA	micro RNA
MKL1	Megakaryoblastic leukemic-1
MMP	Matrix Metalloproteinase
MRI	Magnetic resonance imaging
mRNA	Messenger RNA
mRNP	Messenger ribonucleoprotein
MST1R	Macrophage Stimulating 1 Receptor
MYC/MYCN	MYCN proto-oncogene protein
MYH16	Myosin Heavy Chain 16 Pseudogene
NANOG	Nanog Homeobox
ncRNAs	Non-coding RNAs
NEFL	Neurofilament Light Chain
NER	Nucleotide excision repair
NES	Nestin
NF1	Neurofibromin 1
NF-κB	Nuclear factor kappa-light-chain-enhancer of activated B cells
NHEJ	Non-homologous end joining
NKX2-2	NK2 homeobox 2
NOTCH	Notch receptor
NSUN	NOL1/NOP2/SUN domain family members
O-GlcNAcylation	O-Linked β-N-acetylglucosamine modification
OLIG2	Oligodendrocyte transcription factor 2
OSCC	Oesophageal squamous cell carcinoma
OTX2	Orthodenticle Homeobox 2
PARP1	Poly(ADP-Ribose) Polymerase 1
PCR	Polymerase Chain Reaction
PDGFRA	Platelet derived growth factor receptor alpha
PFN2	Profilin 2
Ph-H3	Phosphorylated Histone H3
PI3K	Phosphatidylinositol 3-kinase
PKM1/2	Pyruvate Kinase M1/2
PLK1	Polo Like Kinase 1
PRDM6	PR/SET Domain 6
pre-mRNA	Precursor messenger RNA
PTCH1	Patched 1
PTEN	Phosphatase and tensin homolog
PUS	Pseudouridine synthase
PVT1	Pvt1 Oncogene

qDRIP	Quantitative differentiated DRIP
QMC	Queens Medical Centre
qPCR	Quantitative Polymerase Chain Reaction
RAD51	RAD51 homolog, DNA repair protein
RAD52	RAD52 homolog DNA repair protein
RANBP17	RAN Binding Protein 17
RARα	Retinoic acid receptor-alpha
RARγ	Retinoic acid receptor-γ
RB1	RB Transcriptional Corepressor 1
RBM15/15B	RNA binding motif protein 15/RNA binding motif protein 15B
RF	Replication fork
RNA	Ribonucleic acid
RNAP	RNA polymerase
RNase H	Ribonuclease H
RNase III	Ribonuclease III
RNase T1	Ribonuclease T1
RON	Recepteur d'origine nantais
ROS	Reactive oxygen species
RR-ChIP seq	RNA-specific RNase H1 ChIP sequencing
RRM	RNA recognition motif
rRNA	Ribosomal RNA
RRP8	Ribosomal RNA-processing protein 8
S phase	Synthesis phase
S9.6	Anti-DNA-RNA Hybrid Antibody, clone S9.6
SAH	S-Adenosyl-L-Homocysteine
SAM	S-Adenosyl methionine
SD	Standard deviation
SDR	Short-chain dehydrogenases/reductases
SEM	Standard error of the mean
SHH	Sonic hedgehog activated
shRNA	shRNA
siControl	siRNA control
SID–UPLC–MS/MS	Stable-isotope dilution ultra-performance liquid chromatography with tandem mass spectrometry
siHNRNPA2B1	HNRNPA2B1 siRNA
SINEs	Short interspersed elements
siRNA	Small interfering RNA
SLC12A5	Solute Carrier Family 12 Member 5
SMARCA4	SWI/SNF Related, Matrix Associated, Actin Dependent Regulator of Chromatin, Subfamily A, Member 4
SMN	Survival of Motor Neuron
SMO	Smoothened proteins
SNAI1/SNAI2	Snail1/2
snoRNA	Small nucleolar RNA
SNP	Single nucleotide polymorphisms
snRNA	Small nuclear RNA
snRNPs	Small nuclear ribonucleoproteins

SOX2	SRY-Box Transcription Factor 2
SP1/SP2	Sp1 transcription factor/Sp2 transcription factor
sqrt	Square root
SR	Serine and Arginine-rich proteins
SRA1	Steroid receptor RNA activator 1
SREs	Splicing regulatory elements
SRSF	Serine And Arginine Rich Splicing Factor
ssDNA	Single stranded DNA
ssRNA	Single stranded RNA
STAT3	Signal Transducer and Activator of Transcription 3
SUFU	SUFU Negative Regulator of Hedgehog Signalling
SYT1	Synaptotagmin 1
T	Thymine
Taq	Thermus aquaticus
TCGA	The Cancer Genome Atlas
TERRA	Telomeric-repeat-containing RNA
TERT	Telomerase Reverse Transcriptase
TET	Ten-eleven translocation
TMZ	Temozolomide
TP53	Tumour protein p53
TRMT10C	TRNA Methyltransferase 10C
TRMT6	TRNA Methyltransferase 6 Non-Catalytic Subunit
TRMT61A	TRNA Methyltransferase 61A
tRNA	Transfer RNA
TSA	Tyramide Signal Amplification
TSS	Transcription start sites
TUBB3	Tubulin Beta 3 Class III
TWIST1	Twist family BHLH transcription factor 1
U	Uridine
VEGF	Vascular endothelial growth factor
VEGFRA	Vascular endothelial growth factor receptor A
VIM	Vimentin
VIRMA/KIAA1429	Vir- like m6A methyltransferase associated
WHO	World Health Organisation
WNT	Wingless activated
WT	Wild-type
WTAP	WT1 Associated Protein
WWOX	WW domain containing Oxidoreductase
XRN2	5'-3' exoribonuclease 2
YTHDC1	YTH Domain Containing 1
YTHDF	YTH N6-Methyladenosine RNA Binding Protein
ZC3H13	Zinc finger CCCH-type containing 13
ZMYM3	Zinc Finger MYM-Type Containing 3
γ-H2AX	Phosphorylated H2A histone family member X
α-satellites	Alpha-satellites
Ψ	Pseudouridine

5mC	5-methylcytosine
5hmC	5-hydroxylmethylcytosine
3'UTR	3' untranslated region
5'UTR	5' untranslated region

Chapter 1: Introduction

1.1 Epitranscriptomics

Chemical modifications are a highly specific and effective way to regulate the function of biological macromolecules such as proteins, RNA, DNA, sugars and lipids. RNA modifications have been reported for the last 60 years and now over 150 distinct chemical modifications have been identified on different RNA species (Cohn, 1960; Li and Mason, 2014; Boccaletto *et al.*, 2018). They are present primarily on transfer RNAs (tRNAs), ribosomal RNAs (rRNAs) and messenger RNAs (mRNAs), as well as other non-coding RNAs (ncRNAs) such as small nuclear RNAs (snRNAs), small nucleolar RNAs (snoRNAs), long intergenic non-coding RNAs (lincRNA) and microRNAs (miRNA) (Li and Mason, 2014; Shelton, Reinsborough and Xhemalce, 2016; Roundtree *et al.*, 2017; Zhao *et al.*, 2017; Gebert and MacRae, 2019; Yao, Wang and Chen, 2019). Modifications on these RNA species were first designated 'RNA epigenetics' in 2010 but renamed to what we now know as 'epitranscriptomics' in 2012 (He, 2010; Saletore *et al.*, 2012). In a similar manner to epigenetics-related proteins, proteins that interact or bind to these epitranscriptomic modifications were termed as: 'writers' that modify the RNA, 'erasers' that remove that RNA modification and 'readers' that can directly recognise the modification by a binding pocket or indirectly recognise it via a structural switch mechanism. Epitranscriptomic modifications have the potential to affect transcripts by altering the secondary structure of RNA, base-pair binding, the charge of a nucleoside as well as protein-RNA interactions (Roundtree *et al.*, 2017). Consequently, these modifications can therefore affect the outcome of gene expression by modulating RNA localisation, processing, translation and decay (Roundtree *et al.*, 2017). The most abundant of these epitranscriptomic modifications include pseudouridine (Ψ), 5-methylcytidine (m^5C), 5-hydroxylmethylcytidine (hm^5C), adenosine to inosine editing, N1-methyladenosine (m^1A), N6, 2'-O-dimethyladenosine (m^6Am) and N6-methyladenosine (m^6A) (Fig. 1.1; Table 1.1) (Li, Xiong and Yi, 2017).

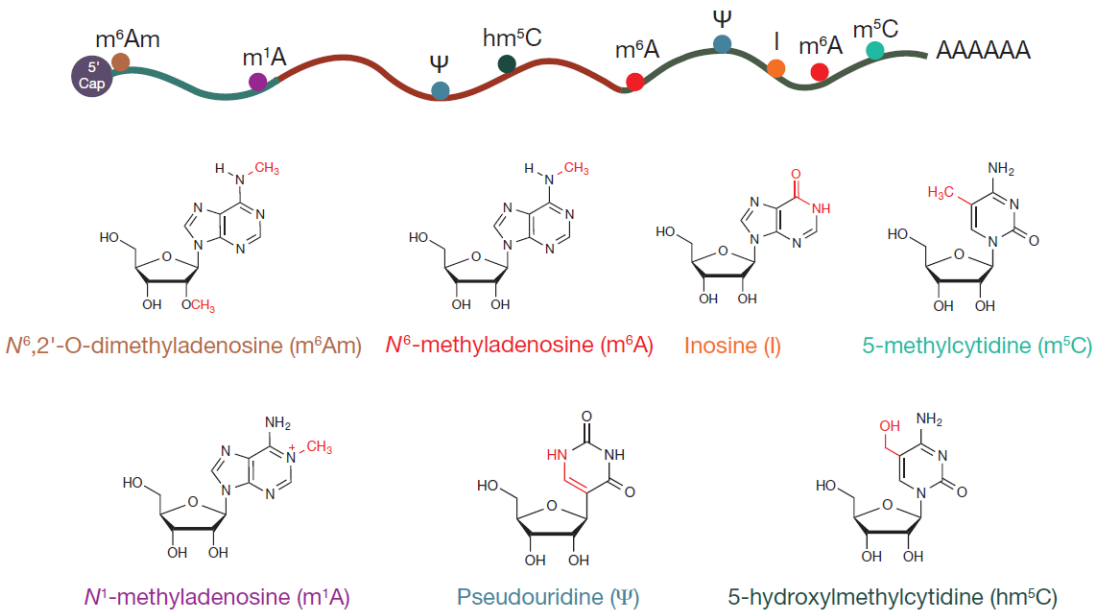


Figure 1.1: Selection of abundant modifications observed on RNA.

Visualisation of the most common RNA modifications including m^6A, m^6Am, m^1A, m^5C, hm^5C, Ψ and adenosine to inosine editing present on various RNA types. Taken from (Li, Xiong and Yi, 2017).

1.1.1 Pseudouridine (Ψ)

Pseudouridine (Ψ) often referred to as the fifth nucleotide of RNA is the most abundant post-transcriptional modification found on rRNA, tRNA, snRNA, snoRNA and mRNA (Davis and Allen, 1957; Cohn, 1960; Karijolich, Yi and Yu, 2015). Two distinct mechanisms can enzymatically catalyse the isomerisation of uridine: the RNA-independent mechanism with Ψ synthases that include dyskerin pseudouridine synthase 1 (DKC1) and the pseudouridine synthase (PUS) protein family or the RNA-dependent mechanism that relies on box H/ACA ribonucleoproteins (Hamma and Ferré-D'Amaré, 2006; Kiss, Fayet-Lebaron and Jády, 2010; Li, Ma and Yi, 2016). Ψ has exhibited different physiological roles dependent upon the type of RNA in which it is located. For instance, Ψ that is found on tRNAs has been associated with stabilising and maintaining tRNA structure whereas, Ψ located on rRNAs is necessary for proper folding of rRNA, ensuring translational fidelity and assembly of the ribosome (Decatur and Fournier, 2002; Baudin-Baillieu *et al.*, 2009; Jack *et al.*, 2011; Karijolich, Yi and Yu, 2015;

Li, Ma and Yi, 2016; Penzo and Montanaro, 2018). Ψ has also been identified on a specific type of snRNAs known as U RNAs that are essential for mRNA splicing (Bohnsack, Höbartner and Bohnsack, 2019). Pseudouridylation of U in RNAs is seen as essential for efficient splicing of mRNA particularly if under cellular stresses such as heat shock and nutrient deprivation (Bohnsack, Höbartner and Bohnsack, 2019). The presence of Ψ was recently identified on mRNAs with a suggested abundance between 0.2 – 0.6% Ψ/uridine ratio (Li *et al.*, 2015). Although the role of Ψ on mRNA remains elusive, Ψ sites appear enriched in the coding region and 3' untranslated region (3'UTR) of mRNAs but are not associated with a particular feature in these regions (Li *et al.*, 2015). Currently, only pseudouridylases have been identified in eukaryotic cells and no known readers or erasers have been identified for Ψ (Penzo and Montanaro, 2018). Pseudouridylases have been associated with various cancers and their impact on the phenotype of cancer cells. PUS1 is primarily a nuclear protein that pseudouridylases tRNA, snRNA and mRNA (Penzo and Montanaro, 2018). PUS1 targets steroid receptor RNA activator 1 (SRA1) allowing SRA1 to interact with several nuclear receptors including retinoic acid receptor-γ (RARγ) in melanoma cells, and oestrogen receptor (ER) in breast cancer cell lines enhancing their transcriptional activity (Zhao *et al.*, 2004). Another well-studied writer for Ψ, primarily in rRNA, snRNA and snoRNA, is DKC1. Mutations in DKC1 cause a rare genetic condition known as dyskeratosis congentia which results in the inability of the bone marrow to produce sufficient blood cells and a predisposition to cancer (Heiss *et al.*, 1998). A mouse model of DKC1 loss of function produced a similar phenotype to dyskeratosis congentia and found that reduced pseudouridylation on rRNA leads to dysfunctional translation of key mRNAs, particularly *TP53,* in human breast cancer samples (Ruggero, 2003; Montanaro *et al.*, 2010).

1.1.2 5-methylcytidine (m^5C)

5-methylcytosine (5mC) has been extensively studied as a DNA modification (Wyatt, 1950; Roy and Weissbach, 1975; Jahner *et al.*, 1982; Bestor and Ingram, 1983; Goll and Bestor, 2005; Kohli and Zhang, 2013) but has also been identified on RNA known as 5-methylcytidine (m^5C) (Desrosiers, Friderici and Rottman, 1974; Dubin and Taylor, 1975). Currently, m^5C has been detected on rRNA, tRNA, and other ncRNAs and with a lower abundance on mRNA

compared to the other RNA classes (Legrand *et al.*, 2017; Bohnsack, Höbartner and Bohnsack, 2019). On tRNA, m^5C presence is found to regulate and stabilise RNA secondary structure as well as being necessary for translation accuracy by influencing the anticodon stem-loop conformation (Motorin and Helm, 2010; Squires and Preiss, 2010; Trixl and Lusser, 2019). Whereas m^5C present on rRNA can impact translational precision with loss of m^5C at position 2278 permitting the translational readthrough of stop codons (Chow, Lamichhane and Mahto, 2007; Schosserer *et al.*, 2015). The low presence of m^5C on mRNA has made identifying functions and roles difficult, yet with improved detection methods, studies have proposed that m^5C is involved in the nuclear export of mature mRNAs via Aly/REF export factor (ALYREF) (Yang *et al.*, 2017; Huang *et al.*, 2019). The methyltransferases responsible for m^5C modification on RNA include the NOL1/NOP2/SUN domain family members 1 - 7 (NSUN1 – NSUN7) and DNA methyltransferase-like 2 (DNMT2) (Bohnsack, Höbartner and Bohnsack, 2019). NSUN2 and DNMT2 have been found to methylate cytoplasmic tRNAs and mRNAs, NSUN1/NSUN5 can modify 28S rRNA, and NSUN3/NSUN4 modify mitochondrial tRNAs and rRNAs (Bohnsack, Höbartner and Bohnsack, 2019). NSUN2 was found to methylate lincRNA (*NMR* or LINC01672) which, in turn, controls the expression of matrix metalloproteinases 3 and 10 (*MMP3/MMP10*) and consequently promoted tumour progression in oesophageal cancer (Li *et al.*, 2018).

In DNA, 5mC can be oxidised by ten-eleven translocation (TET) proteins into 5-hydroxylmethylcytosine (5hmC) which is viewed as an important epigenetic modification (Kriaucionis and Heintz, 2009; Tahiliani *et al.*, 2009). Therefore, researchers started to investigate whether this oxidation occurs similarly to m^5C in RNA (Li and Mason, 2014). 5-hydroxylmethylcytidine (hm^5C) was first identified in the rRNA of wheat seedlings and since has been observed in *Drosophila melanogaster* mRNA within coding regions favouring translation of mRNA transcripts (Rácz, Király and Lásztily, 1978; L. Fu *et al.*, 2014; Delatte *et al.*, 2016).TET proteins have also been reported to oxidise m^5C to hm^5C in RNA in both mammalian species and *Drosophila* (L. Fu *et al.*, 2014; Delatte *et al.*, 2016).

Table 1.1: Overview of RNA modification sites, roles, and cancer implications.

RNA Modifications	Symbol	RNA types	Suggested roles	Writer proteins (Addition of modification)	Eraser proteins (Removal of modification)	Cancer implications
Pseudouridine	Ψ	rRNA, tRNA, snRNA, snoRNA, mRNA	Maintenance of tRNA structure mRNA splicing	DKC1 PUS protein family	Not currently identified	Melanoma Breast Cancer
Adenine to Iodine Editing	A to I	mRNA, miRNA, tRNA	mRNA splicing Secondary RNA structure of tRNAs Regulation of miRNA biogenesis Target specificity of miRNAs	ADAR1/2	Not currently identified	Not currently identified
5-methylcytidine	m^5C	rRNA, tRNA, mRNA, ncRNAs	Stabilise tRNA secondary structure The presence on rRNA impacts translational precision	NSUN1 – NSUN7 DNMT2	Can be oxidised by TET proteins	Oesophageal cancer

			Nuclear export of mature mRNAs			
N1-methyladenosine	m^1A	tRNA, rRNA, mRNA	Alter protein-mRNA interactions Upregulation of translation Stabilise tRNA tertiary structure rRNA biogenesis	TRMT6/TRMT61A complex	ALKBH1 ALKBH3	Not currently identified
N6, 2'-O-dimethyladenosine	m^6Am	mRNA	Prevent miRNA-mediated mRNA degradation and MRNA 2 (DCP2)-mediated decapping	Not currently identified	Not currently identified	Not currently identified
N6-methyladenosine	m^6A	mRNA, lincRNA, rRNA, miRNA	mRNA stability, decay, exportation, splicing and transportation miRNA processing and maturation	METTL3 METTL14 WTAP RBM15/RBM15B VIRMA/KIAA1429 ZC3H13 CBLL1 METTL16	FTO ALKBH5	Acute Myeloid Leukaemia, Breast Cancer Glioblastoma Multiforme Hepatocellular Carcinoma Lung Cancer Pancreatic Cancer

1.1.3 Adenosine to Inosine editing

Adenosine to inosine editing is the most prevalent type of RNA editing observed in higher eukaryotes, with the phenomenon initially observed in amphibian (*Xenopus laevis*) eggs (Bass and Weintraub, 1987, 1988; Rebagliati and Melton, 1987). Initially, it was found that the unwinding of double-stranded RNA (dsRNA) is dependent on the conversion of adenosine to inosine which is mediated by adenosine deaminase acting on dsRNA1 and 2 (ADAR1 and ADAR2) (Bass and Weintraub, 1987, 1988; Rebagliati and Melton, 1987; Nishikura, 2010, 2016). RNA editing from adenosine to inosine has also been observed in mRNA primary transcripts, tRNAs and miRNAs (Nishikura, 2016). Uniquely, inosine will preferentially pair with cytidine over adenosine usually paired with uridine which leads inosine to be read as guanosine by the ribosome (Nishikura, 2016). This conversion consequently has implications for the secondary RNA structure, altering alternative splicing, the regulation of miRNA biogenesis and changing the target specificity of miRNAs (Wulff, Sakurai and Nishikura, 2011; Nishikura, 2016).

1.1.4 N1-methyladenosine (m^1A)

Methylation at the N1 position of adenosine is found at the Watson-Crick interface which produces a positive charge on that nucleotide (Behm-Ansmant, Helm and Motorin, 2011; Hauenschild *et al.*, 2015). N1-methyladenosine (m^1A) is mainly found on tRNAs and 28S rRNAs but also on a small subset of cytosolic mRNAs where its presence is debated among researchers, potentially due to lack of specific m^1A antibody (Saikia *et al.*, 2010; Dominissini *et al.*, 2016; Safra *et al.*, 2017; Sloan *et al.*, 2017; Zhou *et al.*, 2019; Barbieri and Kouzarides, 2020).

The presence of m^1A on mRNA and other RNA species can electrostatically impact the RNA secondary structure and alter protein-RNA interactions (Dominissini *et al.*, 2016; Li *et al.*, 2016; Zhou *et al.*, 2016; You, Dai and Wang, 2017). The positive charge generated by m^1A can also lead to the generation of truncated cDNAs and misincorporation of nucleosides at

the site of m^1A in the readthrough cDNA (Behm-Ansmant, Helm and Motorin, 2011; Hauenschild *et al.*, 2015). The presence of m^1A has been suggested to be positioned at the 5' untranslated region (5'UTR) and first splice site of coding transcripts with its presence associated with upregulation of translation (Dominissini *et al.*, 2016; Li *et al.*, 2016). Additionally, levels of m^1A on RNA were found to react dynamically to cellular stresses such as nutrient deprivation and heat shock (Dominissini *et al.*, 2016; Li *et al.*, 2016).

On cytoplasmic tRNA, m^1A stabilises the tertiary structure whereas, at position 9 of metazoan mitochondrial tRNA methylated by TRNA Methyltransferase 10C (TRMT10C), it affects the folding of tRNA (Schevitz *et al.*, 1979; Vilardo *et al.*, 2012). Furthermore, in human 28S rRNA, m^1A methylation at position 1322 by ribosomal RNA-processing protein 8 (RRP8) is necessary for correct rRNA biogenesis (Hauenschild *et al.*, 2015; Waku *et al.*, 2016).

Currently, only one methyltransferase has been suggested as an m^1A writer on mRNA known as the TRNA Methyltransferase 6 Non-Catalytic Subunit (TRMT6)/TRNA Methyltransferase 61A (TRMT61A) complex, however, this only appears to account for a small number of m^1A present on mRNAs (Dominissini *et al.*, 2016; Safra *et al.*, 2017). Erasers for m^1A depend on the RNA species in which m^1A resides with AlkB Homolog 3, Alpha-Ketoglutarate Dependent Dioxygenase (ALKBH3) demethylating m^1A on mRNA while AlkB Homolog 1, Histone H2A Dioxygenase (ALKBH1) suggested to demethylate m^1A on tRNA (Liu *et al.*, 2016; Chen *et al.*, 2019; Woo and Chambers, 2019).

1.1.5 N6, 2'-O-dimethyladenosine (m^6Am)

The second base of many mRNAs, adjacent to the 5' cap, is capable of becoming 2' O-methylated with a fraction of these bases methylated from m^6A bases by an unidentified methyltransferase to form N6, 2'-O-dimethyladenosine (m^6Am) (Schibler and Perry, 1977; Linder *et al.*, 2015). This modification is found in an overall low abundance in mRNA (Linder *et al.*, 2015) with a study proposing that m^6Am can stabilise mRNA by preventing miRNA-mediated mRNA degradation and MRNA 2 (DCP2)-mediated decapping (Mauer *et al.*, 2017).

1.2 N6-methyladenosine (m^6A)

Methylation of adenosine at position 6 produces N6-methyladenosine (m^6A) which is one of the best characterised mRNA modifications. This post-transcriptional regulatory marker is found on many RNA species including mRNA, lincRNA, rRNA and miRNA (Desrosiers, Friderici and Rottman, 1974; Maden, 1986, 1988; C. R. Alarcón *et al.*, 2015; Fazi and Fatica, 2019; van Tran *et al.*, 2019). m^6A is found at consensus RNA motif DRACH (D = G, A or U, R = G or A, H = A, C or U), with this modification enriched in mRNA in the 3'-untranslated regions (3'UTR), the stop codon and within the coding region (Dominissini *et al.*, 2012; Meyer *et al.*, 2012; Y. Fu *et al.*, 2014). Within mRNA, m^6A has been identified to impact mRNA stability, decay, export, splicing and translation (Desrosiers, Friderici and Rottman, 1974; Perry and Kelley, 1974; Roundtree *et al.*, 2017). Intriguingly, m^6A can be dynamically added and removed from mRNA. This process is mediated by methyltransferases ("writers") and demethylases ("erasers"). Additionally, m^6A present on mRNA can interact with binding proteins ("readers"), either directly or indirectly.

1.2.1 m^6A writers

Methyltransferase Like 3 (METTL3) and methyltransferase like 14 (METTL14) form a catalytic core complex that adds a methyl group to the N6 position of adenosine (Bokar *et al.*, 1997; Dominissini *et al.*, 2012; Meyer *et al.*, 2012; Schwartz *et al.*, 2014; Linder *et al.*, 2015). Structurally, METTL3 and METTL14 both contain a highly similar MTase region, but, within the METTL3/METTL14 catalytic complex, the S-Adenosyl methionine (SAM) cofactor only binds and transfers the methyl group to METTL3 changing SAM to S-Adenosyl-L-Homocysteine (SAH) (Śledź and Jinek, 2016; Wang, Doxtader and Nam, 2016; Wang *et al.*, 2016). METTL14 was found to have a degenerative active site that is unable to accept or donate methyl groups and therefore is catalytically inactive (Śledź and Jinek, 2016; Wang, Doxtader and Nam, 2016). However, the structural role that METTL14 provides is essential for METTL3 catalytic activity, requiring METTL3 and METTL14 to form a stoichiometric complex at a 1:1 ratio (Śledź and Jinek, 2016; Wang, Doxtader and Nam, 2016).

The METTL3/METTL14 heterodimer functions in conjunction with a regulatory protein complex that includes Wilms' tumour 1-associating protein (WTAP), RNA binding motif protein 15 (RBM15) / RNA binding motif protein 15B (RBM15B), Vir- like m^6A methyltransferase associated (VIRMA or KIAA1429), zinc finger CCCH-type containing 13 (ZC3H13) and Casitas B-lineage lymphoma-transforming sequence-like protein 1 (CBLL1 or E3 ubiquitin-protein ligase Hakai) (Knuckles *et al.*, 2018) (Fig. 1.2). Although this regulatory protein complex does not possess the catalytic methyltransferase activity, it can guide the METTL3/METTL14 heterodimer to specific RNA sites within nuclear speckles for methylation of RNAs (Lee *et al.*, 2020). WTAP initially was shown to interact with Wilm's tumour 1 protein as a splicing factor as well as play a regulatory role in early embryo development and cell cycle progression (Little, Hastie and Davies, 2000; Horiuchi *et al.*, 2006, 2013). With m^6A, WTAP interacts with the METTL3/METTL14 heterodimer to promote the localisation of the complex to nuclear speckles and methylate specific mRNA targets (Ping *et al.*, 2014). RBM15 and its paralog RBM15B are dependent on WTAP to target the METTL3/METTL14 complex to U-rich sequences proximal to the m^6A consensus motif (Patil *et al.*, 2016; Knuckles *et al.*, 2018). In mouse embryonic stem cells, ZC3H13 is necessary for nuclear localisation of the ZC3H13-WTAP-VIRMA-CBLL1 complex, as well as enabling efficient methylation by acting as an adaptor protein between WTAP and RBM15 (Knuckles *et al.*, 2018; Wen *et al.*, 2018). VIRMA or KIAA1429 was reported to recruit and guide the METTL3/METTL14/WTAP complex towards 3'UTR and stop codons at selected m^6A methylation sites (Schwartz *et al.*, 2014; Yue *et al.*, 2018). CBLL1 or HAKAI is found to have strong interactions with VIRMA, ZC3H13, WTAP and RBM15 as well as share many common targets with WTAP, but its role within the m^6A methyltransferase complex remains elusive (Horiuchi *et al.*, 2013; Knuckles *et al.*, 2018; Wen *et al.*, 2018; Yue *et al.*, 2018).

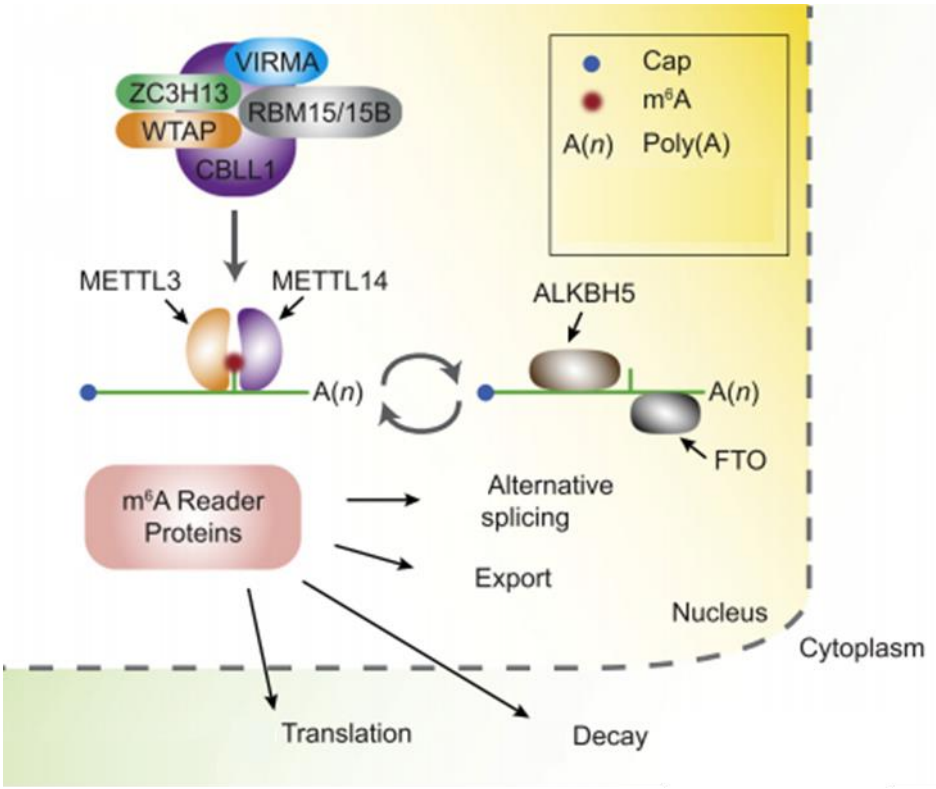


Figure 1.2: The dynamic methylation and demethylation of m^{6}A.

METTL3 and METTL14 form the main catalytic complex introducing m^{6}A to RNA transcripts and a regulatory protein complex comprising of WTAP, RBM15, VIRMA, ZC3H13 and CBLL1 localises to specific regions with nascent transcripts. Numerous m^{6}A readers determine the functional role of m^{6}A-containing RNAs within alternative splicing, nuclear export, decay and translation. Adapted from (Lee *et al.*, 2020).

Methyltransferase like 16 (METTL16) has also been identified as m^{6}A methyltransferase acting on U6 spliceosomal snRNA (Pendleton *et al.*, 2017; Shima *et al.*, 2017). METTL16 regulates the gene expression for a SAM synthase known as methionine adenosyltransferase 2A (*MAT2A*) therefore regulating SAM homeostasis (Pendleton *et al.*, 2017; Shima *et al.*, 2017; Doxtader *et al.*, 2018). Furthermore, METTL16 has been found to methylate lincRNA metastasis associated lung adenocarcinoma transcript 1 (*MALAT1*) as well as multiple precursor mRNAs (pre-mRNAs) (Brown *et al.*, 2016; Warda *et al.*, 2017). Unlike METTL3 which recognises the DRACH consensus motif, METTL16 requires a specific stem-loop structure and a longer UACAGAGAA sequence for methylation (Pendleton *et al.*, 2017; Shima *et al.*, 2017; Warda *et al.*, 2017).

1.2.2 Erasers of m^{6}A

The removal of m^{6}A from mRNA transcripts has been described as a reversible post-transcriptional modification mediated by Fat mass and obesity-associated protein (FTO) and α-ketoglutarate-dependent dioxygenase alkB homolog 5 (ALKBH5) (Fig. 1.2) (Jia *et al.*, 2011; Zheng *et al.*, 2013). FTO was first reported in 2007 to be associated with elevated body mass and obesity in humans (Dina *et al.*, 2007; Frayling *et al.*, 2007; Scuteri *et al.*, 2007; Zhao *et al.*, 2014). FTO was then observed to demethylate m^{6}A in both RNA and DNA (Jia *et al.*, 2011; Fu *et al.*, 2013). This enzyme is suggested to oxidise m^{6}A to return to unmodified adenosine creating intermediate products like N6-hydroxymethyladenosine and further oxidised products like N6-formyladenosine that functions are yet to be explored (Jia *et al.*, 2011; Fu *et al.*, 2013). The current perception is that FTO demethylates a broad spectrum of RNA modifications including m^{6}Am in mRNA and m^{1}A in tRNA, rather than targeting m^{6}A demethylation specifically (Mauer *et al.*, 2017; J. Wei *et al.*, 2018). ALKBH5 is another identified m^{6}A demethylase that favourably demethylates m^{6}A in a DRACH consensus motif-dependent manner suggesting that it could play a larger global role in m^{6}A demethylation compared with FTO (Zheng *et al.*, 2013; Lee *et al.*, 2020).

1.2.3 m^{6}A readers

The m^{6}A mRNA modification is interpreted by reader proteins within the cell. Proteins interacting with m^{6}A are present both within the nucleus and in the cytoplasm playing a variety of roles including modulating the mRNAs localisation as well as, their processing, translation and decay (Fig. 1.4) (Liu and Pan, 2016; Nachtergaele and He, 2017; Roundtree *et al.*, 2017; Zhao *et al.*, 2017).

YTH domain containing protein 1 (YTHDC1) is widely distributed in the nucleus where it recognises and binds to GG(m^{6}A)CU sequences in RNA transcripts (Xu *et al.*, 2014; Y. Li *et al.*, 2019). YTHDC1 is mainly known for its role in alternative splicing by recruiting serine and arginine rich splicing factor 3 (SRSF3) and blocking mRNA binding of serine and arginine rich splicing factor 10 (SRSF10) to promote exon inclusion (Xiao *et al.*, 2016). Other roles of YTHDC1 include facilitating the nuclear export of m^{6}A-methylated RNAs; promoting the

transcriptional silencing of X chromosome genes and the maintenance of intracellular levels of SAM that could regulate m^{6}A methylation levels (Patil *et al.*, 2016; Roundtree *et al.*, 2017; Shima *et al.*, 2017). YTH domain containing protein 2 (YTHDC2) is an acknowledged RNA helicase that contains the YTH domain, R3H domain, helicase domain and ankyrin repeats and is suggested to promote translation elongation of mRNAs (Hsu *et al.*, 2017; Mao *et al.*, 2019).

YTH N6-methyladenosine RNA binding protein 1 (YTHDF1) is a cytoplasmic m^{6}A reader that interacts with eukaryotic initiation factor 3 (eIF3) enhancing the translation efficiency of its target RNAs (X. Wang et al., 2015). YTH N6-methyladenosine RNA binding protein 2 (YTHDF2) is involved in augmenting mRNA degradation by reducing the stability of m^{6}A marked RNA transcripts, recruiting the carbon catabolite repression 4 — negative on TATA-less (CCR4-NOT) multiprotein complex and directing m^{6}A marked RNA targets towards processing bodies (X. Wang et al., 2014; Du et al., 2016). YTH N6-methyladenosine RNA binding protein 3 (YTHDF3) cooperates with YTHDF1 to regulate mRNA translation and supports YTHDF2 in mRNA decay sharing a substantial number of common targets with both YTHDF1 and YTHDF2 (A. Li *et al.*, 2017; Shi *et al.*, 2017).

HNRNP protein family members such as heterogeneous nuclear ribonucleoproteins A2/B1 (HNRNPA2B1) and heterogeneous nuclear ribonucleoproteins C (HNRNPC) have also been proposed to interact with m^{6}A marked mRNA and ncRNAs (Meyer *et al.*, 2012; Meyer and Jaffrey, 2014). It was initially thought that the nuclear protein HNRNPA2B1 binds and regulates alternative splicing as well as accelerates the processing of primary-miRNA via interaction with METTL3, microprocessor complex DiGeorge syndrome critical region 8 protein (DGCR8) and Drosha Ribonuclease III (DROSHA) (C. Alarcón *et al.*, 2015; C. R. Alarcón *et al.*, 2015). HNRNPC has been found to have an important role in the processing of pre-mRNAs (McCloskey *et al.*, 2012; Zarnack *et al.*, 2013). Intriguingly, the current consensus from various approaches is that, unlike other m^{6}A readers, HNRNPA2B1 and HNRNPC do not bind directly to m^{6}A (Liu *et al.*, 2015; Wu *et al.*, 2018). Instead, HNNRP proteins rely on a mechanism known as the “m^{6}A switch” mechanism (Fig. 1.3) (Liu *et al.*, 2015; Wu *et al.*, 2018).

The presence of m^{6}A on mRNA and lincRNA promotes their local unfolding as the base pairing between U and m^{6}A is weaker than that between U and A (Roost *et al.*, 2015).

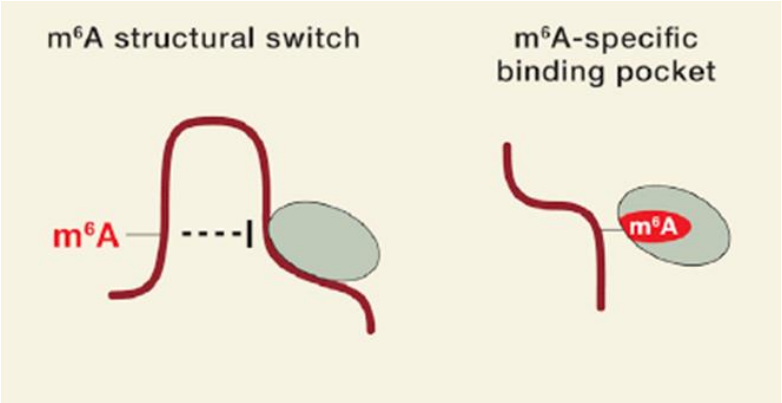


Figure 1.3: Types of direct and indirect binding mechanisms for m^{6}A reader proteins.

Comparing the different mechanisms in which m^{6}A readers can interact with m^{6}A either directly via m6A-specific binding sites or indirectly via m^{6}A promoted structural remodelling of the RNA to reveal a binding site. Figure adapted from (Roundtree *et al.*, 2017).

And finally, insulin-like growth factor-2 mRNA-binding proteins (IGF2BP) consist of two RNA recognition motif (RRM) binding domains and four K homology (KH) domains in which only KH3 and KH4 domains are capable of binding to m^{6}A sites on RNA (Bell *et al.*, 2013; Huang *et al.*, 2018). IGF2BP1-3 are proposed to strengthen the stability of m^{6}A-marked transcripts and promote their translation (Bell *et al.*, 2013; Huang *et al.*, 2018).

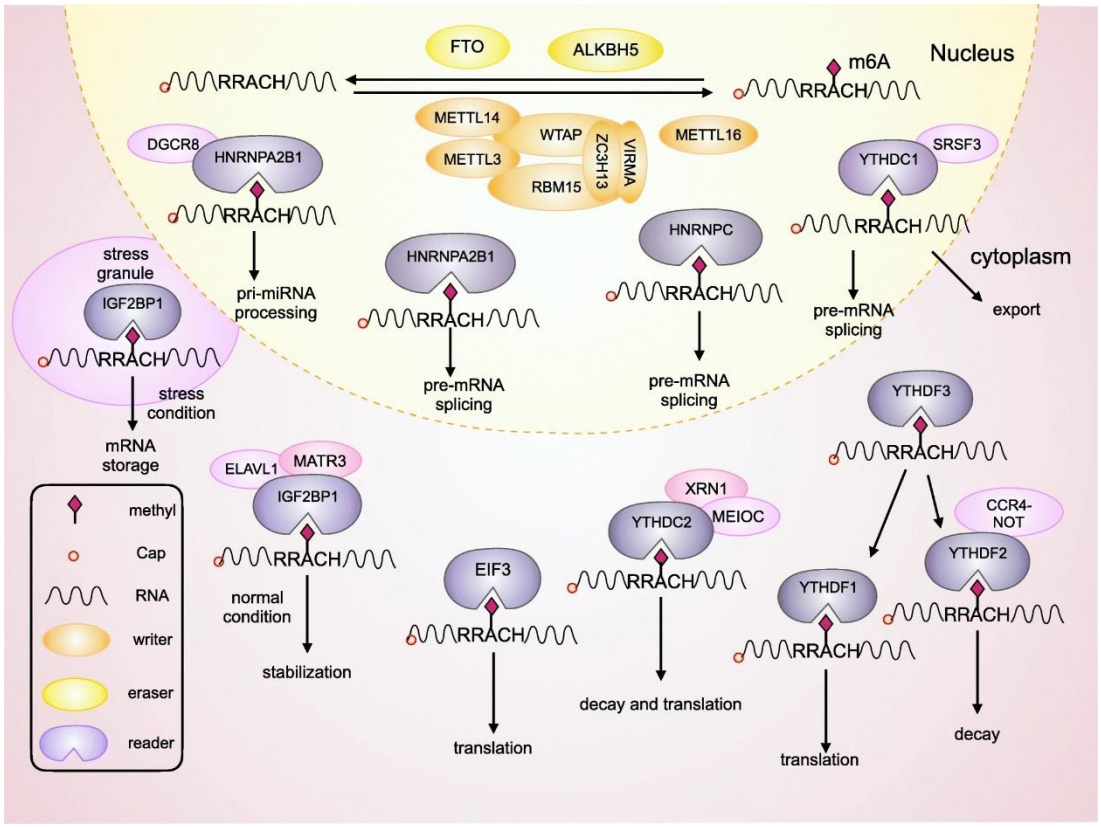


Figure 1.4: Overview of m^{6}A reader proteins impact on mRNA functions.

The fate of m^{6}A marked RNA with m^{6}A readers both within the nuclear and cytoplasmic leads to implications in mRNA stability, alternative splicing, nuclear export, decay and translation. Taken from (He *et al.*, 2019).

1.2.4 Relevance of m^{6}A to cancer

Recent scientific advances have allowed the study of epitranscriptomic modifications such as m^{6}A within various tumours including acute myeloid leukaemia (Z Li *et al.*, 2017; Weng *et al.*, 2018), breast cancer (Cai et al., 2018; L. Wu et al., 2019; Wang, Xu and Shi, 2020), glioblastoma multiforme (Golan-Gerstl et al., 2011; Deng et al., 2016; Cui et al., 2017; Zhang et al., 2017; Visvanathan et al., 2018; C. Xu et al., 2020; L. Wang et al., 2020; Dixit et al., 2021), hepatocellular carcinoma (M. Chen *et al.*, 2017; Zhong *et al.*, 2019), lung cancer (J. Li *et al.*, 2019), pancreatic cancer (J. Chen *et al.*, 2017; Taketo *et al.*, 2017; Y. He *et al.*, 2018; Kong *et al.*, 2020), colorectal cancer (Deng *et al.*, 2019; Peng *et al.*, 2019; T. Li *et al.*, 2019) and renal clear cell carcinoma (X. Li *et al.*, 2017; Zhuang *et al.*, 2019). However, dependent

upon the tumour, m^{6}A can possess either an oncogenic role or a tumour suppressant role (Yang, Sun and Zhang, 2020). In this section, we will focus on the three types of tumours in which m^{6}A has been extensively researched and studied: acute myeloid leukaemia (AML), breast cancer (BC) and glioblastoma multiforme (GBM).

1.2.4.1 Acute myeloid leukaemia (AML)

AML is an aggressive cancer with a poor prognosis where m^{6}A writers, erasers and readers have been investigated for their role and as potential therapeutic targets. METTL3 acts as an oncogene and plays a vital role in AML pathogenesis (Barbieri *et al.*, 2017; Vu *et al.*, 2017). METTL3 was found to be essential for the growth of AML cells, with its depletion leading to cell cycle arrest, inducing cell differentiation, apoptosis and failure to establish leukaemia in immunodeficient mice (Barbieri *et al.*, 2017; Vu *et al.*, 2017). Molecularly, METTL3 methylated BCL2 apoptosis regulator (*BCL2*) and MYC proto-oncogene, BHLH transcription factor (*MYC*) mRNAs promote translation of these transcripts critical for regulating apoptosis and differentiation in AML cell lines (Vu *et al.*, 2017). Recruitment of METTL3 by CCAAT enhancer binding protein zeta (CEBPZ) to chromatin results in induction of m^{6}A deposition at transcription start sites (TSS) of active genes within AML including Sp1 transcription factor (*SP1*) and Sp2 transcription factor (*SP2*) (Barbieri *et al.*, 2017). The addition of m^{6}A by METTL3 in a CEBPZ-dependent manner enhances the translation of these transcripts by relieving ribosome stalling (Barbieri *et al.*, 2017). Recent work has been focussing on the potential of inhibiting METTL3 in AML via the treatment of these tumours with a METTL3 inhibitor known as STM2457 (Yankova *et al.*, 2021). It was identified that STM2457 was capable of catalytically inhibiting METTL3 in AML cells leading to reduced AML growth as well as an increase in differentiation of leukemic cells and apoptosis (Yankova *et al.*, 2021). This METTL3 inhibitor is now progressed into clinical trials phase 1, with the hope that it can be used in combination with other chemotherapy agents. METTL14 was found to be highly expressed in haematopoietic stem and progenitor cells (HSPCs), and depletion of this factor resulted in METTL3-dependent promotion of terminal myeloid differentiation (Yao *et al.*, 2018). METTL14 was observed to be upregulated in AML carrying cytogenetic abnormalities such as t(11q23). t(15;17) or t(8:21) (Weng *et al.*, 2018). Depletion of METTL14 promoted terminal

myeloid differentiation of AML cells and inhibited AML cell proliferation (Weng et al., 2018). WTAP has an oncogenic role in leukemogenesis where its expression positively correlates with anti-apoptotic proteins, stem cell-, cell and proliferation-related proteins (Bansal *et al.*, 2014). RBM15 has been linked to a rare form of AML, acute megakaryoblastic leukaemia (AKML), common in children and infants and produced by the fusion of the *RBM15* gene and megakaryoblastic leukemic-1 (*MKL1*) gene via the translocation of t(1;22)(p13.3; q13.1) resulting in recurrent aberrations (Wiseman, Bonney and Wynn, 2012).

ALKBH5 has not been as extensively studied in AML as another m^6A eraser, FTO. Yet recently, ALKBH5 expression has been correlated with poor prognosis in AML patients, with ALKBH5 selectively promoting leukemogenesis and regulating self-renewal of leukaemia stem cells (J. Wang *et al.*, 2020; Shen *et al.*, 2020), whereas, single nucleotide polymorphisms (SNPs) of FTO have been strongly linked to increased risk of malignancies including various types of blood cancers (Deng *et al.*, 2018). FTO acts as an oncogenic protein in AML promoting AML cell growth, self-renewal and metastasis of AML cells as well as regulating leukemic stem cell functions (Zejuan Li *et al.*, 2017; Chen and Du, 2019). Specifically, FTO was observed to demethylate ankyrin repeat and SOCS box containing 2 (*ASB2*) and retinoic acid receptor-alpha (*RARα*) transcripts leading to elevated leukemogenesis and inhibited all-trans-retinoic acid (ATAR) induced cell differentiation in AML (Zejuan Li *et al.*, 2017).

Readers of m^6A such as YTHDF2 and the IGF2BP proteins have been associated with AML and other haematological malignancies. YTHDF2 was observed to be upregulated in AML with depletion of this factor resulting in hindered propagation of leukemic stem cells and enhanced myeloid reconstitution in haematopoietic stem cells (Paris *et al.*, 2019). IGF2BP1 was found to be upregulated in AML with low expression in AML patients associated with better survival, and depletion of IGF2BP1 reducing cell proliferation (Zhou *et al.*, 2017; Elcheva *et al.*, 2020). IGF2BP2 is overexpressed in AML patients with its knockdown inhibiting cell growth of these tumours (X. He *et al.*, 2018). IGF2BP2 expression has been associated with poor prognostic indicators such as mutations in Isocitrate Dehydrogenase (NADP(+)) 1 (*IDH1*) and Fms-related receptor tyrosine kinase 3 (*FLT3*) – internal tandem duplication (ITD) and negatively correlated with good prognostic CCAAT enhancer-binding protein alpha

(*CEBPA*) mutation status (X. He *et al.*, 2018). IGF2BP3 affected the stability of prostaglandin-endoperoxide synthase 2 (*COX2* or *PTGS2*) mRNA by binding to the 3'UTR region leading to inhibition of apoptosis in AML cells (Ko *et al.*, 2016; Carter *et al.*, 2019).

1.2.4.2 Breast cancer (BC)

In BC, m^6A and its writers, readers and erasers can benefit or disrupt key cancer hallmarks such as cell proliferation, apoptosis, migration, invasion and metastasis (Fig. 1.5) (Hanahan and Weinberg, 2000, 2011). METTL3 was found to be upregulated in BC tissues and cell lines (Wang, Xu and Shi, 2020). Knockdown of METTL3 led to the acceleration of apoptosis, reduced methylation and proliferation as well as inhibition of tumour growth by targeting m^6A sites present on *BCL2* mRNA transcripts (Wang, Xu and Shi, 2020). Additionally, METTL3 was found to be a part of a positive feedback loop with hepatitis B X-interacting protein (HBXIP), which is linked to increased aggressiveness of BC (Cai *et al.*, 2018). By HBXIP suppressing miRNA let-7g that would normally target the 3'UTR region of METTL3 and downregulate, this action allows an increase in METTL3 expression that upregulates HBXIP in the form of a positive feedback loop HBXIP/let-7G/METTL3/HBXIP axis, enhancing BC cell proliferation (Cai *et al.*, 2018). METTL14 was similarly found to be significantly upregulated in BC tissues compared to non-cancerous breast tissues (Yi *et al.*, 2020). LincRNA-942 functions as an oncogene via recruiting the methyltransferase complex by METTL14 to target m^6A methylation on C-X-C motif chemokine receptor 4 (*CXCR4*) and cytochrome P450 family 1 subfamily B member 1 (*CYP1B1*) leading to increased proliferation, colony formation and suppression of apoptosis in BC cells (Sun *et al.*, 2020). METTL14 was found to modulate the expression of tumour suppressor miRNA, hsa-miR-146a-5p, via the m^6A modification and, subsequently, promote migration and invasion of BC cells (Hsieh et al., 2013; C. Wang et al., 2018; G. Wei et al., 2018; Yi et al., 2020). Another m^6A writer, KIAA1429 or VIRMA, functions as an oncogene in BC with high expression observed in BCs but is downregulated in non-tumorigenic breast tissues (Qian *et al.*, 2019). High KIAA1429 expression was linked to a significantly shorter overall patient survival time, high BC cell proliferation, colony formation by stabilising cyclin-dependent kinase 1 (*CDK1*) mRNA and metastasis compared to those with low KIAA1429 expression (Qian *et al.*, 2019).

m^{6}A erasers FTO and ALKBH5 have also been associated with BC tumour progression and metastasis. FTO is suggested to demethylate 3'UTR of BCL2 interacting protein 3 (*BNIP3*) mRNA and induce decay mediated by YTHDF2 leading to BC cell proliferation, colony formation and metastasis (Niu *et al.*, 2019). ALKBH5 was found to be stimulated by hypoxia to stabilise Nanog Homeobox (*NANOG*) and Kruppel-like factor 4 (*KLF4*) mRNAs inducing a similar phenotype observed in BC stem cells and BC metastasis (Chuanzhao Zhang *et al.*, 2016; C Zhang *et al.*, 2016). HNRNPA2B1 is found to be overexpressed in BC tissues and cell lines where its knockdown inhibits Signal Transducer and Activator of Transcription 3 (STAT3) and activates extracellular signal-regulated protein kinase 1/2 (ERK1/2) leading to the prolongation of the S phase *in vitro*, reduced BC cell proliferation and induced apoptosis (Hu et al., 2017; Y. Liu et al., 2020). Epithelial-to-mesenchymal transition (EMT) is known to accelerate the progression of tumour metastasis (Yang *et al.*, 2020). HNRNPA2B1 is found to inhibit EMT and metastasis in BC by binding to a specific locus, UAGGG, within the 3'UTR on Profilin 2 (*PFN2*) mRNA, where it reduces its stability, interfering with PFN2 promotion of BC cell migration and invasion (Y. Liu et al., 2020). However, there is no indication that HNRNPA2B1 binding to *PFN2* mRNA was m^{6}A-dependent. IGF2BP2 was found to regulate BC stemness by binding to lincRNA FGF13-AS1 and c-Myc forming a positive feedback loop, whereas a subunit of eIF3 was found to interact with heterogeneous nuclear ribonucleoprotein U (HNRNPU), HS2FP36 and β-Actin to promote metastasis of BC cells within the lymph nodes (Zheng *et al.*, 2016; Ma *et al.*, 2019).

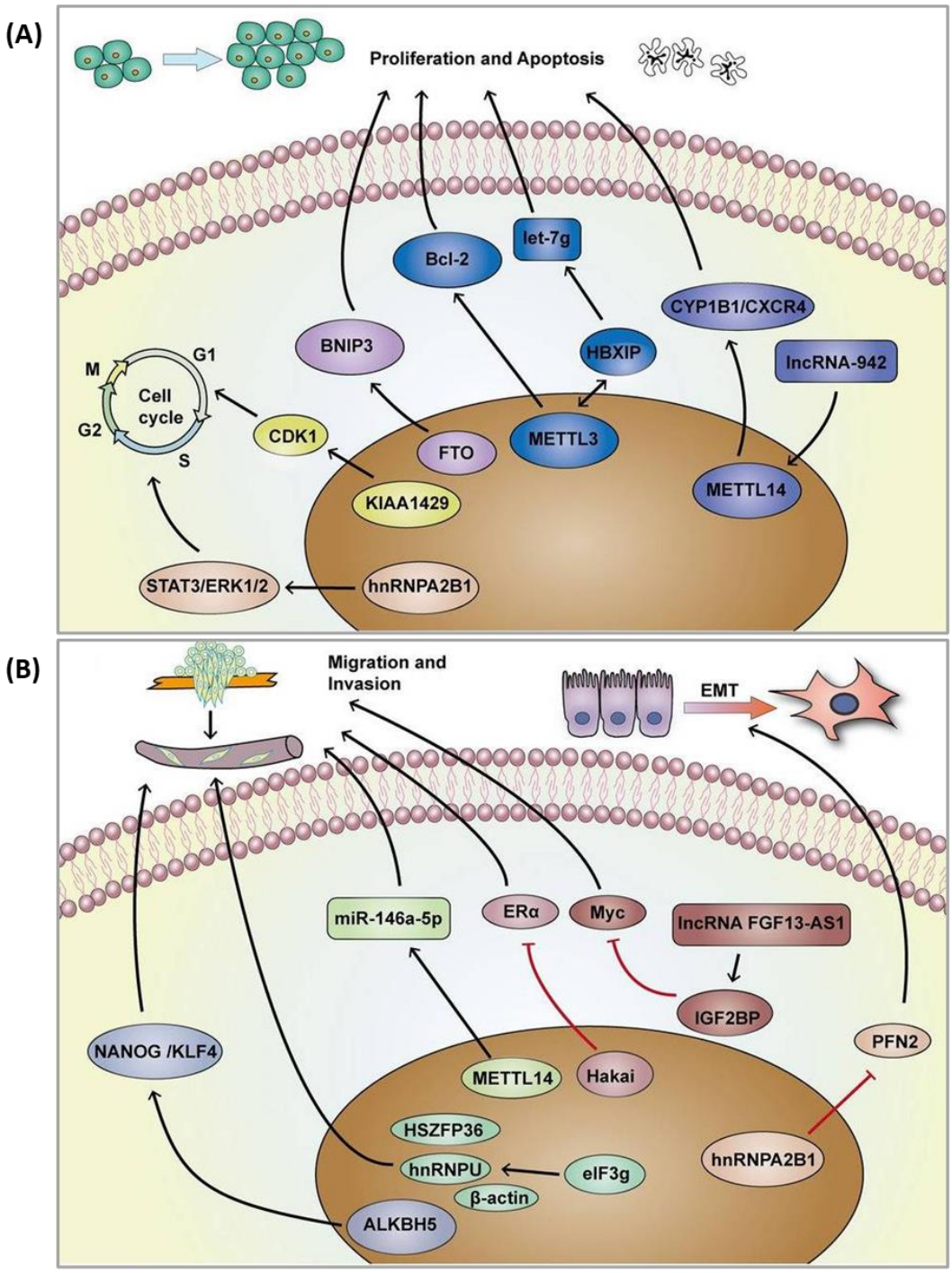


Figure 1.5: Molecular mechanisms involving the m^{6}A modification in breast cancer.

Summary of the current mechanisms where m^{6}A-related proteins have been identified to suppress apoptosis and induce proliferation, migration, invasion and metastasis. Adapted from (Y. Wang *et al.*, 2020).

1.2.4.3 Glioblastoma multiforme (GBM)

In GBM, the recurrence of the tumour may be due to the presence of glioblastoma stem cells (GSCs) (Singh et al., 2004; Yan, Yang and Rich, 2013; A. K. Singh et al., 2015; Jackson, Hassiotou and Nowak, 2015; Safa et al., 2015; Taga and Tabu, 2020; Vieira de Castro et al., 2020). With this, researchers focussed on m^{6}A 'writer' genes and whether the expression of these genes impacted the presence of GSCs. Thus, silencing of *METTL3* and *METTL14* by small hairpin RNAs (shRNAs) within primary GSCs enhanced relative growth and sphere formation by these cells, *in vitro* (Cui *et al.*, 2017). Furthermore, the combined knockdown of *METTL3* and *METTL14* in murine xenografted GSCs caused enlarged tumour formation *in vivo* (Cui *et al.*, 2017). In line with the m^{6}A writers, a proposed m^{6}A eraser *ALKBH5* is overexpressed in GSCs and was found to be associated with increased proliferation and tumorigenesis (Zhang *et al.*, 2017). Another study showed that increases in m^{6}A levels and *METTL3* were responsible for the GSC progression suggesting a tumour suppressor role (Visvanathan *et al.*, 2018), contrasting with other publications that proposed an oncogenic role for increased m^{6}A and METTL3 levels (Cui *et al.*, 2017; Zhang *et al.*, 2017). Furthermore, when *METTL3* is silenced in GSCs, SRY (sex-determining region Y)-box 2 (*SOX2)* transcript and protein levels were both downregulated, suggesting a positive correlation between *METTL3* and *SOX2* in GSCs (Visvanathan *et al.*, 2018). This was supported by looking at four GBM transcriptome datasets which also corroborated that METTL3 and SOX2 have a high binding affinity to each other (Visvanathan *et al.*, 2018).

Readers of m^{6}A, YTHDF1 and HNRNPC are found to be upregulated within glioma patients as well as in GBM cell lines including, U87 and SHG-44 (C. Xu et al., 2020). Utilising silencing and overexpression techniques in U87 and SHG-44 cells, YTHDF1 was found to promote the proliferation of these cells (C. Xu et al., 2020). Using TCGA datasets to compare normal brain and GBM tissues, Wang found that the majority of m^{6}A-related genes; *METTL3*, *WTAP*, *VIRMA*, *ZCH3H13*, *YTHDC1*, *YTHDF1*, *YTHDF2*, *HNRNPC*, *FTO* and *ALKBH5* displayed differential expression between GBM patient tissue and normal brain tissue (L. Wang *et al.*, 2020). On the GEPIA web server, which incorporates over 9,736 GBM tumours and 8657 normal brain samples from the TCGA and GTEx projects, only YTHDF1, YTHDF2, WTAP and

HNRNPC have significantly elevated expression in GBM tumour samples (L. Wang *et al.*, 2020). Additionally, Wang identified a correlation between HNRNPC presence and GBM progression/development (L. Wang *et al.*, 2020). Moreover, YTHDF2 was shown to stabilise oncogenic drivers *MYC* and Vascular endothelial growth factor receptor A (*VEGFRA)* transcripts in GSCs in an m^6A-dependent manner (Dixit *et al.*, 2021).

1.3 DNA:RNA hybrids

DNA:RNA hybrids or R-loops are nucleic acid structures formed when a nascent G-rich RNA strand or transcript hybridises with the DNA template strand, leaving a displaced non-template DNA strand (Thomas, White and Davis, 1976; Aguilera and García-Muse, 2012) (Fig. 1.6). DNA:RNA hybrid only refers to the double structure with RNA annealing to the template DNA, whereas the term R-loop denotes the three-stranded structure formed by the DNA:RNA hybrid and the single-stranded DNA (ssDNA) with both terms commonly interchanged.

1.3.1 Formation and removal of DNA:RNA hybrids

The formation of DNA:RNA hybrids is more thermodynamically stable than that of dsDNA interactions (Roberts and Crothers, 1992). A possible reason for this more stable interaction for DNA:RNA hybrids could be due to the preference for R-loops to form when the non-template DNA strand is G-rich, as G-rich RNA when bound to a C-rich DNA template strand has increased thermodynamic stability (Sugimoto *et al.*, 1995). For a DNA:RNA hybrid to form in the genome, it is reliant on three features: DNA nicks, high G density and negative supercoiling (Roy *et al.*, 2010). DNA:RNA hybrids typically range between lengths of 200-500 base pairs but have been observed to reach kilo-bases in length (Yu *et al.*, 2003; Huang *et al.*, 2006, 2007; Kao *et al.*, 2013; Kouzine *et al.*, 2017; Malig *et al.*, 2020). Surprisingly, DNA:RNA hybrids were found to occupy approximately 5% of the human genome with their accumulation preferentially observed in highly transcribed genes, rRNA and tRNA loci, transposable elements, centromeres, telomeres, ncRNA regions and anti-sense RNAs (Ginno et al., 2012; Chan et al., 2014; el Hage et al., 2014; Sanz et al., 2016; Wahba et al., 2016; L. Chen et al., 2017). Within these highly active genes, DNA:RNA hybrids tend to occur and accumulate at promoter and terminator regions within sequences prone either to CpG islands,

GC-rich sequences, G-quadruplex (G4)-containing sequences or transcription termination sites with high GC-skew (Ginno *et al.*, 2012; Sanz *et al.*, 2016; Stork *et al.*, 2016; L. Chen *et al.*, 2017). It was initially assumed that DNA:RNA hybrids are predominantly formed as by-products of transcription, however, it appears that R-loops formation is not exclusive to transcription and these structures are also able to form at distinct sites separate from transcription *in trans* (Aguilera and García-Muse, 2012; Wahba *et al.*, 2016).

DNA:RNA hybrids can be detected using anti-DNA:RNA hybrid antibody (clone S9.6), the fusion of Green fluorescent protein (GFP) to the hybrid-binding domain of RNase H or by an inactive RNase H (Boguslawski *et al.*, 1986; Ginno *et al.*, 2012; Bhatia *et al.*, 2014; L. Chen *et al.*, 2017) (Fig. 1.6), whereas R-loops can be detected by the identification of the displaced ssDNA indirectly via the mutagenesis of sodium bisulfite-induced deamination of cytidines in the ssDNA that can provide a size of the DNA:RNA hybrid when sequenced (Yu *et al.*, 2003). Interestingly, human activation-induced cytidine deaminase (hAID) works comparably to this method but is not as processive as bisulfite in converting all the cytidines to thymines (Gomez-Gonzalez and Aguilera, 2007; Garcia-Pichardo *et al.*, 2017).

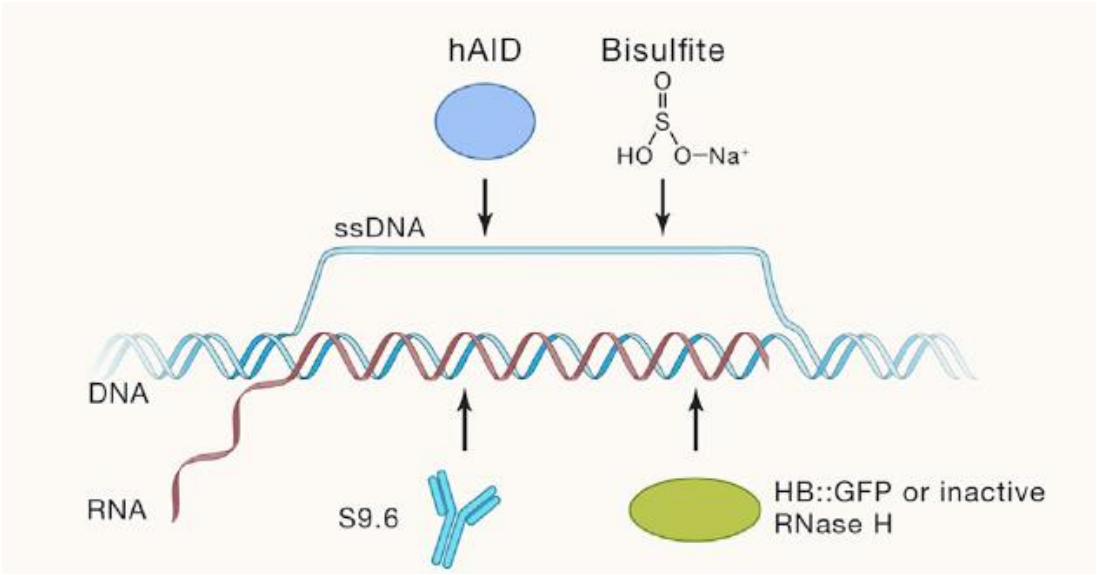


Figure 1.6: Structure of DNA:RNA hybrid and their methods of detection.

Adapted from (García-Muse and Aguilera, 2019).

In different organisms from bacteria to humans, there are highly conserved mechanisms in place to remove DNA:RNA hybrids from the genome (Cerritelli and Crouch, 2009). Ribonuclease H (RNase H) enzymes are non-sequence specific endonucleases which degrade exclusively the RNA which is annealed to template DNA within DNA:RNA hybrids (Cerritelli and Crouch, 2009). In eukaryotes, there are two types of RNase H enzymes. RNase H1 is monomeric and requires a sequence of at least 4 ribonucleotides to hydrolytically cleave RNA from the DNA:RNA hybrid (Cerritelli and Crouch, 2009). While RNase H2 is a heterotrimeric protein with one catalytic subunit and two others required for other enzymatic activities resulting in RNase H2's capability to cleave single ribonucleotides incorporated in the DNA (Cerritelli and Crouch, 2009). Both RNase H proteins can cleave and remove DNA:RNA hybrids from the genome as well as have different specialised roles depending on where the R-loop is located in the genome (Cerritelli *et al.*, 2003; Wahba *et al.*, 2011; Reijns *et al.*, 2012; Stirling *et al.*, 2012; Chan *et al.*, 2014; el Hage *et al.*, 2014; Skourti-Stathaki and Proudfoot, 2014; Boque-Sastre *et al.*, 2015). An alternative pathway that is utilised by the cells is removing DNA:RNA hybrids from the genome with help of DNA-RNA helicases, such as Rho factor, senataxin and DExH-Box Helicase (DHX9) that unwind DNA:RNA hybrids and can limit DNA:RNA hybrid formation (Richardson, 2003; Chakraborty and Grosse, 2011; Mischo *et al.*, 2011; Cristini *et al.*, 2018).

1.3.2 Roles and functions of DNA:RNA hybrids

DNA:RNA hybrids have been attributed to play both beneficial and detrimental roles within the genome, with studies observing their functions in class switch recombination, modulating DNA repair, genome stability, telomere dynamics and regulating gene expression (Yu *et al.*, 2003; Li and Manley, 2005; Ginno *et al.*, 2012; Balk *et al.*, 2013; Hamperl *et al.*, 2017; Yasuhara *et al.*, 2018).

1.3.2.1 Class switch recombination

Class switch recombination (CSR) is the change of immunoglobulin isotype within the immunoglobulin genes from the constant μ region (corresponding to IgM) to other isotypes such as γ (IgG), α (IgA) and ε (IgE) in activated B cells (Stavnezer, Guikema and Schrader,

2008). CSR requires regions known as ‘switch regions’ to have no identifiable consensus sequence, yet produce GC-rich non-protein coding RNA transcripts that allow for CSR to take place (Stavnezer, Guikema and Schrader, 2008). In 2003, it was first found that these GC-rich RNA transcripts could lead to the formation of 1 kilobase long stable DNA:RNA hybrid (Yu *et al.*, 2003). It was proposed that the DNA:RNA hybrid formation in the ‘switch region’ provided the ssDNA structure available for activation-induced cytidine deaminase (AID) to convert cytosine to uracil which created a DNA nick within the ssDNA processed by the base excision repair (BER) machinery (Yu *et al.*, 2003). Subsequently, DNA mismatch repair and end-joining DNA repair recognise and repair resulting in the Ig class switch (Yu *et al.*, 2003; Huang *et al.*, 2006, 2007). Further work has identified that the activated B cell must be entering the S phase and exhibiting active DNA replication for efficient CSR (Wiedemann, Peycheva and Pavri, 2016).

1.3.2.2 Telomere modulation

DNA:RNA hybrids are found to form in telomeres, specifically where non-coding (TERRA) hybridises onto telomeric DNA (Luke *et al.*, 2008; Balk *et al.*, 2013). It was found that loss of telomerase enzyme within cells allowed the formation of DNA:RNA hybrids resulting in delays of cell senescence as well as mediating telomere elongation (Luke *et al.*, 2008; Balk *et al.*, 2013; Arora *et al.*, 2014).

1.3.2.3 Gene expression

Presence of DNA:RNA hybrids can have both a positive and negative outcome on gene expression dependent on the location of the R-loop within the gene. For instance, positioning the DNA:RNA hybrid at the 3’ end of mammalian genes can stall RNA polymerase (RNAP) by recruiting senataxin helicase, which in turn, recruits 5'-3' exoribonuclease 2 (XRN2), promoting the termination of transcription (Skourti-Stathaki, Proudfoot and Gromak, 2011; Ginno *et al.*, 2012; Skourti-Stathaki and Proudfoot, 2014; Nadel *et al.*, 2015; Morales *et al.*, 2016; Sanz *et al.*, 2016; Yanling Zhao *et al.*, 2016; Dumelie and Jaffrey, 2017; L. Chen *et al.*, 2017). Conversely, DNA:RNA hybrids located upstream from promoter sequences can block transcription starting as well as hinder the binding of transcription factors (Boque-Sastre *et al.*,

2015; Bonnet *et al.*, 2017; Hamperl *et al.*, 2017; Lang *et al.*, 2017). Additionally, DNA:RNA hybrids can impact gene expression at an epigenetic level since DNA methyltransferases DNMT will bind poorly with DNA:RNA hybrids, therefore R-loops may protect CpG islands located within promoter regions from methylation (Ginno *et al.*, 2012; Grunseich *et al.*, 2018).

1.3.2.4 DNA repair

Understanding the role of DNA:RNA hybrids in DNA repair is still in its infancy, but several studies have suggested that reduced levels of R-loops can impact the efficiency of homologous recombination and non-homologous end-joining repair (Ohle *et al.*, 2016; Lu *et al.*, 2018; Yasuhara *et al.*, 2018). The presence of a DNA:RNA hybrid promotes the recruitment of nucleotide excision repair (NER) factors, which in turn, recruit RAD52 homolog DNA repair protein (RAD52) (Teng *et al.*, 2018; Yasuhara *et al.*, 2018). RAD52 has been shown to promote homologous recombination at sites of DNA damage caused by reactive oxygen species (ROS) (Keskin *et al.*, 2014; Mazina *et al.*, 2017; Teng *et al.*, 2018).

1.3.2.5 DNA damage

It has been observed that the presence of DNA:RNA hybrids can lead to DNA damage and eventually genomic instability which have been associated in pre-mRNA splicing, biogenesis and export of messenger ribonucleoprotein (mRNP) complexes (Huertas and Aguilera, 2003; Li and Manley, 2005; Paulsen *et al.*, 2009). Initially, researchers theorised that this DNA damage could be due to the R-loop structure containing a displaced ssDNA which is vulnerable to the action of nucleases or the genotoxics such as ROS species (Fig. 1.7 A) (Aguilera, 2002; Li and Manley, 2005). However, more evidence within bacteria, yeast and human cells suggests that DNA:RNA hybrids cause genomic instability within the S or G_2 phase of the cell cycle by either stalling replication fork (RF) progression as well as potentially causing RF breakage (Fig. 1.7 B) (Wellinger, Prado and Aguilera, 2006; Gomez-Gonzalez and Aguilera, 2007; Tuduri *et al.*, 2009; Gan *et al.*, 2011; Salas-Armenteros *et al.*, 2017). Within these cycling cells, the transcription-replication collisions can occur in two ways, either by head-on orientation (Fig. 1.7 B - top) or by the co-directional collisions of the RNAP and the RF (Fig. 1.7 B - bottom). Head-on collisions between RNAP and the RF activate the

serine/threonine-specific protein kinase (ATR) DNA damage pathway in response to ssDNA leading to DNA breakage and ultimately cell cycle arrest (Hamperl *et al.*, 2017). Co-directional collisions between RNAP and RF leads to the activation of the ATM serine/threonine kinase – mediated DNA damage in response to dsDNA breaks (Hamperl *et al.*, 2017). DNA:RNA hybrids have also been reported to be elevated in the regions possessing chromosomal breaks such as common fragile sites (CFS) (Helmrich, Ballarino and Tora, 2011; Groh *et al.*, 2014; Costantino and Koshland, 2018). CFS are genomic regions that can consist of repetitive sequences which are problematic to replicate and are prone to undergo DNA breaks under replication stress (Glover, 2006). Although R-loops are reported to accumulate at CFS that can influence transcription-replication conflicts (Helmrich, Ballarino and Tora, 2011; Groh *et al.*, 2014), CFS fragility cannot completely be explained by the presence of R-loops with fragile sites also correlated with specific chromatin status and gene expression profile (Letessier *et al.*, 2011).

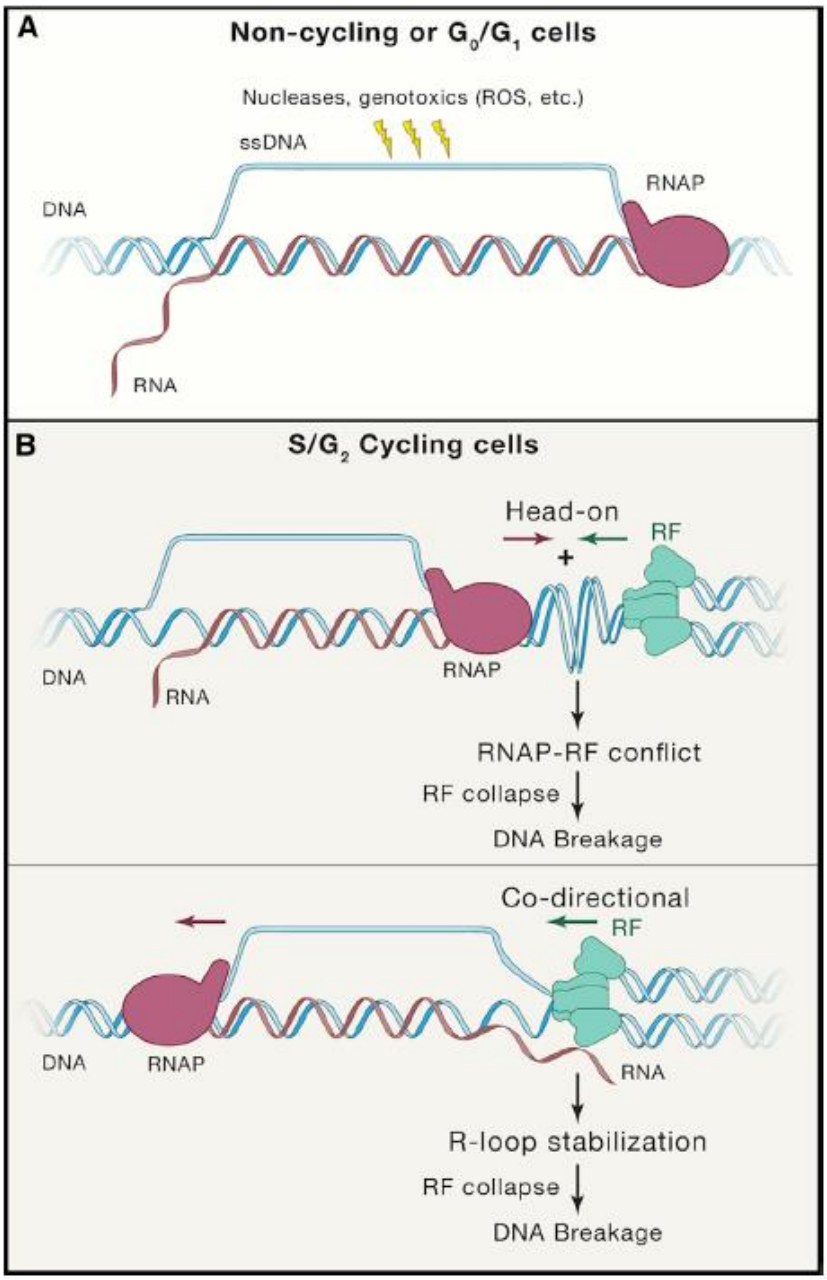


Figure 1.7: DNA:RNA hybrid presence gives rise to DNA damage.

(A) *In non-cycling or in G_0/G_1 cells the displaced ssDNA in R-loops are susceptible to DNA damage via the action of genotoxics or nucleases.* ***(B)*** *In S/G_2 phase cells, DNA damage is caused by transcription-replication conflicts. Head-on (top) collisions between the RNAP and the RF cause stalling RF progression and potential RF breakage. Co-directional (bottom) orientation collisions cause stabilisation of the DNA:RNA hybrid ultimately producing DNA breaks. Taken from* (García-Muse and Aguilera, 2019).

1.3.3 DNA:RNA hybrids role in human disease

DNA:RNA hybrids have been strongly implicated in repeat expansion disorders such as Friedreich's ataxia, fragile X syndrome and amyotrophic lateral sclerosis/frontotemporal dementia (Grabczyk, Mancuso and Sammarco, 2007; Colak *et al.*, 2014; Haeusler *et al.*, 2014; Loomis *et al.*, 2014). Friedreich's ataxia is a rare inherited disease that causes movement difficulties and progressive nervous system damage which is primarily caused by the unstable GAA repeat expansion within intron 1 of the frataxin (*FXN*) gene (Grabczyk, Mancuso and Sammarco, 2007; Groh *et al.*, 2014). DNA:RNA hybrids have been shown to form on these GAA repeat templates within bacteria and in vitro studies that result in RNAP arrest and ultimately the depleted expression of the *FXN* gene (Grabczyk, Mancuso and Sammarco, 2007; Groh *et al.*, 2014). Fragile X syndrome and fragile X tremor/ataxia syndrome are both inherited neurodegenerative disorders which are both caused by the expansion of the CGG repeat in the 5'UTR of the fragile X mental retardation 1 (*FMR1*) gene (Colak *et al.*, 2014; Groh *et al.*, 2014; Loomis *et al.*, 2014). Transcription-dependent DNA:RNA hybrids are found to form over these expanded CGG repeat regions and are transcriptional-dependent with their dynamics associated with FMR1 gene regulation (Groh *et al.*, 2014; Loomis *et al.*, 2014). Transcriptionally induced DNA:RNA hybrids have also been associated with larger repeat expansions such as the hexanucleotide repeat expansion (GGGGCC repeat) in chromosome 9 open reading frame 72 (*C9orf72*) gene in amyotrophic lateral sclerosis (ALS)/ frontotemporal dementia (Haeusler *et al.*, 2014). Formation of the DNA:RNA hybrids within the GGGGCC repeat of the *C9orf72* gene is a structural feature that contributes to the abortion of the transcription mechanism (Haeusler *et al.*, 2014).

DNA:RNA hybrids have also been implicated in breast and ovarian cancer, eosinophilic leukaemia and mixed lineage leukaemia (Stirling *et al.*, 2012; Hamperl *et al.*, 2017; Gorthi *et al.*, 2018; Shivji *et al.*, 2018). Pathological DNA:RNA hybrid accumulation with cancer cells is known to promote genomic instability and is termed a hallmark of cancer (Hanahan and Weinberg, 2011). DNA:RNA hybrids have been reported to contribute to dysregulation of DNA repair and replication in cancer as well as gene expression of oncogenes (Hamperl *et al.*, 2017). The breast cancer susceptibility gene 1/2 (*BRCA1*/*BRCA2*) acts as a tumour

suppressor gene mutated in breast and ovarian cancer as well as in other cancers (Miki *et al.*, 1994; Ford *et al.*, 1998; Schlacher, Wu and Jasin, 2012; Gorthi *et al.*, 2018). In the regions with double-stranded breaks (DSBs), both BRCA1 and BRCA2 are known to function in homologous recombination to prevent DNA:RNA hybrid formation (Bhatia *et al.*, 2014; Hill *et al.*, 2014; Hatchi *et al.*, 2015). Knockdown of either *BRCA1* or *BRCA2* has been shown to promote DNA damage that correlated with the elevation in DNA:RNA hybrid levels (Bhatia *et al.*, 2014; Hill *et al.*, 2014; Savage *et al.*, 2014; Gorthi *et al.*, 2018; Shivji *et al.*, 2018). Loss of BRCA1 promoted the formation of DNA:RNA hybrid at both the 5' and 3' end of genes whereas depletion of BRCA2 only promotes the formation of DNA:RNA hybrids at the 5' end of genes (Hatchi *et al.*, 2015; Gorthi *et al.*, 2018; Shivji *et al.*, 2018). DNA:RNA hybrids are also implicated in eosinophilic leukaemia and mixed lineage leukaemia via oncogenic translocation of polyadenylation factor leaving the protein inactive which triggers an accumulation of DNA:RNA hybrids, chromosome instability and DNA damage (Stirling *et al.*, 2012).

1.3.4 The presence of m^{6}A on DNA:RNA hybrids within the genome

Recently, RNA modifications such as m^{6}A have been reported to be present in DNA:RNA hybrids within the genome (Yang *et al.*, 2019; Abakir *et al.*, 2020; Zhang *et al.*, 2020). The first mention of m^{6}A presence on DNA:RNA hybrids was by Yang and colleagues in October 2019 where they proposed that m^{6}A presence on the RNA of DNA:RNA hybrids promote the formation of R-loops to facilitate transcription termination within HeLa and transformed HEK293 cells (Yang *et al.*, 2019). Another publication suggests that m^{6}A addition by METTL3 promoted DSB repair (Zhang *et al.*, 2020). The authors of this study proposed that ATM-mediated phosphorylation of METTL3 at serine 43 promotes the m^{6}A methylation of DNA damage-associated DNA:RNA hybrids (Zhang *et al.*, 2020). The m^{6}A then recruits YTHDC1 that, in turn, forms DNA:RNA hybrids at these dsDNA break sites and promotes the recruitment of BRCA1 and RAD51 homolog, DNA repair protein (RAD51), to these DSBs allowing for homologous recombination mediated DSB repair to ultimately prevent genomic instability (Zhang *et al.*, 2020).

Contrastingly to Yang et al., who proposed that knockdown of METTL3 caused a reduction in R-loop levels, our group reported that siRNA-mediated knockdown of METTL3 led to the

accumulation of DNA:RNA hybrids in human induced pluripotent stem cells (hiPSCs) (Abakir *et al.*, 2020). DNA:RNA hybrids marked with m^6A localised in repetitive sequences such as alpha-satellites (*α-satellites*) and long interspersed nuclear element-1 (*LINE1*) were found to accumulate through the S phase of the cell cycle to max out their presence within the G_2/M phase and finally getting depleted during G_0/G_1 phases (Abakir *et al.*, 2020). Similarly, m^6A marked DNA:RNA hybrids levels were at their highest during S and G_2/M cell cycle phases with a significant reduction in m^6A – DNA:RNA hybrid levels again in G_0/G_1 phases (Abakir *et al.*, 2020). Furthermore, the m^6A reader YTHDF2 was found to interact with DNA:RNA hybrids (Abakir *et al.*, 2020), corroborating previous studies reporting that YTHDF2 can promote genomic stability (Paulsen *et al.*, 2009). Moreover, our group found that YTHDF2 is localised to the nucleus during the G_2/M cell cycle phases where it helps prevent the accumulation of m^6A marked DNA:RNA hybrids and therefore contributes to the inhibition of R-loop dependent DNA damage in human cell lines (Fig. 1.8) (Abakir *et al.*, 2020).

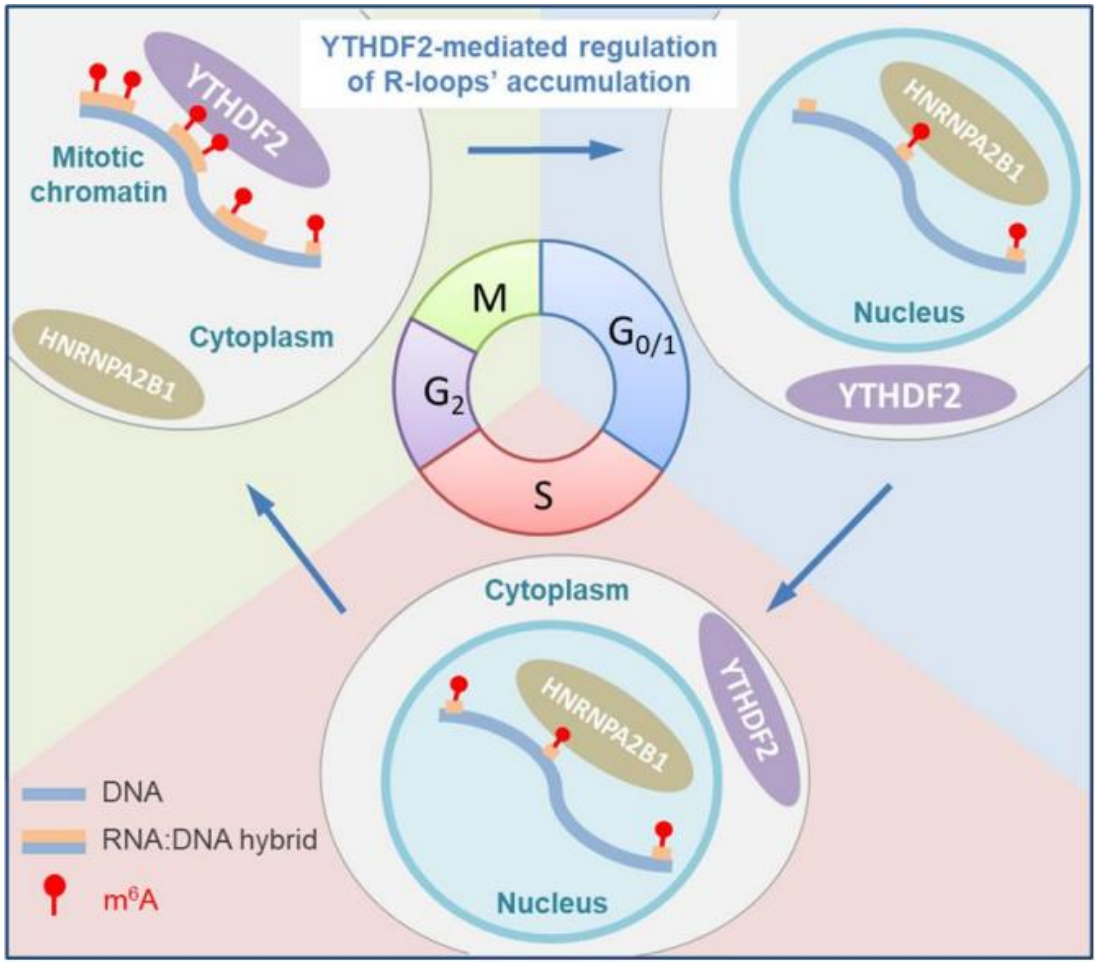


Figure 1.8: Dynamics of m^{6}A-marked DNA:RNA hybrids and the interacting m^{6}A readers YTHDF2 and HNRNPA2B1 during the cell cycle.

Figure taken from (Abakir *et al.*, 2020).

1.4 Hypothesis and Aims

Previous work from our lab showed that m^{6}A readers such as YTHDF2 interact with m^{6}A marked DNA:RNA hybrids, particularly during the G_2/M phase of the cell cycle (Abakir *et al.*, 2020). Within this study, other m^{6}A readers such as YTHDF1 and HNRNPA2B1 were also evaluated to understand whether they could interact with DNA:RNA hybrids (Fig. 1.9) (Abakir *et al.*, 2020). HNRNPA2B1 was shown to strongly interact with DNA:RNA hybrids in HeLa cells (Fig. 1.9), but the immunostaining showed that HNRNPA2B1 did not interact with mitotic chromatin when the cell was dividing (Abakir *et al.*, 2020). Additionally, ChIP indicated that HNRNPA2B1 had predominantly interacted with m^{6}A marked DNA:RNA hybrids found in

intronic regions but not in repetitive sequences such as *α-satellites* or *LINE1* (Fig. 1.10 A) (Abakir *et al.*, 2020). Furthermore, HNRNPA2B1 ChIP showed that its binding to these intronic sequences was decreased after siRNA knockdown of *METTL3* (Fig. 1.10 C) but increased after knockdown of *RNASEH1* (Fig. 1.10 B) (Abakir *et al.*, 2020). Moreover, the siRNA-mediated knockdown of *HNRNPA2B1* displayed elevated accumulation of a marker for DNA DSBs, histone variant γ-H2AX, yet to a lesser extent compared to YTHDF2 knockout cells (Abakir *et al.*, 2020).

Therefore, HNRNPA2B1 was shown to interact directly with DNA:RNA hybrids (Cristini *et al.*, 2018; Abakir *et al.*, 2020) as well as interact (likely indirectly) with m^6A marked RNA sequences (C. Alarcón *et al.*, 2015; Wu *et al.*, 2018). Both m^6A, and to a lesser extent, HNRNPA2B1, have been implicated in GBM with roles such as GBM proliferation, migration capability, tumorigenesis, and apoptosis (Deng et al., 2016; Cui et al., 2017; Zhang et al., 2017; C. Xu et al., 2020; L. Wang et al., 2020). Thus, in this thesis, we aimed to test two hypotheses. Firstly, we hypothesised that HNRNPA2B1 has a role in preventing the accumulation of m^6A marked DNA:RNA hybrids and therefore may act as a factor promoting genomic stability. Secondly, we hypothesised that m^6A marked DNA:RNA hybrids present in brain tumours may be impacted by the loss of *HNRNPA2B1*.

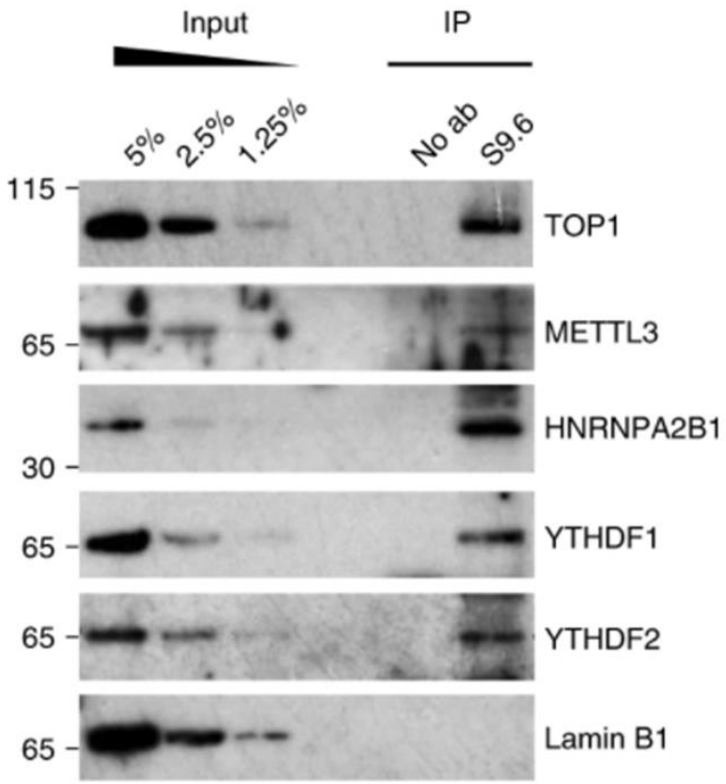


Figure 1.9: Writers and readers of m^{6}A interact with DNA:RNA hybrids in HeLa cells.

Immunoblotting of DNA:RNA hybrid co-immunoprecipitation probed with METTL3, HNRNPA2B1, YTHDF1 and YTHDF2 antibodies in HeLa cells. TOP1 and Lamin B1 were used as positive and negative control, respectively. Figure taken from (Abakir *et al.*, 2020).

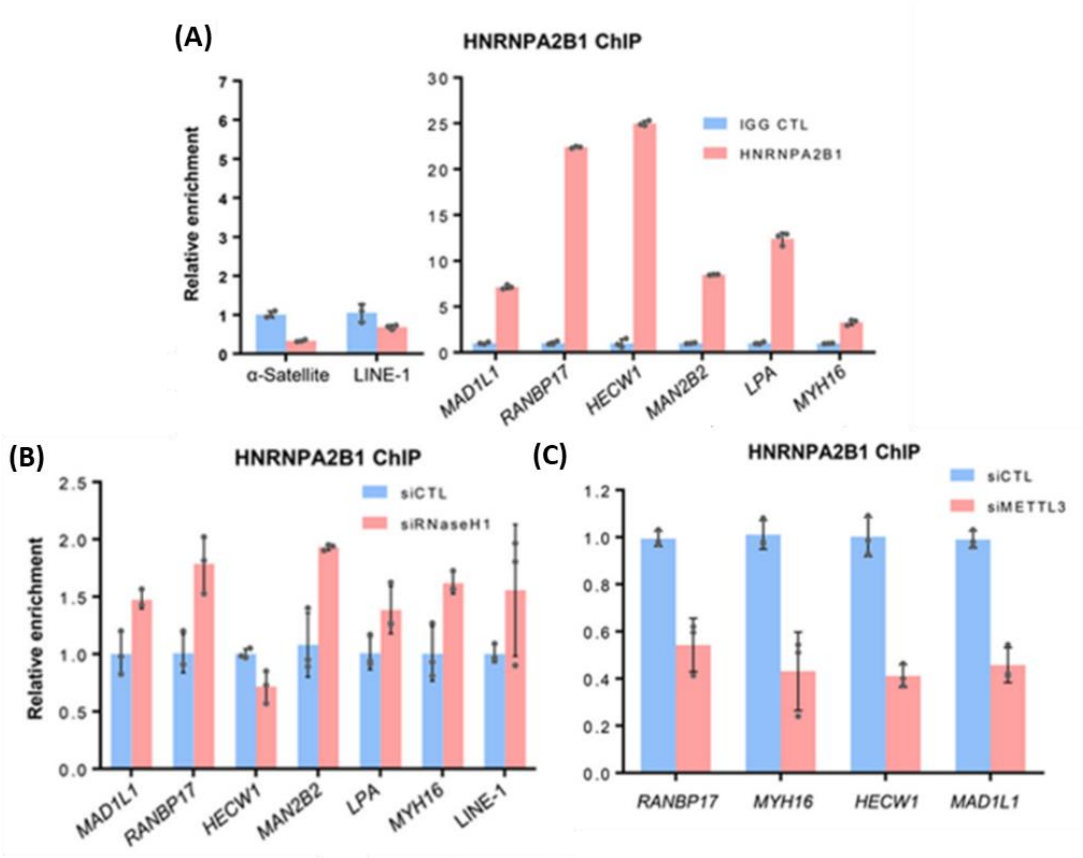


Figure 1.10: HNRNPA2B1 preferentially binds to m^{6}A marked DNA:RNA hybrids in intronic sequences which can affected by the loss of *RNaseH1* or *METTL3*.

(A) *HNRNPA2B1 ChIP comparing HNRNPA2B1 binding of m^{6}A-marked DNA:RNA hybrids in repetitive sequences (α-satellites and LINE1) to intronic sequences (MAD1L1, RANBP17, HECW1, MAN2B2, LPA, MYH16) in hiPSCs.* ***(B)*** *HNRNPA2B1 ChIP comparing binding of HNRNPA2B1 in RNASEH1 siRNA mediated knockdown hiPSCs to siRNA control hiPSCs within intronic sequences and LINE1.* ***(C)*** *HNRNPA2B1 ChIP comparing binding of HNRNPA2B1 in METTL3 siRNA mediated knockdown hiPSCs to siRNA control hiPSCs within intronic sequences. Figure adapted from* (Abakir *et al.*, 2020).

Therefore, **the central goal of this thesis was to understand the distribution and function of m^{6}A-marked DNA:RNA hybrids and their functional interaction with HNRNPA2B1 in human non-tumorigenic and cancer cell lines.** The thesis was split into four main aims:

1) To examine the impact that HNRNPA2B1 knockout has on accumulation of m^{6}A-marked DNA:RNA hybrids in human semi-haploid HAP1 cells.
2) To get an insight into functional significance of the interaction of HNRNPA2B1 with another m^{6}A reader, YTHDF2, and its potential impact on the dynamics of m^{6}A-marked DNA:RNA hybrids.
3) To assess the expression of m^{6}A related genes and the abundance of m^{6}A-marked DNA:RNA hybrids in adult and paediatric brain tumour cell lines.
4) To test if HNRNPA2B1 may represent a potential oncogene in adult and paediatric brain tumour cell lines.

Chapter 2: Materials and Methods

2.1 Cell culture

2.1.1 Cell lines

Human haploid (HAP1) matched wild-type (WT), HNRNPA2B1 knockout (KO) and YTHDF2 KO cell lines are commercially available cell lines purchased from Horizon Discovery by Dr Alexey Ruzov (University of Nottingham) and cultured as the company advised. HAP1 cells are haploid cells are generated based on the KBM-7 cell line that are transformed male chronic myelogenous leukaemia (CML) patient-derived cell line (Kotecki, 1999; Carette *et al.*, 2011; Essletzbichler *et al.*, 2014).

The FB83 cell line was obtained from Dr Beth Coyle (University of Nottingham) having been established from human foetal brain tissue received from the Joint MRC/Wellcome Trust (Grant #099175/Z/12/Z, Ethics committee approval 08/H0906/21 + 5, Health Research authority NRES Committee North East – Newcastle & North Tyneside 1) Human Developmental Biology Resource (www.hdbr.org) as previously described (Ivanov et al., 2016).

Four continuous GBM cell lines (LN18, LN229, U251 and U87MG) and one medulloblastoma cell line (UW228-3) were used in this study (Table 2.1). UW228-3 was obtained from Dr Beth Coyle (University of Nottingham) and cultured as advised. Dr Sebastien Serres (University of Nottingham) provided a flask of SVGA (human astrocytes) that was cultured as advised. Dr Stuart Smith (University of Nottingham) provided the primary GBM GIN cells for culturing.

Table 2.1: Cancer cell line characteristics.

Cell lines	Organism	Tissue	Disease	Other Characteristics
LN18	Human	Brain; Cerebrum; Right temporal lobe	GBM	65 years, Male. Mutated p53 and wild-type PTEN

LN229	Human	Brain; Right frontal parieto-occipital cortex	GBM	60 years, Female. Mutated p53 and wild-type PTEN
U251	Human	Brain	GBM/ Malignant Astrocytoma	75 years, Male.
U87MG	Human	Brain	Likely GBM	Male
UW228-3	Human	Brain; posterior fossa	MB	9 years, Female.

2.1.2 Preparation of media and cell culture

All media formulations are described in Table 2.2. LN18, LN229, U251, U87MG, GIN28, and GIN31 were cultured in Dulbecco's Modified Eagles Medium (DMEM, Gibco™, Life Technologies – 31885023) supplemented with 10% heat-inactivated foetal bovine serum (FBS, ThermoFisher – SH30541.03). GIN8 and FB83 were cultured in DMEM supplemented with 15% FBS. SVGA was cultured in DMEM High Glucose (Gibco™, Life Technologies, 4.5 g/L D-Glucose – 41965039) supplemented with 10% FBS and 1% Penicillin-Streptomycin (Gibco™, Life Technologies, 10,000 U/mL – 11548876). UW228-3 was cultured in DMEM/F12 (Gibco™, Life Technologies – 11320074) supplemented with 15% FBS, 1% L-Glutamine (Gibco™, 200 mM – 25030149) and 1% Sodium Pyruvate (Gibco™, 100 mM – 11360070). HAP1 WT, HAP1 HNRNPA2B1 KO and HAP1 YTHDF2 KO were cultured in DMEM/F12 supplemented with 20% FBS and 1% Penicillin-Streptomycin. All the above cell lines were cultured in tissue culture flasks and incubated at 37 °C with 5% CO_2.

Table 2.2: Media formulation.

Cell line	Media Components
LN18, LN229, U251, U87MG, GIN28, GIN31	DMEM + 10% FBS
GIN8, FB83	DMEM + 15% FBS

SVGA	DMEM (High glucose – 4.5 g/L) +10% FBS + 1% Penicillin-Streptomycin
UW228-3	DMEM/F12 + 15% FBS +1% L-Glutamine +1% Sodium Pyruvate
HAP1 WT, HAP1 HNRNPA2B1 KO, HAP1 YTHDF2 KO	DMEM/F12 + 20% FBS + 1% Penicillin-Streptomycin

2.1.3 Cryopreservation and thawing of cells

After dissociating $1x10^6$ cells from the flask with Trypsin and PBS, the cells were centrifuged between 200 - 500 G depending on the cell line for 5 minutes. The supernatant was carefully aspirated; the pellet was gently resuspended in a 1:10 solution of Dimethyl sulfoxide (DMSO) (Sigma – C6164) in FBS. This was placed in a 1 mL cryovial and quickly transferred to a Mr Frosty that once placed in a -80 °C freezer, chills the samples at -1 °C per minute. Following a 24-hour incubation within the -80 °C freezer, the cryovials were moved to long-term storage within the liquid nitrogen tank.

For thawing cells from liquid nitrogen, cryovials were warmed in a 37 °C water bath and taken out just before completely thawed. Cells in the 1 mL cryovial were then carefully resuspended in 9 mL of warmed DMEM media in a drop-by-drop manner. These were centrifuged at 200 G for 5 minutes. The supernatant was carefully aspirated off, and the cells were resuspended in 5 mL of warmed media dependent upon cell line (Table 2.2) and put in T25 flasks. After 24 hours, the media was replaced with fresh media, ensuring that the remaining DMSO was removed.

2.1.4 Sub-culturing of cells

For HAP1 WT, HAP1 HNRNPA2B1 KO and HAP1 YTHDF2 KO media was changed daily and passaged when reaching 70-80% confluency. LN18, LN229, U251, U87MG, UW228-3, FB83, SVGA, GIN8, GIN28, and GIN31 were cultured in media that was replaced every 2-3 days. The cells were passaged once 70-80% confluency was reached. 2 mL of 0.25% Trypsin-EDTA (Phenol-red, Gibco™ – 25200056) was used for dissociation of cells from T25 flasks. The

cells were incubated at 37 °C with 5% CO_2 for anywhere from 3 minutes to 10 minutes depending upon the cell line. Flasks with Trypsin-EDTA were gently tapped to dissociate adherent cells followed by neutralisation with PBS and spun in a centrifuge at between 200 - 500 G (depending upon cell line) for 5 minutes. The pellet was then resuspended for continued culturing.

2.1.5 Human pluripotent stem cell culture

REBL-PATs (R-Pat) are human induced pluripotent stem cells (hiPSCs) that were reprogrammed from skin fibroblasts using the Sendai virus by Gary Duncan at the University of Nottingham to produce a monoclonal hiPSC cell line. R-Pat cells were cultured in Essential 8™ Basal Medium (Gibco™ – A1516901) supplemented with Essential 8™ medium supplement (Gibco™ – A1517001) and 1% Penicillin-Streptomycin on coated Matrigel™ tissue-culture flasks at 37 °C with 5% CO_2. Cells were passaged every 3-4 days using TrypLE Select Enzyme (1x) (No Phenol Red, Gibco™, Life Technologies – 12563029) and ROCK Inhibitor (Y-27632, Sigma-Aldrich – SCM075) was added to R-Pat cells just before re-seeding in new coated Matrigel™ tissue-culture flask.

2.2 Cell culture assays

2.2.1 siRNA knockdown

To make a 10 µM stock, Silence Select human HNRNPA2B1 5 nmol siRNAs (ID: s6714, ThermoFisher – #4390824) were dissolved in 500 µL of dH_2O. Cells were seeded and cultured for 24 hours before transfection until reaching 40-50% confluency in either a 6-well plate for gene expression analysis or an 8-well glass chamber slide (Chamber slide, Lab-Tek, Glass, 8-well, Thermo Scientific Nunc – #177402) for immunostaining. In one tube, 10 µM of siRNA was diluted in Opti-MEM Reduced Serum Media (No phenol red, ThermoFisher – #31985070) to achieve a total volume of 200 µL for transfection in the 6-well plate or 40 µL for 8-well glass chamber slide. In another tube, DharmaFECT transfection reagent (DharmaFECT 1, Dharmacon – #T-2001-01/02) was diluted in OptiMEM depending upon the optimised concentration for each cell line and plating format. U251 cells required 6 µL of DharmaFECT

diluted in 194 µL OptiMEM media for 6-well plates and 1.2 µL DharmaFECT in 38.8 µL for 8-well glass chamber slides. Whereas LN18 and UW228-3 required 8 µL of DharmaFECT diluted in 192 µL OptiMEM media for 6-well plates and 1.6 µL DharmaFECT in 38.4 µL for 8-well glass chamber slides. The two tubes were incubated separately at room temperature for 5 minutes before combining both tubes of diluted siRNA and DharmaFECT into one tube to incubate at room temperature for 20 minutes. OptiMEM reduced serum media was then added to make a total transfection volume of 2 mL in 6-well plates and 200 µL for 8-well glass chamber slides with a final concentration of 50 nM of HNRNPA2B1 siRNA per well. Cells were incubated for 24 hours at 37 °C and 5% CO_2. After 24 hours, transfection media was replaced with a complete medium and returned to incubate for another 24 hours at 37 °C and 5% CO_2 before harvesting the cells for gene expression or immunocytochemical analyses.

2.2.1.1 Use of Attachment factor on growth surface

Before seeding the cells for siRNA transfection, 6-well plates and glass chamber slides were coated in Attachment Factor Protein 1X (Gibco, ThermoFisher Scientific – #S006100) at room temperature for 3 hours or incubated at 37 °C and 5% CO_2 for 1 hour. Plates and chamber slides were washed with PBS before seeding cells, and then, after 24 hours, the siRNA transfection protocol was performed as described above.

2.2.2 Growth curves

Cells were seeded in tissue culture-treated 24-well plates at a density of 2,000 cells per well and their growth was monitored for over 10 days. To exclude dead cells from the count, Trypan Blue 0.4% solution (ThermoFisher – #15250061) was used to count viable cells daily by a haemocytometer.

2.2.3 Flow cytometry cell sorting

Flow cytometry sorting for G_0/G_1, S and G_2/M phases of the cell cycle was performed according to the previously described method (Pozarowski and Darzynkiewicz, 2004). In short, enzymatically dissociated U251 and UW228-3 cells were washed in PBS and fixed in 70% ethanol for 2 hours. These were washed in PBS and stained with 10 µg/mL propidium iodide

(PI) (Sigma Aldrich – #P3566) in PBS supplemented with 0.1% Triton X-100 and 100 ug/mL RNase A (QIAgen – #19101). PI treated U251 and UW228-3 were sorted based on the DNA content into G_0/G_1, S and G_2/M cells using Beckman Coulter Astrios EQ and Beckman Coulter Kaluza 2.1 software carried out by Nicola Croxall and David Onion in the University of Nottingham Flow Cytometry Facility.

2.3 Molecular biology

2.3.1 RNA extraction

RNA extraction was performed either using the Qiagen RNeasy kit (#74106) or the Macherey-Nagel NucleoSpin RNA kit (#740955-250) following the supplier's instructions. RNA was quantified using NanoDrop™ spectrophotometry measurements at 260/280 nM and 260/230 nM to analyse the RNA quality and for detection of organic compound contamination, respectively.

2.3.2 Complementary DNA (cDNA) synthesis

Synthesis of cDNA was performed by reverse transcription PCR. Depending on the sample, 1 or 2 µg of RNA was added to a 20 µL reaction mix containing 1 µL of 10mM dNTPs (New England Biolabs - #N0447S), 2 µL of 10X random hexamers (Thermo Scientific - #N8080127) and dH_2O. The reaction mixture was heated to 65 °C for 5 minutes followed by incubation on ice. During the incubation, 4 µL of 5X first strand buffer, 1 µL of Dithiothreitol (DTT) and 1 µL of Superscript III Reverse Transcriptase (ThermoFisher – #18080093) were added to the reaction mix and incubated at room temperature for 5 minutes. The reaction mixture was then heated at 50 °C for 1 hour, followed by the inactivation of the enzyme for 15 minutes at 70 °C. The reaction was adjusted with dH_2O for a total volume of 200 µL for 2 µg of RNA used and 100 µL for 1 µg of RNA used.

2.3.3 Gene expression analysis by Real time Quantitative Polymerase Chain Reaction (qPCR)

Gene expression was measured using the Applied Biosystems FAST 7500 qPCR machine and the manufacturer's software. The primers were designed using Primer3 and checked for self-complementarity and potential hairpin formation using the OligoCalc online software tool (http://biotools.nubic.northwestern.edu/OligoCalc.html), verified by the UCSC In-Silico PCR software tool (Table 2.2). The 10 µL reaction mix consisted of 2.5 µL of dH_2O, 5 µL of GoTaq qPCR Master Mix (Promega - #A6001/2), 0.25 µL of forward and reverse primers (10 µM) (Sigma Aldrich) and 5 µL of cDNA sample (100 ng). The samples were run on a qPCR machine for 40 cycles, using the following parameters: 95 °C denaturation for 15 seconds, annealing temperature at 60 °C for 1 minute and extension temperature at 72 °C for 30 seconds. The samples underwent melt curve analysis after 40 cycles, which involves increasing the temperature in 0.3 °C increments from 60 to 95 °C. Gene expression was analysed using the $2^{-\Delta\Delta CT}$ method (Livak and Schmittgen, 2001) and normalised to Glyceraldehyde 3-phosphate dehydrogenase (GAPDH) as an endogenous reference for gene expression.

Table 2.3: List of qPCR 5' and 3' primers

Gene name	Forward Primer Sequence	Reverse Primer Sequence
GAPDH	GATGCTGGCGCTGAGTACG	GCAGAGATGATGACCCTTTTGG
METTL3	CAAGCTGCACTTCAGACGAA	GCTTGGCGTGTGGTCTTT
METTL14	AGAAACTTGCAGGGCTTCCT	TCTTCTTCATATGGCAAATTTTCTTC
WTAP	AGAACAGTCAGAGGCCACAA	TACCCCGCACTGAGTTGATT
YTHDF2	ACCTTACTTGAGTCCACAGG	AGCCAATGGAGGGACTGTAG
YTHDC1	AGGAAAGTCAGCCACAGAGT	CCTTTTCCGGACACAGGTTT
HNRNPA2B1	AACCAGGGGCTCATGTAACT	CCTCTTTTCTTTCCAGACTGCC
FTO	GCTAATGAGGATGCTGTGCC	TCACTGCCATTTTCCCCATG
ALKBH5	TCATCAACGACTACCAGCCC	GAAAGCACTGGTTCCGACAC

DHX9	AGATGGCCCGATACGACAAT	AGTTGCCTCTAAAGCCACCT
DDX3X	GGAGTGATTACGATGGCATTGG	TTGGTGGGAGTGGTTTTGAC
***HNRNPA2* isoform**	TGGAGAGAGAAAAGGAACAGTTC	AAGCTTTCCCCATTGTTCGT
***HNRNPB1* isoform**	GAAACTGTTCCTTTGGAGAGGA	CCCCATTGTTCGTAGTAGTT

2.3.4 Polymerase Chain Reaction (PCR)

For the PCR reactions, we made a reaction mix totalling 50 µL that included 10 µL of 5X Phusion High-Fidelity buffer (6 mL, NEB – #B0518S), 10 µM each of forward and reverse primers (Table 2.3), 10 mM of dNTPs, 100 ng of genomic DNA and 1 U of Phusion Polymerase (Phusion High-Fidelity DNA polymerase, 100 units, NEB – #M0530S/L). An initial denaturation of 98°C for 5 minutes was carried out before running the PCR for 35 cycles using the following programme: denaturation at 98 °C for 30 seconds, annealing at a gradient temperature depending upon the reaction ranging from 52.7 to 57.3 °C for 30 seconds, extension at 72 °C for 45 seconds. There was a final extension for 5 minutes at 72 °C before holding the samples at 4 °C.

Table 2.4: Phusion PCR 5’ and 3’ primers

Primer Sequences	
HNRNPA2B1 Exon 1 (Forward Primer)	AGGTGCTCCTCGCAGAGT
HNRNPA2B1 Exon 5 (Reverse Primer)	TCCTAGAACTCTGAACTTCCTGC

2.3.5 Agarose gel electrophoresis

To detect the products of PCR reactions we used agarose gel electrophoresis. We cast a 1% agarose gel and visualised DNA bands with ethidium bromide (10 mg/mL, Invitrogen – #15585011) at a final concentration of 250 mg/µL. DNA samples were mixed with a 6X loading dye (Quick-Load® Purple 1 kb DNA ladder, 50 µg/mL, NEB – #N0552S) to a final concentration of 1X loading dye in each reaction and loaded alongside 5 µg of DNA ladder (1 kb ladder, 50 µg/mL, NEB – #N3232S/L). The gel was then run at 90 volts and 400 milliamperes (mA) for 1 hour, visualised using the Fujifilm LAS 4000 UV transilluminator, and the image were captured by LAS 4000 image acquisition software. PCR product run through gels was extracted by QIAquick Gel Extraction Kit (QIAgen – #28704) following the manufacturer's instructions. DNA was eluted in nuclease-free dH_2O and then quantified in the NanoDrop-1000 spectrophotometer (ThermoFisher).

2.3.6 Genomic DNA extraction and Sonication

To prepare the genomic DNA, a cell pellet of a T75 flask was lysed in 1 mL of lysis buffer (20 mM Tris pH 8.0, 4 mM EDTA, 20 mM NaCl, 1% SDS), pipetting up and down until no longer viscous. 3.6 µg/mL of RNase A (100 mg/ml, 17500 U, QIAgen – #19101) was added to lysed cells for 1 hour at 37 °C, followed by the addition of 33.3 µL of proteinase K (20 mg/mL, Promega – #MC5005) and incubation of the mixture at 55 °C for overnight. Using 1 volume of phenol/chloroform (Saturated with 10 mM Tris, pH 8.0, 1 mM EDTA, Sigma – #P2069), the samples were vortexed and centrifuged at 14,000 G for 5 minutes. The aqueous and interphase phase were collected and placed into a fresh tube. The phenol-chloroform extraction was repeated, except only the aqueous phase was taken. The genomic DNA was precipitated with 1:10 volume of 5 M NaCl and 1 volume of isopropanol, placed at -20 °C for 30 minutes, and then centrifuged at 14,000 G for 10 minutes. The isopropanol was removed and the pellet was resuspended in 1 volume of 70% ethanol. After centrifuging at 14,000 G for 5 minutes, the ethanol was removed, the pellet dried at room temperature and resuspended in 100 µL of RNase/DNase-free water. Genomic DNA samples were then tested on Nanodrop™ for concentration, quality and any organic contamination. Genomic DNA was

also tested for exact concentration on Qubit® Fluorometer as per the manual in the dsDNA BR assay kit (Molecular probes Life technologies – #Q32850). Samples were diluted to a total of 130 µL and placed in a microtube (AFA fiber, pre-slit, Snap-cap, Covaris – #520045) before sonication in the Covaris S220 Focussed-Ultrasonicator with the S-series holder microTUBE (Adaptor, Covaris – #500114). Samples were sonicated for 60 seconds at 10% Duty cycle, Intensity 4, Cycle/Burst 200 for ~350 base pair fragments.

2.3.7 DNA:RNA hybrid and m^{6}A marked DNA:RNA hybrid immunoprecipitation (S9.6 DRIP and m^{6}A DRIP)

Our group has previously described used the immunoprecipitation of DNA:RNA hybrids and m^{6}A-marked DNA:RNA hybrids in (Abakir *et al.*, 2020). Firstly, 4 µg of sonicated sample for m^{6}A DRIP, S9.6 DRIP and No Antibody control for each immunoprecipitation which were made up to 400 µL with DNase/RNase free H_2O. Samples being used for the m^{6}A-marked DNA:RNA hybrid immunoprecipitation was denatured at 95 °C for 10 minutes, then immediately placed on ice. The samples for the DNA:RNA hybrid immunoprecipitation with the S9.6 clone antibody were not denatured. 51 µL of 10 x IP buffer (100 mM Na-Phosphate pH 7.0, 1.4 M NaCl, 0.5% Triton X-100) was added to all samples before either 3 µL of m^{6}A antibody (N6-methyladenosine, m^{6}A, Rabbit polyclonal antibody, Synaptic Systems – #202-003) or 5 µL of S9.6 antibody (DNA:RNA hybrid, clone S9.6, Mouse monoclonal antibody, Merck Millipore – #MABE1095) (Table 2.5) was added to corresponding immunoprecipitation samples. The No Antibody control samples were processed in parallel without the addition of either antibody. All immunoprecipitation samples with or without antibodies were shaken/spun overnight at 4 °C. Next, after washing in PBS, Dynabeads M-280 Sheep anti-mouse IgG (Invitrogen – #11202D) and Dynabeads M-280 Sheep anti-rabbit IgG (Invitrogen – #11203D) beads were resuspended in 1 x IP buffer (1:10 of 10 x IP buffer) and 20 µL of the corresponding beads were added to each sample. These were spun at 4 °C for 2 hours and then placed in a magnetic rack to remove the supernatant. Samples with attached beads were washed 3 times with 1 x IP buffer before the addition of 250 µL of Proteinase K (20 mg/mL, Promega – #MC5005). Samples were incubated for at least 5 hours at 55 °C in a shaking incubator.

Samples were then placed on a magnetic rack, and the supernatant was carefully removed from the detached beads and placed in a new Eppendorf. Samples were then purified using the QIAquick PCR purification kit (QIAgen – #28104) and resuspended in 200 µL. For input samples, 1% of each experimental non-RNase treated sample was diluted in 400 µL of DNase/RNase free H_2O and 51 µL of 10 x IP buffer and stored at 4 °C until the purification step. Samples were quantified by locus-specific qPCR using 2 µL of sample per reaction, the primers listed in Table 2.4, as well as the commercial primers for alpha-satellites (α-satellites) (Novus – #NBP1-71654SS), were used.

Table 2.5: List of DRIP and ChIP primers

Gene name	Forward Primer sequence	Reverse Primer sequence
LINE1 **(L1PA1 and L1PA2 classes)**	AGGCCACTGTGTGCGCGC	CCAGGTGTGGGATATAGTCTC
Alu-Y	AGATCGAGACCATCCTGGCT	CCGCCTCCCGGGTTCACGCC
Alu-S	GCCGAGGCGGGCGGATCACC	GCCTCCCGAGTAGCTGGGAT
MYH16	AGAGCAGAGCAACAGAGACT	TTCCCTACTGAGTCCTCCCA
HECW1	CCCTTGACTCCCTTTCTCCC	AGGGAGGGGAAGAAAGAGAG
WWOX **(Intron 4)**	TAGGAAGGAAGGAAGGAAGAGAG G	GACAAGTCAAGCCCACAGACC
WWOX **(Intron 5)**	TTCTTCTATCCATCCAACCGTCCT	AAAGGAAAGGAAGACAGGAGGAA G
WWOX **(Intron 8)**	CTGCCATAAAAATGTCTGTCAGAG	ATGCATCATTTATCCATCCATCCAA
GLI2	GCAGACACATACCACACAG	TGTGGATATGCTGTGTGTTGTA
CDK6	GAAAGGGGAAGGAGAAGGGG	TCAGCCAGCATCTATCAGGG
NF1	TGGTGTTCTTTCTCTCTGTCTCT	ACACCAAAGCTAGCAGAAGAA
RB1	CTCCCTCAATTTCAGAACGTGT	TCACCACAGATCCCACAGAA

2.3.8 Chromatin immunoprecipitation (ChIP)

ChIP was performed according to the Magna ChIP A (EZ-Magna ChIP A kit – Milipore #17-408) manufacturer's instructions using one 80% confluent T75 flask of either HAP1 WT, HAP1 HNRNPA2B1 KO or HAP1 YTHDF2 KO cells. Crosslinked and lysed DNA was made up to 1 mL with PBS containing 0.05% Protease Inhibitor Cocktail II (PIC) mix. The lysate samples were sonicated using the Covaris S220 Focused Ultrasonicator in 1 mL militubes (miliTUBE 1 mL AFA fiber – Covaris #520135) and Covaris adaptor (miliTUBE 1 mL adaptor - Covaris #500371) for 30 minutes (2 x 15 minutes) at a 5% Duty Cycle, Intensity 4 and Cycle/Burst 200. Sonicated fragments were verified by Agilent Tapestation D5000 screen tapes ensuring that fragments between 200-1000 base pairs were generated. Samples were then centrifuged and supernatant aliquoted into 5 x 200 µL samples, with each sample being roughly equivalent to $1x10^6$ cells. The protocol was carried out with 200 µL sheared crosslinked chromatin and 300 µL Dilution buffer/ 0.05% PIC to allow for a more diluted sample. An input sample (1%) was obtained from HAP1 WT, HAP1 HNRNPA2B1 KO and HAP1 YTHDF2 KO cells before an immunoprecipitating antibody was added. For each cell line, there was a sample with 2.5 µL of Normal Rabbit IgG (included in the EZ-Magna ChIP A kit), samples with 2.5 µL of anti-mouse HNRNPA2B1 antibody (DP3B3, Novus Biologicals (Bio-techne) – #NB120-6102SS), samples with 5 µL of anti-rabbit YTHDF2 antibody (Proteintech – #24744-1-AP) and samples without any antibody added. Next, fully suspended 20 µL protein A magnetic beads were added to the samples, and the samples were left at 4°C overnight on a rotating wheel. For the rest of the protocol, we followed the manufacturer's instructions except for the final elution step where samples were diluted in 100 µL of DNase/RNase-free H_20. ChIP samples were then analysed by qPCR, with 2 µL of the sample used per reaction. The ChIP primers are listed in Table 2.4. Commercial primers (Novus – #NBP1-71654SS) were used for α-satellites primers.

2.3.9 Immunocytochemistry

The immunocytochemistry protocol described below was optimised based on the methodology used in several previous publications (Wheldon et al., 2014; Hamperl et al.,

2018). Before seeding for immunostaining, glass chamber slides (Chamber slide, Lab-Tek, Glass, 8-well, Thermo Scientific Nunc – #177402) were either coated with Matrigel for R-Pat cells (as described in 2.1.4 Human Pluripotent Stem Cell Culture) or with Attachment Factor Protein 1X for HAP1 and cancer cell lines (as described in 2.2.1.1 Use of Attachment factor on growth surface). HAP1 and R-Pat cells were seeded at 30,000 cells per well (0.8 cm^2) and LN18, U251, SVGA and UW228-3 were seeded at 15,000 cells per well on a glass slide. When cells were at 70-80% confluency, the media was washed off with PBS before fixing the cells with ice-cold 4% PFA for 15 minutes at room temperature. To remove the PFA, slides were then washed in PBS for 5 minutes at room temperature. Cells were permeabilised with PBX (PBS with 0.001% Triton-X – Sigma #T8787-100ML) for 30 minutes at room temperature then washed several times with PBS. For immunostaining with YTHDF2 and HNRNPA2B1, chamber slides were gently washed with PBS before depurination with 4 M HCl for 1 hour. After several washes with PBS, slides were blocked with 10% FBS in PBS blocking solution for at least 1 hour at room temperature. For immunostaining with S9.6 DNA:RNA hybrid antibody and γ-H2AX antibody (Phospho-Histone H2A.X (Ser139) antibody clone JBW301, mouse monoclonal, Merck Millipore – #05-636), no depurination stage was required and the cells were instead blocked with the 10% FBS in PBS solution for at least 1 hour. Slides then were stained with their respective primary antibody listed in Table 2.5 using the following dilutions: 1:200 of DNA:RNA hybrid (clone S9.6) antibody, 1:200 Phospho-Histone γ-H2AX antibody, 1:200 HNRNPA2B1 antibody and 1:500 YTHDF2 antibody. Followed by 3 washes with PBT (PBS with 0.01% Tween-20 – Sigma #P1379), complementary secondary goat anti-rabbit IgG HRP conjugate (Invitrogen – #65-6120) and goat anti-mouse IgG (Invitrogen – #A-21052) antibodies were added to the blocking solution at 1:400 dilution (Table 2.5) and incubate for 1 hour at room temperature. After further 3 PBT washes, tyramide amplification solution (1:200 tyramide mix with provided buffer, TSA Plus Fluorescein System – Perkin Elmer #NEL741001KT) was added to chamber slides stained with HNRNPA2B1 and YTHDF2 for 2 minutes before being washed off with PBT 3 times. Chamber slides stained with either S9.6 antibody or γ-H2AX antibody did not require tyramide amplification. Rubber grommets of the glass chamber slides were then gently removed, mounting medium added (Fluoroshield™

with DAPI, Sigma – #F6057) and coverslips (SLS Coverslips No 0 22x64mm, 100 pk – Scientific Laboratory Supplies #MIC3208) applied.

Table 2.6: The antibodies and other reagents used for immunostaining.

Primary Antibody	Specifications	Dilution
S9.6	DNA:RNA hybrid, clone S9.6 – Mouse monoclonal antibody – Merck Millipore (MABE1095)	1:200
γ-H2AX	Phospho-Histone H2A.X (Ser139) antibody clone JBW301 – Mouse monoclonal – Merck Millipore (05-636)	1:200
m^{6}A	N6-methyladenosine (m^{6}A) – Rabbit polyclonal antibody – Synaptic Systems (202-003)	1:200
YTHDF2	YTHDF2 antibody – Rabbit polyclonal antibody – Proteintech (24744-1-AP)	1:500
HNRNPA2B1	hnRNPA2b1 antibody (DP3B3) – Mouse monoclonal antibody – Novus Biologicals (Bio-techne) (NB120-6102SS)	1:200
Ph-H3	Phospho-Histone H3 (Ser10) (6G3) – Mouse monoclonal antibody – Cell signalling (9706S)	1:200
Secondary Antibody	**Specifications**	**Dilution**
Anti-Rabbit	Goat Anti-Rabbit IgG (H+L), HRP conjugate – Invitrogen (65-6120)	1:400
Anti-Mouse	Alexa Fluor ™ 633 Goat Anti-Mouse IgG (H+L) highly crossed-absorbed – Invitrogen (A-21052)	1:400
Other reagents	**Specifications**	**Dilution**
Tyramide Signal Amplification (488 Fluor)	TSA Plus Fluorescein System – Perkin Elmer (NEL741001KT) – now known as Akoya Biosciences	1:200
Fluoroshield ™ with DAPI	Histology Mounting Medium with DAPI – Sigma (F6057)	N/A

2.3.9.1 m^6A marked DNA:RNA hybrid immunostaining

Immunostaining of m^6A-marked DNA:RNA hybrids, cells were either left untreated, treated with RNase A only or treated with RNase A and RNase H (Figure 2.1). Before depurination with 4 M HCl, 100 µL of RNase H at a 1:10 dilution in 1x RNase H buffer (5000 units per mL, NEB – #M0297S/M0297L) were added to the control wells that required RNase H treatment. DNase/RNase-free H_2O was added to the non-treated wells. The slides were put in a humidity chamber and incubated at 37 °C overnight. The RNase H was removed and then designated wells were treated with 50 µL of RNase A at a 1:4 dilution with DNase/RNase free H_2O or left with only DNase/RNase free H_2O at 37 °C for 1 hour. Following 4 M HCl depurination and incubation in blocking solution, 1:200 N6-methyladenosine (m^6A) antibody and 1:200 of Phospho-Histone H3 antibody (Phospho-Histone H3 (Ser10) (6G3), Mouse monoclonal antibody, Cell signalling – #9706S) (Table 2.5) diluted with 10% FBS in PBS blocking solution were added to the samples. The samples were incubated for 1 hour at room temperature or overnight in a humidity chamber at 4 °C. Immunostaining was continued as described above including the Tyramide amplification step.

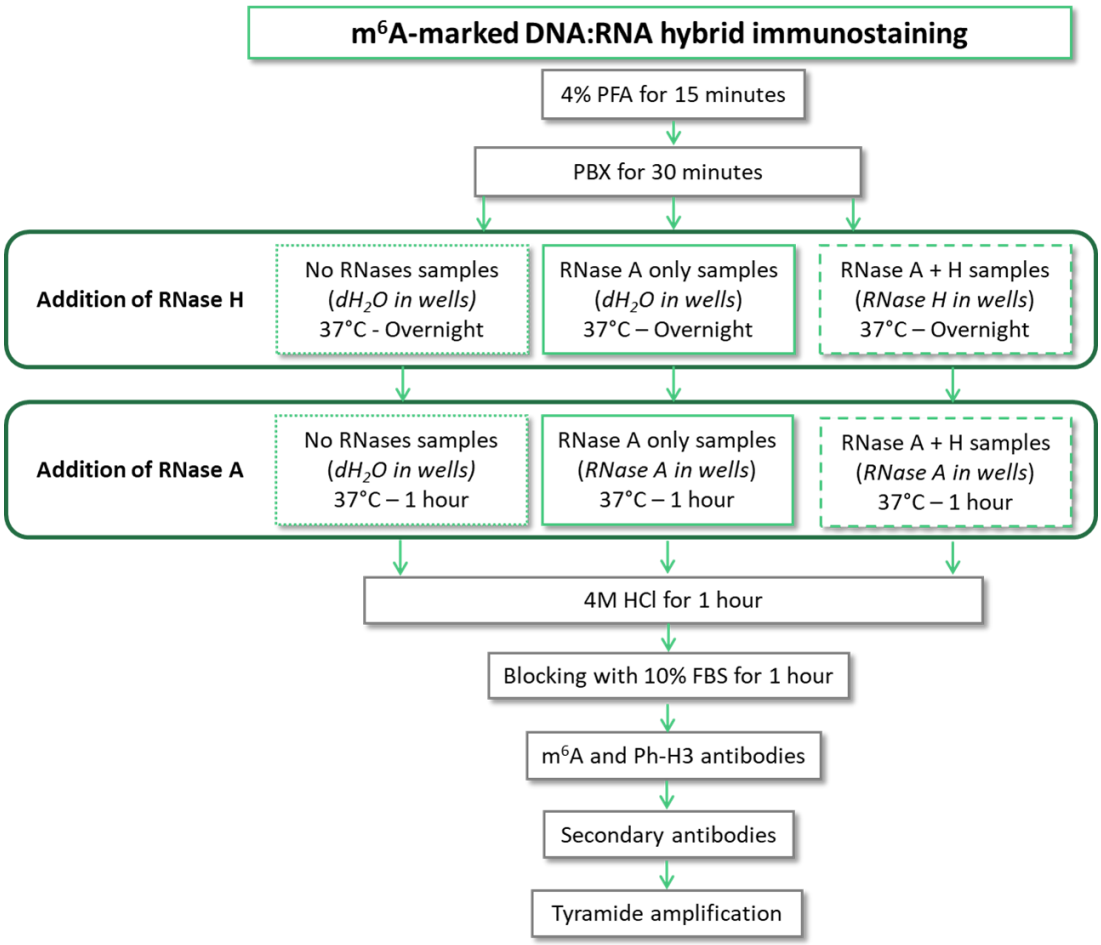


Figure 2.1: m^{6}A marked DNA:RNA hybrid immunostaining methodology.

2.4 Confocal microscopy imaging

Fluorescence images were taken with the Zeiss LSM 700 AxioObserver confocal microscope using a C-Apochromat 63x1.2 Water Korr M27 objective lens. Immunostaining without the primary antibody was used as the control immunostaining and produced no detectable signal. All images were captured at identical exposure settings and acquisition protocols for all the channels with images processed using Zeiss Zen Black 2012 software. Mean values of the average of 10 – 20 nuclei signal intensities were calculated for each experimental point. GraphPad Prism 8 software was used for data visualisation and statistical analysis.

2.5 Stable-isotope dilution ultra-performance liquid chromatography with tandem mass spectrometry (SID-UPLC-MS/MS)

The samples tested by SID-UPLC-MS/MS were carried out by Ryszard Olinski laboratory to analyse m^6A and adenosines as described in the methods and supplementary methods in the previous study (Abakir *et al.*, 2020).

2.6 Bioinformatics

Bioinformatics analysis was performed on IGV software of m^6A DRIP and S9.6 DRIP hiPSCs datasets (Abakir et al., 2020).

2.7 Statistical Analysis

All experiments were performed in two biological replicates unless stated otherwise and each figure has reported or plotted the mean and standard deviation or standard error (as stated). Statistical analysis was performed using GraphPad Prism 8 Software. Normality tests were performed in all datasets to check for normal distribution. For normally distributed data, paired and unpaired two-tailed parametric Student's t-tests were performed. For non-normally distributed data, Mann-Whitney tests were performed. All statistical tests were conducted using 95% confidence interval and were denoted by ns = $p \geq 0.05$, * $p < 0.05$, ** $p < 0.01$, *** $p < 0.001$, **** $p < 0.0001$.

Chapter 3: Characterisation of HNRNPA2B1 knockout in HAP1 cells.

3.1 Introduction

Heterogeneous nuclear ribonucleoproteins (HNRNPs) belong to a large protein family with involvement in alternative splicing (Dreyfuss *et al.*, 1993; Caputi *et al.*, 1999; del Gatto-Konczak *et al.*, 1999; Bilodeau *et al.*, 2001; Domsic *et al.*, 2003; Geuens, Bouhy and Timmerman, 2016), transcriptional regulation (Listerman, Sapra and Neugebauer, 2006), mRNA stability (Fähling et al., 2006; Goodarzi et al., 2012), RNA transport (Hoek *et al.*, 1998; Muslimov *et al.*, 2014) and translation (Kwon, Barbarese and Carson, 1999). The HNRNPA2B1 protein is a part of the HNRNP A/B subfamily that has two main isoforms, HNRNPA2 and HNRNPB1 (Burd *et al.*, 1989; Kozu, Henrich and Schäfer, 1995). Compared to the A2 isoform, the B1 isoform has an additional 12 amino acids at the N-terminal. (Burd *et al.*, 1989; Kozu, Henrich and Schäfer, 1995; Wu *et al.*, 2018). HNRNPA2B1 contains two N-terminal RNA recognition motif (RRM) domains and a C-terminal glycine-rich low complexity area also known as a Prion-like domain (Mears and Rice, 1996; Kim *et al.*, 2013; Harrison and Shorter, 2017; Wu *et al.*, 2018). Isoforms of HNRNPA2B1 have around 80% amino acid homology within the RRM domains but only 30% amino acid commonality in the glycine-rich low complexity area (Burd *et al.*, 1989; Mayeda *et al.*, 1994). The RRM domain structure is comprised of a four-stranded antiparallel beta-sheet, two alpha-helices and amino- and carboxy-terminal regions (Daubner, Cléry and Allain, 2013; Wu *et al.*, 2018). Both RRM domains within HNRNPA2B1 are involved in the recognition of RNA with RRM1 exclusively recognising purine-rich AGG motif-containing RNA sequences, whereas RRM2 has broader compatibility recognising RNA sequences including a UAG motif, purine-rich GAG motif and pyrimidine-rich UU sequences (Wu *et al.*, 2018). Wu and his colleagues found that, both RRM1 and RRM2 binding surfaces aligned on the same plane which resulted in HNRNPA2B1 being capable of binding to a single-stranded RNA in a long-connecting loop or two anti-parallel RNA strands (Wu *et al.*, 2018).

The RRM domain is one of over 600 different domains found within RNA binding proteins (RBPs), with the RRM domain size ranging between 60 to 100 amino acids long (Gerstberger, Hafner and Tuschl, 2014). RBPs can bind to any RNA sequence providing that the RNA either coding or non-coding has regulatory *cis*-acting sequence elements present to bind to (G. Singh et al., 2015). Post-translational modifications such as acetylation, isomerisation, methylation, O-linked β-N-acetylglucosamine modification (O-GlcNAcylation), phosphorylation and ubiquitination have been shown to regulate RBPs interaction with RNA sequences (García-Mauriño *et al.*, 2017; Hofweber and Dormann, 2019; Zanzoni *et al.*, 2019). In addition to RBP's ability to bind to RNA sequences, it is estimated that 40% of the currently identified RBPs can also bind to double-stranded DNA, including HNRNPA2B1 (Hudson and Ortlund, 2014; Coppin *et al.*, 2018). DNA and RNA binding proteins (DRBP) are thought to be involved in a range of cellular processes including transcription, translation, gene silencing, telomere maintenance, apoptosis, and DNA damage response (Hudson and Ortlund, 2014; Coppin *et al.*, 2018).

RBPs such as HNRNPA2B1 and other members of the HNRNP protein family have been demonstrated to be a key part of alternative splicing (AS) (Dreyfuss *et al.*, 1993; Caputi *et al.*, 1999; del Gatto-Konczak *et al.*, 1999; Bilodeau *et al.*, 2001; Domsic *et al.*, 2003; Geuens, Bouhy and Timmerman, 2016). AS is known as the deviation from the DNA sequence by the skipping of exons or by intron retention, leading to numerous variations of mature mRNAs (Zheng, Fu and Gribskov, 2005; Blencowe, 2006), whereas constitutive splicing removes introns and retains exons in the order set by the DNA sequence (Zheng, Fu and Gribskov, 2005) (Fig. 3.1 A). Mutually exclusive exons will appear adjacent to one another in precursor messenger RNA (pre-mRNA) resulting in one mRNA containing one exon and another mRNA containing the other exon, but not within the same transcript (Fig. 3.1 B) (Breitbart, Andreadis and Nadal-Ginard, 1987; Wang and Burge, 2008). Cassette or skipped exons are observed as the most prevalent pattern accounting for an estimated 30% of splicing events (Kim, Magen and Ast, 2007). These occur when an exon is skipped in one mRNA isoform but included in another mRNA isoform of one gene (Fig. 3.1 C) (Breitbart, Andreadis and Nadal-Ginard, 1987; Wang and Burge, 2008). When an alternative 3' splice site (acceptor sites) is selected it changes the 5' boundary of the downstream exon (Fig. 3.1 D) (Breitbart, Andreadis and Nadal-

Ginard, 1987; Wang and Burge, 2008). On the other hand, when an alternative 5' donor site has been accepted, it changes the 3' boundary of the upstream exon (Fig. 3.1 E) (Breitbart, Andreadis and Nadal-Ginard, 1987; Wang and Burge, 2008). Intron retention, more commonly noted in plants and single-celled eukaryotes, is essentially the absence of splicing (Fig. 3.1 F), which tends to involve smaller introns in these organisms (Breitbart, Andreadis and Nadal-Ginard, 1987; Kim, Magen and Ast, 2007). Whereas intron retention in human transcripts tends to be positioned in untranslated regions (UTRs) (Galante *et al.*, 2004).

These simplified mechanisms outlined in Figure 3.1, are all carried out in a dynamic macromolecular RNA-protein complex identified as a spliceosome (Black, 2003; Chen and Manley, 2009; Wahl, Will and Lührmann, 2009; Mozaffari-Jovin *et al.*, 2014). This complex consists of small nuclear ribonucleoproteins (snRNPs) called U1, U2, U4, U5 and U6 as well as numerous auxiliary protein factors (Black, 2003; Chen and Manley, 2009; Wahl, Will and Lührmann, 2009). Spliceosomes rely upon splicing signals to recognise sequences within the pre-mRNA that include a 5' splice site, a branchpoint and a 3' splice site (Wahl, Will and Lührmann, 2009), as well as splicing regulatory elements (SREs) that are motifs found in pre-mRNA that can have regulatory roles in splice site selection (Black, 2003). SREs can often represent targets for trans-acting factors such as RBPs including Serine and Arginine-rich (SR) proteins and HNRNP proteins. SREs have been classified into exonic splicing silencers (ESS), exonic splicing enhancers (ESE), intronic splicing silencers (ISS) and intronic splicing enhancers (ISE) (Mayeda and Krainer, 1992; Fu, 1995; Long and Caceres, 2009; Busch and Hertel, 2012; Huelga *et al.*, 2012; Zhou and Fu, 2013).

HNRNP A/B protein subfamily members act by binding to ESS or ISS cis-elements on the RNA strand and can disrupt the effect of SR proteins (Mayeda and Krainer, 1992; Caceres *et al.*, 1994; Mayeda *et al.*, 1994; Caputi *et al.*, 1999; Zhu, Mayeda and Krainer, 2001; Olsen *et al.*, 2014; Bruun *et al.*, 2016). Within the HNRNP A/B family, HNRNPA2 and HNRNPA1 have 70% protein homology as well as similar splicing functions like inhibiting 5' and 3' splice site recognition, inhibiting proximal splicing sites and promoting distal 5' splicing site selection (Mayeda *et al.*, 1994). It has also been suggested that HNRNPA2 can bind to the same motif as HNRNPA1 and therefore could compensate for the function of HNRNPA1 protein during

alternative splicing (Mayeda *et al.*, 1994; Caputi *et al.*, 1999; Bilodeau *et al.*, 2001; Zhu, Mayeda and Krainer, 2001; Hutchison *et al.*, 2002; Wu *et al.*, 2018). Despite the protein similarities, HNRNPA2B1 has a relatively weak binding to RNA but higher activity in promoting the selection of distal 5' splice sites compared to HNRNPA1 (Mayeda *et al.*, 1994). HNRNPA2B1 is involved in the alternative splicing of various genes and promotes exon exclusion (Mayeda and Krainer, 1992; Mayeda *et al.*, 1994; Caputi *et al.*, 1999; Bilodeau *et al.*, 2001; Clower *et al.*, 2010; David *et al.*, 2010; Golan-Gerstl *et al.*, 2011; Singh and Singh, 2011; Singh *et al.*, 2011).

Within intron 7 of the Survival of Motor Neuron 1/2 (*SMN1/2)* gene, HNRNPA2B1 binds to an ISS region, leading to a truncated non-functional SMN2 protein as well as depletion of SMN1 protein found to be responsible for spinal muscular atrophy (Hua *et al.*, 2008; Singh and Singh, 2011; Singh *et al.*, 2011).

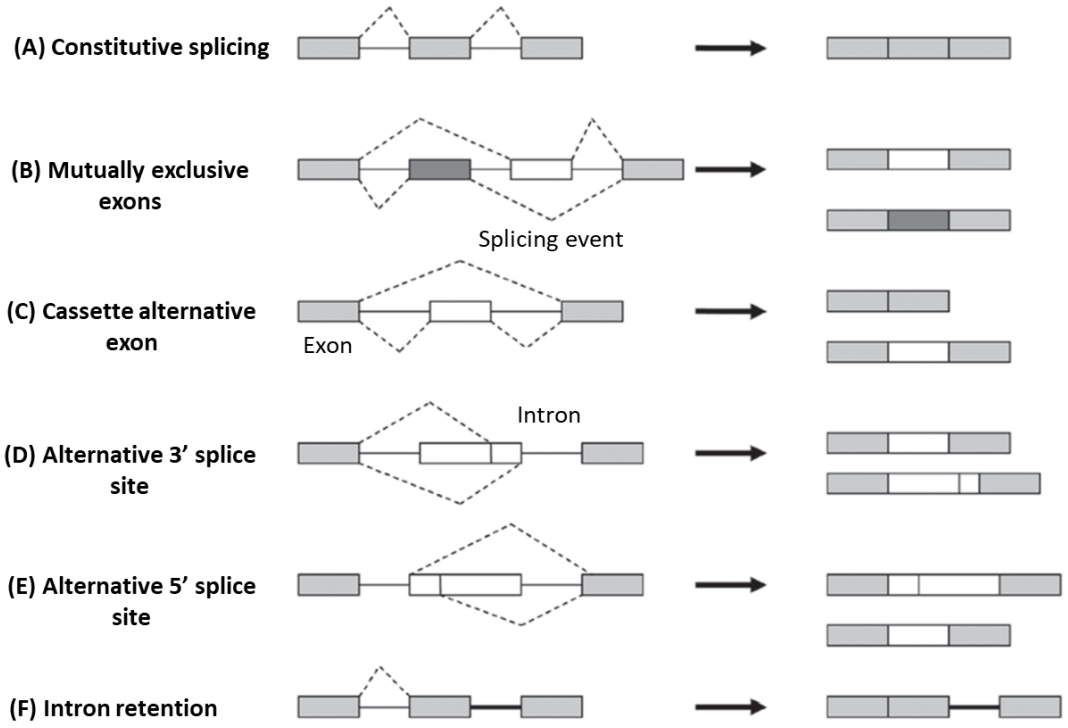


Figure 3.1: Main mechanisms of constitutive and alternative splicing.

(A) *Constitutive splicing,* ***(B)*** *Mutually exclusive exons,* ***(C)*** *Cassette alternative exon,* ***(D)*** *Alternative 3' splice site,* ***(E)*** *Alternative 5' splice site,* ***(F)*** *Intron retention. Modified figure from* (Y. Wang et al., 2015).

HNRNPA1 and HNRNPA2 proteins have also been linked to alternative splicing of the Pyruvate Kinase M1/2 (*PKM*) gene (Clower *et al.*, 2010; David *et al.*, 2010). PKM has two mutually exclusive exons, exon 9 is exclusive to PKM1 protein and exon 10 is exclusive to PKM2 protein, with PKM1 being the predominant isoform in most cell types (Clower *et al.*, 2010; David *et al.*, 2010). HNRNPA1 and HNRNPA2 can either directly or indirectly mediate the repression of exon 9 (the PKM1 protein), resulting in the inclusion of exon 10 (the PKM2 protein) (Clower *et al.*, 2010; David *et al.*, 2010). These changes can be reversed upon the depletion of both HNRNPA1 and HNRNPA2, causing increases in PKM1 transcripts and a decrease in the PKM2 isoform (Clower *et al.*, 2010; David *et al.*, 2010). This increased expression of PKM2 protein over PKM1 protein has been shown to promote aerobic glycolysis, proliferation and tumorigenesis in tumour cell lines and mouse tissues (Clower *et al.*, 2010; David *et al.*, 2010).

Tyrosine kinase receptor, recepteur d'origine nantais (*RON*), is a tumour suppressor gene modulated by the HNRNPA2B1 splicing factor. High HNRNPA2B1 levels in glioblastoma cells promoted the skipping of exon 11 activating a *RON* isoform that promotes invasion (Golan-Gerstl *et al.*, 2011). In the same publication, another tumour suppressor gene known as WW domain-containing oxidoreductase (*WWOX*) was also identified to be targeted by HNRNPA2B1 causing the skipping of exons 6 to 8 (Golan-Gerstl *et al.*, 2011). Other published results observed truncated isoforms of *WWOX* transcripts within breast cancer (Driouch *et al.*, 2002) and oesophageal squamous cell carcinoma samples (Kuroki *et al.*, 2002) by the skipping of exons 5, 6, 7 and 8.

The human *WWOX* gene is located on chromosome 16 and resides within the common fragile site (CFS) known as FRA16D (Ried *et al.*, 2000). Spanning over 1.1 million bases, *WWOX* is comprised of 9 exons with an open reading frame (ORF) of 2241 base pairs long resulting in the transcription of 414-amino acid (46 kDa) protein (Ried *et al.*, 2000). The encoded WWOX protein encompasses two WW domains with two signature tryptophan (W) residues at the N-terminal and a short-chain alcohol dehydrogenase/reductase (ADH/SDR) domain at the C-terminal (Bednarek *et al.*, 2000; Aqeilan *et al.*, 2009; Abu-Odeh, Bar-Mag, *et al.*, 2014). WWOX proteins have over 570 potential interactions currently identified with suggested

involvement in apoptosis, DNA damage response, localisation, metabolism, RNA processing, tight junctions, transactivation, and transcription (Aqeilan *et al.*, 2005; Abu-Odeh, Bar-Mag, *et al.*, 2014; Aqeilan, Abu-Remaileh and Abu-Odeh, 2014; Hussain *et al.*, 2018). One key role WWOX has is to maintain the integrity of the genome (Abu-Odeh, Salah, *et al.*, 2014; Aqeilan, Abu-Remaileh and Abu-Odeh, 2014). The DNA damage response is a complex signalling process, that can either trigger DNA repair, cell cycle arrest or apoptosis if the damage is extensive and unrepairable (Bartek and Lukas, 2007; Harper and Elledge, 2007; Abu-Odeh, Salah, *et al.*, 2014). The positive regulation of the E3 ligase activity of E3 ubiquitin-protein ligase Itchy homologue (ITCH) by ataxia telangiectasia mutated (ATM) can induce the ubiquitination and translocation of WWOX to the nucleus and its association with ATM (Abu-Odeh, Salah, *et al.*, 2014; Taouis *et al.*, 2021). The interaction of nuclear WWOX and ATM leads to the monomerization of ATM and activation of the non-homologous end joining (NHEJ) and homologous recombination (HR). Depletion of WWOX results in delayed activation of the ATM and impeded DNA damage repair (Abu-Odeh, Salah, *et al.*, 2014; Taouis *et al.*, 2021).

Collectively, the literature suggests that the m^{6}A reader HNRNPA2B1 could have either direct or indirect involvement in the DNA damage response as well as resolution of DNA:RNA hybrids. In this chapter, I first aimed to characterise HAP1 HNRNPA2B1 knockout (KO) cells then secondly, examine whether the presence of HNRNPA2B1 affected the metabolism of m^{6}A-marked DNA:RNA hybrids in HAP1 cells.

3.2 Aims

The aim of this chapter is to examine the potential impact of HNRNPA2B1 depletion on the dynamics of DNA:RNA hybrids and m^{6}A that decorate these structures. Using the commercially available HNRNPA2B1 KO cell line and matched wild-type (WT) cell line obtained from Horizon Discovery, we firstly aimed to corroborate the type of HNRNPA2B1 KO present and determine its possible consequences on cell proliferation. Next, we performed immunocytochemistry and m^{6}A-DNA:RNA hybrid and DNA:RNA hybrid immunoprecipitation qPCR in WT and HNRNPA2B1 KO cells to understand whether the removal of HNRNPA2B1

affects the spatial distribution and/or enrichment of DNA:RNA hybrids and m^{6}A-marked DNA:RNA hybrids.

Previously, our group has demonstrated that another m^{6}A interacting gene known as YTH N6-Methyladenosine RNA Binding Protein 2 (YTHDF2), interacts with m^{6}A-marked DNA:RNA hybrids (Abakir *et al.*, 2020). However, unlike YTHDF2 which binds directly to m^{6}A modified RNA, recent publications have suggested that HNRNPA2B1 may not bind directly to m^{6}A on RNA but interact with it by an indirect mechanism known as the "m^{6}A switch" (Wu *et al.*, 2018). To explore whether HNRNPA2B1 acts independently or in association with YTHDF2 when interacting with m^{6}A-marked DNA:RNA hybrids we utilised a YTHDF2 KO cell line and techniques such as immunocytochemistry and chromatin immunoprecipitation qPCR.

Finally, HNRNPA2B1 has a published role in alternative splicing as exonic or intronic splicing silencers (Mayeda *et al.*, 1994). Focussing on one alternative splicing target of HNRNPA2B1, known as *WWOX* (Golan-Gerstl *et al.*, 2011), we used hiPSCs m^{6}A-DRIP and S9.6 DRIP next-generation sequencing datasets, described in (Abakir *et al.*, 2020), to visualise DNA:RNA hybrid loci specific regions in *WWOX* identify potential gene targets and quantify by S9.6 DRIP-qPCR within HNRNPA2B1 KO cells and HAP1 WT cells. We further evaluated whether HNRNPA2B1 or YTHDF2 binding to these regions in *WWOX* introns is altered within HNRNPA2B1 KO cells or YTHDF2 KO cells.

3.3 Results

3.3.1 Characterisation of HAP1 HNRNPA2B1 KO cell line.

The HNRNPA2B1 protein has been associated with several cellular functions (Caputi *et al.*, 1999; Kwon, Barbarese and Carson, 1999; Bilodeau *et al.*, 2001; Domsic *et al.*, 2003; Listerman, Sapra and Neugebauer, 2006; Muslimov *et al.*, 2014) and has been reported to bind to both DNA and RNA (Hudson and Ortlund, 2014; Coppin *et al.*, 2018). Therefore, to determine the importance of HNRNPA2B1 in the biology of m^{6}A-marked DNA:RNA hybrids, an HNRNPA2B1 KO cell line was used. A stable KO was produced using CRISPR/Cas9 technology in a HAP1 cell line (Kotecki, 1999; Carette *et al.*, 2011; Essletzbichler *et al.*, 2014).

Using the CRISPR/Cas-9 editing system, one nucleotide was inserted within the first RRM domain that is present within the 2 isoforms of *HNRNPA2B1* (*HNRNPA2* and *HNRNPB1*).

3.3.1.1 Sanger sequencing confirms the insertion of nucleotide which leads to a frameshift mutation in HNRNPA2B1.

Using PCR, sanger sequencing and online translation tool software, we sought to verify that the HNRNPA2B1 KO cell line disrupts the *HNRNPA2B1* gene and protein expression within HAP1 cells (Fig 3.2). Using primers targeting between exon 1 to exon 5 of HNRNPA2B1 (diagram shown in Fig. 3.4 A) we wanted to identify if the HNRNPA2B1 gene was disrupted past the point of the nucleotide insertion in HAP1 HNRNPA2B1 KO cells (Fig. 3.2). Compared to HAP1 WT cells, the intensity of the band within HNRNPA2B1 KO cells appeared weaker but not completely absent. We next isolated bands from the gels shown in Fig. 3.2 for both HAP1 WT and HNRNPA2B1 KO and performed sanger sequencing. In the forward strand of the HAP1 WT DNA sequence of *HNRNPA2B1*, the red arrow displayed the position of the base pair insertion (Fig 3.3 A). Within the HNRNPA2B1 KO DNA, we identified a nucleotide insertion leading to a possible codon frameshift (Fig. 3.3 B).

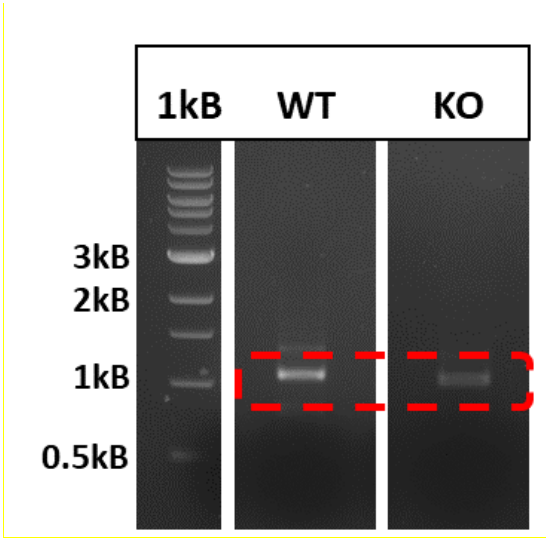


Figure 3.2: PCR analysis of HNRNPA2B1 knockout impacted *HNRNPA2B1* gene transcripts within HNRNPA2B1 KO and WT HAP1 cells.

Phusion PCR with annealing temperature at 55.2°C using HNRNPA2B1 primers spanning exon 1 – 5 in HAP1 WT and HAP1 HNRNPA2B1 KO cells. 1 kb ladder was used.

To comprehend whether a change in the reading frame would impact HNRNPA2B1 protein formation, we analysed the DNA sequence obtained by our Sanger sequencing by an online translation tool (https://web.expasy.org/translate/). The HAP1 WT sequence illustrates the full amino acid sequence for the HNRNPA2B1 protein (Fig. 3.3 C), whereas the HNRNPA2B1 KO sequenced DNA revealed that after insertion of the nucleotide, there is a disruption in the codon reading frame with downstream amino acid sequence changes resulting in an early stop codon (Fig. 3.3 D).

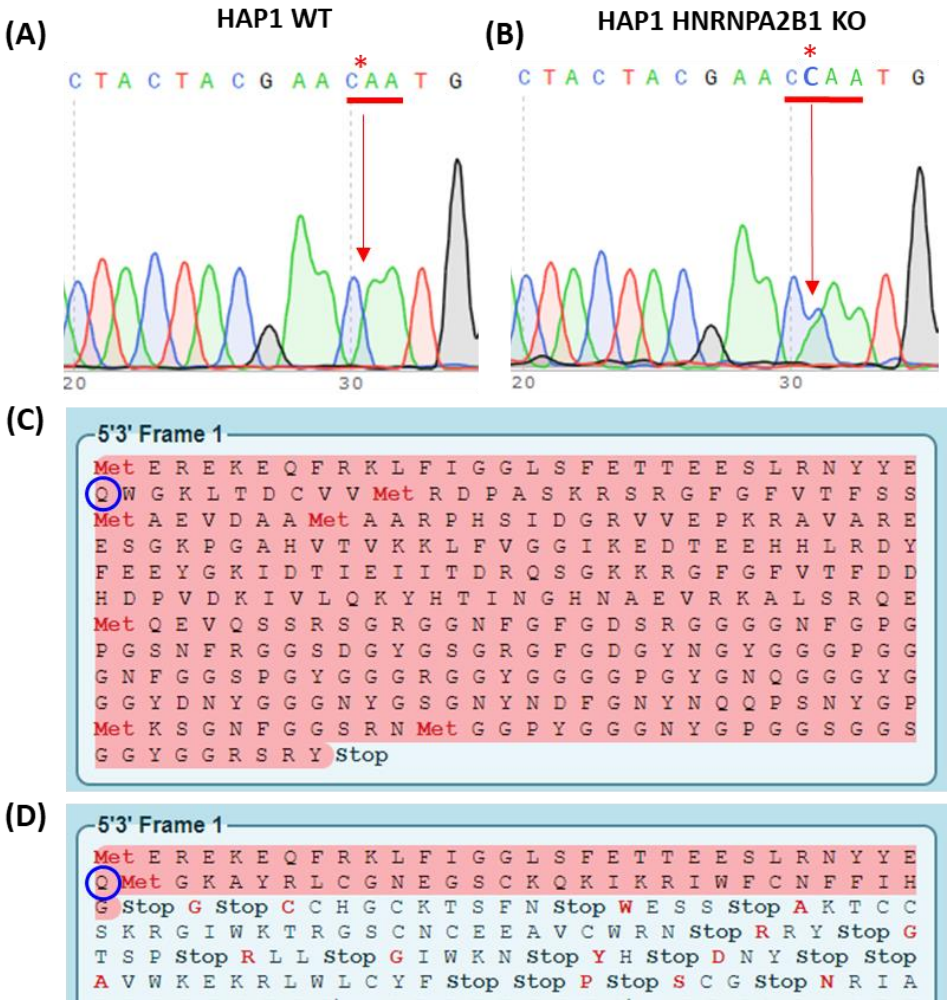


Figure 3.3: Nucleotide insertion causes frame shift mutation within HAP1 HNRNPA2B1 KO cell line from Horizon Discovery.

*Chromas screenshot of HAP1 WT DNA **(A)** and HAP1 HNRNPA2B1 KO **(B)**. Sanger sequencing of the forward strand of HNRNPA2B1. Red arrow and asterisk show the position of base pair insertion.*

*Translation of HNRNPA2B1 WT **(C)** and HNRNPA2B1 KO **(D)** coding sequence (CDS) to amino acid sequence. Blue circle represents the amino acid impacted by nucleotide insertion.*

Together, these results demonstrate that the nucleotide insertion disrupts HNRNPA2B1 functional domains, RRM1 and RRM2 (Fig. 3.4). Compared to the full-length HNRNPA2B1 gene and protein domain structure found in HAP1 WT cells (Fig. 3.4 A), the nucleotide insertion site observed within exon 3 of HNRNPA2B1 in HAP1 HNRNPA2B1 KO cells (Fig. 3.4 B), interrupts the RRM1 domain in HNRNPA2B1 and abolishes the RRM2 domain, suggesting a likely loss of HNRNPA2B1 protein function.

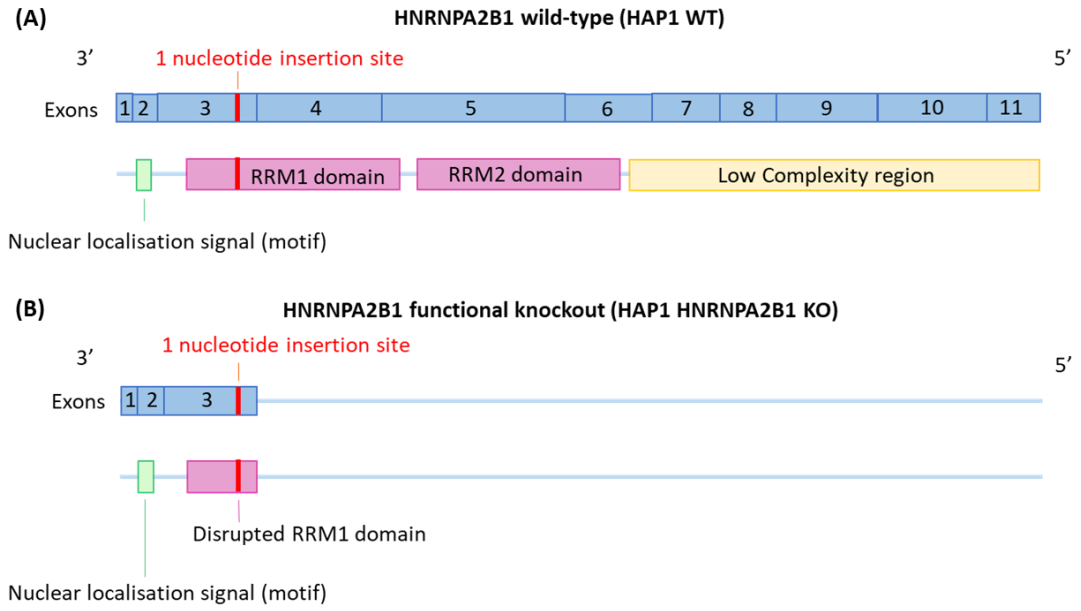


Figure 3.4: Nucleotide insertion results in disruption of both RRM1 and RRM2 domains in HAP1 HNRNPA2B1 KO cells.

*Illustration of the impact of the nucleotide insertion (red line) on the protein structure of HNRNPA2B1 within **(A)** HAP1 WT and **(B)** HAP1 HNRNPA2B1 KO cells. The HNRNPA2 isoform protein structure is shown.*

3.3.1.2 Both isoforms of HNRNPA2B1 are impacted by nucleotide insertion within RRM domains

HNRNPA2B1 has two functional isoforms known as *HNRNPA2* and *HNRNPB1* (Fig. 3.5) (Burd *et al.*, 1989; Kozu, Henrich and Schäfer, 1995). Both isoforms contain RRM1 and RRM2

domains, only differing by a cassette exon that is alternatively spliced out from the *HNRNPA2* isoform but retained in the *HNRNPB1* isoform. The nucleotide insertion site identified in the HAP1 HNRNPA2B1 KO cells resides within a conserved region of both isoforms (Fig. 3.5).

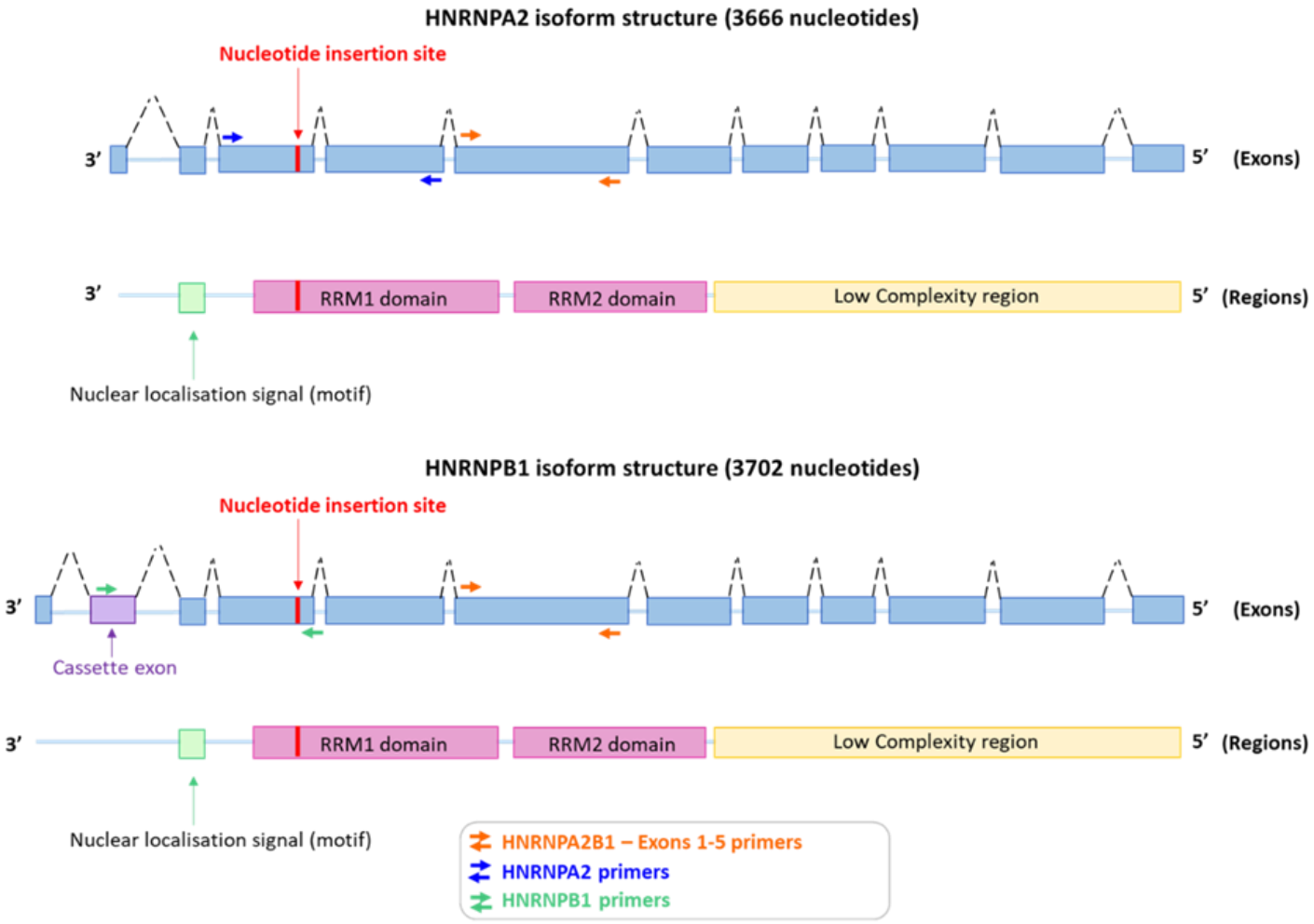


Figure 3.5: Structural differences between HNRNPA2B1 isoforms, HNRNPA2 and HNRNPB1.

Alternative splicing differences between HNRNPA2 and HNRNPB1 isoform structure. The inclusion of the cassette exon within the HNRNPB1 isoform is shown by an additional purple exon which is excluded in the HNRNPA2 isoform. The red line illustrates the nucleotide insertion in both isoforms. Primer positions for downstream HNRNPA2B1 primers (orange arrows) shown in (Fig. 3.6 A); HNRNPA2 isoform primers over nucleotide insertion (blue arrows) and HNRNPB1 isoform primers over nucleotide insertion (green arrows) shown in (Fig. 3.6 B).

To test if the gene expression of *HNRNPA2B1* downstream from the frameshift mutation is affected, primers were designed to span from exon 1 to exon 5 (primers location indicated by the orange arrows in Fig 3.5). The expression of the *HNRNPA2B1* mRNA region containing exons 1–5 had a significant decrease of 97.5% in HAP1 HNRNPA2B1 KO cells compared to HAP1 WT ($p = 0.000071$, Fig. 3.6 A). Primers were also designed around the base pair insertion in the *HNRNPA2* isoform (primers location indicated by the blue arrows in Fig 3.5) and in *HNRNPB1* including the cassette exon (primers location indicated by the green arrows in Fig 3.5). The expression of these mRNA regions within both the *HNRNPA2* isoform and the *HNRNPB1* isoform had a reduction of 97% and 70%, respectively (Fig. 3.6 B).

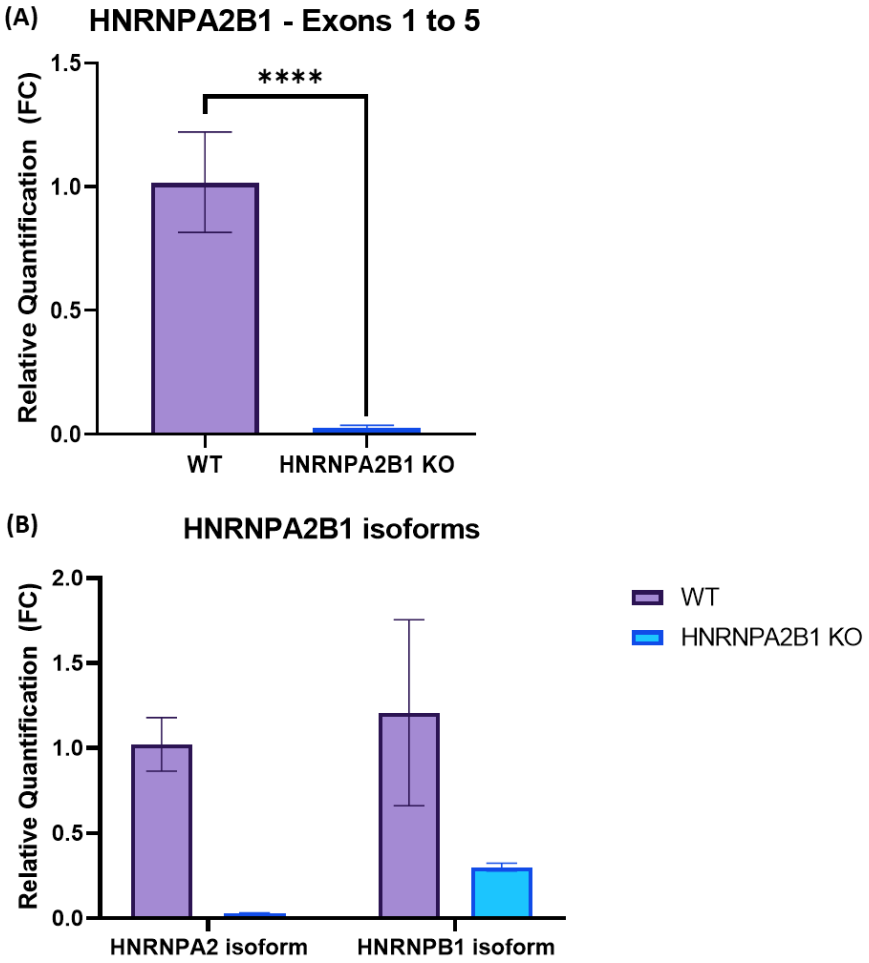


Figure 3.6: Nucleotide insertion reduces the mRNA transcripts of both *HNRNPA2* and *HNRNPB1* isoforms.

(A) *The results of the qPCR showing HNRNPA2B1 gene expression with exons 1 – 5 primers comparing WT to HNRNPA2B1 KO cells. Mean ± SEM, 2 biological replicates each with 3 technical replicates, unpaired t-test, **** = p < 0.0001* ***(B)*** *HNRNPA2 and HNRNPB1 isoform gene expression of HNRNPA2B1 KO compared to WT. Mean ± SEM, 1 biological replicate with 3 technical replicates.*

3.3.1.3 Cell proliferation is marginally affected by KO of HNRNPA2B1 in HAP1 cells.

Previous work from our group identified that the loss of an m^6A interacting protein YTHDF2 impacted cell proliferation of HAP1 cells (Abakir *et al.*, 2020). To observe whether HNRNPA2B1 has a similar impact on cell proliferation, we cultured HAP1 WT and HNRNPA2B1 KO cells over 10 days starting with 2000 cells seeded on 24-well plates (Fig. 3.7). On day 5 ($p = 0.5974$), day 6 ($p = 0.9807$) and day 7 ($p = 0.5072$) no significant difference

was observed in the proliferation rate between WT and HNRNPA2B1 KO cells. After 8 days in culture, there was a mean difference of 897,000 cells between WT cells and HNRNPA2B1 KO cells (p = 0.0969). This difference was continued to be observed in day 9 (p = 0.02427) and day 10 of culture (p = 0.4339).

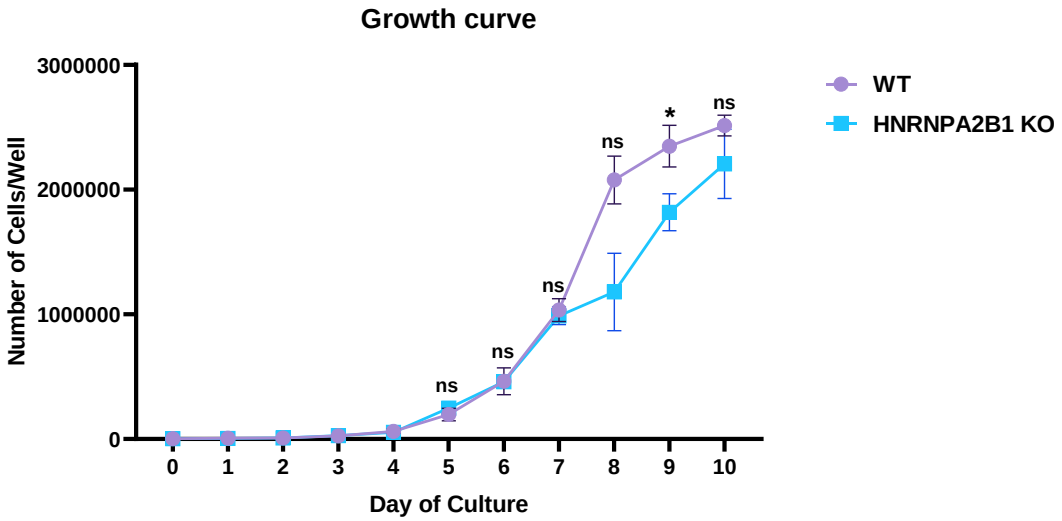


Figure 3.7: Silencing of *HNRNPA2B1* has no significant impact on cell proliferation.

*Growth curve comparing cell proliferation rates of HNRNPA2B1 KO cells and its WT counterpart. Mean ± SEM, paired t-test, * = p < 0.05, 3 biological replicates.*

3.3.2 Knockout of HNRNPA2B1 impacts the levels of DNA:RNA hybrids dependent upon their location in the genome.

After validation of the KO of HNRNPA2B1 in HAP1 cells, our next aim was to examine if silencing HNRNPA2B1 had any impact on DNA:RNA hybrids or m^6A-DNA:RNA hybrids within HAP1 cells. Previous results from our lab used siRNA transfection to silence HNRNPA2B1 in human pluripotent stem cells (hiPSCs) (Abakir *et al.*, 2020) and showed that siHNRNPA2B1 knockdown (KD) leads to increased immunostaining of a double-strand DNA damage repair marker, γ-H2AX. Therefore, we wanted to corroborate and expand on previous HNRNPA2B1 siRNA transfections by using HAP1 HNRNPA2B1 KO cells and using qPCR, immunostaining, SID-UPLC-MS/MS, S9.6 DRIP qPCR and m^6A DRIP qPCR.

3.3.2.1 Depletion of HNRNPA2B1 has a mixed influence on gene expression of m^{6}A related genes and DNA:RNA hybrid related genes.

To examine whether KO of *HNRNPA2B1* impacts the gene expression of other m^{6}A-related genes, we compared the expression of genes involved in the addition of m^{6}A (*METTL3* and *METTL14*) and interacting with m^{6}A modified RNA (*YTHDF2*, *YTHDC1*) in HAP1 WT and HAP1 HNRNPA2B1 KO cells (Fig. 3.8 A). There was a non-significant increase in *METTL3* by 3.45 – fold within HNRNPA2B1 KO cells ($p = 0.1097$) as the error bars indicate variance between the replicates. Likewise, there was no notable change in *METTL14* (24.4% decrease, $p = 0.2083$) and *YTHDF2* (1.97 – fold increase, $p = 0.3503$). Yet, we observed a significant (by 1.83 – fold, $p = 0.0363$) increase in the expression of *YTHDC1* mRNA. Next, we evaluated whether the loss of HNRNPA2B1 impacted genes involved in the resolution of DNA:RNA hybrids (Fig 3.8 B). An increase of 4.1 – fold ($p = 0.0527$) was observed in *DHX9* in HNRNPA2B1 KO cells compared to WT cells, but no significant change was noted for *DDX3X* helicase (13.8% decrease, $p = 0.0904$).

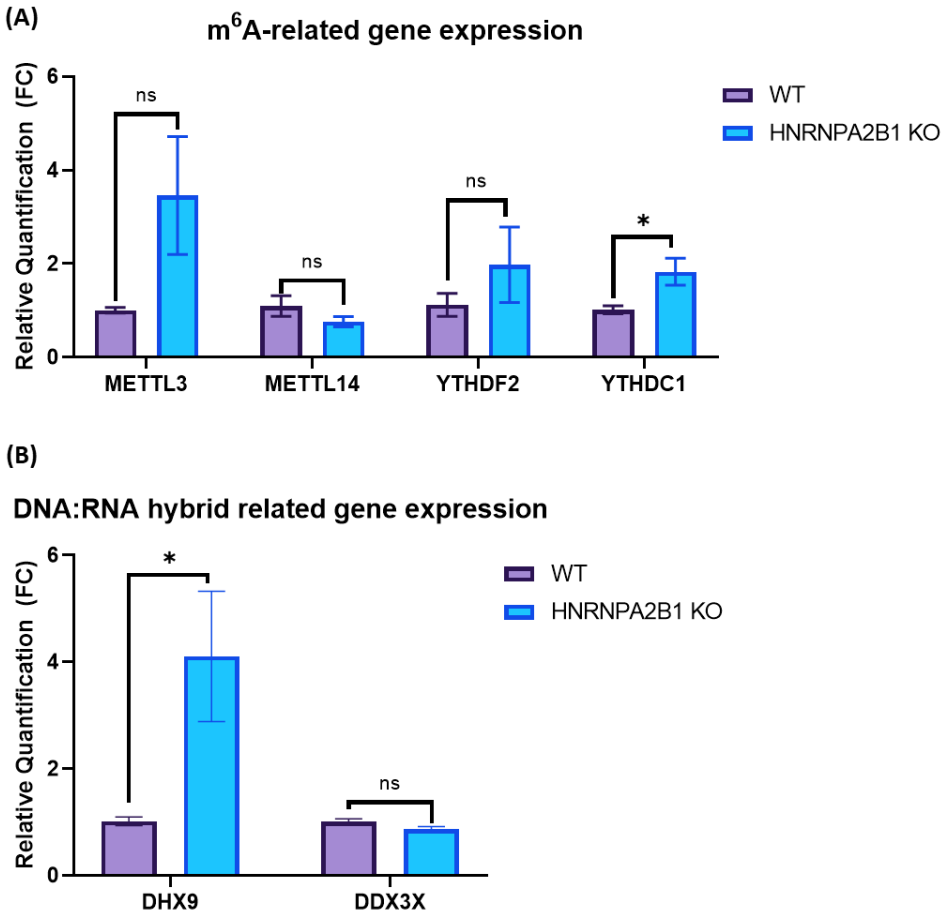


Figure 3.8: Knockout of HNRNPA2B1 significantly increases expression of DNA:RNA hybrid helicase gene, *DHX9*.

The results of the qPCR showing the expression of genes related to m^{6}A and DNA:RNA hybrids separately, comparing WT to HNRNPA2B1 KO cells. ***(A)*** *Key genes involved in the addition of m^{6}A (METTL3 and METTL14) and interaction with RNA transcripts with m^{6}A present (YTHDF2 and YTHDC1).* ***(B)*** *Genes involved in the maintenance of DNA:RNA hybrid levels within the genome (DHX9 and DDX3X). Mean ± SEM, 2 biological replicates each with 3 technical replicates. Unpaired t-test, ns = p ≥ 0.05, * = p < 0.05.*

3.3.2.2 HNRNPA2B1 KO cells display no difference in the levels of DNA:RNA hybrids in immunostaining experiments.

Gene expression analysis suggested an elevated expression of the DNA:RNA hybrid helicase, *DHX9*, within HNRNPA2B1 KO cells compared to WT expression (Fig. 3.8). Therefore, we next checked the levels of DNA:RNA hybrids in HNRNPA2B1 KO cells, as HNRNPA2B1 is an

m^{6}A reader, we wanted to observe any changes in DNA:RNA hybrid signal in a similar manner to KO of another m^{6}A reader, *YTHDF2* (Abakir *et al.*, 2020). We performed immunostaining of DNA:RNA hybrids in WT and HNRNPA2B1 KO cells using an anti-DNA:RNA hybrid antibody known as clone S9.6 (Fig. 3.9). Looking at the immunocytochemical images in Fig. 3.9 A - B, there is non-specific cytoplasmic immunostaining despite DNA:RNA hybrids remaining primarily in the nucleus. Other studies have also observed this in their DNA:RNA hybrid immunostaining experiments and have attributed it to the S9.6 antibody having a binding affinity for both DNA:RNA hybrids and double-stranded RNA (Boguslawski *et al.*, 1986; Hu *et al.*, 2006; Phillips *et al.*, 2013). Next, we quantified the pixel intensity of the DNA:RNA hybrid signal in the nuclei of WT and HNRNPA2B1 KO cells (Fig. 3.9 C). In these experiments, we did not detect any significant difference ($p = 0.7808$) but noticed large variations in the individual pixel staining intensity in both WT and HNRNPA2B1 KO cells.

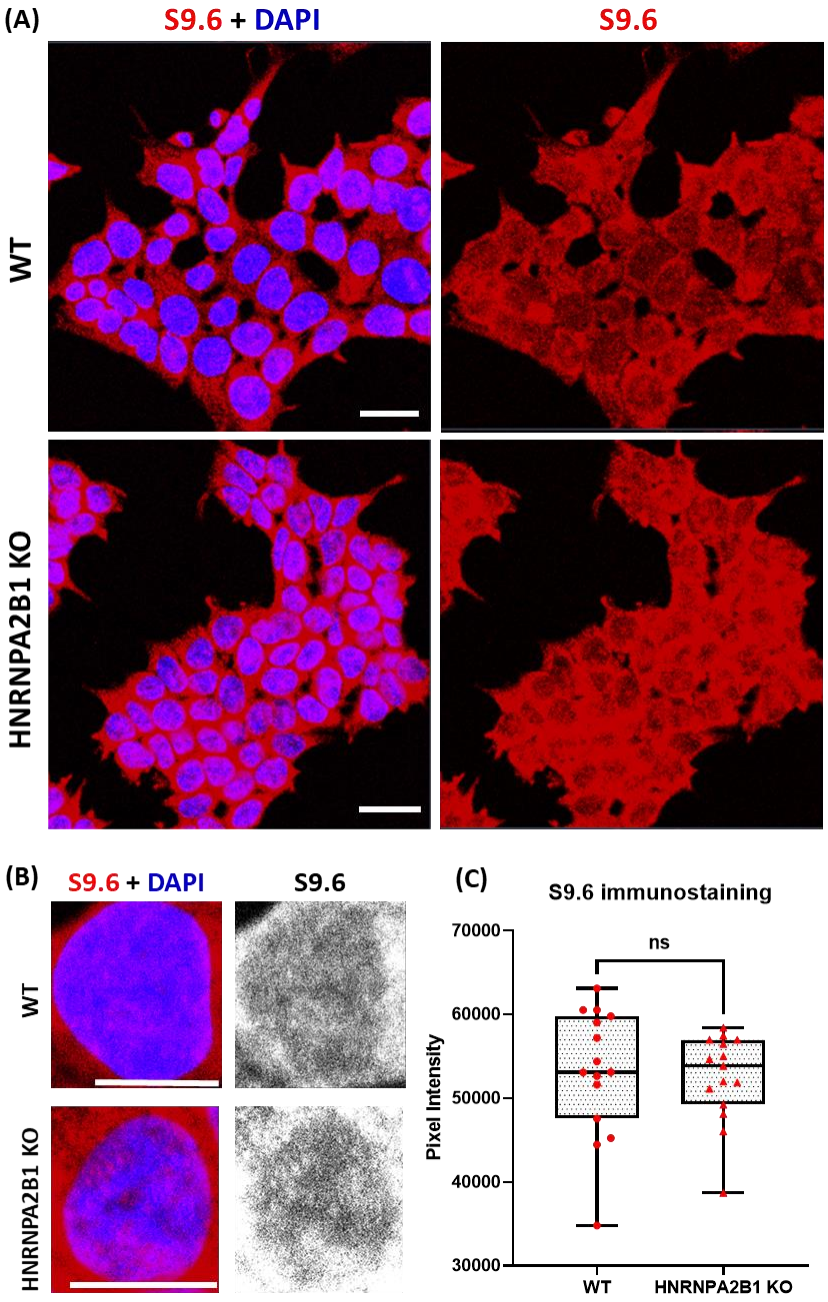


Figure 3.9: High variability of DNA:RNA hybrid staining in HAP1 wild-type and HNRNPA2B1 KO cells.

(A) *Immunostaining with DNA:RNA hybrid antibody (S9.6 clone) and DAPI nuclear staining in HAP1 WT and HNRNPA2B1 KO cells. Representative image shown from 4 technical replicates. Scale bar represents 20 µM.* ***(B)*** *Single cell comparison of S9.6 immunostaining within WT and HNRNPA2B1 KO cells. Scale bar represents 5 µM.* ***(C)*** *Quantification boxplot of HAP1 WT and HNRNPA2B1 KO cells in 15 nuclei. Values had normal distribution and were evaluated using unpaired t-test, ns = $p \geq 0.05$.*

3.3.2.3 HNRNPA2B1 KO and WT cells display no significant difference in the levels of immunostaining of DNA damage indicator, γ-H2AX.

To examine whether HNRNPA2B1 depletion promotes double-stranded breaks similar to YTHDF2 depletion in HAP1 cells, we performed immunostaining for an indicator of DNA damage repair, phosphorylated histone variant of H2AX known as γ-H2AX (Fig. 3.10 A). In immunostaining with anti – γ-H2AX antibody in HAP1 WT and HAP1 HNRNPA2B1 KO cells (Fig. 3.10 B), we observed variations in the presence of γ-H2AX between different nuclei in both WT and HNRNPA2B1 KO cells. When we quantified the pixel intensity of 20 nuclei in WT and HNRNPA2B1 KO nuclei, we observed a large amount of disparity in pixel intensity within WT cells and less in variation the HNRNPA2B1 KO cells but overall, no significant difference in γ-H2AX signal was detected in our experiments ($p = 0.0730$, Fig. 3.10 C).

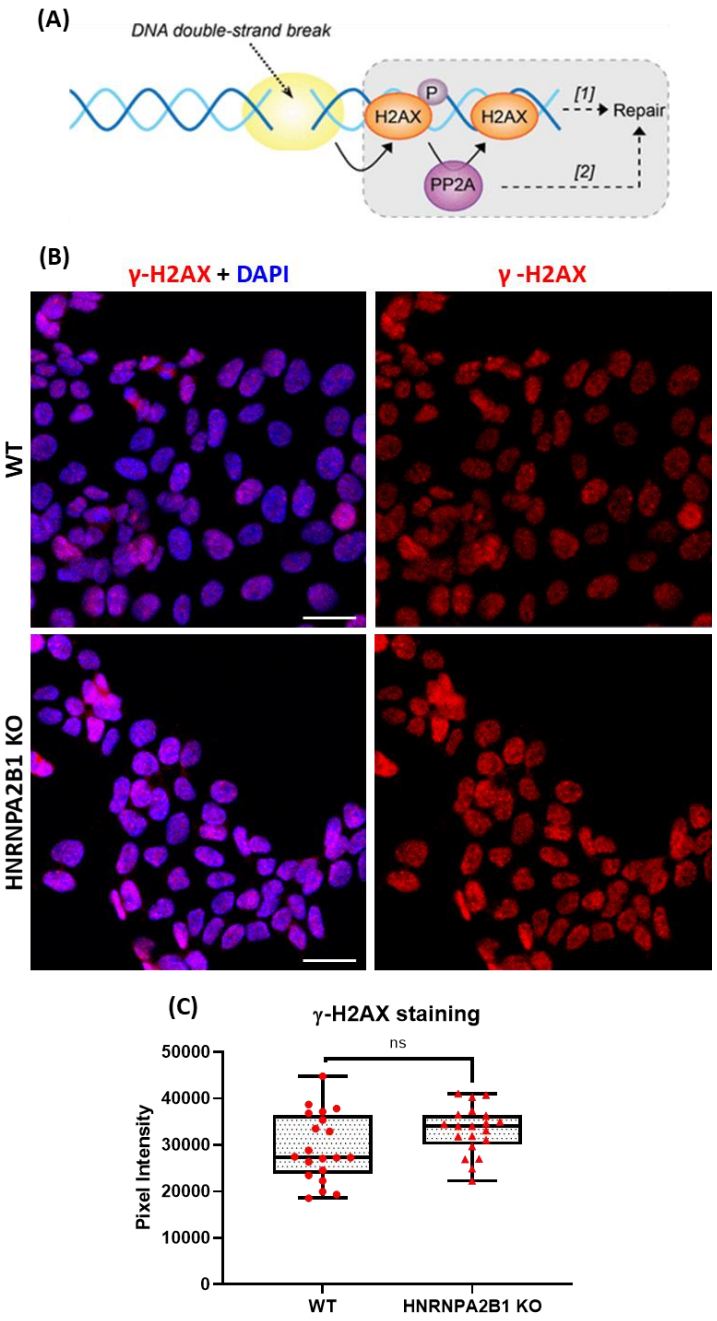


Figure 3.10: No difference in γ-H2AX immunostaining in HNRNPA2B1 KO compared to HAP1 WT cells.

(A) *Diagram illustrating histone H2AX role in repairing double stranded breaks. Modified* from (Mamouni *et al.*, 2014). ***(B)*** *Immunostaining for phosphorylated histone variant γH2AX and DAPI in WT and HNRNPA2B1 KO cells. Representative image shown from 4 technical replicates. Scale bar represents 20 μM.* ***(C)*** *Quantification boxplot of WT and HNRNPA2B1 KO cells in 20 nuclei of each. Values had normal distribution and were evaluated using unpaired t-test, ns = p ≥ 0.05.*

3.3.2.4 Mass spectrometry suggests a decrease in the levels of m^{6}A on DNA:RNA hybrids within HNRNPA2B1 KO cells.

To confirm our results on DNA:RNA hybrids, we aimed to test if HNRNPA2B1 depletion impacts the global levels of m^{6}A-marked DNA:RNA hybrids in the genome. To analyse the genome levels of m^{6}A-DNA:RNA hybrids, we utilised a technique to detect the release of m^{6}A in the filtrate by stable-isotope dilution ultra-performance liquid chromatography with tandem mass spectrometry (SID-UPLC-MS/MS) with and without RNase H treatment (Abakir *et al.*, 2020). We used this technique to examine the m^{6}A levels on DNA:RNA hybrids in both HAP1 WT and HNRNPA2B1 KO cells (Fig. 3.11). We focused on the small fragments that pass through the filtrate after treatment with RNase H, as these fragments almost certainly originate in RNase H degraded DNA:RNA hybrids (Fig. 3.11 A). We observed a non-significant decrease in m^{6}A-marked DNA:RNA hybrids from 5.52 fmol of m^{6}A per 1 µg of genomic DNA in WT RNase H treated filtrate to 3.43 fmol/µg of methylated adenosines in HNRNPA2B1 KO RNase H-treated filtrate ($p = 0.1631$). Although our main focus was HNRNPA2B1 role in the biology of m^{6}A marked DNA:RNA hybrids, HNRNPA2B1 initially was linked to m^{6}A presence on single-stranded RNA (Fig. 3.11 B). Similar to DNA:RNA hybrids results, we did not detect any significant difference in methylated adenosine present on non-treated filtrate samples from 0.16% (m^{6}A/A) in WT to 0.19% (m^{6}A/A) of methylated adenosines on RNA in HNRNPA2B1 KO samples ($p = 0.2056$).

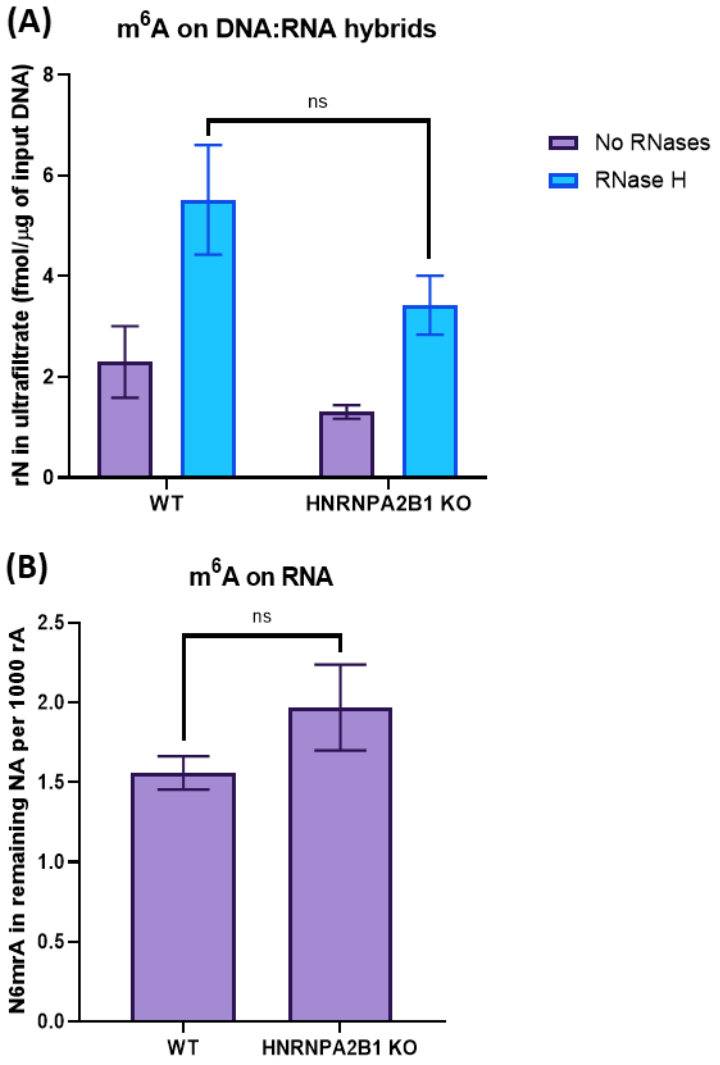


Figure 3.11: Knockout of HNRNPA2B1 appears to affect the genomic levels of m^{6}A-marked DNA:RNA hybrids differently compared to m^{6}A modified RNA.

(A) *SID–UPLC–MS/MS quantification of m^{6}A within the fractions of HAP1 WT-derived and HAP1 HNRNPA2B1 KO-derived nucleic acids released following RNase H treatment.* ***(B)*** *Ribonucleotides obtained from the quantification of SID–UPLC–MS/MS peaks in untreated HAP1 WT and HNRNPA2B1 KO RNA. Mean ± SD, 3 biological replicates, unpaired t-test, ns = $p \geq 0.05$.*

3.3.2.5 DNA:RNA hybrids are enriched within repetitive and specific intronic sequences in HNRNPA2B1 KO cells.

DNA:RNA hybrid immunoprecipitation (DRIP) is an antibody-based approach to looking at the genomic distribution of DNA:RNA hybrids that can be used for locus-specific assessment of their enrichment. Using this technique, we wanted to examine if the loss of HNRNPA2B1 led

to changes in the levels of DNA:RNA hybrids in the R-loop prone loci previously identified by next-generation sequencing in human-induced pluripotent stem cells (hiPSCs). Firstly, we compared the enrichment of DNA:RNA hybrids between WT and HNRNPA2B1 KO cells in Alpha-satellites (*α-satellites*) (Fig. 3.12 A) and *LINE1* (Fig. 3.12 B). We observed an enrichment of DNA:RNA hybrids in HNRNPA2B1 KO by 1.512 – fold in *α-satellites* and 1.379 – fold enrichment within *LINE1* in comparison to WT cells. Other repetitive sequences such as *Alu-Y* (Fig. 3.12 C) and *Alu-S* (Fig. 3.12 D) possessed an increase in DNA:RNA hybrid enrichment of 5.92 – fold and 9.33 – fold, correspondingly in HNRNPA2B1 KO compared to WT cells.

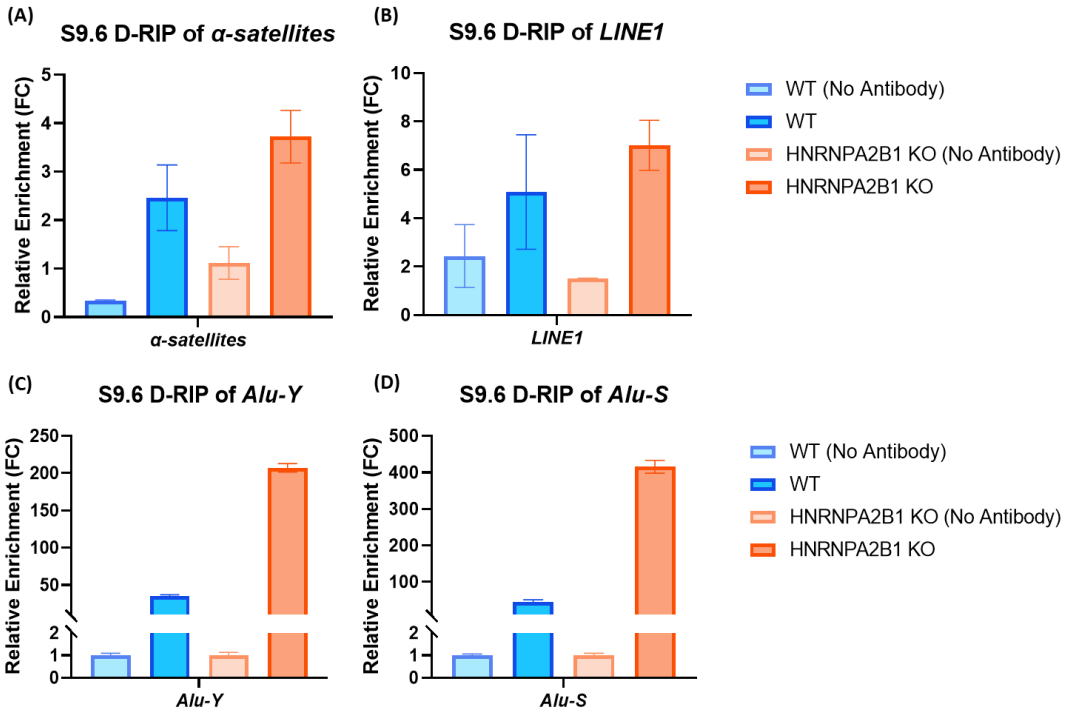


Figure 3.12: Knockout of HNRNPA2B1 led to increased enrichment of DNA:RNA hybrids in SINE/*Alu* elements.

DNA:RNA hybrid immunoprecipitation qPCR comparison of repetitive elements: ***(A)*** *α-satellites,* ***(B)*** *LINE1, SINE elements* ***(C)*** *Alu-Y and* ***(D)*** *Alu-S within HAP1 WT and HNRNPA2B1 KO cells. No antibody controls were used for both HAP1 WT and HNRNPA2B1 KO cells. FC = Fold change. Mean ± SEM, 1 biological replicate with 3 technical replicates.*

Subsequently, we wanted to evaluate whether increases in DNA:RNA hybrids had a similar pattern in intronic sequences. Contrasting with repetitive sequences that exhibited a degree of enrichment from WT to HNRNPA2B1 KO cells, it appears that DNA:RNA hybrid presence in intronic sequences depends upon the gene (Fig. 3.13). While *MYH16* (Fig. 3.13 A) has a fold enrichment of 25.14 – fold, *HECW1* (Fig. 3.13 B) has an 80.87 – fold decrease of DNA:RNA hybrids from WT to HNRNPA2B1 KO.

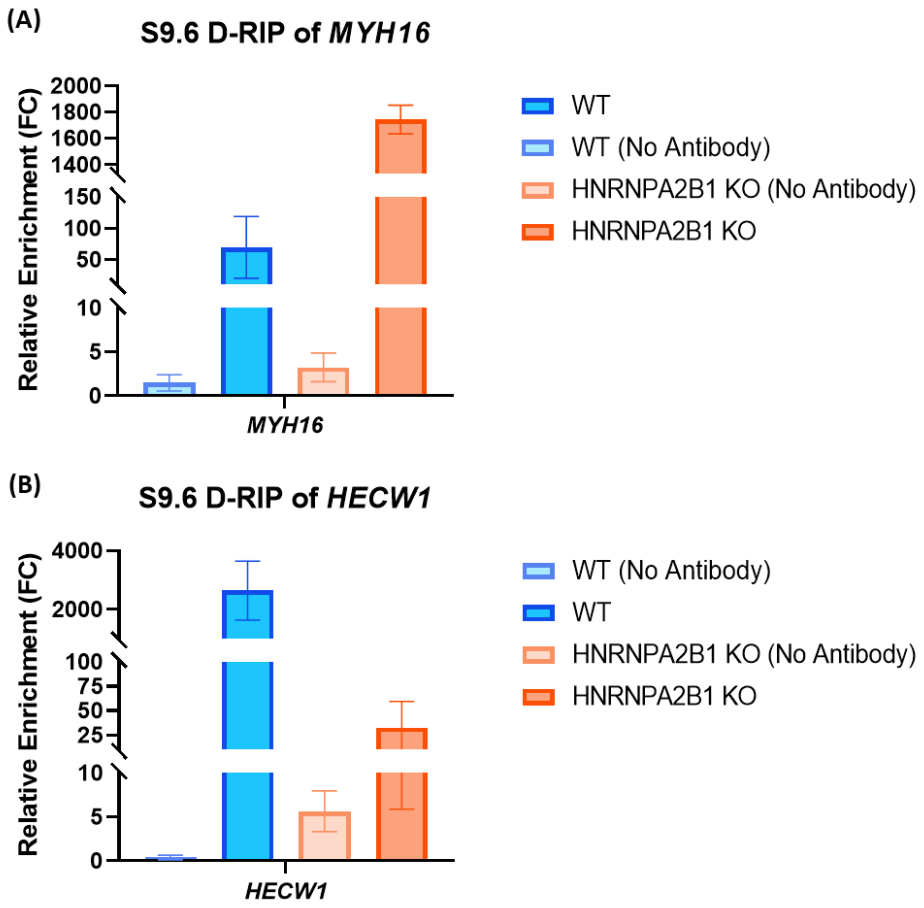


Figure 3.13: Knockout of HNRNPA2B1 led to increased enrichment of DNA:RNA hybrids in *MYH16* and decreased in *HECW1*.

DNA:RNA hybrid immunoprecipitation qPCR comparison of intronic sequences, ***(A)*** *MYH16 and* ***(B)*** *HECW1, within WT and HNRNPA2B1 KO cells. No antibody controls were used for both HAP1 WT and HNRNPA2B1 KO cells. FC = Fold change. Mean ± SEM, 1 biological replicate with 3 technical replicates.*

3.3.2.6 m^{6}A-marked DNA:RNA hybrids are reduced within repetitive sequences but increased in specific intronic sequences in HNRNPA2B1 KO cells.

To quantify m^{6}A-DNA:RNA hybrids within locus-specific sequences, we used a modified DRIP protocol that utilises an m^{6}A antibody instead of a DNA:RNA hybrid antibody (Fig. 2.1) (Abakir *et al.*, 2020). Looking at m^{6}A-DNA:RNA hybrids presence within repetitive elements, we observed a decrease in m^{6}A-enrichment within *α-satellites* by 10.42 – fold decrease (Fig. 3.14 A), *LINE1* by 7.41 – fold decrease (Fig. 3.14 B), *Alu-Y* by 16.42 – fold decrease (Fig. 3.14 C) and *Alu-S* by 46.71 – fold decrease (Fig. 3.14 D) sequences in HNRNPA2B1 KO comparing HAP1 WT. In HNRNPA2B1 KO cells, for nearly all repetitive sequences, except *LINE1* elements, m^{6}A relative signal was lower than the no antibody control representing the background signal, suggesting that m^{6}A-DNA:RNA hybrids are present at very low levels in the HNRNPA2B1 KO cells at these loci. Next, we wanted to determine if m^{6}A marked DNA:RNA hybrids within intronic sequences showed a similar pattern to what was observed in repetitive sequences (Fig. 3.15). Remarkably, both *MYH16* (Fig. 3.15 A) and *HECW1* (Fig. 3.15 B) have an increase of m^{6}A-enrichment by 18.17 – fold and 1937.85 – fold, respectively compared to HAP1 WT cells.

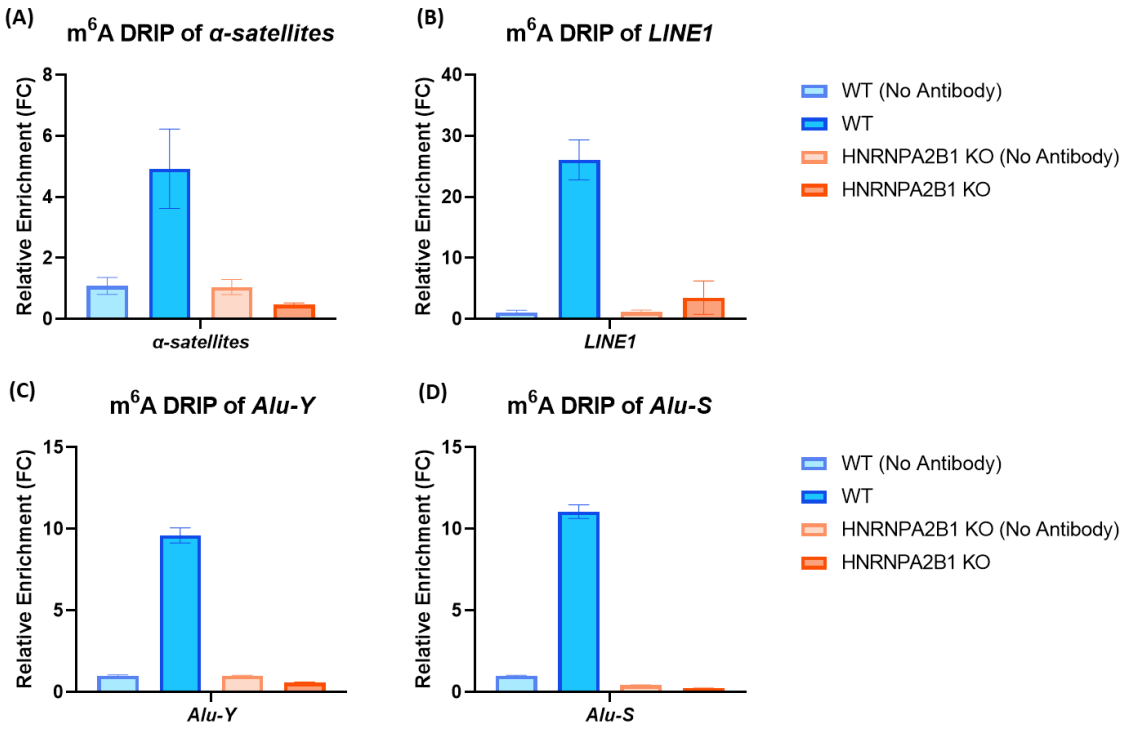


Figure 3.14: HNRNPA2B1 KO led to decreased levels of m^{6}A-DNA:RNA hybrids within repetitive elements.

m^{6}A-DNA:RNA hybrid immunoprecipitation qPCR comparison of repetitive elements: ***(A)*** *α-satellites,* ***(B)*** *LINE1 and SINE elements* ***(C)*** *Alu-Y and* ***(D)*** *Alu-S within WT and HNRNPA2B1 KO cells. No antibody controls were used for both HAP1 WT and HNRNPA2B1 KO cells. FC = Fold change. Mean ± SEM, 1 biological replicate with 3 technical replicates.*

Overall, the results in this section suggest that knockout of HNRNPA2B1 in HAP1 cells has a mixed impact on DNA:RNA hybrids dependent upon the gene and type of repetitive elements. Yet, the knockout of HNRNPA2B1 in HAP1 cells appeared to decrease levels of m^{6}A-marked DNA:RNA hybrids in all tested repetitive elements but increased enrichment in the examined intronic sequences. The pattern observed in m^{6}A-marked DNA:RNA hybrids after depletion of HNRNPA2B1 could suggest a direct or indirect interaction and possible involvement of HNRNPA2B1 in regulating the dynamics of m^{6}A on DNA:RNA hybrids.

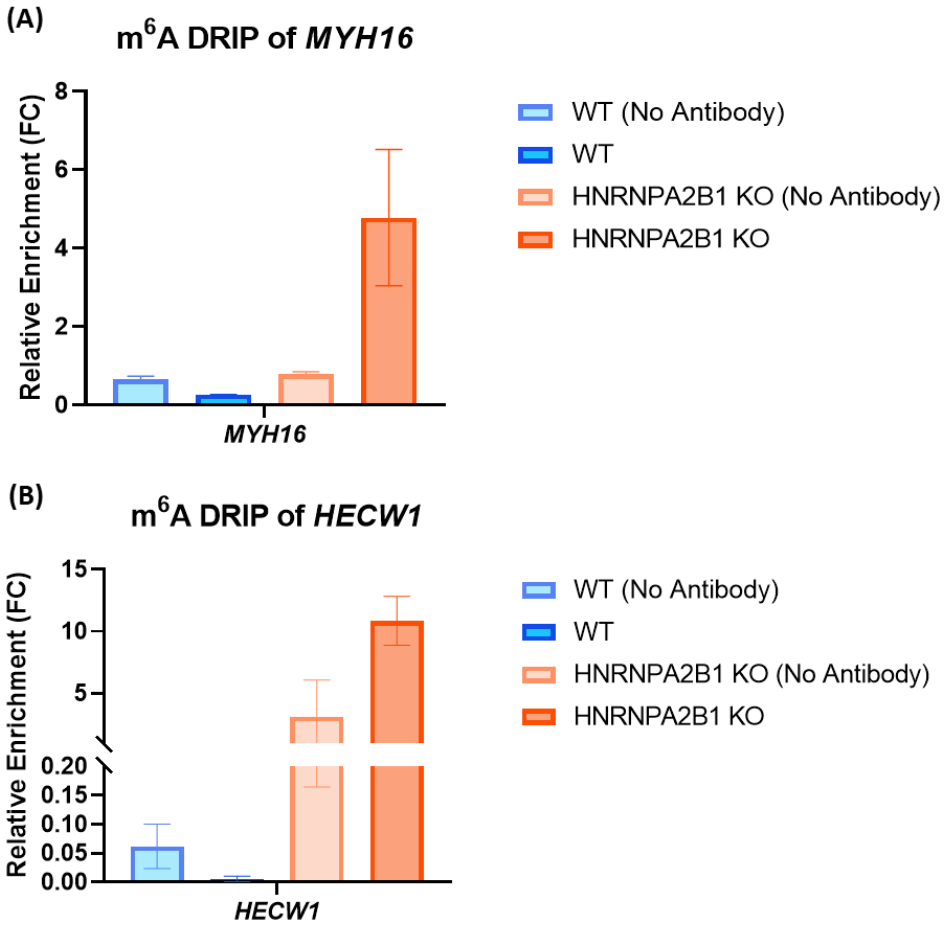


Figure 3.15: Knockout of HNRNPA2B1 led to increased enrichment of m^{6}A-DNA:RNA hybrids within *MYH16* and *HECW1*.

m^{6}A-*DNA:RNA hybrid immunoprecipitation qPCR comparison of intronic sequences,* ***(A)*** *MYH16 and* ***(B)*** *HECW1, within WT and HNRNPA2B1 KO cells. No antibody controls were used for both HAP1 WT and HNRNPA2B1 KO cells. FC = Fold change. Mean ± SEM, 1 biological replicate with 3 technical replicates.*

3.3.3 Interplay between HNRNPA2B1 and YTHDF2 when interacting with m^{6}A-marked DNA:RNA hybrids.

In this chapter, we have found that knockout of HNRNPA2B1 in HAP1 cells impacts m^{6}A-marked DNA:RNA hybrids differently depending upon where they reside in the genome. Yet, a recent publication has suggested that HNRNPA2B1 does not bind directly with m^{6}A but indirectly by an "m^{6}A switch" mechanism (Wu *et al.*, 2018). Thus, we decided to explore whether HNRNPA2B1 interacts with other proteins to impact m^{6}A-marked DNA:RNA hybrid

genome levels. One possible candidate was YTHDF2 since previous work by our group has identified that this m^{6}A-interacting gene can also interact with DNA:RNA hybrids and could be involved in their regulation (Abakir *et al.*, 2020). Using database analysis, gene expression analysis, immunocytochemistry, and chromatin immunoprecipitation (ChIP), we aimed to understand if there is a possible interplay between HNRNPA2B1 and YTHDF2.

3.3.3.1 HNRNPA2B1 protein interactome suggests co-expression and interaction with YTHDF2, spliceosome and DNA:RNA hybrid maintenance proteins.

To understand if m^{6}A-, DNA:RNA hybrids and the spliceosome-related proteins might interact with HNRNPA2B1 in human cells, we used a STRING database (https://string-db.org/) that evaluates known and predicted interactions of proteins in various human cell types (Fig. 3.16 – 3.18). This analysis demonstrated that HNRNPA2B1 protein has the strongest interaction with two spliceosome proteins (SRSF3 and SRSF10) and a DNA:RNA hybrid maintenance protein, DHX9, representing curated databases (light blue), experimentally determined (pink), text mining (light green) and co-expression (black) edges. HNRNPA2B1 interaction with YTHDF2 is only a suggested interaction by text-mining and co-expression data (Fig. 3.16 A – B).

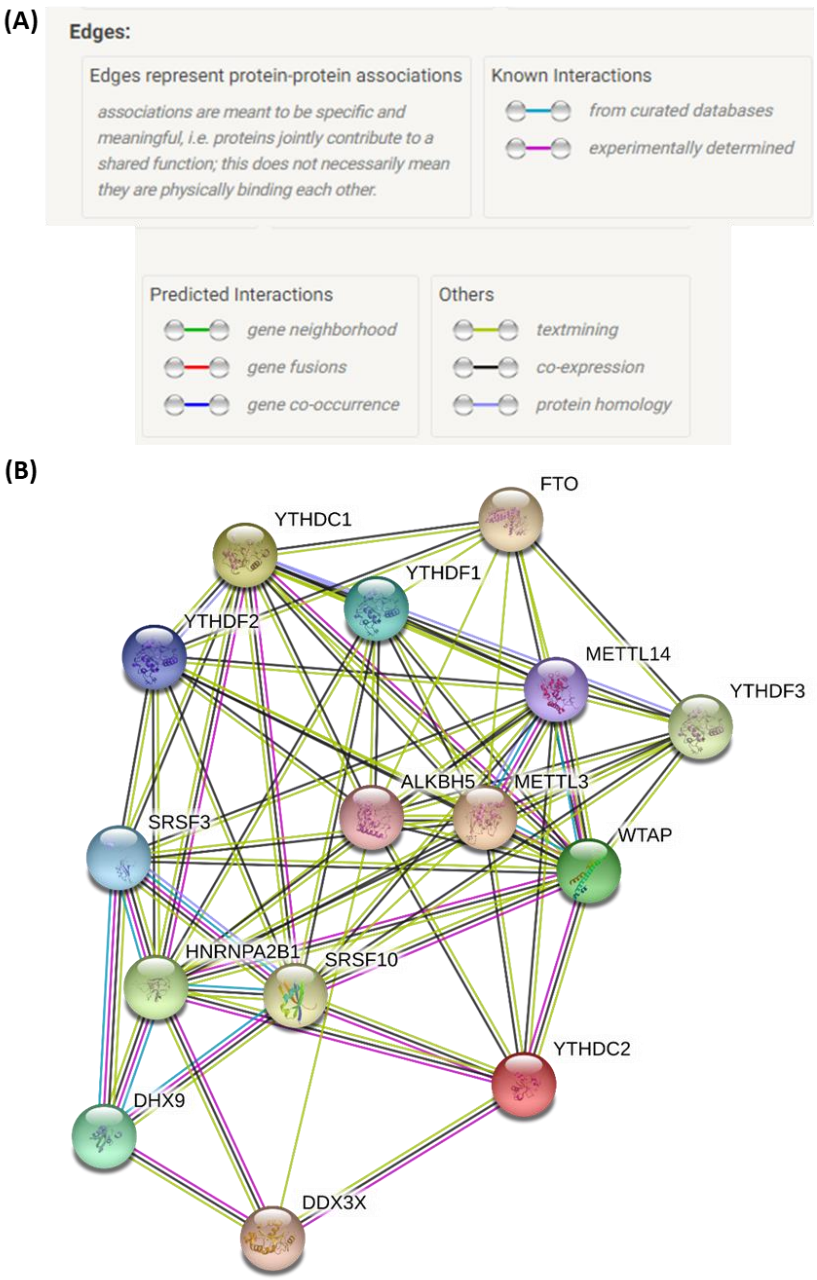


Figure 3.16: Protein-protein interactome network suggests functional protein interactions between HNRNPA2B1, SRSF3, SRSF10, DHX9 and DDX3X.

(A) *Description of the meaning of the coloured lines/edges seen in the protein-protein interactome diagram.* ***(B)*** *STRING known and predicted protein-protein interactome map of m^{6}A-related proteins (METTL3, METTL14, WTAP, YTHDF1, YTHDF2, YTHDF3, YTHDC1, YTHDC2, HNRNPA2B1, FTO, ALKBH5), spliceosome related proteins (SRSF3 and SRSF10) and DNA:RNA hybrid related proteins (DHX9 and DDX3X). Edges indicate functional and possible physical protein interactions. Medium confidence interaction score (0.400).*

Following this, we explored if these proteins with known and predicted interactions shared biological processes in common (Fig. 3.17). In Figure 3.17 A, a list of biological processes is shown ordered by lowest to highest false discovery rate shown as p-values which indicates how significant the enrichment is for each gene ontology. This list includes the regulation of mRNA metabolic process (red), mRNA splicing, via spliceosome (blue), regulation of mRNA processing (green), regulation of RNA splicing (yellow), mRNA transport (pink), posttranscriptional regulation of gene expression (dark green), mRNA export from the nucleus (light blue) and mRNA splice site selection (orange).

Firstly, we observed that HNRNPA2B1, HNRNPC, YTHDC1, SRSF1, SRSF3, SRSF10 and DHX9 all have a strong association with mRNA splicing via the spliceosome (blue), with HNRNPA2B1, YTHDC1, SRSF1, SRSF3 and SRSF10 being involved in the regulation of RNA splicing (yellow) and only YTHDC1, SRSF1 and SRSF10 linked to mRNA splice site selection (orange) (Fig. 3.17 B). Additionally, YTHDC1 and HNRNPA2B1 were found to have the most associations in common that comprise mRNA processing, splicing, transport, export, and posttranscriptional regulation of gene expression.

However, HNRNPC appears to have fewer associated biological processes linked with its enrichment compared to HNRNPA2B1 and YTHDC1. YTHDF2 was also only found to have regulation of mRNA metabolic process and post-transcriptional regulation of gene expression biological processes in common with HNRNPA2B1, DHX9, DDX3X, HNRNPC and YTHDC1.

The protein network analysis shown in Fig. 3.16 – 3.17 provided a general indication of the possible interaction network between HNRNPA2B1, YTHDF2, DHX9 and other proteins involved in DNA:RNA hybrid and m^6A metabolism. This suggests a link at least between HNRNPA2B1 and DHX9 with common involvement in biological processes such as mRNA splicing. However, these databases are made up of several datasets and are yet to inform whether HNRNPA2B1 and YTHDF2 have any involvement concerning DNA:RNA hybrids.

(A)

Biological Process (Gene Ontology)				
GO-term	*description*	*count in network*	*strength*	*false discovery rate*
GO:1903311	regulation of mRNA metabolic process	7 of 238	1.81	1.01e-09
GO:0000398	mRNA splicing, via spliceosome	7 of 284	1.73	1.70e-09
GO:0050684	regulation of mRNA processing	5 of 114	1.98	8.71e-08
GO:0043484	regulation of RNA splicing	5 of 116	1.97	8.71e-08
GO:0051028	mRNA transport	5 of 148	1.87	2.17e-07
GO:0010608	posttranscriptional regulation of gene expression	6 of 441	1.47	5.86e-07
GO:0022618	ribonucleoprotein complex assembly	5 of 203	1.73	6.35e-07
GO:1903312	negative regulation of mRNA metabolic process	4 of 74	2.07	9.86e-07
GO:0048024	regulation of mRNA splicing, via spliceosome	4 of 77	2.05	1.04e-06
GO:0006406	mRNA export from nucleus	4 of 107	1.91	3.55e-06
GO:0006376	mRNA splice site selection	3 of 30	2.34	8.73e-06

(B)

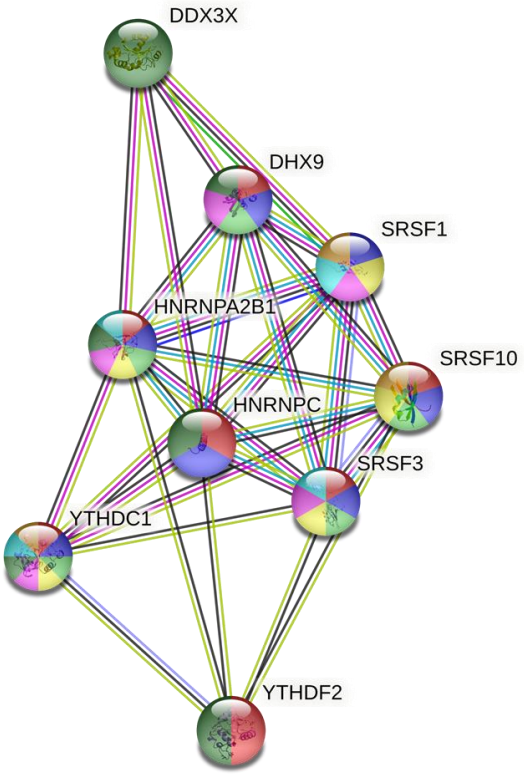


Figure 3.17: HNRNPA2B1 and YTHDC1 have the most involvement in mRNA splicing, processing, transport, and export from the nucleus.

(A) *List of significantly enriched gene ontology pathways. Ordered by false discovery rate that is corrected for multiple testing by Benjamini – Hochberg procedure.* ***(B)*** *STRING protein network of known and predicted protein-protein interactome of m^{6}A-related proteins (HNRNPA2B1, HNRNPC, YTHDC1, YTHDF2), spliceosome related proteins (SRSF1, SRSF3, SRSF10) and DNA:RNA hybrid related proteins (DHX9 and DDX3X).*

3.3.3.2 Immunocytochemistry suggests interplay between YTHDF2 and HNRNPA2B1 localisation within the nucleus.

Previous publications have not identified any correlation between HNRNPA2B1 and YTHDF2. This is supported by their localisation within the cell, with HNRNPA2B1 present in the nucleus (Nichols *et al.*, 2000; Friend *et al.*, 2013; Wang, Wen and Cao, 2019) and YTHDF2 predominantly within the cytoplasm (Zhou *et al.*, 2015; Ries *et al.*, 2019; Zaccara and Jaffrey, 2020). However, results from our group showed that YTHDF2 presence increases in the mitotic chromatin during mitosis (Abakir *et al.*, 2020), suggesting YTHDF2 could change its localisation depending upon the stage of the cell cycle. Therefore, by using established KO cell lines we have for both HNRNPA2B1 and YTHDF2 respectively, we used immunostaining for YTHDF2 and HNRNPA2B1 in these cell lines to examine potential changes in the localisation of these proteins upon depletion of HNRNPA2B1 or YTHDF2.

The immunofluorescence confocal images were taken with a 63x magnification lens (Fig. 3.18 A) in HAP1 WT cells and showed a clear separation between cytoplasmic YTHDF2 and nucleic HNRNPA2B1. However, when the same immunostaining is performed in HNRNPA2B1 KO cells, it firstly reaffirms the KO of HNRNPA2B1 protein in these cells but, more importantly, that the YTHDF2 immunostaining appears to localise to both the cytoplasm and the nucleus. This was corroborated by the cropped single-cell images of WT and HNRNPA2B1 KO cells (Fig. 3.18 B), indicating that the removal of HNRNPA2B1 leads to a change in the spatial distribution of YTHDF2. The pixel intensity within 10 nuclei each, showed a significant increase in YTHDF2 intensity ($p = 0.0003$, Fig. 3.18 C) within the nucleus when HNRNPA2B1 staining is significantly depleted ($p < 0.0001$, Fig 3.18 D).

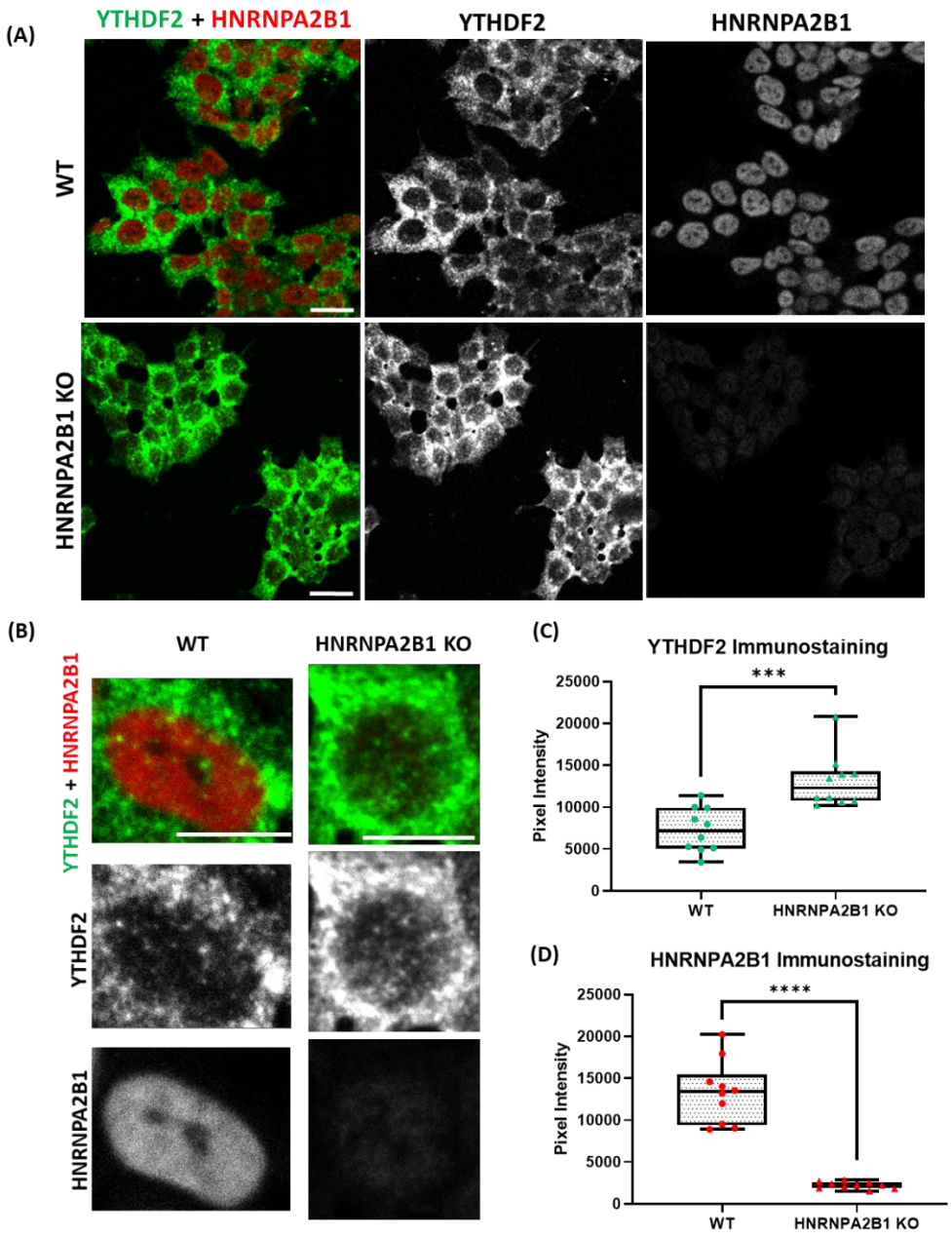


Figure 3.18: YTHDF2 nuclear immunostaining increases within the nucleus in HNRNPA2B1 KO cells.

(A) *Immunostaining with YTHDF2 antibody and HNRNPA2B1 antibody in WT and HNRNPA2B1 KO cells. Representative image shown from 4 technical replicates. Scale bar represents 20 µM.* ***(B)*** *Single cell comparison of YTHDF2 and HNRNPA2B1 immunostaining within WT and HNRNPA2B1 KO cells. Scale bar represents 5 µM.* ***(C)*** *Quantification boxplot of YTHDF2 pixel intensity between HAP1 WT and HNRNPA2B1 KO cells in 10 nuclei.* ***(D)*** *Quantification boxplot of HNRNPA2B1 pixel intensity between HAP1 WT and HNRNPA2B1 KO cells in 10 nuclei. Values had normal distribution and evaluated by unpaired t-test, *** = $p < 0.001$ and **** = $p < 0.0001$.*

Following the immunostaining in HNRNPA2B1 KO cells (Fig. 3.18), we wanted to examine whether the removal of YTHDF2 had a similar shift on the localisation of HNRNPA2B1 within the cell. Using the same combination of YTHDF2 and HNRNPA2B1 antibodies, the immunocytochemical signals of these were then compared between WT and YTHDF2 KO cells (Fig. 3.19). Interestingly, there was no change in localisation of HNRNPA2B1 with immunostaining remaining nucleic (Fig. 3.19 A-B). However, the HNRNPA2B1 immunostaining signal significantly decreased in pixel intensity ($p < 0.0001$, Fig. 3.19 C) in YTHDF2 KO cells compared to HAP1 WT cells. This corresponded with a significant decrease in YTHDF2 immunostaining in YTHDF2 KO cells ($p < 0.0001$, Fig. 3.19 D). Our observations indicate a possible interplay between HNRNPA2B1 and YTHDF2 localisation, where YTHDF2 appears to compensate for HNRNPA2B1 loss, but not vice versa and, therefore, HNRNPA2B1 could functionally be impacted by the loss of YTHDF2.

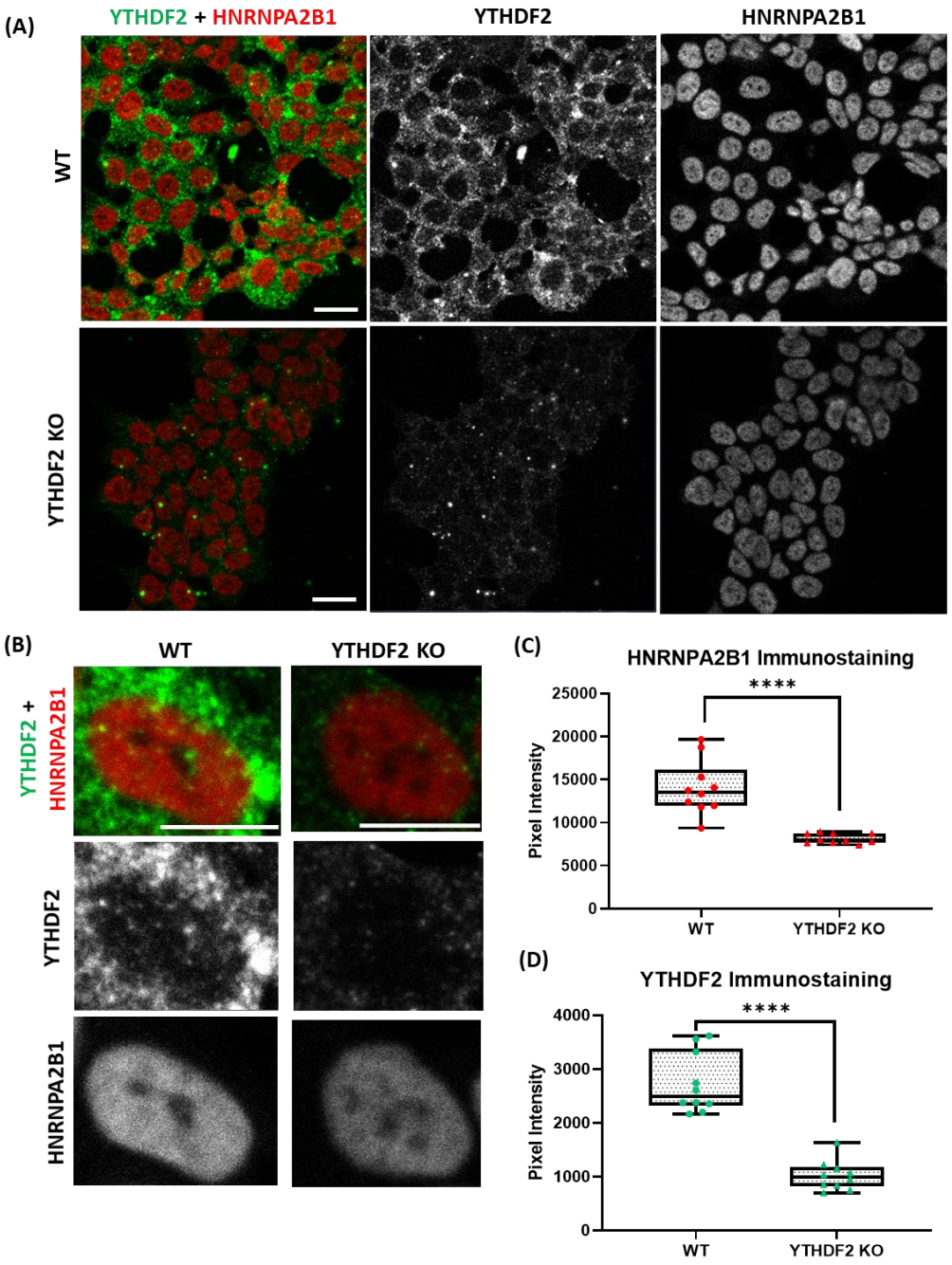


Figure 3.19: HNRNPA2B1 immunostaining decreases within the nucleus in YTHDF2 KO cells.

(A) *Immunostaining with YTHDF2 antibody and HNRNPA2B1 antibody in WT and YTHDF2 KO cells. Representative image shown from 4 technical replicates. Scale bar represents 20 μM.* ***(B)*** *Single cell comparison of YTHDF2 and HNRNPA2B1 immunostaining within WT and YTHDF2 KO cells. Scale bar represents 5 μM.* ***(C)*** *Quantification boxplot of HNRNPA2B1 pixel intensity between HAP1 WT and YTHDF2 KO cells in 10 nuclei.* ***(D)*** *Quantification boxplot of YTHDF2 pixel intensity between HAP1 WT and YTHDF2 KO cells in 10 nuclei. Values had normal distribution and evaluated by unpaired t-test, **** = $p < 0.0001$.*

3.3.3.3 YTHDF2 binding to repetitive and intronic sequences increases within HNRNPA2B1 KO cells.

Immunostaining of YTHDF2 and HNRNPA2B1 within HNRNPA2B1 KO and WT cells suggested that YTHDF2 nuclear presence increases upon loss of HNRNPA2B1 (Fig. 3.18). To further test this hypothesis, we utilised chromatin immunoprecipitation with YTHDF2 antibody followed by qPCR to explore whether this increase in YTHDF2 results in the increase in its binding to locus-specific regions where m^6A-DNA:RNA hybrids and DNA:RNA hybrids reside. Similar to the aforementioned immunostaining, YTHDF2 binding to repetitive elements with m^6A-marked DNA:RNA hybrids had increased enrichment in *α-satellites* by 11.49 – fold, in *LINE1* by 12.13 – fold, in *Alu-Y* elements by 250.56 – fold and in *Alu-S* elements by 5.07 – fold comparing from WT to HNRNPA2B1 KO cells (Fig. 3.20 A). Next, we tested YTHDF2 binding to m^6A marked DNA:RNA hybrids and DNA:RNA hybrids within intronic sequences, YTHDF2 displayed an increased enrichment in *MYH16* locus by 9.44 – fold and in *HECW1* locus by 8.23 – fold comparing from WT to HNRNPA2B1 KO cells (Fig. 3.20 B).

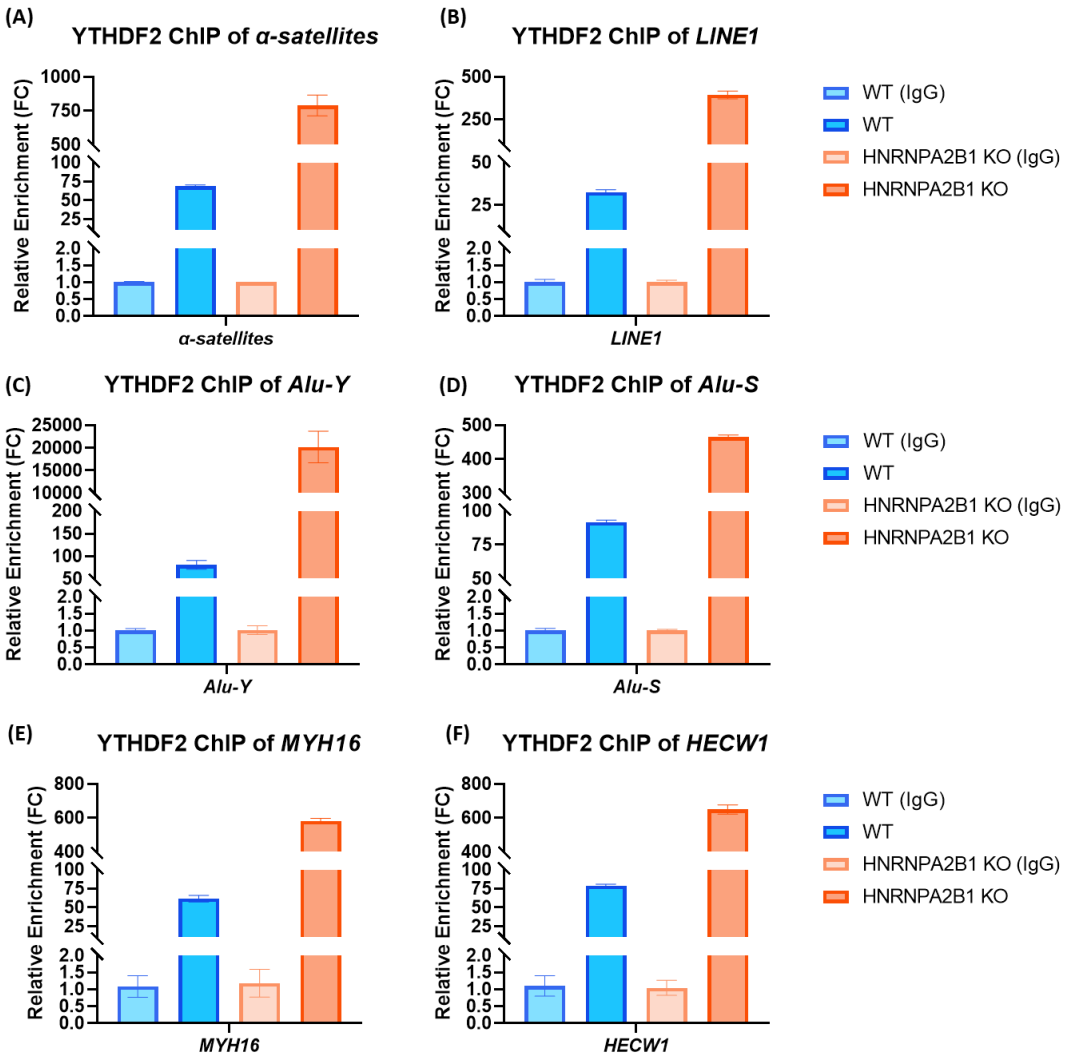


Figure 3.20: YTHDF2 binding in HNRNPA2B1 KO cells increases in both repetitive elements and intronic sequences.

YTHDF2 Chromatin immunoprecipitation qPCR comparison of repetitive elements: ***(A)*** *α-satellites,* ***(B)*** *LINE1 and SINE elements,* ***(C)*** *Alu-Y and* ***(D)*** *Alu-S within WT and HNRNPA2B1 KO. YTHDF2 Chromatin immunoprecipitation qPCR comparison of intronic sequences:* ***(E)*** *MYH16 and* ***(F)*** *HECW1 within WT and HNRNPA2B1 KO cells. IgG negative control was used in both WT and HNRNPA2B1 KO cells. Mean ± SD, 1 biological replicate with 3 technical replicates. FC = Fold change.*

3.3.3.4 HNRNPA2B1 binding to repetitive sequences and individual DNA:RNA-containing loci decreases in YTHDF2 KO cells.

Immunostaining of YTHDF2 and HNRNPA2B1 in YTHDF2 KO and WT cells showed that the HNRNPA2B1 nuclear signal decreases upon depletion of YTHDF2 (Fig. 3.19). Following this, we wanted to examine whether this removal of YTHDF2 impacts HNRNPA2B1 binding to locus-specific regions containing DNA:RNA hybrids by ChIP qPCR. We observed that HNRNPA2B1 binding in repetitive elements was reduced by 104.15 – fold in *α-satellites*, by 34.51 – fold in *LINE1*, by 42.15 – fold in *Alu-Y* and by 107.03 – fold in *Alu-S* when comparing WT to YTHDF2 KO cells (Fig. 3.21 A). HNRNPA2B1 binding to DNA:RNA hybrids within intronic sequences of *MYH16* and *HECW1* were both similarly reduced in YTHDF2 KO cells by 31.72 – fold in *MYH16* and by 109.27 – fold in *HECW1* when comparing WT to YTHDF2 KO cells (Fig. 3.21 B).

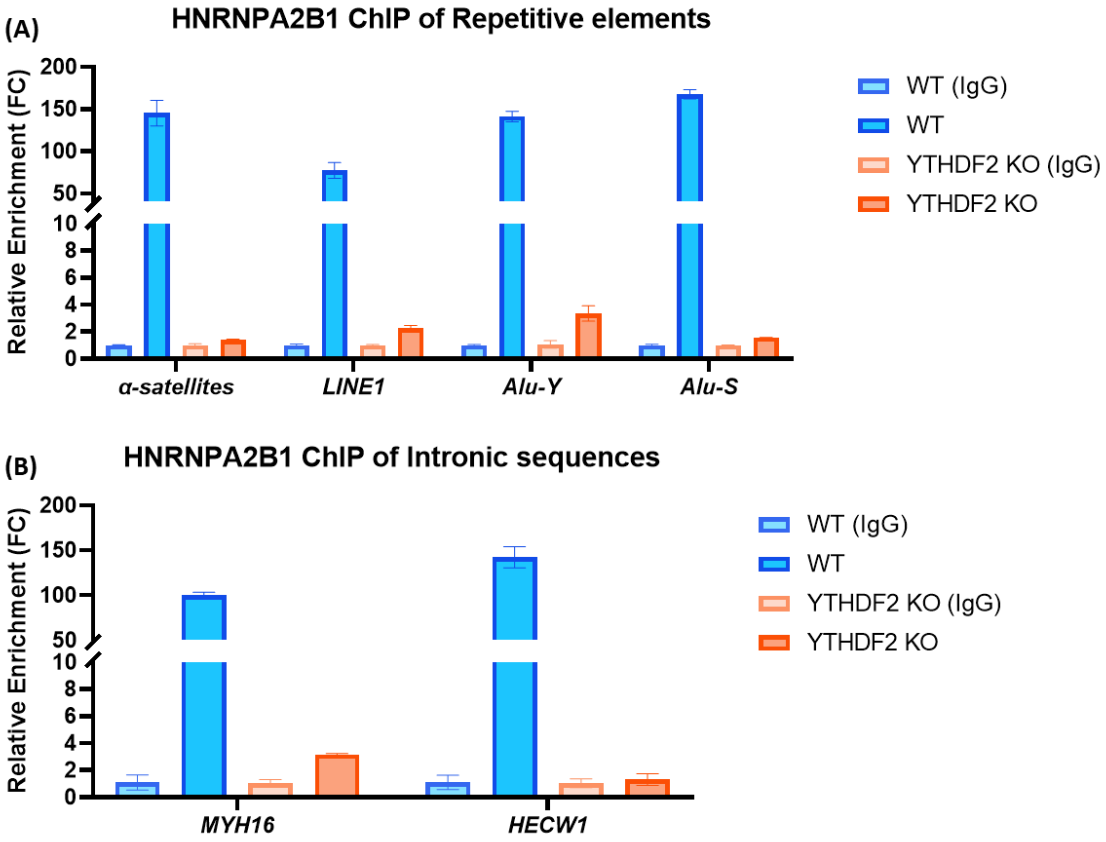


Figure 3.21: HNRNPA2B1 binding in YTHDF2 KO cells decreases in both repetitive elements and intronic sequences.

(A) *HNRNPA2B1 Chromatin immunoprecipitation qPCR comparison of repetitive elements: α-satellites, LINE1 and SINE elements (Alu-Y and Alu-S) within WT and YTHDF2 KO.* ***(B)*** *HNRNPA2B1 Chromatin immunoprecipitation qPCR comparison of intronic sequences: MYH16 and HECW1 within WT and YTHDF2 KO cells. IgG negative control was used in both WT and YTHDF2 KO cells. Mean ± SD, 1 biological replicate with 3 technical replicates. FC = Fold change.*

3.3.4 HNRNPA2B1 differentially interacts with different DNA:RNA hybrid-containing loci in the introns of *WWOX* gene.

Within this chapter, we have explored the dynamics of HNRNPA2B1 and YTHDF2 interaction with DNA:RNA hybrids. Exploration of datasets (Fig. 3.16 – 3.17) has also suggested a close interaction between HNRNPA2B1 and DHX9, a DNA:RNA hybrid helicase related to mRNA splicing. These results provide a reason to explore whether a known splicing target of HNRNPA2B1, firstly has m^{6}A-marked DNA:RNA hybrids or DNA:RNA hybrids present in HAP1 cells and secondly whether KO of HNRNPA2B1 and YTHDF2 interferes with the binding with the splicing target. To answer this question, we used hiPSCs m^{6}A-DRIP and S9.6 DRIP next-generation sequencing datasets, described in (Abakir *et al.*, 2020), to identify potential gene targets that have been suggested to be targeted by HNRNPA2B1 (Golan-Gerstl *et al.*, 2011), then performed S9.6 DRIP qPCR over locus-specific regions found in HAP1 WT, HNRNPA2B1 KO and YTHDF2 KO cells. Finally, we performed ChIP qPCR with HNRNPA2B1 and YTHDF2 antibodies on these cell lines targeting the locus-specific regions identified to evaluate the binding of YTHDF2 and HNRNPA2B1 to these regions.

3.3.4.1 DNA:RNA hybrids and m^{6}A-marked DNA:RNA hybrids found in the introns of WWOX by analysis of m^{6}A-DRIP and S9.6 DRIP next-generation sequencing.

Previous publications showed that depletion and overexpression of *HNRNPA2B1* impact the splicing isoforms of several genes in glioblastoma multiforme (Golan-Gerstl *et al.*, 2011). From this, we evaluated whether any of the genes described in Golan-Gerstl et al., the publication had any DNA:RNA hybrid or m^{6}A-marked DNA:RNA hybrid intronic peaks using hiPSC m^{6}A-DRIP and S9.6 DRIP next-generation sequencing datasets (Abakir *et al.*, 2020). We identified that *WWOX* found on Chromosome 16, has 3 regions where both DNA:RNA hybrid and m^{6}A-

marked DNA:RNA hybrids are suggested to reside in hiPSCs: within intron 4, within the intron 5 and the intron 8 (Fig. 3.22 A-C). To visualise where the location of these peaks within WWOX, we illustrated WWOX canonical structure and indicated each peak with either a green star (intron 4), an orange star (intron 5) or a purple star (intron 8) (Fig. 3.23 A). The first peak, intron 4, is observed in the intron after the WW2 domain and both intron 5 and intron 8 reside within and outside the SDR region, respectively (Fig. 3.23 B). Within the *WWOX* canonical gene structure, 2 of the peaks (intron 5 and intron 8) reside in positions next to exons which in some isoforms are skipped (Driouch *et al.*, 2002; Kuroki *et al.*, 2002; Golan-Gerstl *et al.*, 2011) (Fig. 3.24 C).

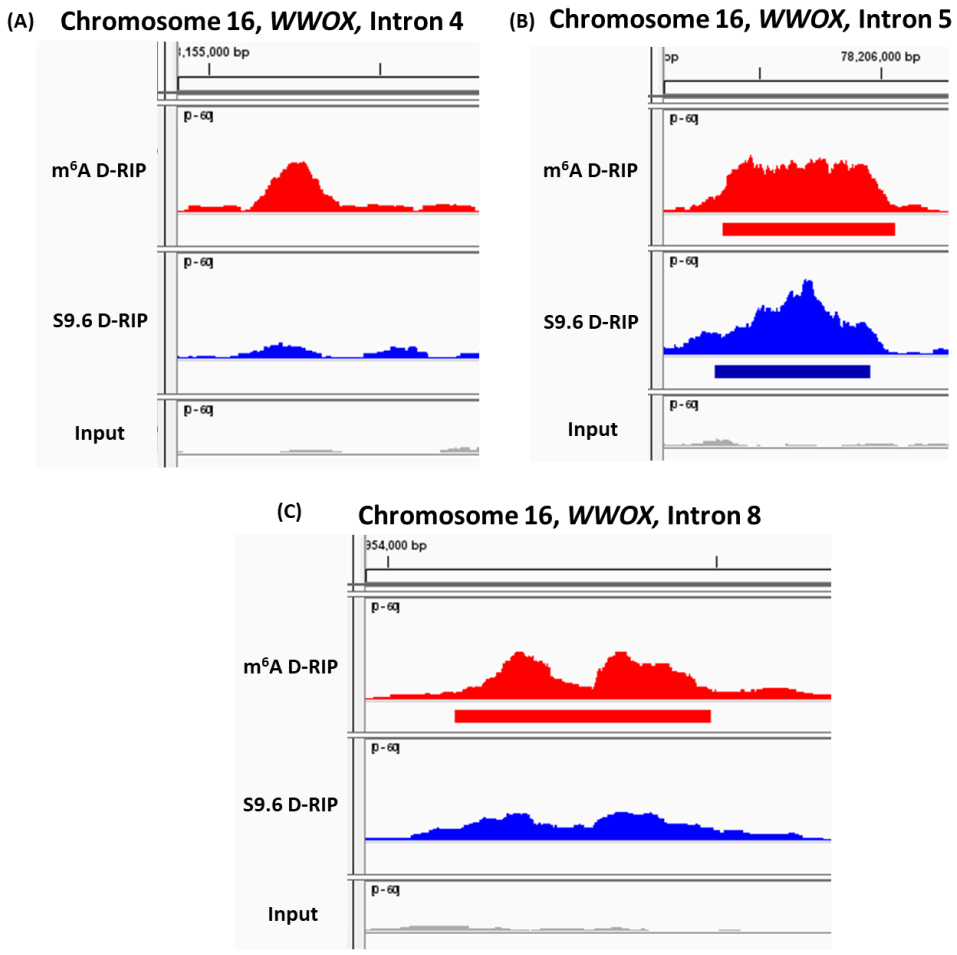


Figure 3.22: m^{6}A-marked DNA:RNA hybrids and DNA:RNA hybrids within intronic regions of *WWOX* in hiPSCs.

*IGV coverage plot of m^{6}A DRIP and S9.6 DRIP next generation sequencing within hiPSCs in **(A)** WWOX intron 4 (green star in Fig. 3.24 A), **(B)** WWOX intron 5 (orange star in Fig. 3.24 A) and **(C)** WWOX intron 8 (purple star in Fig. 3.24 A). Compared to hiPSCs input with the data range set at 60.*

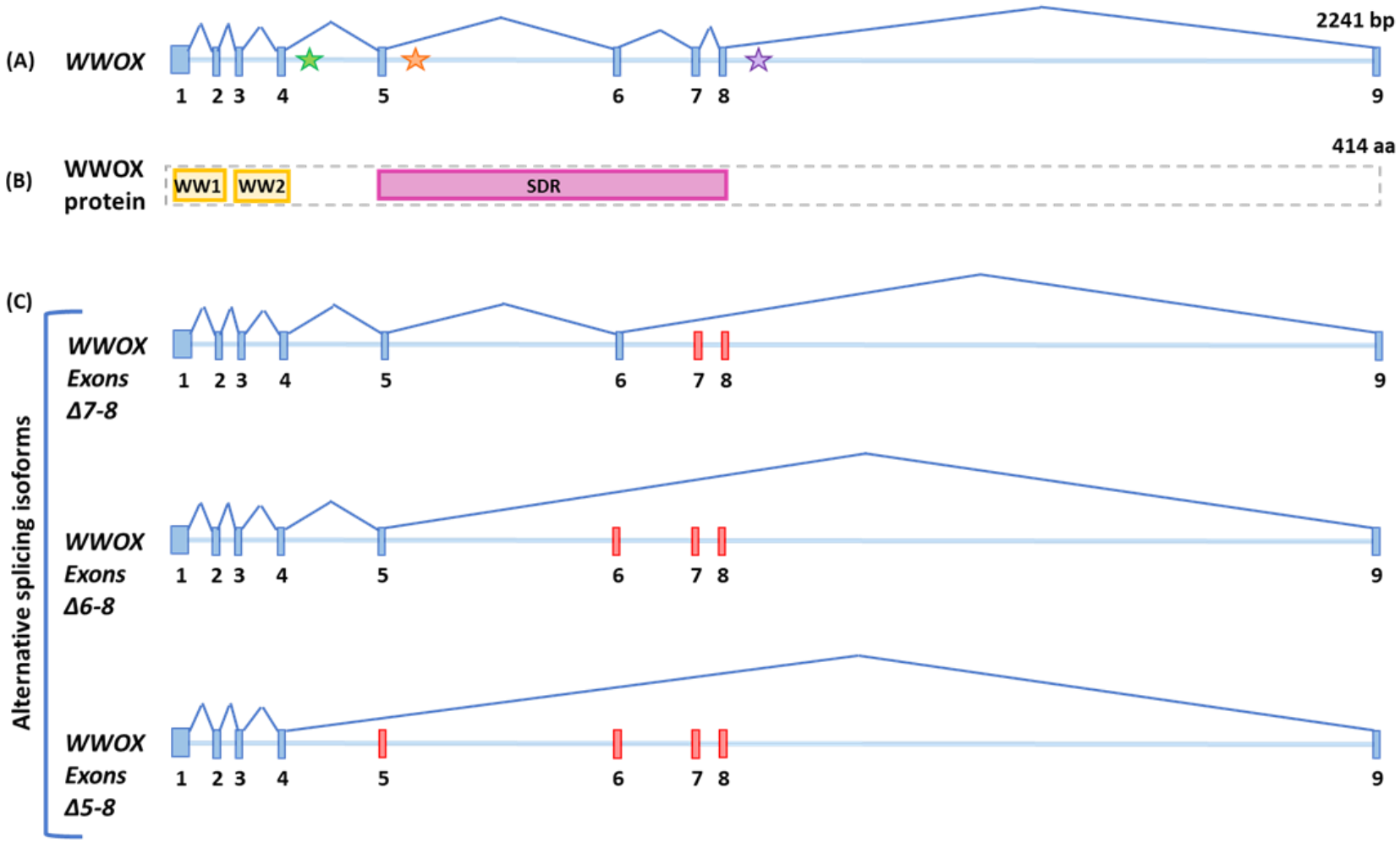


Figure 3.23: *WWOX* canonical gene structure, protein structure and alternative splicing isoforms.

(A) *Illustration of WWOX canonical gene structure, showing 9 exons spanning 2241 base pairs. Green, orange, and purple stars indicate locations of m^{6}A-marked DNA:RNA hybrids shown in Figure 3.23.* ***(B)*** *WWOX protein structure of 414 amino acids with the WW1 domain in exons 1-2, WW2 domain in exons 3-4 and SDR binding domain in exons 5-8.* ***(C)*** *Alternative splicing isoforms of WWOX, that skips exons ∆7-8, exons ∆6-8 and exons ∆5-8, respectively. Isoforms referred to by* (Driouch *et al.*, 2002; Kuroki *et al.*, 2002; Golan-Gerstl *et al.*, 2011).

3.3.4.2 DNA:RNA hybrids have increased enrichment in *WWOX* Intron 4 and 8 but decrease in *WWOX* Intron 5 in HNRNPA2B1 KO compared to HAP1 WT cells.

We identified possible DNA:RNA hybrids and m^{6}A-marked DNA:RNA hybrids peak in the hiPSCs next-generation sequencing. We created primers to span each locus-specific region in *WWOX* and then performed DRIP qPCR to observe the levels of DNA:RNA hybrids within repetitive and intronic sequences in HAP1 WT and HNRNPA2B1 KO cells (Fig. 3.24). For the intron 4 peak identified by IGV software, we found DNA:RNA hybrid levels increased by 4.09 x10^5 – fold from WT to HNRNPA2B1 KO cells (Fig. 3.24 A). The DNA:RNA hybrid signal enrichment is also observed to increase in the intron 8 peak, increasing by 20.34 – fold comparing WT to HNRNPA2B1 KO cell enrichment (Fig. 3.24 C). Whereas, within intron 5 of *WWOX*, there is a decrease of DNA:RNA hybrid enrichment by 17.91 – fold comparing the enrichment between WT to HNRNPA2B1 KO cells (Fig. 3.24 B).

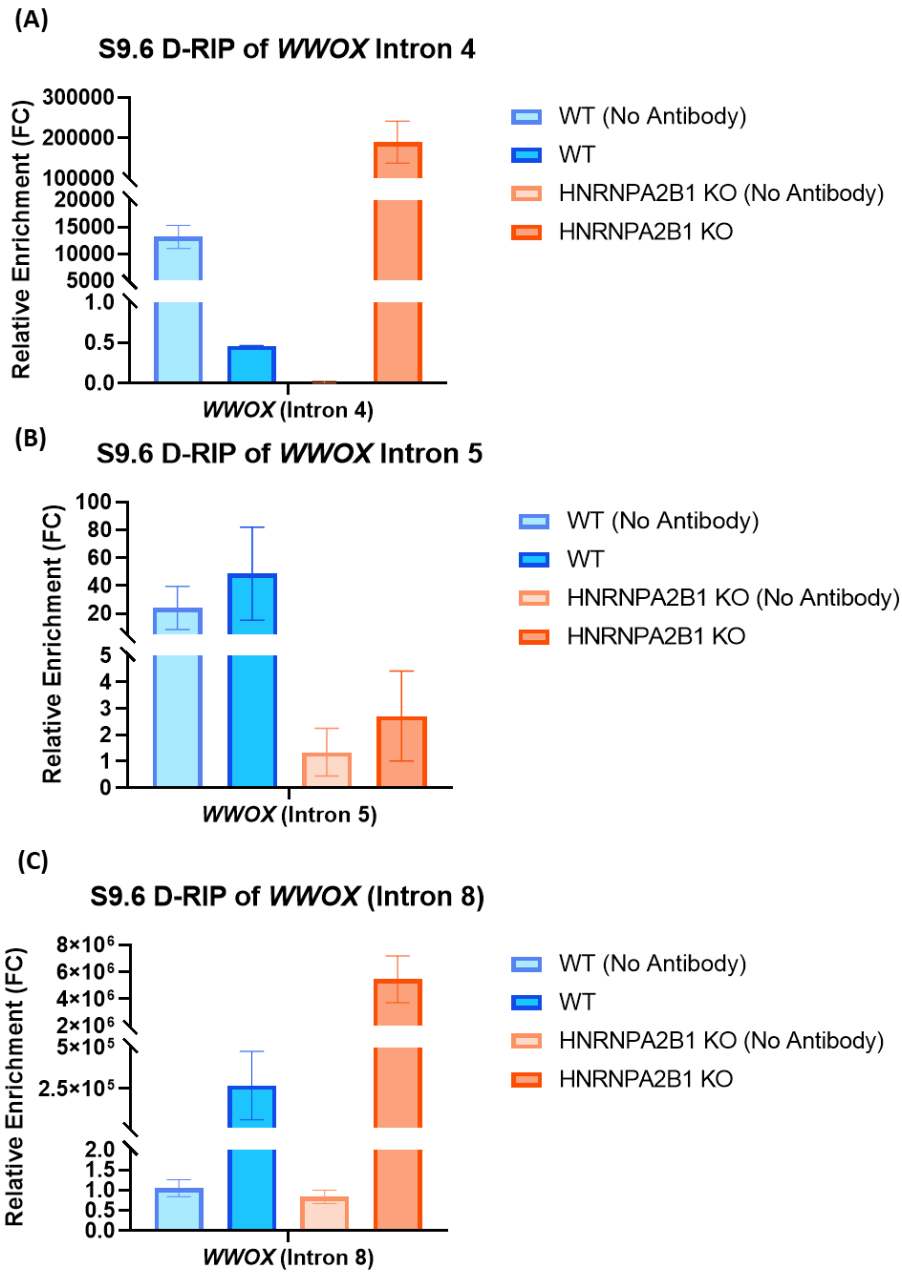


Figure 3.24: Knockout of HNRNPA2B1 leads to decrease of DNA:RNA hybrid enrichment in Intron 5 of *WWOX* but increase in Intron 4 and 8 of *WWOX*.

DNA:RNA hybrid immunoprecipitation qPCR comparison of WWOX sequences: ***(A)*** *WWOX (intron 4) region,* ***(B)*** *WWOX (intron 5) and* ***(C)*** *WWOX (intron 8) in WT and HNRNPA2B1 KO cells. No antibody controls were used for both HAP1 WT and HNRNPA2B1 KO cells. FC = Fold change. Mean ± SEM, 1 biological replicate with 3 technical replicates.*

3.3.4.3 YTHDF2 binding increases to *WWOX* intronic sequences where DNA:RNA hybrids are present in HNRNPA2B1 KO cells.

As we observed the accumulation of DNA:RNA hybrids observed in the majority of *WWOX* introns, we aimed to examine whether YTHDF2 interacts with DNA:RNA hybrids within *WWOX* similar to the other intronic sequences containing DNA:RNA hybrids in HNRNPA2B1 KO cells (Fig. 3.25). In intron 4 of *WWOX*, we observed that the binding of YTHDF2 increased by 229.11 – fold comparing WT to HNRNPA2B1 KO cells (Fig. 3.25 A). In intron 8 of *WWOX,* we also found that YTHDF2 binding was enriched by 7.15 – fold comparing WT to HNRNPA2B1 KO cells (Fig. 3.25 C). Intron 5 of *WWOX* displayed an increase in YTHDF2 binding by 160.01 – fold when comparing WT to HNRNPA2B1 KO enrichment (Fig. 3.25 B). However, the fold-change in WT cells is below the WT IgG control it is compared against, suggesting that YTHDF2 does not bind to the DNA:RNA hybrid within intron 5 of *WWOX* in WT cells.

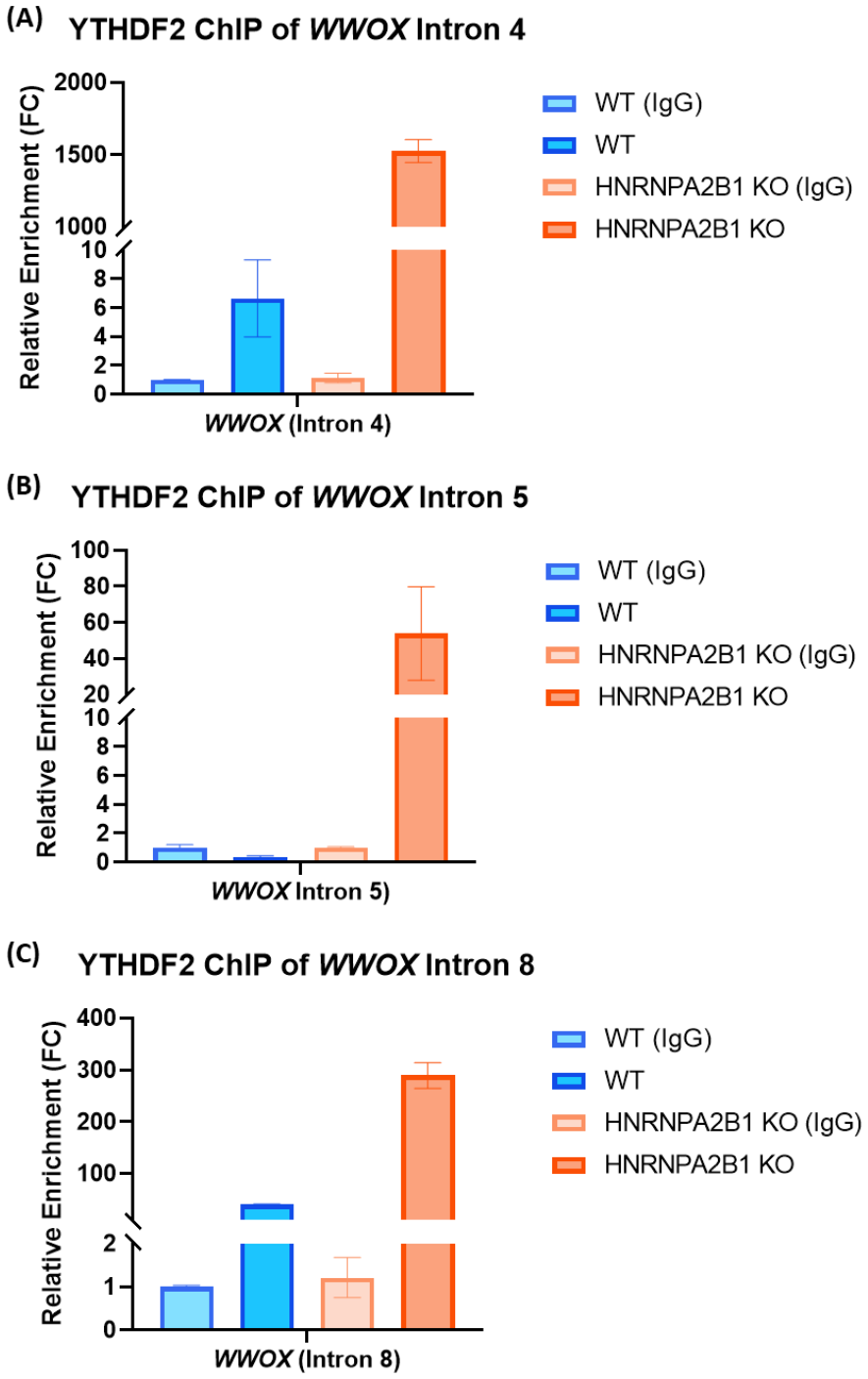


Figure 3.25: YTHDF2 binding increased within *WWOX* Intron 4, 5 and 8 in HNRNPA2B1 KO cells.

*YTHDF2 Chromatin immunoprecipitation qPCR comparison of **(A)** intron 4 of WWOX, **(B)** intron 5 of WWOX and **(C)** intron 8 of WWOX in WT and HNRNPA2B1 KO cells. IgG negative control was used in both WT and HNRNPA2B1 KO cells. FC = Fold change. Mean ± SEM, 1 biological replicate with 3 technical replicates.*

3.3.4.4 HNRNPA2B1 binding differs depending upon the location of the DNA:RNA hybrid within *WWOX* intronic sequences in YTHDF2 KO cells.

Finally, we examined whether HNRNPA2B1 interaction with DNA:RNA hybrids in *WWOX* introns was comparable to the decreased enrichment previously observed in other intronic sequences with DNA:RNA hybrids in YTHDF2 KO cells (Fig. 3.26). In intron 4 of *WWOX*, we found the binding of HNRNPA2B1 decreased by 41.22 – fold from YTHDF2 KO to HAP1 WT cells (Fig. 3.26 A). Likewise, intron 8 of *WWOX* displayed a decreased enrichment in HNRNPA2B1 binding by 40.61 – fold comparing YTHDF2 KO to HAP1 WT cells (Fig. 3.26 C). However, in intron 5 of *WWOX,* the binding of HNRNPA2B1 increased by 9.69 – fold comparing YTHDF2 KO to WT cells (Fig. 3.26 B).

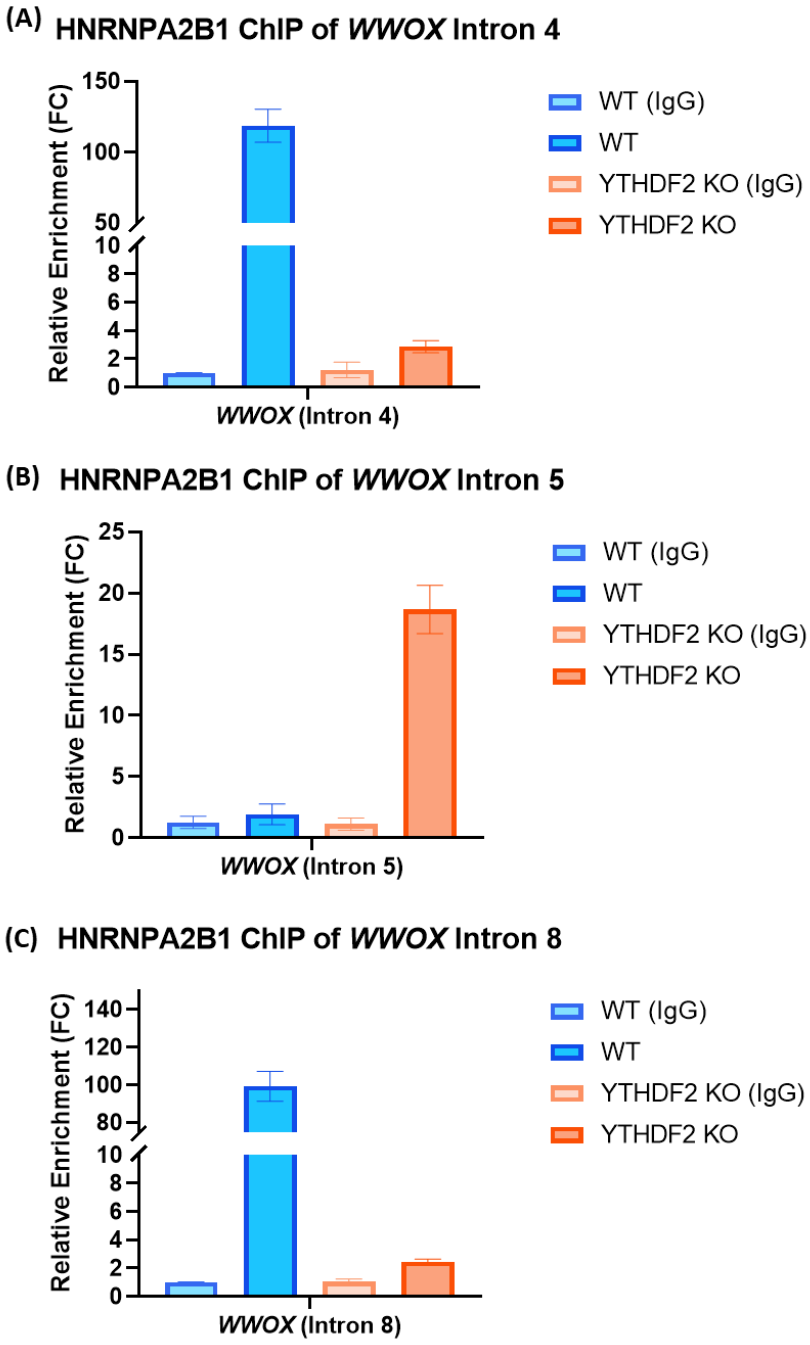


Figure 3.26: HNRNPA2B1 binding decreased in Intron 4 and 8 but increased in Intron 5 of *WWOX* in YTHDF2 KO cells.

*HNRNPA2B1 Chromatin immunoprecipitation qPCR comparison of **(A)** intron 4 of WWOX; **(B)** intron 5 of WWOX; **(C)** intron 8 of WWOX in WT and YTHDF2 KO cells. Both WT and YTHDF2 KO samples were compared to the matched IgG control. FC = Fold change. Mean ± SEM, 1 biological replicate with 3 technical replicates.*

3.4 Technical Discussion

Previous results from our group identified the presence of m^{6}A-marked DNA:RNA hybrids within a range of cell types as well as suggested the involvement of m^{6}A reader protein YTHDF2 in the regulation of accumulation of m^{6}A-marked DNA:RNA hybrids during the cell cycle (Abakir *et al.*, 2020). In this publication, other m^{6}A writers and readers including METTL3, YTHDF1 and HNRNPA2B1 were preliminarily investigated if they could also interact with m^{6}A-marked DNA:RNA hybrids (Abakir *et al.*, 2020). Therefore, we decided to focus on HNRNPA2B1, not only because of the interaction with m^{6}A-marked RNA strands (C. Alarcón et al., 2015; Wu et al., 2018) but because it has been suggested to be capable of binding to both RNA,DNA, and DNA:RNA hybrids (Hudson and Ortlund, 2014; Coppin *et al.*, 2018; Wu *et al.*, 2018).

In the beginning, we validated the KO of HNRNPA2B1 in the HAP1 cell line obtained from Horizon Discovery (Fig. 3.2 – 3.4). We identified that the *HNRNPA2* isoform of *HNRNPA2B1* was completely depleted in HNRNPA2B1 KO cells with an inadvertent depletion of *HNRNPB1* isoform transcripts when compared to HAP1 WT cells (Fig 3.5 – 3.6). Horizon Discovery utilises human near-haploid cells known as HAP1 that are derived from a male chronic myelogenous leukaemia cell line referred to as KBM-7 (Kotecki, 1999; Carette *et al.*, 2011; Essletzbichler *et al.*, 2014). We decided to evaluate the impact of HNRNPA2B1 KO on m^{6}A-marked DNA:RNA hybrids in these cells, as it provided a quicker solution to investigate a functional knockout compared to preparing our own CRISPR-cas9 KO in hiSPCs. Despite the advantages of HAP1 cells for KO experiments, publications have shown that differentiated cells have lower levels of m^{6}A present on RNA compared to their stem cell counterparts which are suggested to contribute to the flexibility required for stem cells to retain pluripotency (Batista *et al.*, 2014). There is also evidence indicating that cells may possess varying levels of m^{6}A depending upon cell type, disease, and tumour type (Jiang *et al.*, 2021; Shen *et al.*, 2021).

To evaluate the impact of HNRNPA2B1 loss on m^{6}A-marked DNA:RNA hybrids and DNA:RNA hybrids, we utilised three techniques: immunostaining (Fig 3.9 – 3.10), m^{6}A and S9.6 DRIP

(Fig 3.12 – 3.15), and SID-UPLC-MS/MS (Fig. 3.11). By immunostaining with DNA:RNA hybrid antibody (S9.6 clone) (Fig. 3.9) and an indicator of DNA damage, γH2AX, antibody (Fig. 3.10), we perceived no significant change in DNA:RNA hybrid levels or DNA damage levels between HAP1 WT and HNRNPA2B1 KO cells. We were able to perform semi-quantitation on these confocal images to obtain the average pixel intensity, a method published by our group in 2017 (Ramsawhook *et al.*, 2017). Our images were taken with a 63x magnification lens to capture the cells and the antibody staining in close detail. This automatically limits the number of cells we can view at once. Moreover, this focus at high magnification will promote unintentional bias towards the cells with the higher pixel intensity, not providing the scale of what might be happening within these experiments. Additionally, within our S9.6 antibody immunostaining, we and others observe unspecific immunostaining within the cytoplasm of the HAP1 cells (Abakir *et al.*, 2020), whereas DNA:RNA hybrids reside predominantly within the nucleus (Fig. 3.9). Publications have proposed that the S9.6 antibody may exhibit cross-reactivity that can recognise then binding to DNA:RNA hybrids and AU-rich RNA:RNA hybrids (Phillips *et al.*, 2013), but not single or double-stranded DNA (Boguslawski *et al.*, 1986; Hu *et al.*, 2006). This was further supported by a recent publication that found that DNA:RNA hybrid immunostaining with S9.6 antibody was sensitive to ribonuclease T1 (RNase T1) and ribonuclease III (RNase III) that degraded both single and double-stranded RNA, respectively (Smolka *et al.*, 2021). Thus, further controls should have been implemented to counter the cross-reactivity of the S9.6 antibody in immunostaining.

SID-UPLC-MS/MS detects the release of m^6A present on small fragments that pass through the filtrate after RNase H treatment to break down DNA:RNA hybrids. Our group has previously utilised this technique as a non-antibody-based assessment of the presence of m^6A on DNA, RNA and DNA:RNA hybrids (Abakir *et al.*, 2020). The results suggested a non-significant decrease in the number of m^6A-marked DNA:RNA hybrids within HNRNPA2B1 KO cells (Fig 3.11 A), yet m^6A present on RNA indicated that HNRNPA2B1 loss caused a non-significant increase in m^6A levels (Fig. 3.11 B). This method offers a view of the whole genome levels of m^6A-marked DNA:RNA hybrids and the impact that loss of HNRNPA2B1 causes. However, this methodology is dependent upon optimised controls, m^6A standards and confidence in the RNase H treatment working effectively.

Another quantitative approach we used was DRIP, which collects genomic DNA from millions of cells in one replicate, providing a broad picture of the location of DNA:RNA hybrids in the genome. This immunoprecipitation provides qualitative data by next-generation sequencing of the locus-specific regions where these DNA:RNA hybrids reside that then are quantified by qPCR using primers designed around these locus-specific regions. DRIP with the S9.6 antibody is the most accepted method of examining DNA:RNA hybrids within the genome (Boguslawski *et al.*, 1986; Phillips *et al.*, 2013), yet our group has modified this method to evaluate m^6A-marked DNA:RNA hybrid by immunoprecipitating with an m^6A antibody as well as denaturing the DNA to allow access to the m^6A epitope. Our results indicated that HNRNPA2B1 KO had a distinctive effect that differed between m^6A-marked DNA:RNA hybrid present on repetitive sequences (Fig. 3.14) and those present on intronic sequences (Fig. 3.15). Whereas the impact of HNRNPA2B1 loss varied with no apparent pattern within S9.6 DRIP samples (Fig. 3.12 – 3.13). Another possibility was to carry out a double immunoprecipitation that would involve an S9.6 DRIP followed by an m^6A DRIP. However, it requires a high starting volume of genomic DNA, due to the potential loss during multiple washing steps during immunoprecipitation. To offset this, we performed the S9.6 DRIP and m^6A-DRIP at the same time, with the same batch of immunoprecipitation reagents as well as running both samples with matched controls on the same qPCR plate for the same locus-specific primers for run temperature consistency. One publication has suggested that sonication can disrupt DNA:RNA hybrids (Halász *et al.*, 2017), however, another reported that although sonication consistently decreases the recovery yield and the alternative method of enzyme restriction digestion also had a loss of product that suggested the loss might not be completely attributed to sonication (Crossley *et al.*, 2020). This publication discussed a recently developed internal synthetic DNA:RNA hybrids that they introduce during the initial cell lysis before genomic DNA collection to act as a normalisation standard signal in next-generation sequencing (Crossley *et al.*, 2020). This method named quantitative differentiated DRIP (qDRIP) is based on the design of four DNA:RNA hybrid spike-ins that include two standard and two longer DNA:RNA hybrids (~130bp and ~280bp) as well as varying low and high GC content to account for any S9.6 antibody bias (Crossley *et al.*, 2020). These additional

controls would have provided higher confidence in the results as well as the potential to modify for m^{6}A-marked DNA:RNA hybrid spike-ins.

In the next section of the chapter, we assessed whether HNRNPA2B1 had any interaction with previously investigated m^{6}A-binding protein YTHDF2 concerning DNA:RNA hybrids and m^{6}A-deposition at these structures. Using two KO cell lines, HAP1 HNRNPA2B1 KO and HAP1 YTHDF2 KO with a matched WT control, we identified that loss of HNRNPA2B1 increased presence of YTHDF2 in the nucleus as well as its binding to m^{6}A-marked DNA:RNA hybrids in HNRNPA2B1 KO cells (Fig. 3.18, Fig. 3.20). Yet, in YTHDF2 KO cells, the loss of YTHDF2 led to the decreased presence of HNRNPA2B1 within the nucleus as well as reduced binding to DNA:RNA hybrid containing loci (Fig 3.19, Fig 3.21). It was determined that ChIP qPCR would be the appropriate method to quantify the potential binding of HNRNPA2B1 or YTHDF2 to m^{6}A-marked DNA:RNA hybrid regions using primers designed based on next-generation sequencing datasets of m^{6}A- and S9.6 DRIP. We used a cross-linking ChIP kit that will minimise nucleosome rearrangements and is optimal for non-histone proteins that bind weakly or indirectly to proteins (Solomon, Larsen and Varshavsky, 1988). A few drawbacks of cross-linking DNA can include disruption of antibody binding to the target epitope, particularly in monoclonal antibodies with one target epitope compared to polyclonal antibodies that bind to epitopes of one gene target. Another disadvantage is that by minimising nucleosome rearrangements, we only observe a snapshot of the steady-state levels, presenting an artefactual view of the interactions within the cells. Even if more biological replicates are examined to find any consistency, depending upon what point in the cell life cycle, when cross-linking occurs the expression of genes may fluctuate, leading to variation, especially when evaluating HNRNPA2B1 or YTHDF2 binding to DNA:RNA hybrid regions within potentially splice targets. Moreover, we should consider the DNA we immunoprecipitated may not be directly bound to HNRNPA2B1, meaning it could be bound to other proteins within a protein complex such as the spliceosome. Therefore, we could be observing an indirect association with HNRNPA2B1 in the ChIP qPCR instead of direct binding of HNRNPA2B1.

Finally, we began to investigate if any published splicing targets of HNRNPA2B1 had DNA:RNA hybrids residing within their introns and if binding changed upon loss of

HNRNPA2B1 or YTHDF2. The next-generation sequencing datasets suggested locations of DNA:RNA hybrids within the introns of HNRNPA2B1 splicing target *WWOX* (Fig. 3.22), in which DNA:RNA hybrid enrichment varied in HNRNPA2B1 KO cells depending upon the position of the DNA:RNA hybrid within *WWOX* introns (Fig. 3.24). We also performed YTHDF2 ChIP on HAP1 WT and HNRNPA2B1 KO cells which displayed a similar pattern with increased binding to DNA:RNA hybrid in *WWOX* introns in HNRNPA2B1 depleted cells (Fig. 3.25). Whereas HNRNPA2B1 ChIP qPCR performed on HAP1 WT and YTHDF2 KO cells displayed decreased binding within two introns where DNA:RNA hybrids reside but increased binding within one intron with DNA:RNA hybrid present in YTHDF2 depleted cells (Fig. 3.26). Our observations suggest that HNRNPA2B1 and YTHDF2 may either directly or indirectly have a functional interaction with m^6A-marked DNA:RNA hybrids We have already covered the drawbacks of both DRIP and ChIP methodologies, but this hypothesis needed other techniques to fully grasp the interactions in which DNA:RNA hybrids and possibly m^6A-marked DNA:RNA hybrids could be involved in alternative splicing. Publications investigating alternative splicing tend to utilise reverse transcription PCR (RT-PCR), high thorough-put RNA sequencing and ChIP next-generation sequencing (Harvey and Cheng, 2016; Halperin *et al.*, 2021).

Chapter 4: Investigating the potential role of HNRNPA2B1 in the metabolism of m^{6}A-marked DNA:RNA hybrids in Glioblastoma Multiforme

4.1 Introduction

Adult diffuse gliomas have been defined into grade II and III astrocytic tumours, grade II and III oligodendrogliomas and grade IV glioblastoma by the World Health Organisation (WHO) (Louis *et al.*, 2016). Glioblastoma multiforme (GBM) is an aggressive malignant brain tumour that makes up to 54% of all gliomas (Ostrom *et al.*, 2013) and is commonly located in the supratentorial region (frontal, occipital, parietal, and temporal lobes) but rarely in the cerebellum or spinal cord (Engelhard *et al.*, 2010; Adams *et al.*, 2013). GBM has a higher incidence rate in males than in females and is primarily diagnosed at a median age of 64 (Chakrabarti *et al.*, 2005; Ostrom *et al.*, 2013). Currently, the best treatment plan includes surgical resection followed by radiation therapy and simultaneous Temozolomide (TMZ) chemotherapy (Stupp *et al.*, 2005). However, GBM has a poor prognosis with the median survival time for GBM patients only 14.6 months and less than 5% of patients surviving 5 years after diagnosis (Stupp *et al.*, 2005; Adams *et al.*, 2013). Several of the challenges that GBM presents in its diagnosis, prognosis, and treatment comprised of the inter-tumoural and intra-tumoural heterogeneity observed genetically and histologically, varying mutations, epigenetic modifications and phenotypic states that can impact genomic stability and consequently will lead to varying clinical outcomes (Homma *et al.*, 2006; Marusyk and Polyak, 2010; Szerlip *et al.*, 2012; Adams *et al.*, 2013).

Initially, microarray and next-generation sequencing were used to classify gene expression profiles within GBM led to the characterisation of its 4 subgroups: Classical, Mesenchymal, Proneural and Neural (Phillips *et al.*, 2006; Verhaak *et al.*, 2010). The classical subgroup is defined by chromosome 7 amplification, chromosome 10 loss, lack of *TP53* mutations, focal 9p21.3 deletion containing cyclin-dependent kinase inhibitor 2A (*CDKN2A*), and inactivation

of retinoblastoma-associated protein pathway (Verhaak *et al.*, 2010). Moreover, the neural precursor and stem cell marker NES and proteins within the sonic hedgehog pathway and the notch signalling pathway are highly expressed in the classical subgroup (Verhaak *et al.*, 2010). GBM classical subgroup tumours that have been treated with aggressive radiotherapy and chemotherapy observed a reduction in mortality (Colman *et al.*, 2010). The mesenchymal subgroup has a focal hemizygous deletion of 17q11.2 containing neurofibromatosis type-1 gene (*NF1*) and co-mutations residing in phosphatase and tensin homolog gene (*PTEN*) which are both a part of the phosphatidylinositol 3-kinase (PI3K)/protein kinase B (Akt) signalling pathway (Verhaak *et al.*, 2010). Expression of genes from the tumour necrosis factor superfamily, nuclear factor kappa-light-chain-enhancer of activated B cells (NF-κB) and mesenchymal and astrocytic markers have higher activity in the mesenchymal subgroup (Phillips *et al.*, 2006; Verhaak *et al.*, 2010). Recently, additional genes such as vascular endothelial growth factor A (*VEGF-A*), vascular epithelial growth factor B (*VEGF-B*), angiopoietin 1 (*ANG1*) and angiopoietin 24 (*ANG24*) have been linked to the mesenchymal class (Sharma *et al.*, 2017). However, despite mesenchymal GBM tumours responding to aggressive radiotherapy and chemotherapy, this subgroup has the worst prognosis among the 4 GBM subgroups (Colman *et al.*, 2010). The proneural subgroup exhibits a high expression of platelet-derived growth factor receptor alpha (*PDGFRA*), oligodendrocyte transcription factor 2 (*OLIG2*) and NK2 homeobox 2 (*NKX2-2*) as well as mutations in the isocitrate dehydrogenase (NADP(+)) 1 (*IDH1*) gene (Verhaak *et al.*, 2010). Patients with a proneural subgroup GBM tumour tend to be found in younger patients and had no subgroup-related difference in responding to radiotherapy and chemotherapy compared to the other GBM subgroups (Colman *et al.*, 2010). The neural subgroup is denoted by the high expression of neuron markers associated with neuron projection and axon/synaptic transmission that include Neurofilament Light Chain (*NEFL*), Gamma-Aminobutyric Acid Type A Receptor Subunit Alpha 1 (*GABRA1*), Synaptotagmin 1 (*SYT1*) and Solute Carrier Family 12 Member 5 (*SLC12A5*) gene (Verhaak *et al.*, 2010). However, the gene expression patterns observed in neural GBM subgroup tumours are similar to normal brain tissue but have shown to be more responsive to radiotherapy and chemotherapy compared to the other GBM subgroups (Colman *et al.*, 2010; Verhaak *et al.*, 2010).

Other subgroup groupings have been described including *IDH* wild-type and mutations (Parsons *et al.*, 2008; Yan *et al.*, 2009; Beiko *et al.*, 2014; Stancheva *et al.*, 2014; Louis *et al.*, 2016) and DNA methylation-based subgroups, in particular, DNA methylation of O-6-Methylguanine-DNA Methyltransferase (*MGMT*) (Brennan *et al.*, 2013; Bell *et al.*, 2018; Johannessen *et al.*, 2018; Ma *et al.*, 2020). As epigenetic changes have provided a prognostic marker for GBM tumours, researchers questioned whether other types of methylation could offer more molecular biomarkers for each subgroup as well as more targets for treatment.

Within GBM, epitranscriptomic modifications such as m^6A have been extensively investigated, with m^6A interacting proteins found to have roles in proliferation, tumorigenesis and GSCs growth (Cui et al., 2017; Zhang et al., 2017; C. Xu et al., 2020; L. Wang et al., 2020; Dixit et al., 2021). Another m^6A reader that has been implicated in GBM is HNRNPA2B1. The first mention of HNRNPA2B1 concerning GBM is by Golan-Gerstl and their colleagues in 2011 (Golan-Gerstl *et al.*, 2011). Using the Oncomine dataset, they found that HNRNPA2B1 was overexpressed in GBM, oligodendroglioma and astrocytoma tumours when compared to normal brain tissues (Golan-Gerstl *et al.*, 2011). They then examined the levels of *HNRNPA2B1* in 22 patient-derived GBM samples and showed that *HNRNPA2B1* levels were 2 – fold higher compared to normal brain samples (Golan-Gerstl *et al.*, 2011). Knockdown of *HNRNPA2B1* in GBM cell lines such as U251 and SHG-44 led to decreased colony size and number, impacted the ability to attach to growth surfaces and reduced migration capability, suggesting HNRNPA2B1 role in tumour cell invasion in GBM (Deng *et al.*, 2016). Combining the knockdown of HNRNPA2B1 with TMZ treatment at various concentrations, led to a lower survival rate in treated mice and increased cells undergoing apoptosis in plated GBM cells (Deng *et al.*, 2016).

Overall, various m^6A writers, readers and erasers have been studied in relation to GBM, yet only a few of these studies were focused on HNRNPA2B1 in GBM. In this chapter, I investigated the hypothesis that m^6A-marked DNA:RNA hybrids are present in GBM and that loss of *HNRNPA2B1* impacts m^6A and DNA:RNA hybrid levels in GBM.

4.2 Aims

The aim of this chapter was to examine the potential presence of m^{6}A-marked DNA:RNA hybrids and m^{6}A reader HNRNPA2B1 in GBM cells as it was shown in other cell types (Abakir et al., 2020). Previous studies have suggested the role of m^{6}A and its related genes in GBM development, yet they are not attributed to the presence of m^{6}A-marked DNA:RNA hybrids and genomic instability associated with it. We first aimed to examine the expression and nuclear localisation of m^{6}A-related genes in GBM continuous and primary cells. Next, using m^{6}A and DNA:RNA hybrid immunoprecipitation, mass spectrometry and immunocytochemistry, we sought to quantify the levels of m^{6}A-marked DNA:RNA hybrids within repetitive and individual intronic sequences in GBM genomic DNA. Finally, we employed HNRNPA2B1 siRNA-mediated knockdown and examined how the loss of *HNRNPA2B1* affected gene expression and nuclear localisation in GBM cells.

4.3 Results

4.3.1 Elevated levels of m^{6}A writers and readers in GBM.

Our first aim was to establish what m^{6}A-related genes are expressed in GBM. This was accomplished by evaluating public expression datasets of GBM patients, followed by gene expression experiments in available GBM continuous- and primary cell lines.

4.3.1.1 Expression of m^{6}A related genes show similar pattern in GBM patient samples and GBM continuous cell lines.

Initially, to understand the expression levels of m^{6}A-related genes in GBM cells, we utilised public microarray expression data sets available on R2: Genomics Analysis and Visualization Platform (http://r2.amc.nl). We focused on the expression of four key m^{6}A-related genes, *HNRNPA2B1*, two genes linked to *HNRNPA2B1* activity (*METTL3* and *YTHDF2*) and m^{6}A reader that is similar to *HNRNPA2B1* that has previously been linked to splicing (*YTHDC1*). We also included βIII-tubulin (*TUBB3*) as it is expressed in all subgroups of GBM (Abbassi *et al.*, 2019) and therefore we used *TUBB3* as an expression control for GBM cells. We looked

at 2 different datasets, TCGA (540 samples – GBM patient tumours) and Lee (101 samples – a mix of GBM patient samples and GBM cell lines presented in (Lee *et al.*, 2006) (Fig. 4.1). In the TCGA dataset, *HNRNPA2B1* expression has a similar pattern to *TUBB3* except for the expression with Mesenchymal GBM subgroup which was increased from an average square root (sqrt) of expression at 32.72 in *TUBB3* to 34.49 in *HNRNPA2B1* (Fig. 4.1 A). The expression of *METTL3*, *YTHDF2, YTHDC1, HNRNPA2B1, and TUBB3* ranged from 12.68 – 15 sqrt of expression in *METTL3*, 15.24 – 16.27 in *YTHDF2*, 15.75 – 19.07 in *YTHDC1*, 29.95 – 41.26 in *HNRNPA2B1* and 32.72 – 44.12 sqrt of expression in *TUBB3*. Utilising the Lee dataset, we wanted to compare the expression patterns in GBM cell lines with those of a normal non-transformed neural stem cell line, again focussing on *METTL3*, *HNRNPA2B1*, *YTHDF2*, *YTHDC1* and *TUBB3* expression (Fig. 4.1 B). Expression for all the m^6A-related genes observed in GBM cell lines and normal neural stem cells (Lee's dataset) has a similar pattern to what was observed in GBM patient samples (TCGA dataset), but at a higher rate of expression within GBM cell lines compared to GBM patient samples. However, between both the TCGA and Lee datasets, the continuous GBM cell lines tested in Lee's microarray data have a higher square root of expression in all GBM cell lines compared to patient GBM samples in the TCGA dataset.

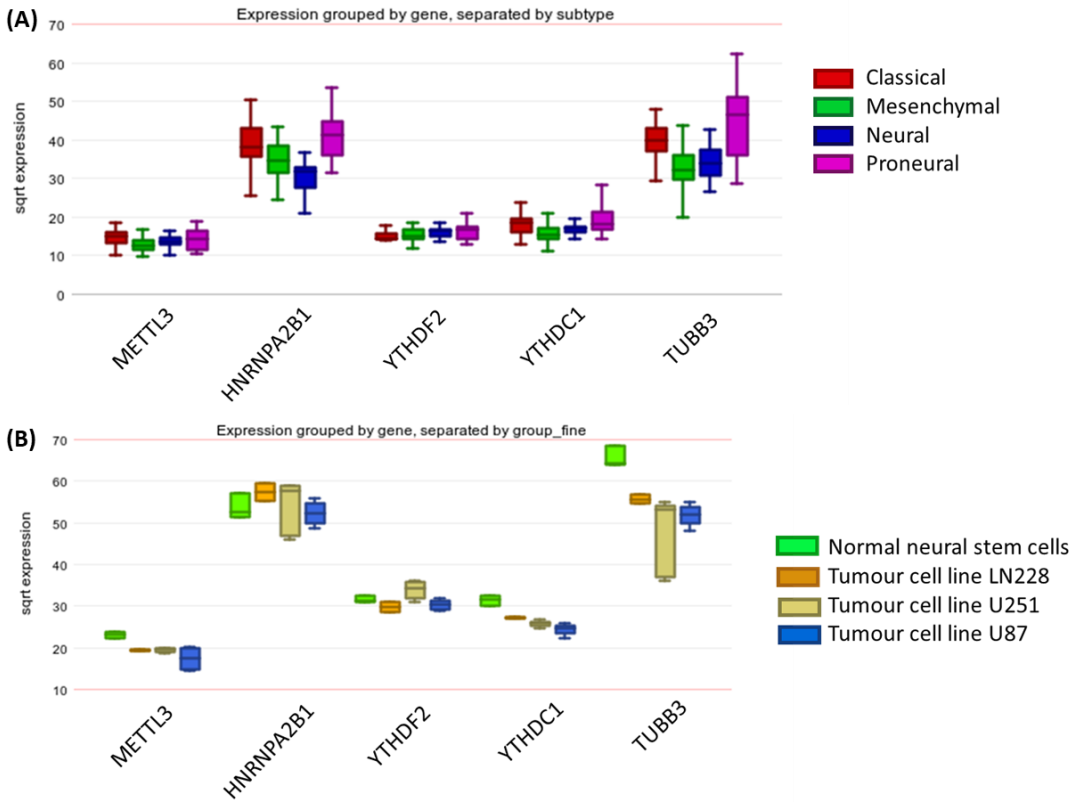


Figure 4.1: GBM patient samples and cell lines exhibit similar expression patterns of m^{6}A-related genes.

(A) *Microarray expression dataset from TCGA (540 total samples) looking at sqrt of expression in METTL3, HNRNPA2B1, YTHDF2, YTHDC1 and TUBB3. Separated by GBM subgroups: Classical (17 samples), Mesenchymal (27 samples), Neural (17 samples) and Proneural (24 samples).* ***(B)*** *Microarray expression dataset from Lee (101 total samples) looking at sqrt expression in METTL3, HNRNPA2B1, YTHDF2, YTHDC1 and TUBB3. Focussed on normal neural stem cells (3 samples), and glioblastoma cell lines: LN228 (2 samples), U251 (6 samples) and U87 (4 samples). Both datasets were analysed by MAS5.0, available on R2: Genomics Analysis and Visualization Platform (http://r2.amc.nl).*

4.3.1.2 HNRNPA2B1 high expression is not linked to one GBM subgroup but it is prevalent in non-disclosed GBM patients.

The TCGA patient datasets indicated that HNRNPA2B1 expression was high in all GBM subgroups, particularly pro-neural and classical subgroups. We, next, wanted to examine whether the high expression of HNRNPA2B1 is linked to GBM prognosis.

Using the R2: Genomics Analysis and Visualization Platform (http://r2.amc.nl) we visualise the TCGA 540 patient samples dataset for GBM as Kaplan curves observing overall survival probability depending upon high or low HNRNPA2B1 expression (Fig. 4.2). Separating the GBM patients into the 4 known subgroups as well as the non-disclosed patient samples, we found no significant impact that high or low expression of *HNRNPA2B1* led to a worse prognosis for the mesenchymal subgroup (p = 0.223, Fig 4.2 A, Supplementary figure 2 A), neural subgroup (p = 0.202, Fig. 4.2 B, Supplementary figure 2 B), pro-neural subgroup (p = 0.204, Fig. 4.2 C, Supplementary figure 2 C), classical subgroup (p = 0.449, Fig. 4.2 D, Supplementary figure 2 D) and non-disclosed subgroup (p = 0.056, Fig. 4.2 E, Supplementary figure 3). Yet, 411 patients exhibited high HNRNPA2B1 expression in non-disclosed subgroup patients compared to only 8 with low HNRNPA2B1 expression.

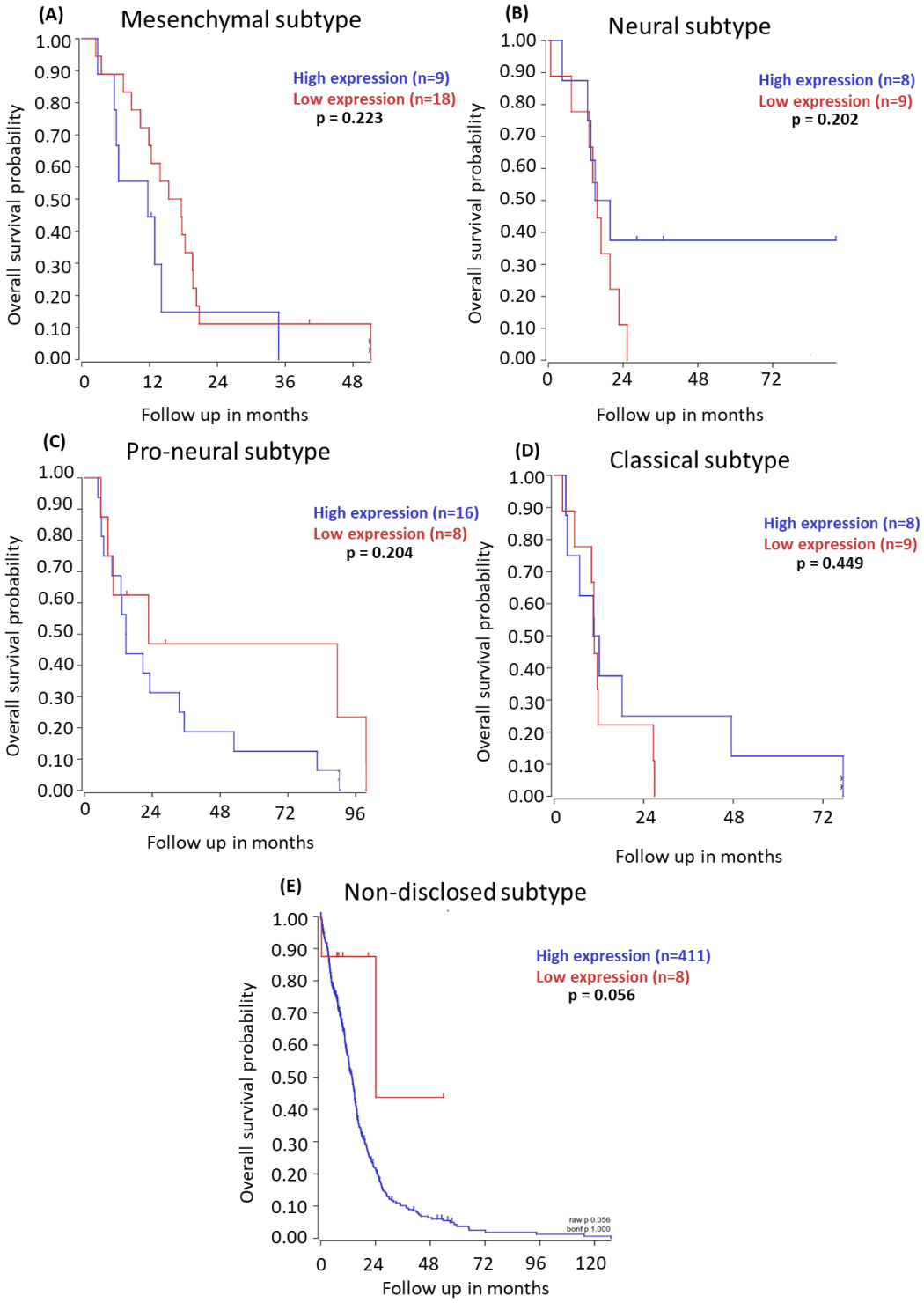


Figure 4.2: HNRNPA2B1 expression is not linked to any known GBM subgroup.

Kaplan curves on HNRNPA2B1 expression were generated on TCGA (540) GBM dataset available on R2: Genomics Analysis and Visualization Platform (http://r2.amc.nl), separated by subgroup: ***(A)*** *Mesenchymal,* ***(B)*** *Neural,* ***(C)*** *Pro-neural,* ***(D)*** *Classical and* ***(E)*** *Non-disclosed.*

4.3.1.3 m^{6}A-related genes show similar gene expression pattern in foetal brain cells, LN18, LN229, U251 and U87MG GBM cell lines.

We then sought to determine whether genes involved in the addition, removal and interaction with m^{6}A were altered in our GBM cell lines: LN18, LN229, U251 and U87MG. To answer this, we performed gene expression analysis by qPCR. As control cell lines, a foetal brain cell line (FB83) and adult astrocyte cell line (SVGA) were included as lineage-specific expression comparisons. All these were compared to induced pluripotent stem cell line known as REBL-PAT (hiPSCs) as m^{6}A writers, readers and erasers have been previously reported to be highly expressed in pluripotent stem cells (Batista *et al.*, 2014; Geula *et al.*, 2015).

Firstly, we looked at the gene expression of m^{6}A writer, *METTL3* (Fig 4.3 A). We found that *METTL3* expression was elevated in FB83 (39.1 – fold, $p = 0.000082$), LN18 (36.1 – fold, $p < 0.000001$), LN229 (51.5 – fold, $p = 0.000007$) and U87MG (32.8 - fold, $p < 0.000001$) compared to hiPSCs. Whereas in the adult astrocyte cell line, SVGA, *METTL3* levels were decreased by 81% ($p < 0.000001$) compared to hiPSCs. Furthermore, U251 displayed non-significant increase in *METTL3* expression (10.3 – fold, $p = 0.0613$) compared to hiPSCs, but displayed large variations between replicates, therefore, more biological replicates were needed to understand *METTL3* gene expression levels in U251. Like *METTL3*, *METTL14* had elevated mRNA levels in FB83 (8.9 – fold, $p = 0.000064$), LN18 (9.1 – fold, $p = 0.000238$), LN229 (9.3 – fold, $p = 0.000028$), U251 (6.04 – fold, $p = 0.00494$) and U87MG (9.2 – fold, $p = 0.00005$) with a 94% decrease of *METTL14* in SVGA ($p = 0.000001$) (Fig 4.3 B) compared to hiPSCs. Unlike the other m^{6}A writers, WTAP expression is relatively low in comparison to *METTL3* and *METTL14* (Fig 4.3 C), with FB83 (2.9 – fold, $p = 0.027$), LN18 (1.3 – fold, $p = 0.558$), U251 (3.7 – fold, $p = 0.0872$) and U87MG (1.3 – fold, $p = 0.549$) showing increased expression but SVGA (59%, $p = 0.00153$) and LN229 (68%, $p = 0.000414$) with markedly decreased *WTAP* expression compared to hiPSCs.

Readers of m^{6}A, such as *YTHDC1* (Fig. 4.3 D), had increased expression in FB83 (680.4 – fold, $p = 0.071$), SVGA (3.2 – fold, $p = 0.0451$), LN18 (2.1 – fold, $p = 0.272$) and U251 (2.5 – fold, $p = 0.106$) but decreased expression in LN229 (54%, $p = 0.0045$) and U87MG (15%, $p = 0.575$) compared to hiPSCs. Contrasting to *YTHDC1*, *YTHDF2* (Fig. 4.3 E) had significant

elevation in gene expression in FB83 (159.9 – fold, $p < 0.000001$), LN18 (61.5 – fold, $p = 0.000005$), LN229 (65.5 – fold, $p < 0.000001$), U251 (48.2 – fold, $p = 0.054$) and U87MG (111.4 – fold, $p = 0.000046$) but a 65% reduction in *YTHDF2* gene expression in SVGA ($p < 0.000001$) compared to hiPSCs. Similar to *YTHDF2*, *HNRNPA2B1* (Fig. 4.2 F) has elevated mRNA levels in FB83 (9.5 – fold, $p = 0.00367$), LN18 (5.8 – fold, $p = 0.00935$), LN229 (8.2 – fold, $p = 0.000046$), U251 (30.5 – fold, $p = 0.0562$) and U87MG (9.4 – fold, $p = 0.0675$) but 80% reduction in gene expression in SVGA ($p = 0.000043$) compared to hiPSCs.

One of the genes involved in the removal of m^6A, *FTO* (Fig. 4.2 G), displayed significantly higher levels of expression in FB83 (10.3 – fold, $p = 0.000002$) and U251 (3.9 – fold, $p = 0.0256$) but was decreased by 32% in SVGA ($p = 0.0484$), 19% in LN18 ($p = 0.624$), 78% in LN229 ($p = 0.000004$) and 55% in U87MG ($p < 0.000001$) compared to hiPSCs. Another gene involved in the removal of m^6A, *ALKBH5* (Fig. 4.2 H), has elevated gene expression in FB83 (82.8 – fold, $p = 0.000010$), LN18 (5.9 – fold, $p = 0.249$), U251 (6.6 – fold, $p = 0.0256$) and U87MG (2.3 – fold, $p = 0.0109$) and reduction in gene expression by 48% in SVGA ($p = 0.00096$) and 35% in LN229 ($p = 0.267$) compared to hiPSCs.

Next, using a heat map of the median gene expression of the replicates, we wanted to examine if there was a specific pattern of expression common for the GBM cell lines we used (Fig. 4.4). Expression profiles of *METTL3* and *YTHDF2* were similar in LN18, LN229 and U87MG but in U251, *METTL3* gene expression was lower in comparison to the other GBM cell lines. Moreover, U251 has a higher level of *HNRNPA2B1* gene expression compared to LN18, LN229 and U87MG.

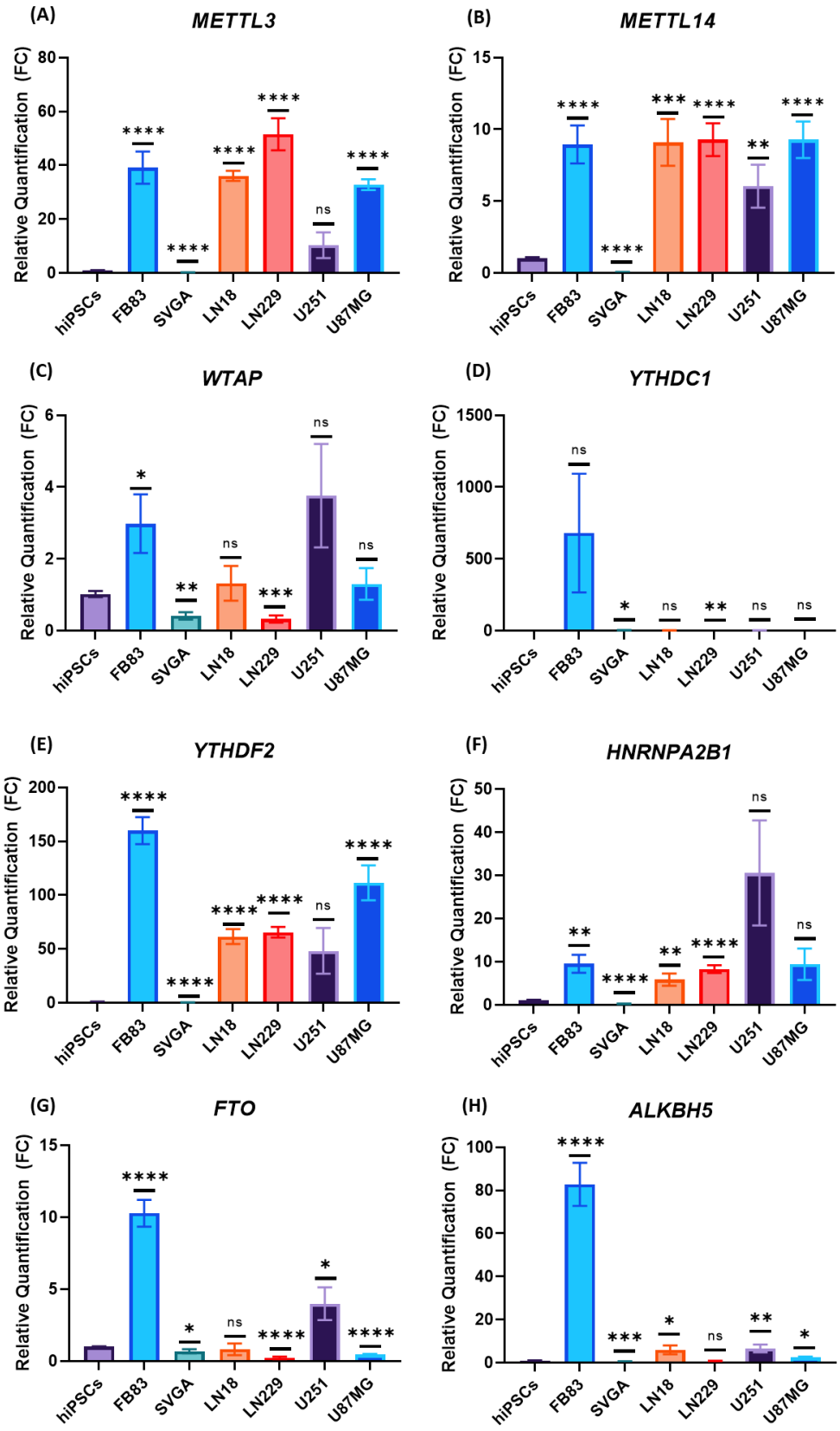


Figure 4.3: *METTL3*, *METTL14*, *YTHDF2* and *HNRNPA2B1* gene expression is significantly increased in glioblastoma cell lines compared to hiPSCs.

Gene expression qPCR of m^{6}A related gene levels, ***(A)*** *METTL3,* ***(B)*** *METTL14,* ***(C)*** *WTAP,* ***(D)*** *YTHDC1,* ***(E)*** *YTHDF2,* ***(F)*** *HNRNPA2B1,* ***(G)*** *FTO and* ***(H)*** *ALKBH5 in foetal brain cell line (FB83), adult human immortalised astrocytes (SVGA) and GBM cell lines: LN18, LN228, U251 and U87MG compared to hiPSCs. Mean ± SEM, 2 biological replicates each with 3 technical replicates. Unpaired t-test, ns = p ≥ 0.05, * = p < 0.05, ** = p < 0.01, *** = p < 0.001, **** = p < 0.0001.*

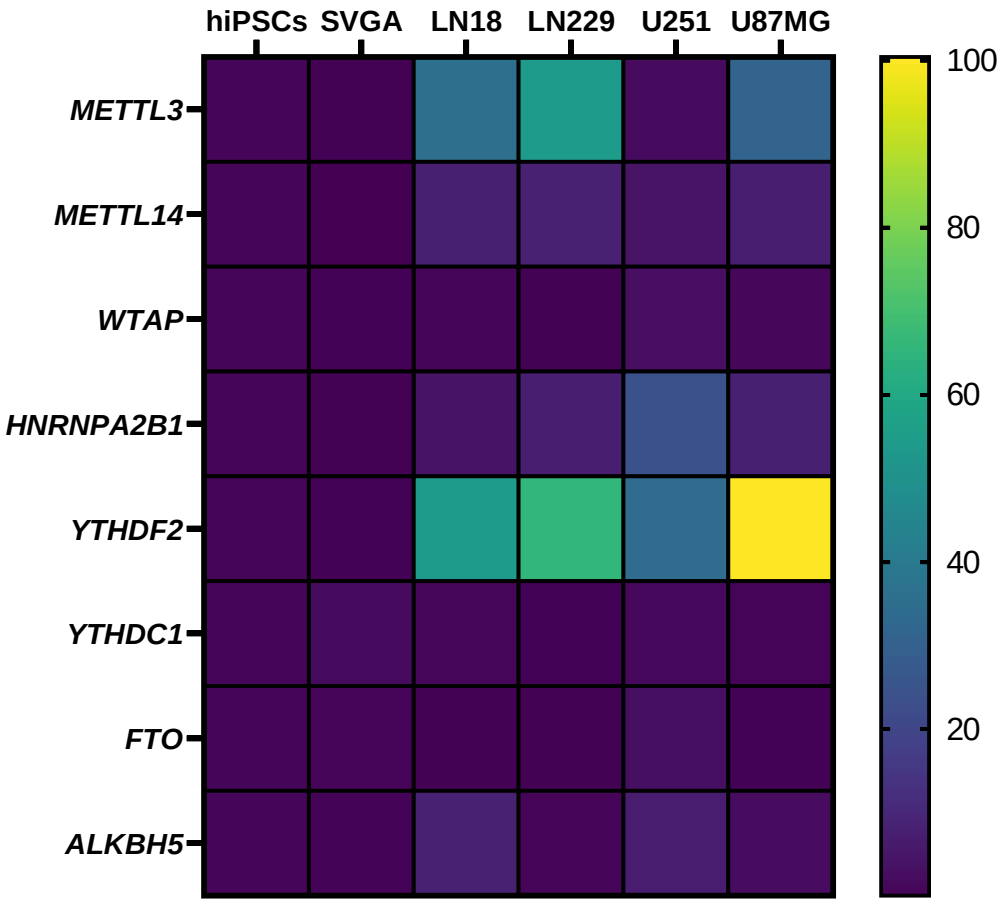


Figure 4.4: LN18, LN229 and U87MG cells have similar expression pattern of m^{6}A related genes.

Heat Map of hiPSCs, SVGA, LN18, LN229, U251 and U87MG gene expression of m^{6}A genes: METTL3, METTL14, WTAP, YTHDF2, YTHDC1, HNRNPA2B1, FTO and ALKBH5. Map of the median of side-by-side replicates. All cell lines had 2 biological replicates each with 3 technical replicates.

4.3.1.4 Primary GBM cells have lower expression of m^{6}A-related genes compared to continuous GBM cell lines.

To examine whether the gene expression seen in GBM cell lines was similar to that of GBM patients, we initially used public microarray expression data sets available on R2: Genomics Analysis and Visualization Platform (http://r2.amc.nl) (Pollard *et al.*, 2009). Using *TUBB3* as a control, we looked at Pollard's dataset (Pollard *et al.*, 2009) focusing on comparing GBM cell lines (14 samples) to primary cells (6 samples) for *METTL3*, *HNRNPA2B1*, *YTHDF2* and *YTHDC1* expression(Fig. 4.5). The microarray expression dataset suggests that expression of *METTL3* ($p = 8.66 \times 10^{-6}$), *HNRNPA2B1* ($p = 1.46 \times 10^{-9}$), *YTHDF2* ($p = 1.08 \times 10^{-8}$) and *YTHDC1* ($p = 0.011$) was lower in GBM primary cells compared to GBM cell lines.

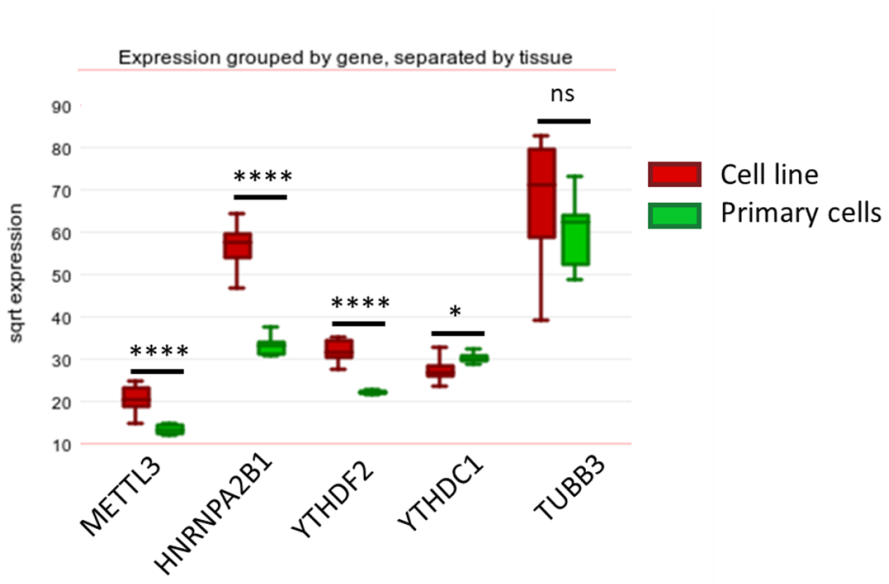


Figure 4.5: Primary glioblastoma cell line have lower expression of m^{6}A-related and DNA:RNA hybrid related genes compared to continuous cell lines.

*Microarray expression dataset from Pollard (20 samples: 14 cell line samples and 6 primary tissues) looking at sqrt of expression in METTL3, HNRNPA2B1, YTHDF2, YTHDC1 and TUBB3. ANOVA analysis comparing between glioblastoma cell lines to primary glioblastoma cells, ns = $p \geq 0.05$, * = $p < 0.05$, **** = $p < 0.0001$. Datasets were analysed by MAS5.0, available on R2: Genomics Analysis and Visualization Platform (http://r2.amc.nl).*

Next, we used three primary GBM cell lines, obtained from patients at Queens Medical Centre (QMC) Nottingham, isolated from the invasive margins of the tumour, GIN8, GIN28 and GIN31 (Glioblastoma INvasive). We examined the expression of four m^6A-related genes (*METTL3*, *METTL14*, *YTHDF2* and *HNRNPA2B1*) from continuous GBM cell lines previously shown in Fig 4.2, with primary GBM cells (Fig 4.6). For *METTL3* (Fig. 4.6 A), there was only a slight increase in expression by 1.8 – fold in GIN8 ($p = 0.157$), 1.6 – fold in GIN28 ($p = 0.373$) but a 14% decrease in GIN31 ($p = 0.093$) compared to hiPSCs. There was a small elevation in *METTL14* levels by 1.7 – fold in GIN8 ($p = 0.478$), 1.04 – fold in GIN28 ($p = 0.888$) and 3.8 – fold in GIN31 ($p = 0.133$) compared to hiPSCs (Fig 4.6 B). *YTHDF2* had increased gene expression by 2.4 – fold in GIN8 ($p = 0.144$), 2.4 – fold in GIN28 ($p = 0.166$) and 1.5 – fold in GIN31 ($p = 0.181$) compared to hiPSCs (Fig. 4.6 C). *HNRNPA2B1* also had increased gene expression in GIN8 by 1.8 – fold ($p = 0.237$), GIN28 by 2 – fold ($p = 0.234$) and GIN31 by 2.5 – fold ($p = 0.046$) compared to hiPSCs (Fig. 4.6 D). Overall, the gene expression levels of *METTL3*, *METTL14*, *YTHDF2* and *HNRNPA2B1* were lower in primary GBM cell lines GIN8, GIN28 and GIN31 compared to the continuous GBM cell line counterparts.

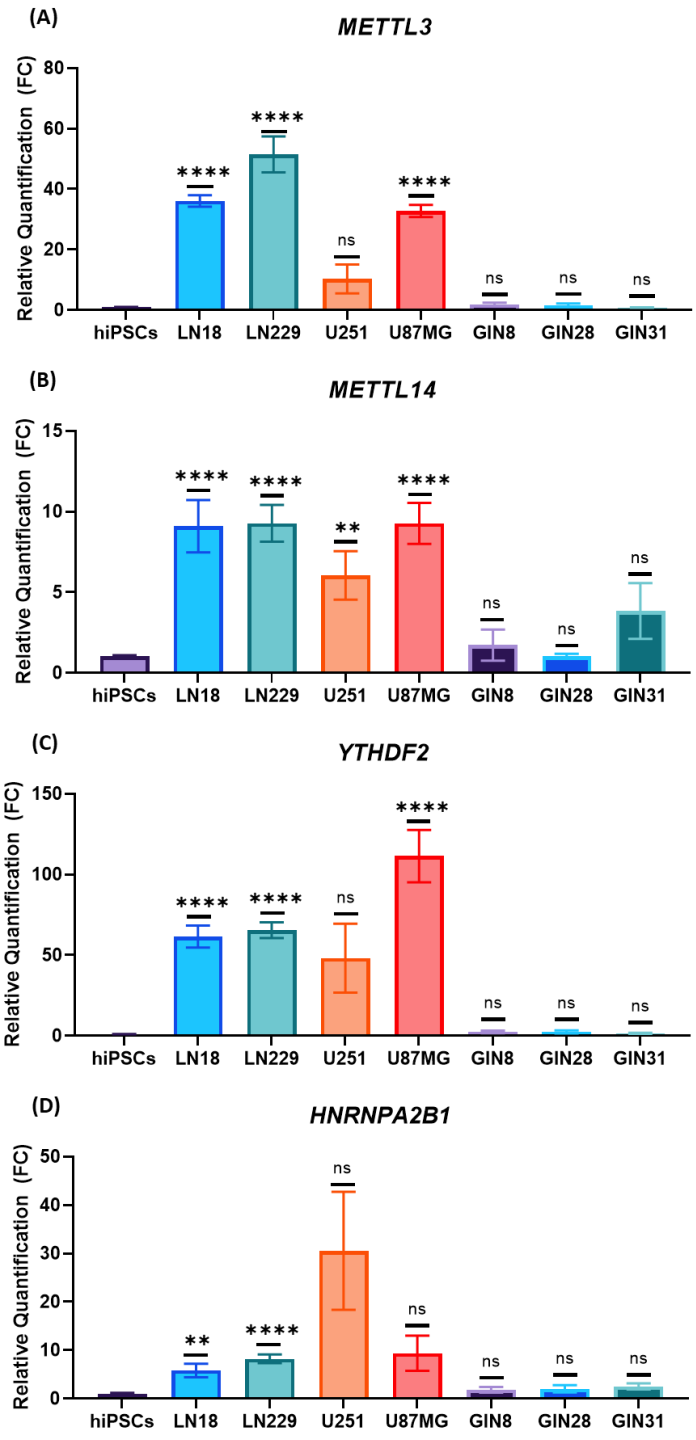


Figure 4.6: Gene expression for m^{6}A-related genes is lower in primary glioblastoma cell lines compared to hiPSCs.

Gene expression of m^{6}A related genes, ***(A)*** *METTL3,* ***(B)*** *METTL14,* ***(C)*** *YTHDF2 and* ***(D)*** *HNRNPA2B1 in continuous cell lines: LN18, LN229, U251, U87MG and primary glioblastoma cell lines GIN8, GIN28 and GIN31 compared to hiPSCs. Mean ± SEM, 2 biological replicates each with 3 technical replicates. Unpaired t-test, ns = $p \geq 0.05$, ** = $p < 0.01$, **** = $p < 0.0001$.*

4.3.2 Levels of m^{6}A-marked DNA:RNA hybrids varied between GBM cell lines.

Gene expression analysis and analysis of public expression datasets have alluded to the presence of m^{6}A interacting genes in GBM cells, revealing high gene expression levels of *METTL3*, *YTHDF2* and *HNRNPA2B1*. Subsequently, our next aim was to examine the presence of m^{6}A marked DNA:RNA hybrids within GBM cells. Preliminary immunostaining by our group identified that m^{6}A-marked DNA:RNA hybrids are present in hiPSCs and GBM cell line LN229 (Abakir *et al.*, 2020). We employed techniques such as m^{6}A DRIP, S9.6 DRIP, SID-UPLC-MS/MS and immunocytochemistry to provide answers to the extent of the presence of m^{6}A-marked DNA:RNA hybrids in LN18 and U251 cells.

4.3.2.1 DNA:RNA hybrids and m^{6}A-DNA:RNA hybrids levels in repetitive sequences are both lower in U251 compared to hiPSCs.

We previously described a method for identifying the presence as well as the genomic distribution of m^{6}A-marked DNA:RNA hybrids in the genome by immunoprecipitation using m^{6}A and DNA:RNA hybrid (Clone S9.6) antibodies followed by qPCR (Boguslawski *et al.*, 1986; Phillips *et al.*, 2013; Abakir *et al.*, 2020). Previous next-generation sequencing data from our group has shown that the majority of m^{6}A-DNA:RNA hybrids reside on repetitive elements in hiPSCs (Abakir *et al.*, 2020). Therefore, we wanted to examine whether m^{6}A-marked DNA:RNA hybrids are present at the same genomic locations in GBM as in hiPSCs.

Using hiPSCs genomic DNA as a control (Fig. 4.7 A – D), we determined that U251 had lower levels of m^{6}A-marked DNA:RNA hybrids in repetitive elements compared to hiPSCs. In *α-satellites* (Fig. 4.7 A), there was a decrease in the enrichment of m^{6}A on DNA:RNA hybrids by 640.59 – fold between U251 and hiPSCs. Similarly, in *LINE1* (Fig. 4.7 B), there was also a decreased m^{6}A enrichment on DNA:RNA hybrids by 1.45 x 10^4 – fold comparing U251 to hiPSCs. In *Alu-Y* (Fig. 4.7 C) and *Alu-S* (Fig. 4.7 D), we detected a decrease in the enrichment of m^{6}A on DNA:RNA hybrids in U251 by 27.22 – fold and 80.21 – fold, respectively compared to hiPSCs.

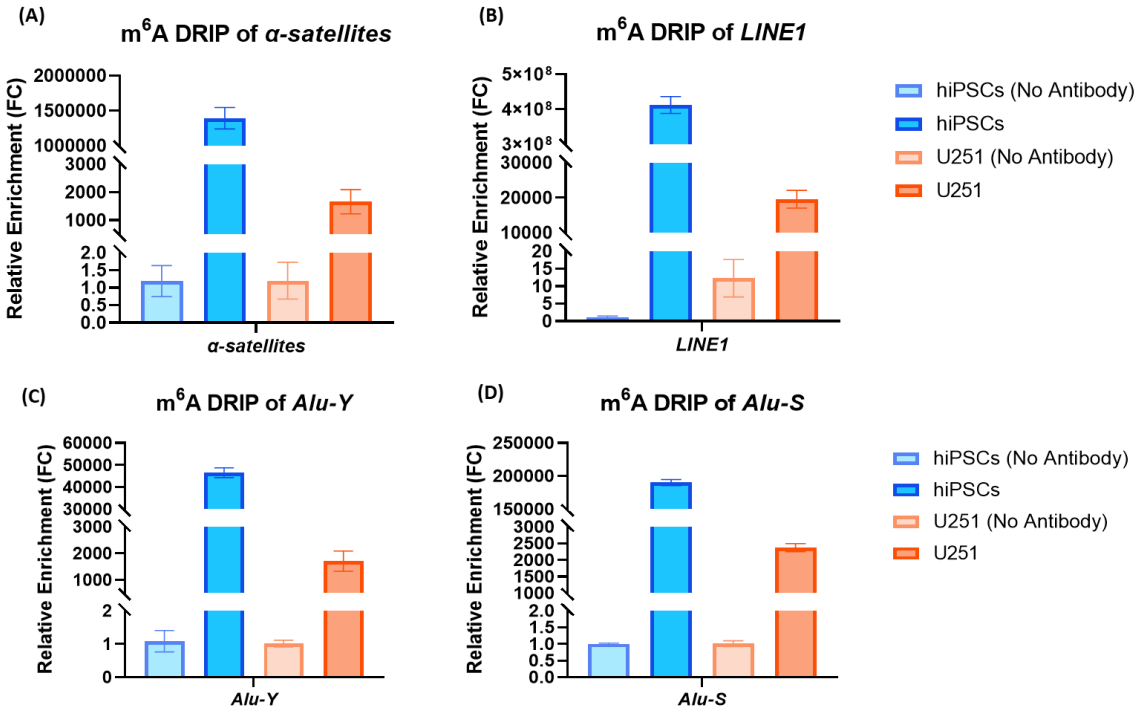


Figure 4.7: Levels of m^{6}A marked DNA:RNA hybrids in repetitive elements are lower in U251 compared to hiPSCs.

m^{6}A DRIP qPCR comparison of repetitive elements: ***(A)*** *α-satellites,* ***(B)*** *LINE1 and SINE elements* ***(C)*** *Alu-Y and* ***(D)*** *Alu-S between hiPSCs and U251. Mean ± SEM, 1 biological replicate with 3 technical replicates.*

A similar pattern was observed in our S9.6 DRIP experiments (Fig. 4.8). In *LINE1* (Fig. 4.8 B), there was a decrease in DNA:RNA hybrid enrichment by 33.74 – fold. Similarly, *Alu-Y* (Fig. 4.8 C) and *Alu-S* (Fig. 4.8 D) also observed a decrease in levels of DNA:RNA hybrids in U251 compared to hiPSCs by 63.22 – fold and 30.18 – fold, respectively. Whereas there was no difference in the levels of DNA:RNA hybrids between U251 and hiPSCs in *α-satellites* (Fig. 4.8 A, 1.15 – fold). Overall, U251 had lower enrichment levels compared to hiPSCs levels with both m^{6}A-marked DNA:RNA hybrids and DNA:RNA hybrids within repetitive elements.

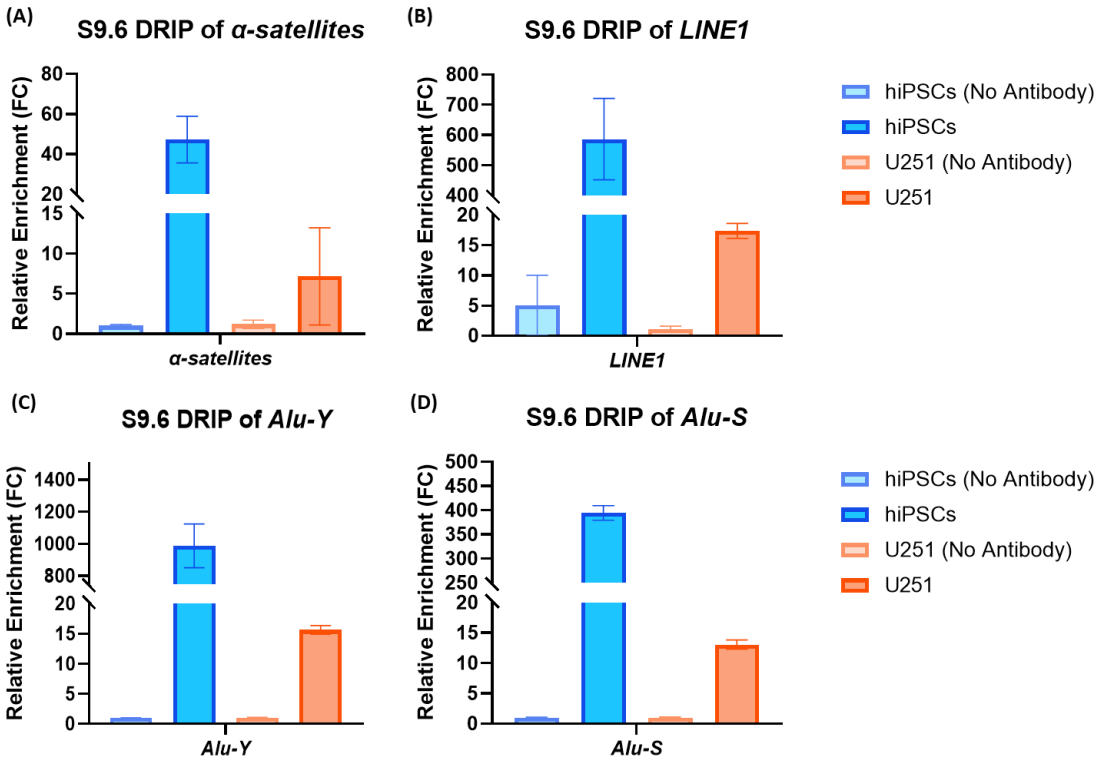


Figure 4.8: Levels of DNA:RNA hybrids in repetitive elements are lower in U251 compared to hiPSCs.

S9.6 DRIP qPCR comparison of repetitive elements: ***(A)*** *α-satellites,* ***(B)*** *LINE1 and SINE elements* ***(C)*** *Alu-Y and* ***(D)*** *Alu-S between hiPSCs and U251. Mean ± SEM, 1 biological replicate with 3 technical replicates.*

4.3.2.2 The levels of m^{6}A on DNA:RNA hybrids in intronic regions of *CDK6*, *RB1* and *NF1* genes are lower in U251 GBM line compared to hiPSCs.

To examine whether m^{6}A-marked DNA:RNA hybrids were present on chosen GBM-related genes, we used data retrieved from next-generation sequencing of m^{6}A DRIP and S9.6 DRIP in hiPSCs (Abakir *et al.*, 2020).

Bioinformatics analysis revealed lists of peaks that overlapped between m^{6}A DRIP and S9.6 DRIP. From this list, we visualised the data using IGV to create coverage plots to search for potential m^{6}A-DNA:RNA hybrids within GBM-linked genes (Fig. 4.9 – 4.11). We identified three candidates with important roles within GBM: in the 4th intron of cyclin-dependent kinase

6 (*CDK6*) (Fig. 4.9 A), in the 2nd intron of RB Transcriptional Corepressor 1 (*RB1*) (Fig. 4.10 A) and the 8th intron of Neurofibromatosis type-1 (*NF1*) (Fig. 4.11 A).

The cyclin-dependent kinase 4 (CDK4)/CDK6 pathway controls cell cycle progression from Growth 1 (G1) phase to Synthesis (S) phase within the cell cycle (Biernat *et al.*, 1997; Wemmert *et al.*, 2009; Chen and Pan, 2017). Both cyclin-dependent kinase 4 (CDK4) and cyclin-dependent kinase 6 (CDK6) can phosphorylate Retinoblastoma protein (pRB) triggering the release of E2 factor (E2F) transcription factors (Bartek, Bartkova and Lukas, 1997; Biernat *et al.*, 1997; Gil and Peters, 2006). This enables the transition from the G1 phase to begin DNA replication in the S phase of the cell cycle. Cyclin-dependent kinase inhibitor 2A (CDKN2A) and cyclin-dependent kinase inhibitor 2B (CDKN2B) regulate CDK4 and CDK6 activity by binding and preventing phosphorylation of pRB that resulting in cell cycle arrest (Bartek, Bartkova and Lukas, 1997; Biernat *et al.*, 1997). Within GBM, CDK4 and/or CDK6 are observed to be upregulated, giving rise to gliomagenesis and tumour progression (Biernat *et al.*, 1997; Chow *et al.*, 2011). Mutations, deletions and expressional abnormalities are seen commonly in *CDKN2A*, *CDK4*, *CDK6* or *RB1* leading to aggressive GBM tumorigenesis (Jen *et al.*, 1994; Biernat *et al.*, 1997; Parsons *et al.*, 2008). Whereas *NF1* is a tumour suppressor protein with marked mutations that are prominent in the mesenchymal subgroup of GBM (Phillips *et al.*, 2006; Verhaak *et al.*, 2010). Primers were designed over the regions with m^6A-marked DNA:RNA hybrids identified in hiPSCs by next-generation sequencing analysis of *CDK6* (Fig. 4.9 A), *RB1* (Fig. 4.10 A) and *NF1* (Fig. 4.11 A). Using these primers, we wanted to quantify the levels of m^6A-DNA:RNA hybrids in hiPSCs and U251.

Examining these candidates by m^6A DRIP qPCR, we observed an overall lower enrichment of m^6A-marked DNA:RNA hybrids in U251 cells compared to hiPSCs. In *CDK6*, we observed a decrease in the enrichment of m^6A on DNA:RNA hybrids by 2.5 $x10^{12}$ – fold in U251 compared to hiPSCs (Fig. 4.9 B). Similarly, in *RB1* (Fig. 4.10 B) we found the enrichment of m^6A on DNA:RNA hybrids decreased by 6.7 $x10^4$ – fold in U251 compared to hiPSCs. In *NF1* (Fig. 4.11 B), we detected a decrease in m^6A on DNA:RNA hybrids by 1.47 $x10^7$ – fold in U251 compared to hiPSCs. Overall, the levels of m^6A-marked DNA:RNA hybrids were lower in U251 cells compared to hiPSCs within GBM-related genes.

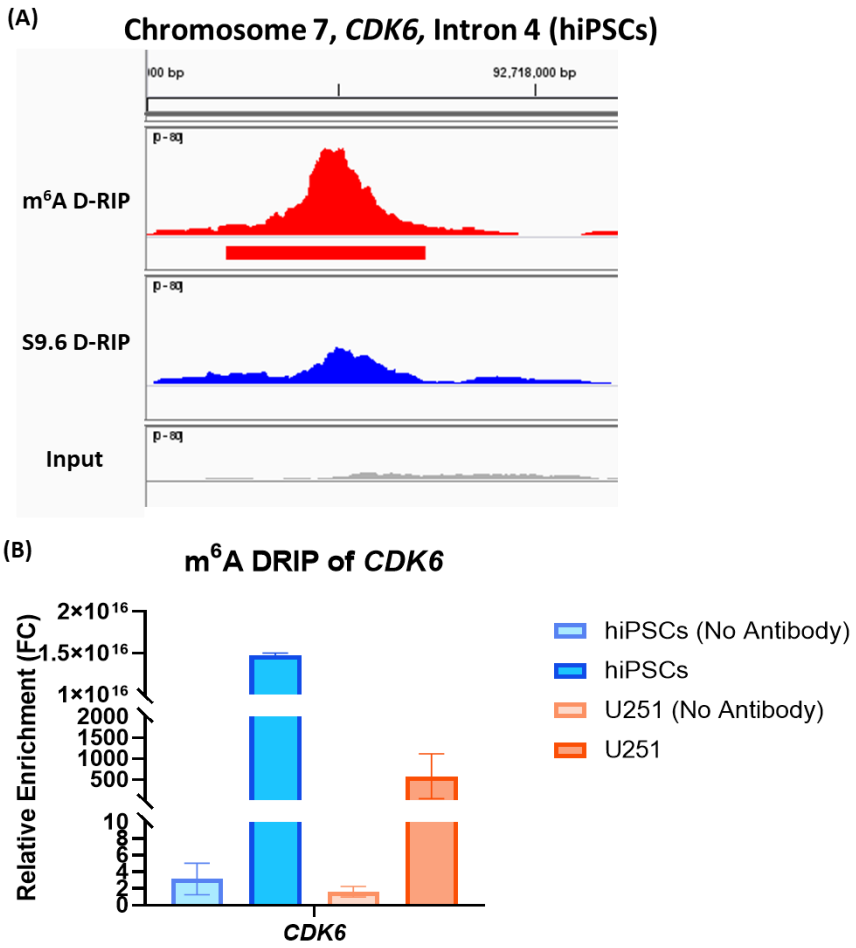


Figure 4.9: Enrichment levels of m^{6}A-marked DNA:RNA hybrids within *CDK6* introns are lower in U251 compared to hiPSCs.

(A) *CDK6 IGV coverage plot of m^{6}A DRIP and S9.6 DRIP next-generation sequencing within hiPSCs. IGV coverage plots were compared to hiPSCs input with the data range set at 80 for CDK6.* ***(B)*** *m^{6}A DRIP qPCR comparison between hiPSCs and U251 for CDK6 with matched no antibody controls. Mean ± SEM, 1 biological replicate with 3 technical replicates.*

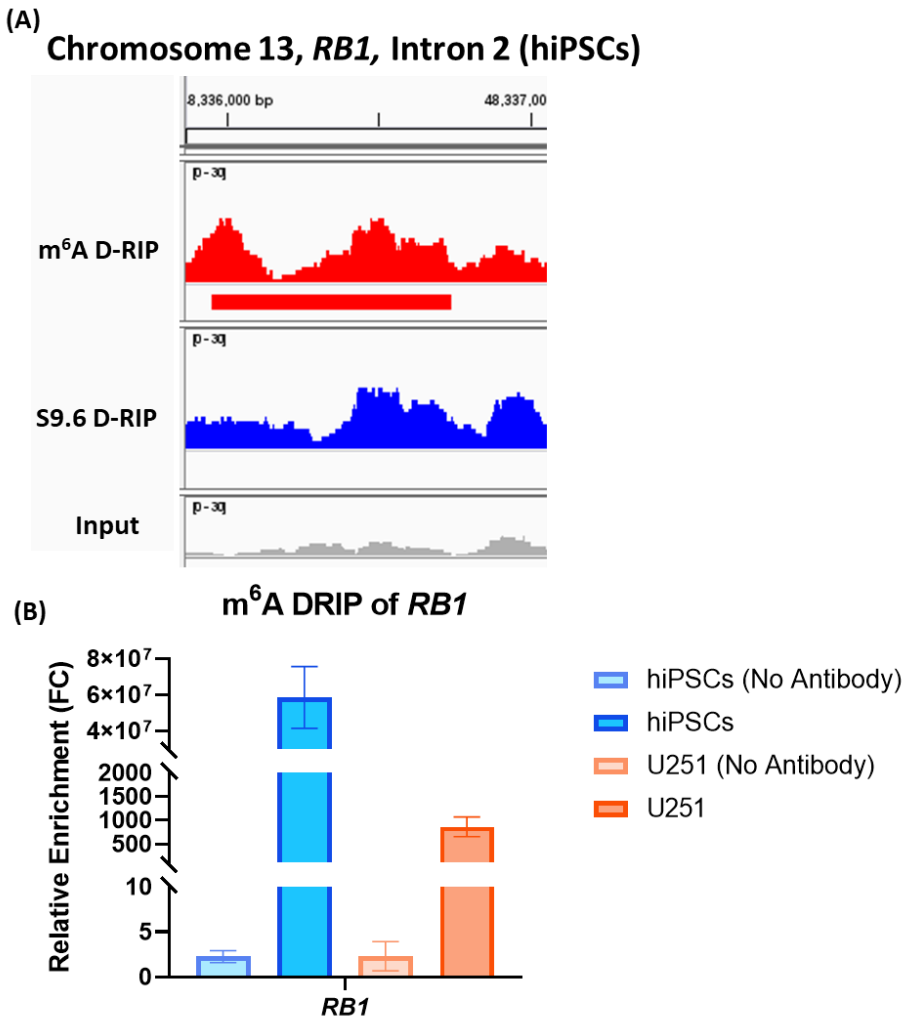


Figure 4.10: Enrichment levels of m^{6}A-marked DNA:RNA hybrids within *RB1* introns are lower in U251 compared to hiPSCs.

(A) *RB1 IGV coverage plot of m^{6}A DRIP and S9.6 DRIP next-generation sequencing within hiPSCs. IGV coverage plots were compared to hiPSCs input with the data range set at 30 for RB1.* ***(B)*** *m^{6}A DRIP qPCR comparison between hiPSCs and U251 for RB1 with matched no antibody controls. Mean ± SEM, 1 biological replicate with 3 technical replicates.*

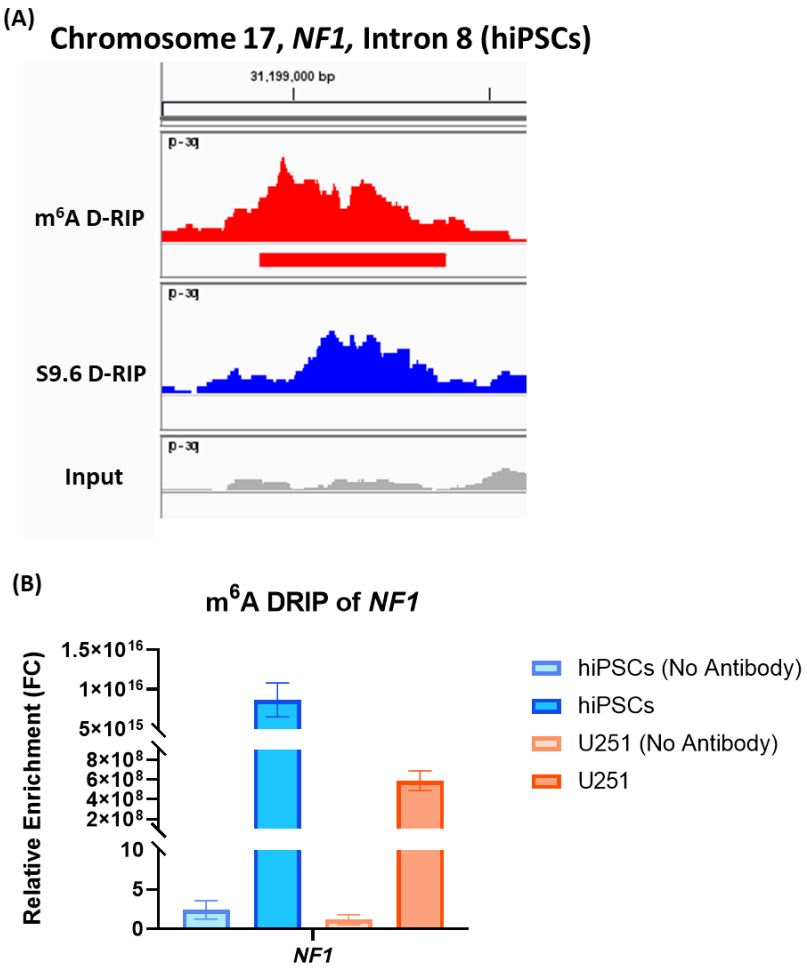


Figure 4.11: Enrichment levels of m^{6}A-marked DNA:RNA hybrids within *NF1* introns are lower in U251 compared to hiPSCs.

(A) *NF1 IGV coverage plot of m^{6}A DRIP and S9.6 DRIP next-generation sequencing within hiPSCs. IGV coverage plots were compared to hiPSCs input with the data range set at 30 for NF1.* ***(B)*** *m^{6}A DRIP qPCR comparison between hiPSCs and U251 for NF1 with matched no antibody controls. Mean ± SEM, 1 biological replicate with 3 technical replicates.*

4.3.2.3 SID-UPLC-MS/MS demonstrates the levels of m^{6}A on DNA:RNA hybrids in GBM cell lines.

SID-UPLC-MS/MS has been used to evaluate the overall levels of m^{6}A-marked DNA:RNA hybrids, as was previously shown (Abakir *et al.*, 2020). Since hiPSCs have already been recognised to have m^{6}A-marked DNA:RNA hybrids present with this technique (Abakir *et al.*, 2020) and used in Chapter 3, we used hiPSCs to compare the levels of m^{6}A-DNA:RNA hybrid

presence to GBM cell line (LN18) and human adult astrocyte cell line (SVGA) (Fig. 4.12). In line with previously published results, we observed elevated levels of m^6A on DNA:RNA hybrids in RNase H treated hiPSCs (56.774 fmol/µg of input DNA) compared to non-RNase H treated hiPSCs (18.198 fmol/µg of input DNA). SVGA and LN18 cell lines observed a comparable amount of m^6A-marked DNA:RNA hybrids with RNase H treated samples (20.234 and 19.354 fmol/µg of input DNA, respectively) compared to non-RNase treated SVGA (6.681 fmol/µg of input DNA) and LN18 cells (7.844 fmol/µg of input DNA). These results suggest that both SVGA and LN18 cells have m^6A marked DNA:RNA hybrids present, yet at a lower level in comparison to hiPSCs.

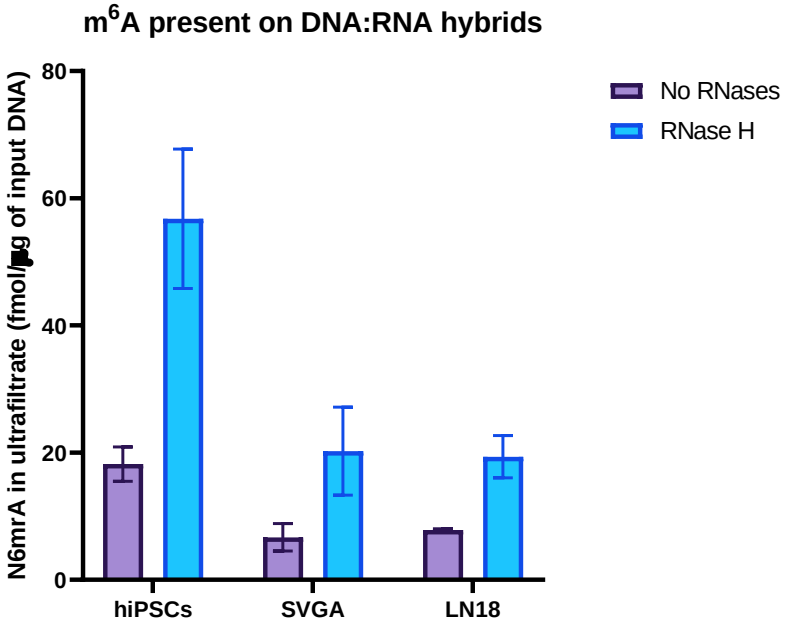


Figure 4.12: SVGA and LN18 cells have lower levels of m^6A present on DNA:RNA hybrids compared to hiPSCs.

SID–UPLC–MS/MS quantification of m^6A within the fractions of hiPSCs-derived, SVGA-derived, LN18-derived nucleic acids released following RNase H treatment. Mean ± SEM, 2 biological replicates.

4.3.2.4 U251 exhibit the lowest levels of m^{6}A-DNA:RNA hybrids immunostaining compared to hiPSCs, LN18 and SVGA cells.

Another technique used to visualise the presence and localisation of m^{6}A-DNA:RNA hybrids are immunocytochemistry. Using m^{6}A and Ph-H3 antibodies and pre-treatment of the samples with RNase A conditions, we compared the m^{6}A signal intensity between hiPSCs, SVGA, U251 and LN18. We used hiPSCs as the control for m^{6}A-DNA:RNA hybrids immunostaining and SVGA as a lineage-specific adult astrocyte cell line control. We also pre-treated the fixed cells with RNase A which degrades single-stranded RNA. With this treatment we remove any single-stranded RNAs that could potentially have m^{6}A present, leaving the remaining signal residing in other RNA species such as the RNA components of DNA:RNA hybrids. Under these conditions (Fig. 4.13), hiPSCs, SVGA and LN18 appeared to have similar levels of m^{6}A-DNA:RNA hybrids in non-mitotic cells. Whereas the level of m^{6}A-marked DNA:RNA hybrids in U251 interphase cells was noticeably lower compared to these cell lines.

Both immunocytochemistry and m^{6}A DRIP qPCR results (Fig. 4.7) suggested a low presence of m^{6}A-marked DNA:RNA hybrids within U251 cells, despite our qPCR data suggesting elevated expression of m^{6}A writer, *METTL3* (Fig. 4.3 A).

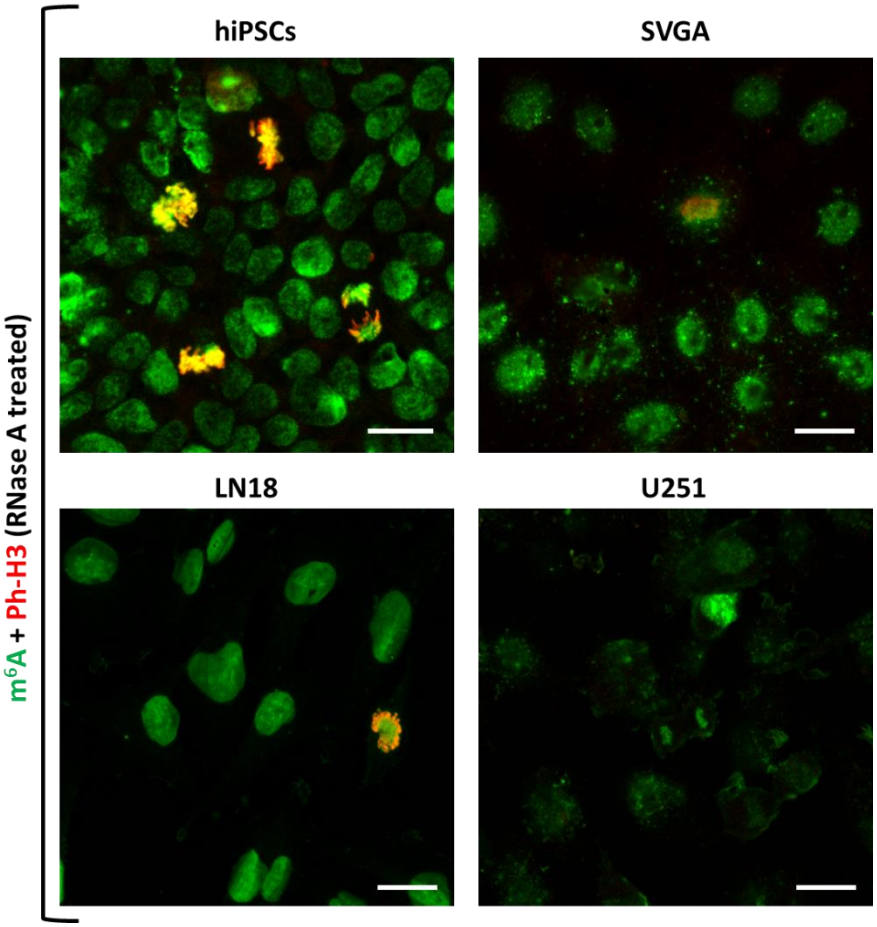


Figure 4.13: m^{6}A DNA:RNA hybrids immunostaining is lower in U251 cells compared to hiPSCs, SVGA and LN18.

Immunostaining of m^{6}A and phospho-Histone H3 (Ph-H3) in RNase A treated hiPSCs, SVGA, LN18 and U251. Representative image shown from 3 technical replicates. Scale bar represents 20 μM.

4.3.3 siRNA mediated knockdown of *HNRNPA2B1* in U251 cells leads to elevated m^{6}A content.

Gene expression analysis of *HNRNPA2B1* suggested its expression was higher in U251 compared to the other GBM cell lines examined. However, according to immunostaining and m^{6}A DRIP qPCR we observed low levels of m^{6}A-marked DNA:RNA hybrids in U251 cells compared to hiPSCs. Therefore, we wanted to examine whether the levels of DNA:RNA hybrid or m^{6}A are altered by HNRNPA2B1-siRNA mediated knockdown. To examine if loss of *HNRNPA2B1* impacts the presence of DNA:RNA hybrids as well as m^{6}A levels, we used *HNRNPA2B1* siRNA transfected into cells with the chemical transfection reagent,

DharmaFECT. Although this method does not cause long-term removal of *HNRNPA2B1,* it could indicate if *HNRNPA2B1* has a role in influencing the levels of DNA:RNA hybrids or m^6A levels in U251 cells.

4.3.3.1 Validation of HNRNPA2B1 knockdown in U251 cells.

In our initial experiments, we aimed to choose a concentration of HNRNPA2B1 siRNA and DharmaFECT that have the strongest knockdown efficiency without severely impacting the cell viability (Fig. 4.14). From two biological replicates, we observed that 50 nM siHNRNPA2B1 with 3 µL of DharmaFECT produced the most consistent knockdown efficiency without impacting cell viability (Fig. 4.14 A). Our qPCR experiments, we demonstrated 65.93% siHNRNPA2B1 knockdown efficiency ($p < 0.000001$) compared to the control U251 cells (Fig. 4.14 B). After transfection, we observed lifting of the cells treated with HNRNPA2B1 siRNA compared to OptiMEM media only. It was also noted that the remaining attached cells after transfection exhibited rounded morphology compared to untreated U251 cells which have an elongated and elliptical appearance.

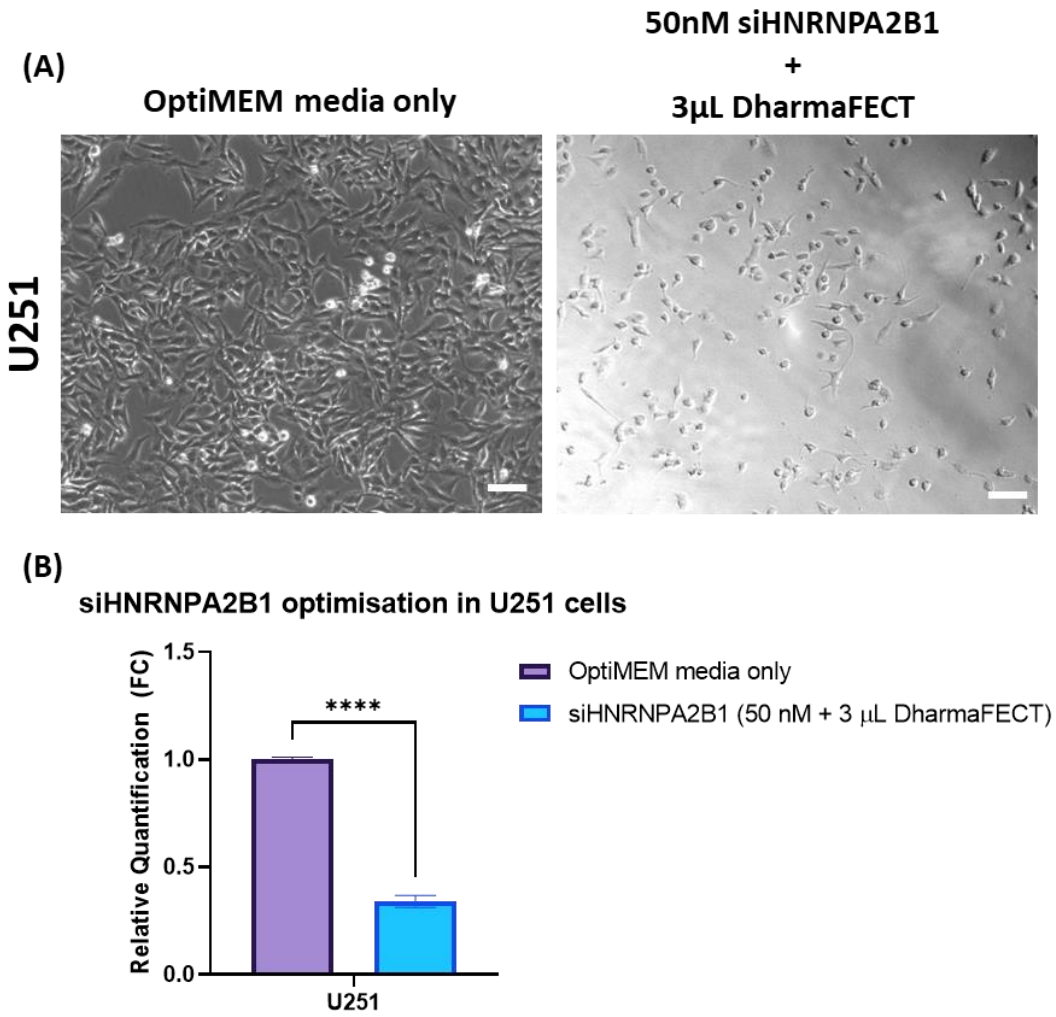


Figure 4.14: Optimisation of siHNRNPA2B1 knockdown in U251 cells.

(A) *Brightfield light microscope images of optimised siRNA treatment of siHNRNPA2B1 in U251 cells 24 hours post-transfection compared to U251 cells in reduced serum OptiMEM media. Transfection of HNRNPA2B1 siRNA was optimised to 50 nM siHNRNPA2B1 with 3 µL per well of DharmaFECT. Scale bar represents 100 µM.* ***(B)*** *RT-qPCR testing of HNRNPA2B1 siRNA knockdown efficiency at 50 nM siHNRNPA2B1 with 3 µL per well of DharmaFECT compared to OptiMEM only media cells. Mean ± SEM, 2 biological replicates with 3 technical replicates. Unpaired t-test, **** = $p < 0.0001$.*

4.3.3.2 Loss of HNRNPA2B1 in U251 cells significantly increases m^{6}A levels within the nucleus without substantial change in the levels of DNA:RNA hybrids.

After optimisation of HNRNPA2B1 siRNA transfection in U251 cells, we next examined whether the levels of DNA:RNA hybrids change upon the loss of HNRNPA2B1. As the siRNA

negative control, we used U251 cells at the same seeding density but only in serum-free OptiMEM media (siControl). Using a DNA:RNA hybrid (clone S9.6) antibody and DAPI nuclear staining, we found no significant difference ($p = 0.0726$) in DNA:RNA hybrid signal between the siControl and the siHNRNPA2B1 U251 cells (Fig. 4.15 A-C). There were several small and rounded cells with very high nuclear pixel intensity of DNA:RNA hybrids, however, it cannot be assumed whether they are in early mitotic stages, beginning stages of apoptosis or displayed this pattern of staining for another unknown reason.

Previous immunostaining with m^6A antibody upon pre-treatment of the samples with RNases in U251 cells suggested low immunocytochemically detectable levels of m^6A-marked DNA:RNA hybrids in these cells. Using HNRNPA2B1 siRNA, we compared the presence of m^6A and HNRNPA2B1 in U251 cells without pre-treatment of the samples with RNases (Fig. 4.16 – 4.17). In siControl cells, similarly to previous m^6A immunostaining, m^6A levels within the nucleus had very low pixel intensity in all cells (Fig. 4.16 A-B; Fig. 4.17 A). Conversely, when U251 cells were transfected with siHNRNPA2B1, m^6A levels were significantly increased (Fig 4.16 C, $p = 0.0002$) whereas HNRNPA2B1 staining was significantly decreased (Fig 4.16 D, $p = 0.0032$). Focussing on single cells of each condition (Fig 4.17 B-C), single-pixel intensity demonstrated the absence of m^6A within the siControl U251 nuclei, whereas, upon depletion of HNRNPA2B1, the m^6A levels increased the m^6A levels found within no RNase, non-mitotic U251 cells. Correlation analysis deduced a positive correlation between HNRNPA2B1 and m^6A (Fig. 4.17 D-E), increasing from $r = 0.3964$ ($p < 0.0001$) to $r = 0.6114$ ($p < 0.0001$).

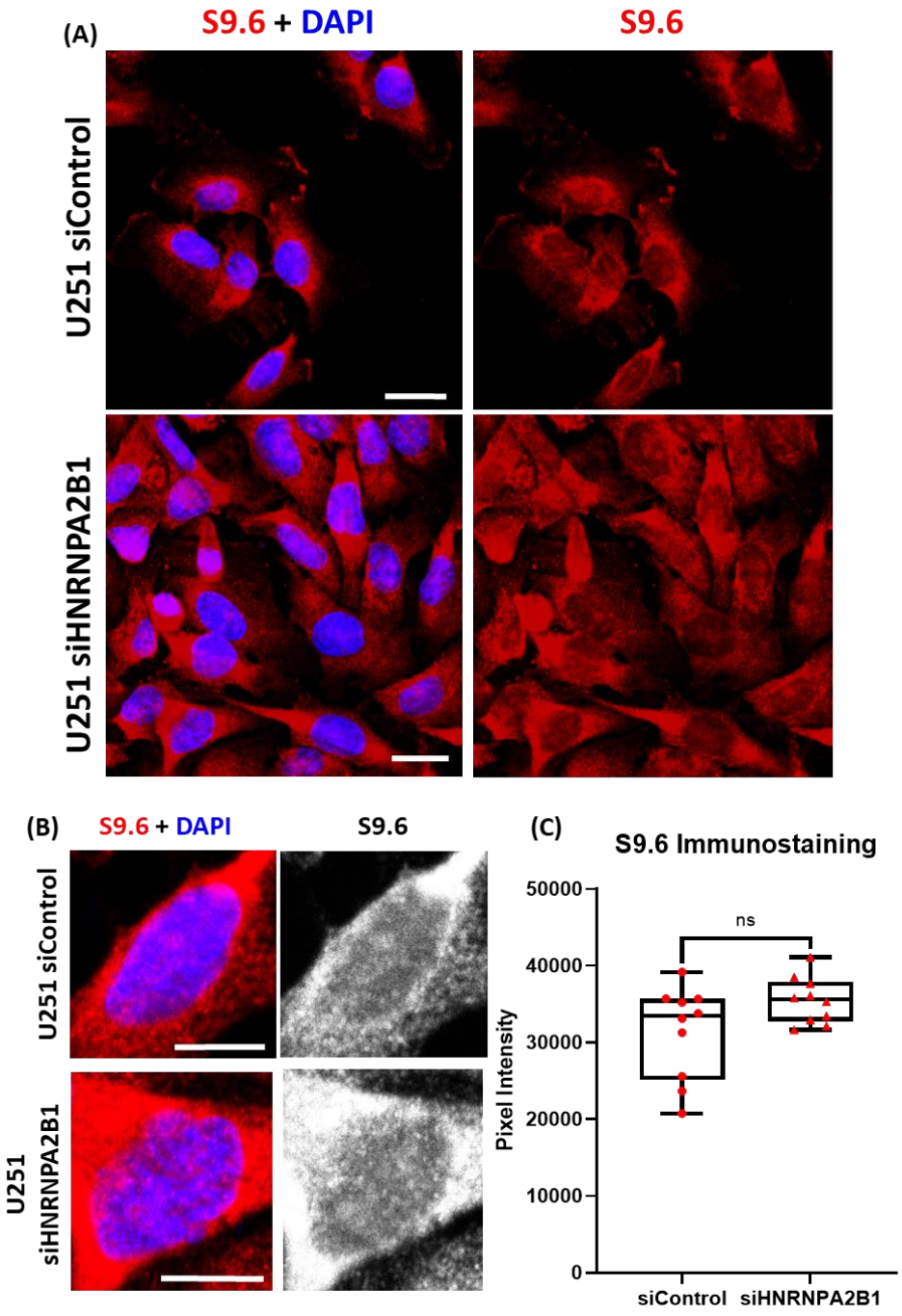


Figure 4.15: No significant difference in DNA:RNA hybrid levels in U251 siHNRNPA2B1 cells.

(A) *Immunostaining with DNA:RNA hybrid antibody (S9.6 clone) and DAPI nuclear staining in siControl and siHNRNPA2B1 U251 cells. Representative image shown from 4 technical replicates. Scale bar represents 20 μM.* ***(B)*** *Single cell comparison of S9.6 and DAPI nuclear immunostaining within siControl and siHNRNPA2B1 U251 cells. Scale bar represents 10 μM.* ***(C)*** *Quantification boxplot of S9.6 pixel intensity between siControl and siHNRNPA2B1 U251 cells in 10 nuclei. Values had normal distribution and evaluated by unpaired t-test, ns = $p \geq 0.05$.*

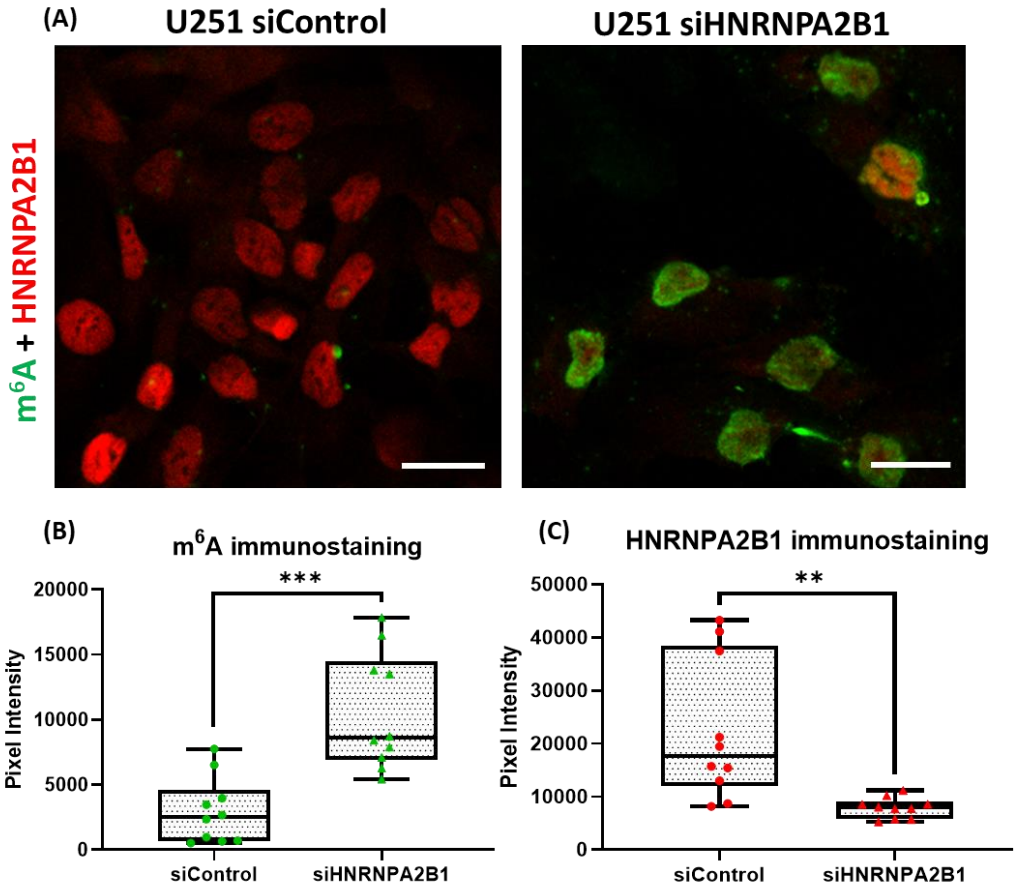


Figure 4.16: m^{6}A levels significantly increase within the nuclei of siHNRNPA2B1 depleted U251 cells compared with non-treated U251.

(A) *Immunostaining with HNRNPA2B1 antibody and m^{6}A antibody in siControl and siHNRNPA2B1 U251 cells. No RNase pre-treatment of the samples. Representative image shown from 4 technical replicates. Scale bar represents 20 μM.* ***(B)*** *Boxplot showing the results of quantification of m^{6}A pixel intensity between siControl and siHNRNPA2B1 U251 cells in 10 nuclei.* ***(C)*** *Boxplot showing the results of quantification of HNRNPA2B1 pixel intensity between siControl and siHNRNPA2B1 U251 cells in 10 nuclei. Values had normal distribution and evaluated by unpaired t-test, ** = $p < 0.01$ and *** = $p < 0.001$.*

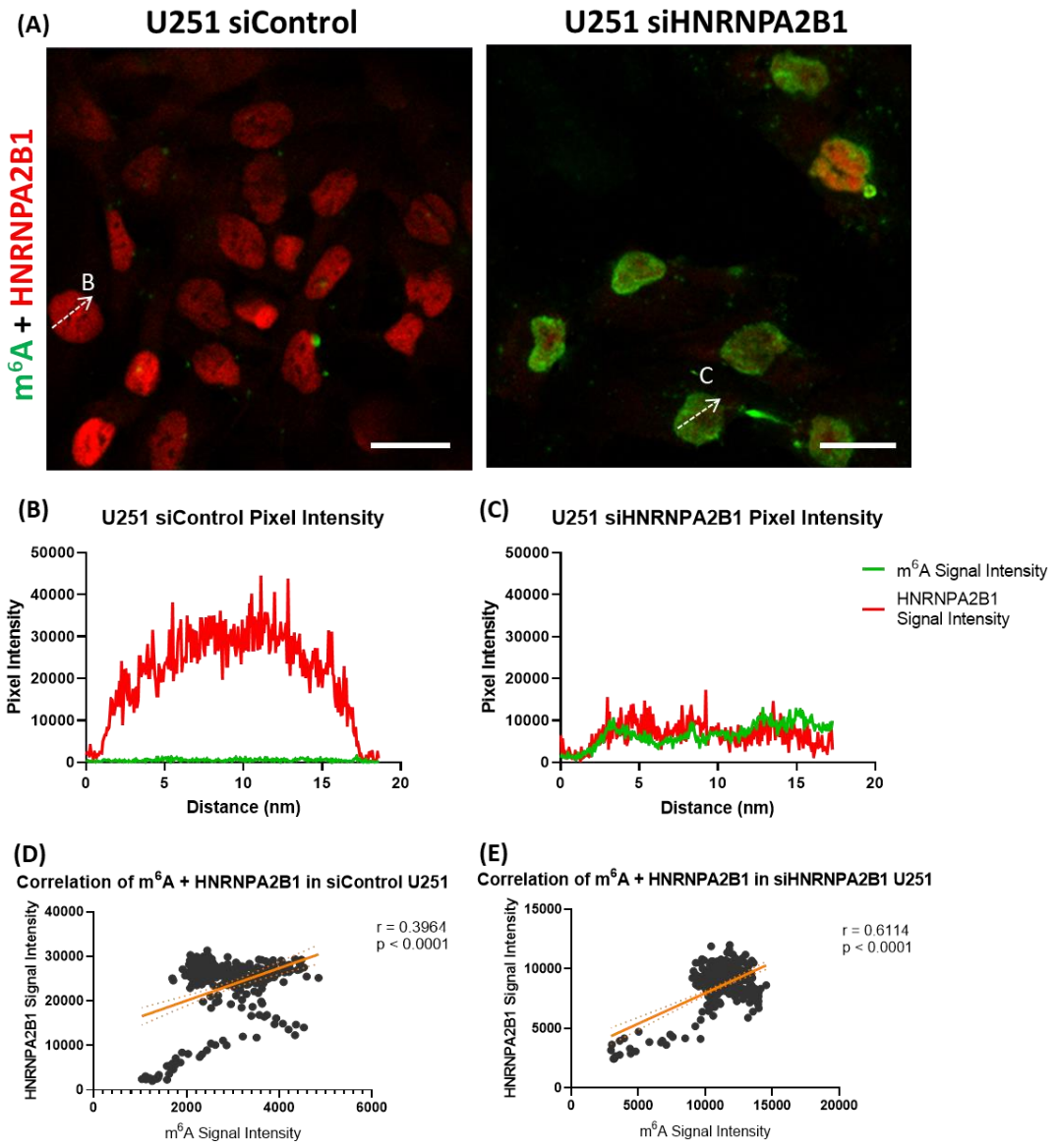


Figure 4.17: Positive correlation between HNRNPA2B1 loss and increased m^{6}A presence within the nucleus.

(A) *Immunostaining with HNRNPA2B1 antibody and m^{6}A antibody in siControl and siHNRNPA2B1 U251 cells. No RNases pre-treatment of the samples. Scale bar represents 20 μM. White dotted line arrows represent single cell pixel intensity to be shown in (B, C).* ***(B)*** *U251 siControl cell pixel intensity following the white arrow depicted in (A) of m^{6}A and HNRNPA2B1 intensity.* ***(C)*** *U251 siHNRNPA2B1 cell pixel intensity following the white arrow depicted in (A) of m^{6}A and HNRNPA2B1 intensity.* ***(D)*** *Linear regression analysis scatterplot of m^{6}A and HNRNPA2B1 signal correlation in U251 siControl cells.* ***(E)*** *Linear regression analysis scatterplot of m^{6}A and HNRNPA2B1 signal correlation in U251 siHNRNPA2B1 cells. 10 nuclei of each siControl and siHNRNPA2B1 U251 were compared.*

4.3.4 Investigating the impact of *HNRNPA2B1* depletion in LN18 GBM cells.

Previous results have suggested that in LN18 cells, the gene expression of *HNRNPA2B1* is significantly elevated in comparison to hiPSCs, yet LN18 cells have the lowest gene expression of HNRNPA2B1 compared with other GBM cell lines. Furthermore, using mass spectrometry and immunocytochemistry, we have observed non-negligible levels of m^6A-marked DNA:RNA hybrids in LN18 cells. With different levels of *HNRNPA2B1* and m^6A-DNA:RNA hybrids in LN18 and U251, we wanted to examine the impact of the knockdown of *HNRNPA2B1* on LN18 cells as well as DNA:RNA hybrids and another m^6A-related gene, *YTHDF2*.

4.3.4.1 Validation HNRNPA2B1 knockdown in LN18 cells.

The previous section aimed to examine whether the levels of DNA:RNA hybrid or m^6A are altered by HNRNPA2B1-siRNA mediated knockdown in U251 cells. Despite the gene expression analysis of *HNRNPA2B1* suggesting a higher expression in U251 compared to the other GBM cell lines examined, we observed low levels of m^6A-marked DNA:RNA hybrids and DNA:RNA hybrids in U251 cells compared to hiPSCs. Therefore, the decision was made to focus on LN18 cells that also exhibited an increase in expression of HNRNPA2B1 mRNA transcripts, instead of continuing to test U251 cells.

With this, optimisation of HNRNPA2B1 siRNA and transfection reagent DharmaFECT was needed in LN18 cells. After testing a range of concentrations at the same seeding density, we identified that 50 nM siHNRNPA2B1 with 4 µL of DharmaFECT worked best (Fig. 4.18 A). It was noted there was a lot of detachment of cells within the siHNRNPA2B1 treated conditions compared with the DharmaFECT only. At 50 nM siHNRNPA2B1 with 4 µL of DharmaFECT, the knockdown efficiency was 78.66% compared to control LN18 cells ($p < 0.000001$) (Fig. 4.18 B).

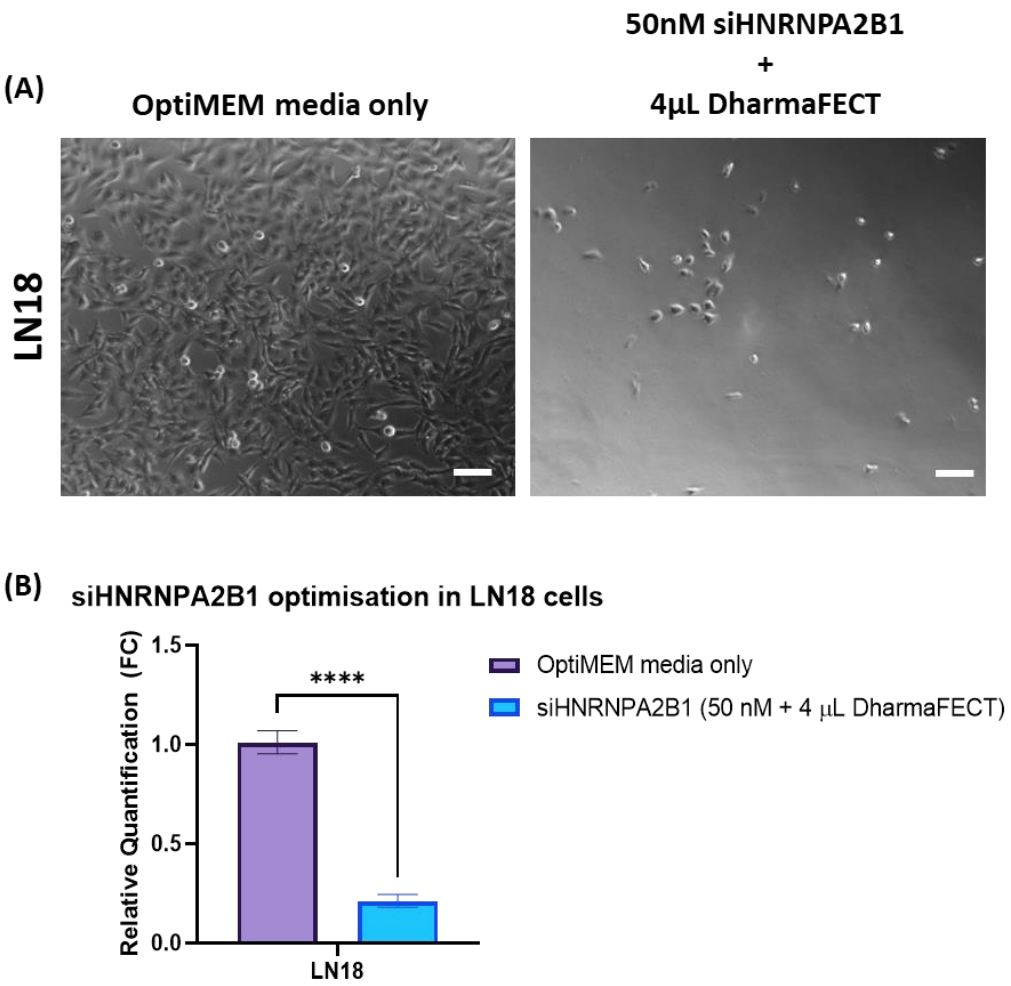


Figure 4.18: Optimisation of siHNRNPA2B1 knockdown in LN18 cells.

(A) *Brightfield light microscope images of optimised siRNA treatment of siHNRNPA2B1 in LN18 cells 24 hours post-transfection compared to LN18 cells in reduced-serum OptiMEM media. Transfection of HNRNPA2B1 siRNA was optimised to 50 nM siHNRNPA2B1 with 4 µL per well of DharmaFECT. Scale bar represents 100µM.* ***(B)*** *RT-qPCR testing of HNRNPA2B1 siRNA knockdown efficiency at 50 nM siHNRNPA2B1 with 4 µL per well of DharmaFECT compared to OptiMEM only media cells. 2 biological replicates with 3 technical replicates. Unpaired t-test, **** = p < 0.0001.*

4.3.4.2 Attachment to growth surface is impaired after knockdown of *HNRNPA2B1* in LN18 cells and is restored with the use of attachment factor.

From the cell images taken 24 hours post-transfection of HNRNPA2B1 siRNA (Fig. 4.19 A), we observed a large number of cells lifting from the growth surface, compared to cells in OptiMEM only media or normal culturing media. To see if the detachment from the growth

surface could be limited, we coated the growth surface in an Attachment factor containing 0.01% gelatin (Fig. 4.19). Using the same seeding density as well as the same optimised concentration of siHNRNPA2B1 and DharmaFECT, we found more cells remaining attached to the surface in these conditions. However, many of the cells have a rounded morphology.

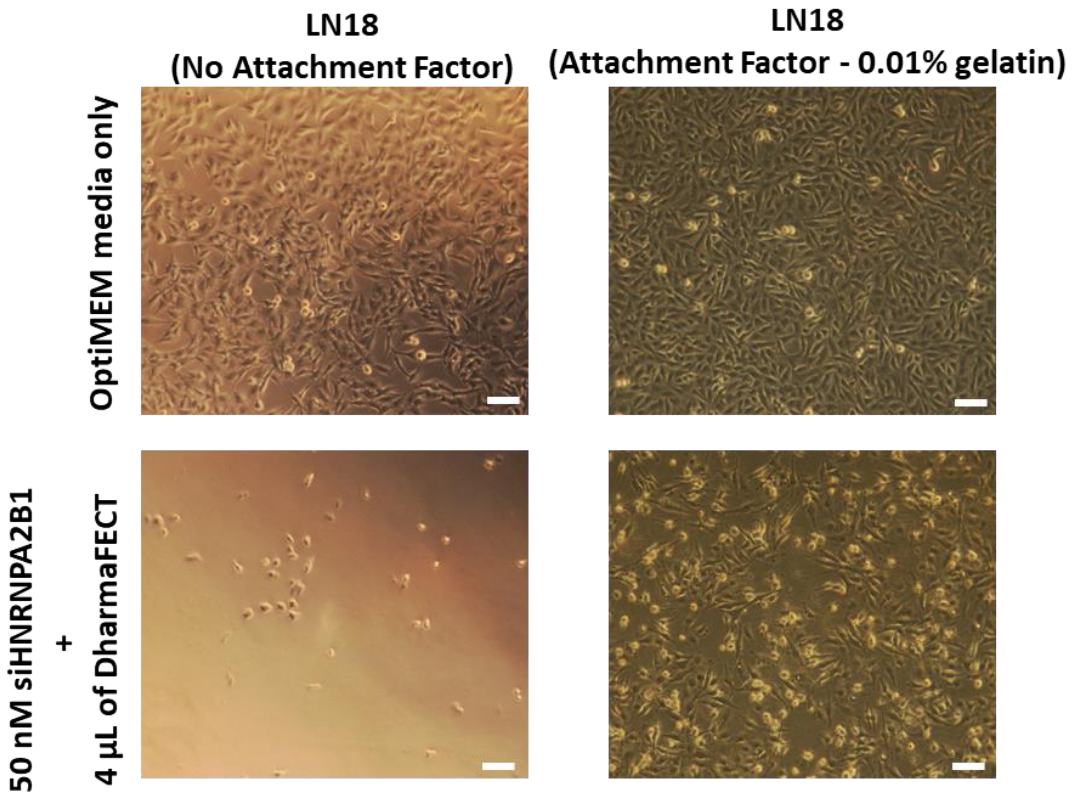


Figure 4.19: Increased level of attachment to growth surface with commercial attachment factor present for LN18 siHNRNPA2B1 knockdown cells.

Brightfield light microscope images of OptiMEM media only and siHNRNPA2B1 transfected LN18 cells at same seeding density and imaged 24 hours post-transfection. Wells were either left untreated in normal growing conditions and other coated first with commercial attachment factor (0.01% gelatin) before seeding. Scale bar represents 100 µM.

4.3.4.3 Knockdown of HNRNPA2B1 increases expression of m^{6}A-related genes with high levels of YTHDF2 maintained within HNRNPA2B1 depleted LN18 cells.

In the previous chapter, we investigated whether gene expression of other m^{6}A and DNA:RNA hybrid-related genes altered upon knockout of *HNRNPA2B1* in HAP1 cells and found

significant increases in *DHX9* expression but smaller increases in m^{6}A writers and readers. However, expression of m^{6}A and DNA:RNA hybrid-related genes are more prominent within LN18 cells, therefore the impact of HNRNPA2B1 knockdown might be different.

We firstly confirmed, in these samples, that *HNRNPA2B1* knockdown was successful in transfected LN18 cells (Fig. 4.20 B) with an efficiency of 82% ($p < 0.0001$). Further analysis of *METTL3*, *METTL14* and *WTAP* gene expression showed increases in expression by 3.04 – fold ($p = 0.039$), 7.05 – fold ($p = 0.0413$) and 2.7 – fold ($p = 0.0537$) respectively, in siHNRNPA2B1 transfected LN18 cells compared to siControl LN18 cells (Fig. 4.20 A). Examination of the other m^{6}A readers showed that *YTHDF2* gene expression increased by 2.2 – fold ($p = 0.0003$) while only a minor increase in *YTHDC1* gene expression (1.3 – fold, $p = 0.4423$) was observed (Fig. 4.20 B). Elevation in both m^{6}A erasers gene expression was seen with 2.9 – fold in *FTO* ($p = 0.0891$) and 6.4 – fold in *ALKBH5* ($p = 0.0029$) (Fig. 4.20 C) between siHNRNPA2B1 and siControl LN18 cells.

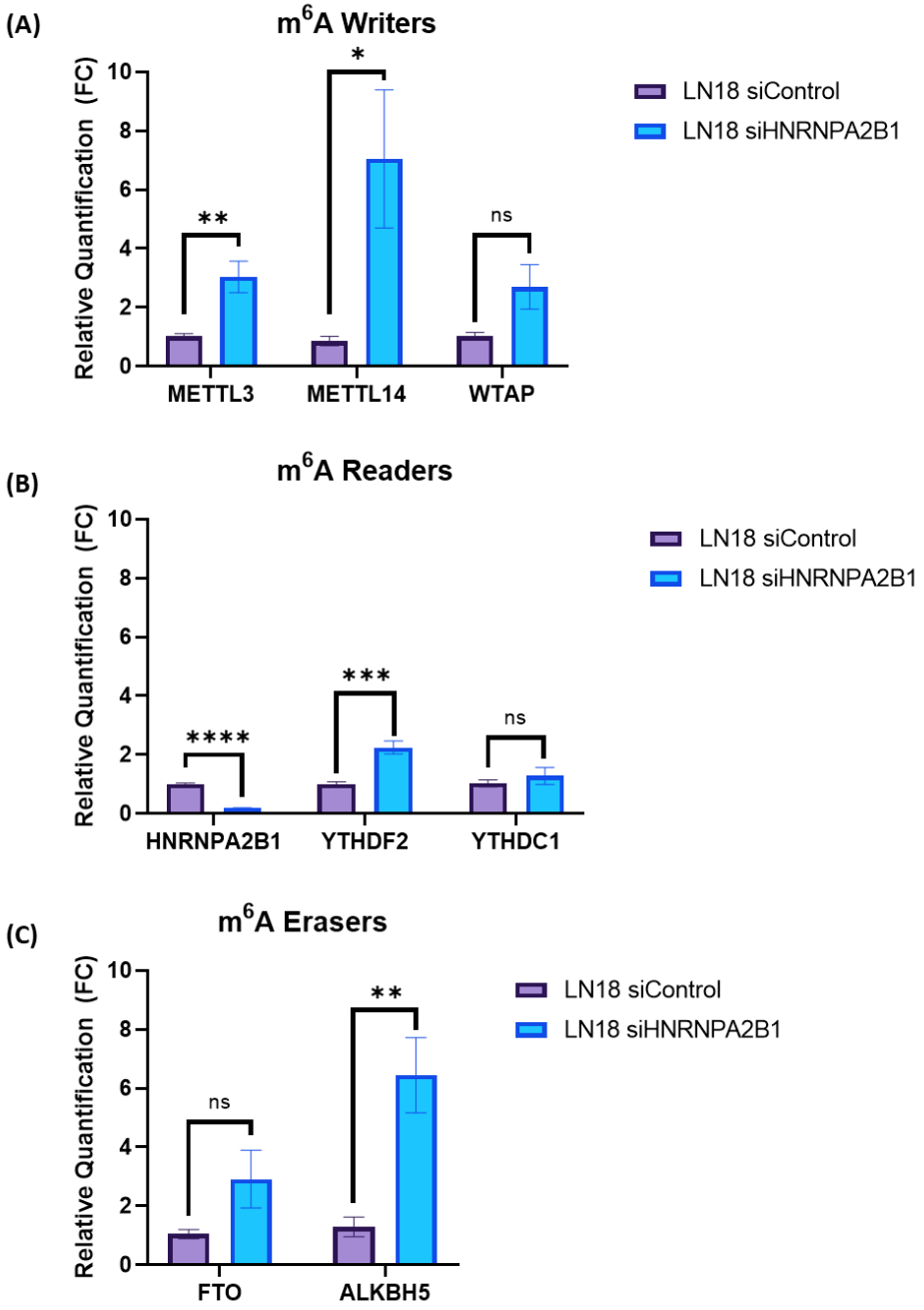


Figure 4.20: Increases in gene expression of m^{6}A writers, readers and erasers upon siHNRNPA2B1 knockdown in LN18.

(A) *Gene expression qPCR showing m^{6}A writers: METTTL3, METTL14 and WTAP comparison between siControl and siHNRNPA2B1 LN18 cells.* ***(B)*** *Gene expression of m^{6}A readers: HNRNPA2B1, YTHDF2 and YTHDC1 comparison between siControl and siHNRNPA2B1 LN18 cells.* ***(C)*** *Gene expression of m^{6}A erasers: FTO and ALKBH5 comparison between siControl and siHNRNPA2B1 LN18 cells. Mean ± SEM, 2 biological replicates each with 3 technical replicates. Unpaired t-test, ns = p ≥ 0.05, * = p < 0.05, ** = p < 0.01, *** = p < 0.001 and **** = p < 0.0001.*

In the previous chapter, we used YTHDF2 and HNRNPA2B1 antibodies for immunostaining in HAP1 wild-type and HNRNPA2B1 knockout cells and found that YTHDF2 is recruited to the nucleus upon loss of HNRNPA2B1. Therefore, we wanted to determine if the same phenomena were occurring in LN18 cells siHNRNPA2B1 transfected cells (Fig. 4.21). We observed no noticeable difference between siControl and siHNRNPA2B1 cells in YTHDF2 localisation to the nucleus in LN18 cells (Fig. 4.21 A-B), which was corroborated when quantifying the pixel intensity of 10 nuclei per treatment (Fig. 4.21 C-D, $p = 0.0896$). However, there were large variations in YTHDF2 pixel intensity of LN18 siHNRNPA2B1 cells, which could suggest differences in the efficiency of HNRNPA2B1 knockdown in these cells.

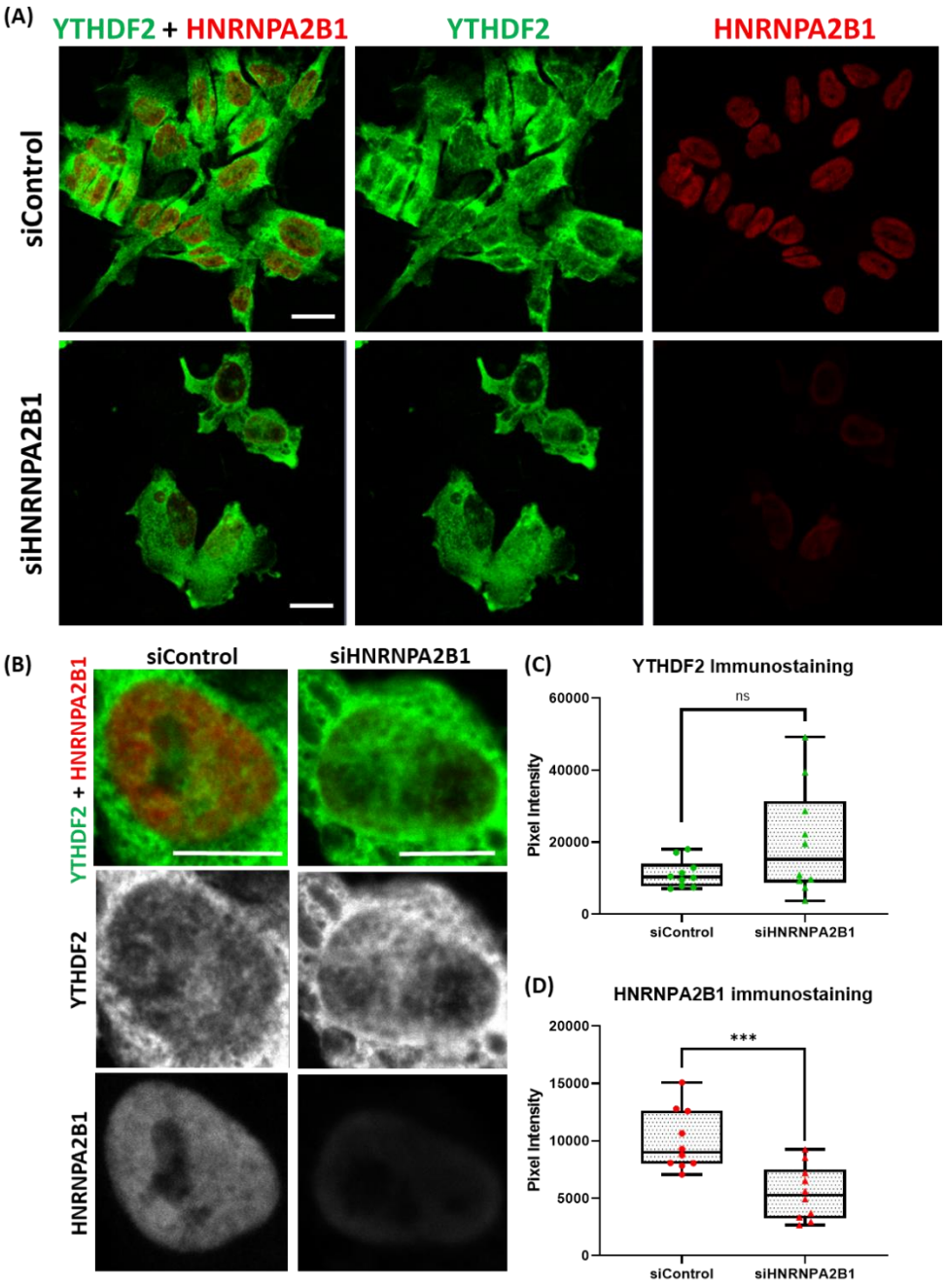


Figure 4.21: No significant increase in YTHDF2 levels in LN18 siHNRNPA2B1 cells.

(A) *Immunostaining with YTHDF2 antibody and HNRNPA2B1 antibody in siControl and siHNRNPA2B1 LN18 cells. Representative image shown from 4 technical replicates. Scale bar represents 20 μM.* ***(B)*** *Single cell comparison of YTHDF2 and HNRNPA2B1 immunostaining within siControl and siHNRNPA2B1 LN18 cells. Scale bar represents 10 μM. Quantification boxplot of* ***(C)*** *YTHDF2 pixel intensity and* ***(D)*** *HNRNPA2B1 pixel intensity between siControl and siHNRNPA2B1 LN18 cells in 10 nuclei. Values had normal distribution and evaluated by unpaired t-test, ns = $p \geq 0.05$ and *** = $p < 0.001$.*

4.3.4.4 Significant increase in the gene expression of DNA:RNA hybrid related genes and immunocytochemical presence of DNA:RNA hybrids in HNRNPA2B1 depleted LN18 cells.

Similar to YTHDF2, HNRNPA2B1 was previously implicated in the recognition of DNA:RNA hybrids (Abakir *et al.*, 2020), we next proposed that genes related to DNA:RNA hybrid maintenance might also be impacted by the knockdown of *HNRNPA2B1* in LN18 cells (Fig. 4.22). Both *DHX9* and *DDX3X* expression increased by 1.9 – fold (p = 0.1077) and 3.05 – fold (p = 0.0019) in siHNRNPA2B1 treated LN18 cells compared to siControl LN18 cells. Overall, the knockdown of *HNRNPA2B1* in LN18 cells lead to the raised gene expression in the majority of m^{6}A and DNA:RNA hybrid-related genes.

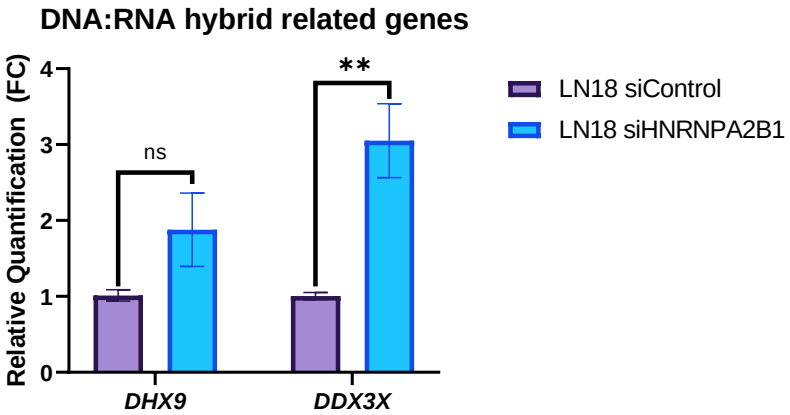


Figure 4.22: Knockdown of HNRNPA2B1 in LN18 increases gene expression of *DHX9* and *DDX3X* compared to siControl LN18 cells.

*Gene expression of DNA:RNA hybrid related genes: DHX9 and DDX3X comparison between siControl and siHNRNPA2B1 LN18 cells. Mean ± SEM, 2 biological replicates each with 3 technical replicates. Unpaired t-test, ns = p ≥ 0.05, ** = p < 0.01.*

Following the qPCR analysis of DNA:RNA hybrid helicases *DHX9* and *DDX3X*, we next wanted to observe whether DNA:RNA hybrids were affected by the knockdown of HNRNPA2B1. Using a DNA:RNA hybrid (clone S9.6) antibody and DAPI nuclear staining, we compared the presence and spatial distribution of DNA:RNA hybrids in siControl and siHNRNPA2B1 LN18 cells (Fig. 4.23). In the majority of LN18 cells transfected with

HNRNPA2B1, there was a significant increase in DNA:RNA hybrid immunostaining within the nucleus compared to siControl LN18 cells (Fig. 4.23 A). This was confirmed by single-cell comparison (Fig. 4.23 B) where the signal was quantified by pixel intensity analysis of 10 nuclei (Fig. 4.23 C, $p < 0.0001$). These immunocytochemistry results along with the increased gene expression of *DHX9* and *DDX3X*, suggest that loss of *HNRNPA2B1* in LN18 cells has a more dramatic impact on the maintenance of DNA:RNA hybrids presence within the genome compared to HAP1 cells.

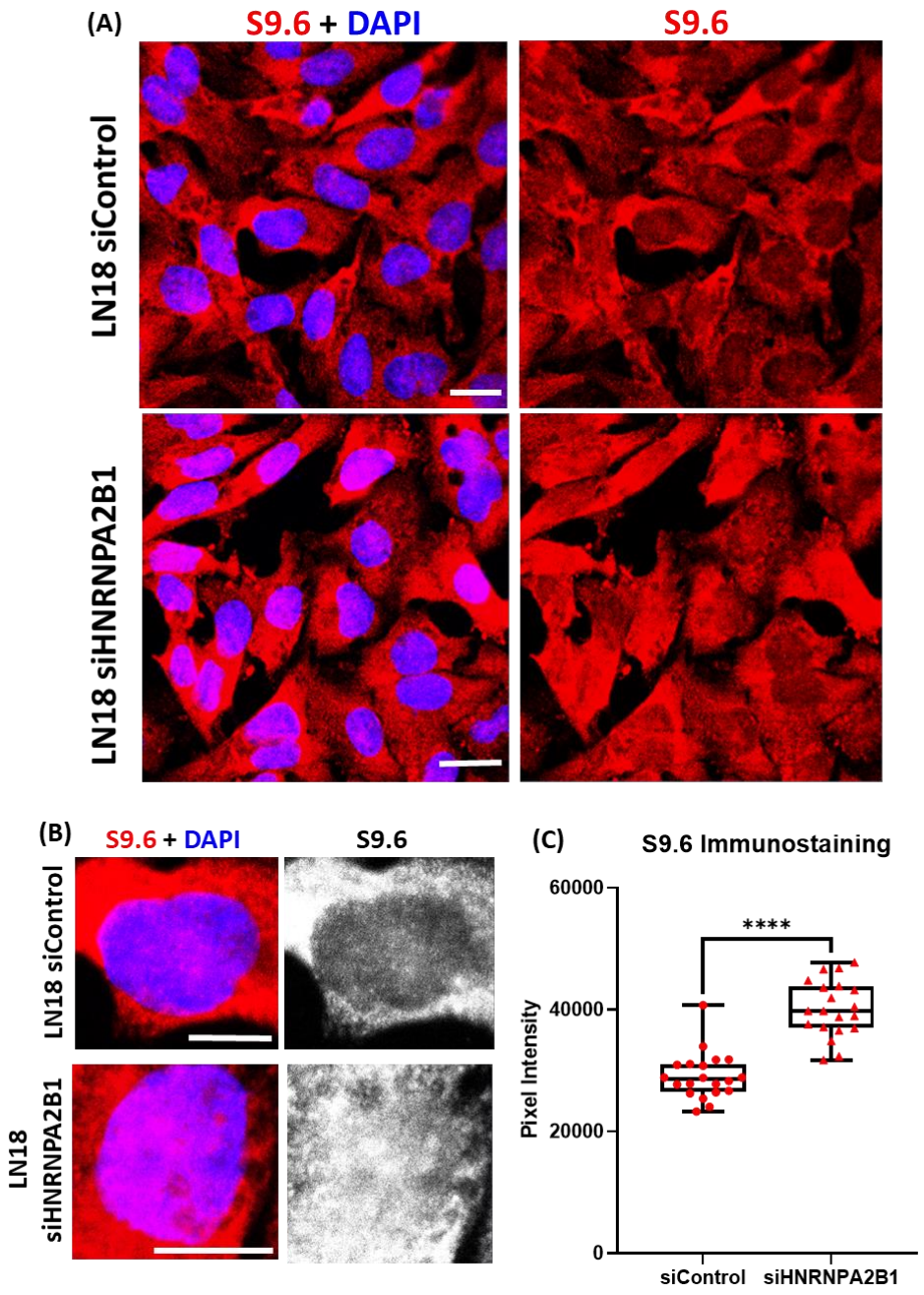


Figure 4.23: DNA:RNA hybrids levels increase in LN18 siHNRNPA2B1 cells.

(A) *Immunostaining with DNA:RNA hybrid antibody (S9.6 clone) and DAPI nuclear staining in siControl and siHNRNPA2B1 LN18 cells. Representative image shown from 4 technical replicates. Scale bar represents 20 μM.* ***(B)*** *Single cell comparison of S9.6 and DAPI nuclear immunostaining within siControl and siHNRNPA2B1 LN18 cells. Scale bar represents 10 μM.* ***(C)*** *Quantification boxplot of S9.6 pixel intensity between siControl and siHNRNPA2B1 LN18 cells in 10 nuclei. Values had non-normal distribution and evaluated by Mann-Whitney test, **** = $p < 0.0001$.*

4.4 Technical Discussion

This chapter aimed to examine the potential presence of m^{6}A-marked DNA:RNA hybrids and m^{6}A reader HNRNPA2B1 in GBM cells and to gain a preliminary understanding of its function in GBM. By using a range of techniques, we made several novel findings: (1) High levels of HNRNPA2B1 transcripts were observed in GBM cell lines and public patient microarray datasets, however, they did not seem to be linked to a significantly worse prognosis in the known GBM subgroups; (2) GBM cell line, U251, exhibited low levels of m^{6}A and m^{6}A-marked DNA:RNA hybrids by immunoprecipitation and immunocytochemically, with HNRNPA2B1 knockdown leading to increase in levels of nuclear m^{6}A; (3) GBM cell line LN18 and human astrocyte cell line SVGA had similar levels of m^{6}A-marked DNA:RNA hybrids present but lower levels respective to hiPSCs; (4) Knockdown of HNRNPA2B1 in LN18 cells led to an increase in DNA:RNA hybrid immunocytochemical levels, gene expression of DNA:RNA hybrid helicases and detachment of the cells from growth surface after siRNA transfection.

Although previous studies have investigated the abundance of HNRNPA2B1 in GBM cells previously (Golan-Gerstl *et al.*, 2011; Deng *et al.*, 2016), it was important to establish the levels of HNRNPA2B1 expression in the GBM cell lines we had available. Gene expression of m^{6}A-related genes indicated that *METTL3*, *METTL14*, *YTHDF2* and *HNRNPA2B1* had the highest expression in FB83 and the continuous GBM cell lines (Fig. 4.3 A-B, E-F, respectively). The mRNA expression we observed for *METTL3*, *METTL14*, *YTHDF2* and *HNRNPA2B1* within GBM cells is comparable to the expression previously published by other groups (Golan-Gerstl et al., 2011; Deng et al., 2016; L. Wang et al., 2020; Dixit et al., 2021). The graphs produced in Figure 4.3 had 2 biological replicates with large variations between replicates in particular samples. This creates uncertainty on which replicates represent the true rate of gene expression therefore, at least another biological replicate would be ideal to straighten these results.

In this section, we wanted to clarify whether the GBM cell lines resemble the gene expression found in GBM patients by examining the gene expression of primary GBM cell lines (Fig. 4.5 – 4.6). Initially, we compared the expression of METTL3, HNRNPA2B1, YTHDF2 and

YTHDC1 between GBM cell lines and primary GBM cells using a public dataset published by Pollard (Pollard *et al.*, 2009). We observed a lower expression for all the m^{6}A-related genes in primary cells compared to GBM cell lines (Fig. 4.5), with this supported by the gene expression comparison between GBM cell lines and the primary GIN cells (Fig. 4.6). These results alongside numerous publications may indicate that our GBM cell lines may have diverged from patient GBM in terms of genetics, epigenetics and epitranscriptomics and may not behave in the same manner as GBM tumours (Lee *et al.*, 2006; Hughes *et al.*, 2007; Robertson *et al.*, 2019). And yet, early analysis and initial investigations such as the work carried out in this chapter provided a cost-effective approach to understanding the potential role of HNRNPA2B1 and m^{6}A-marked DNA:RNA hybrids in GBM.

Since m^{6}A-marked DNA:RNA hybrids have yet to be explored in cancer cells, we wanted to use a wide array of techniques to understand the presence of these nucleic structures in GBM cells. Our results indicated that U251 GBM cells have a comparatively low presence of m^{6}A-marked DNA:RNA hybrids compared to hiPSCs in repetitive and GBM-relevant intronic sequences (Fig. 4.7 – 4.11). However, with this data presented in Figures 4.7 – 4.11, it is difficult to clarify whether the difference is due to the difference in cell type (Jiang *et al.*, 2021; Shen *et al.*, 2021), the difference in frequency of cell cycling between hiPSCs and GBM cells (Supplementary figure 1 D) (Batista *et al.*, 2014) or different sensitivities of the anti-m^{6}A and S9.6 antibodies (Abakir *et al.*, 2020). We followed with SID-UPLC-MS/MS analysis and a pre-established immunoprecipitation method with m^{6}A and DNA:RNA hybrid antibodies (Abakir *et al.*, 2020). While SID-UPLC-MS/MS should detect all m^{6}A-marked DNA:RNA hybrids within the genome, DRIP-qPCR focuses on locus-specific targets identified by m^{6}A and S9.6 DRIP next-generation sequencing of hiPSCs (Fig. 4.7 – 4.12). Optimally, DRIP followed by next-generation sequencing would have been carried out on at least one GBM cell line to understand whether the distribution of m^{6}A-marked DNA:RNA hybrids is comparable to that of hiPSCs. Since that was not possible, we formed a list of possible candidates from the literature with genes of significance in GBM. We compared the list to the DRIP next-generation sequencing to observe if any marked hybrids are present within intronic regions then followed by designing primers over the region which peaked. Not all the primers designed then resulted in successful amplification in U251 DRIP samples leaving three candidates for examination.

Despite the lack of next-generation sequencing on the GBM cell lines, more GBM cell lines could have been used in DRIP-qPCR, allowing a comparison between GBM cell lines as well as including a human astrocyte cell line as a cell type control as non-malignant cell line such as human astrocyte cells have been used by other publications investigating m^6A related genes in GBM (Deng *et al.*, 2016; Dixit *et al.*, 2021).

It was important to use both antibody and non-antibody methods to account for any bias as well as strengthen any consistent results between the methods. Utilising SID-UPLC-MS/MS as our non-antibody technique, we found that SVGA and LN18 have a similar level of m^6A marked small fragments found in the ultrafiltrate after RNase H treatment but relatively low when compared to hiPSCs (Fig. 4.12). The differences observed could either suggest a cell type dependent pattern or could just display the differences in the levels of m^6A-marked DNA:RNA hybrids between pluripotent vs differentiated cells (Batista *et al.*, 2014; Jiang *et al.*, 2021; Shen *et al.*, 2021). To answer this, more cell lines need to be tested including GBM cell lines (LN229, U251 and U87MG), foetal brain cell line (FB83) and possibly GBM spheres formed using these cell lines.

Using the same m^6A antibody, to visualise the cellular distribution we utilised immunocytochemistry that suggested that U251 has a lower presence of m^6A-marked DNA:RNA hybrids compared to hiPSCs, SVGA and LN18 (Fig. 4.13). However, immunostaining is seen as a semi-quantitative method with unintentional user bias that can only focus on a small number of cells. This may influence our results. To overcome this, we took as many images as possible per treatment and cell line, as well as used the same confocal settings established on hiPSCs. Our group has previously performed immunostaining on LN18 and U87MG cells and co-stained m^6A with 5mC antibodies (Abakir *et al.*, 2020). LN18 appears to exhibit similar levels of nuclear m^6A compared to our immunostaining (Fig. 4.13) and U87MG has very little presence of nuclear m^6A, unless in a mitotic state that can only be assumed by the morphology as no mitotic marker was used for immunostaining in this publication (Abakir *et al.*, 2020).

Throughout this chapter, we uncover that both GBM cell lines, U251 and LN18 exhibit HNRNPA2B1 and m^6A-marked DNA:RNA hybrids differently from each other (Fig 4.3; Fig.

4.13). For this reason, we optimised and performed the siRNA knockdown of HNRNPA2B1 on both LN18 and U251 cell lines. In U251 cells, we found knockdown of HNRNPA2B1 caused no notable change in the levels of DNA:RNA hybrids (Fig. 4.15), yet the loss of HNRNPA2B1 correlated with the increase of nuclear m^6A immunostaining (Fig. 4.16 – 4.17). The HNRNPA2B1 immunostaining displayed in Figure 4.16 appears to be similar to previous publications regardless that the HNRNPA2B1 antibodies are sourced from different suppliers (Deng *et al.*, 2016). In LN18 cells, we found that knockdown impacted cell attachment to the growth surface (Fig. 4.19). Furthermore, we observed that loss of HNRNPA2B1 led to an increase in both DNA:RNA hybrid-related genes as well as their nuclear immunostaining signal in LN18 cells (Fig. 4.22 – 4.23). Previous studies investigating HNRNPA2B1 role in GBM cells have found that knockdown of HNRNPA2B1 reduced colony formation in both anchorage-dependent and -independent studies (Golan-Gerstl *et al.*, 2011; Deng *et al.*, 2016).

For our experiments we transfected by siRNA knockdown using a pool of four siRNA allowed larger coverage for the siRNA to target HNRNPA2B1. An improvement could have been to use a GAPDH siRNA positive control or non-targeting siRNAs, whereas we employed serum-free media control cells and DharmaFECT transfection control cells. Knockdown of HNRNPA2B1 with siRNA allowed us to gain a preliminary understanding of HNRNPA2B1 function in GBM cell lines in a relatively quick and cost-effective manner. With siRNA knockdown being a short-term knockdown method, creating larger knockdown samples for methods such as DRIP, next-generation sequencing, flow cytometry and others becomes problematic when the surface attachment is affected by HNRNPA2B1 siRNA transfection. Another technique that has been used to knockdown HNRNPA2B1 in GBM was the use of HNRNPA2B1 short hairpin RNA (shRNA) vector to produce stable knockdowns of HNRNPA2B1 and an overexpression model using a p-BABE-puro retroviral vector and a T7-tagged human HNRNPA2 cDNA (Golan-Gerstl *et al.*, 2011; Deng *et al.*, 2016). These publications suggest the possibility of a stable knockdown of HNRNPA2B1 in GBM, yet the obtaining of a homozygous or heterozygous clone might prove difficult as depletion of HNRNPA2B1 in GBM loss has shown to promote apoptotic markers and lifting from growth surface. A recent publication used a plant extract from the South African medicinal plant, *Cotyledon orbiculata*, which switched splicing into the HNRNPB1 isoform to the HNRNPA2

isoform in the colon and oesophageal cancer cell lines caused downstream interference in splicing isoforms of apoptotic genes (Makhafola *et al.*, 2020). This plant extract along with Pladienolide B, a known mRNA splicing inhibitor and anti-tumour agent, if used as a positive control, would allow us to understand whether HNRNPA2B1 isoforms function similarly in GBM but, furthermore, would permit larger-scale experiments to understand whether HNRNPA2B1 interaction with m^6A-marked DNA:RNA hybrids differ in GBM cells compared to our previous observations in HAP1 cells (Chapter 3).

Chapter 5: Investigating the potential role of HNRNPA2B1 in the metabolism of m^{6}A-marked DNA:RNA hybrids in Medulloblastoma

5.1 Introduction

Medulloblastoma (MB) is a highly malignant cancer that originates in the cerebellum (Bailey, 1925). MB is classed as the most common central nervous system (CNS) tumour and remains one of the leading causes of cancer-related childhood mortality (Pui *et al.*, 2011; Northcott, Jones, *et al.*, 2012; Taylor *et al.*, 2012; Kumar *et al.*, 2015). This common paediatric tumour constitutes over 25% of all intracranial tumours with the average patient age between 4 – 7 years, however, tumours have also been few reported in adults, but is a rarity (Gerber *et al.*, 2014; Kumar *et al.*, 2015). Overall, MB is detected in more male than female patients which is a common occurrence in childhood cancers (Taylor *et al.*, 2012; Sun *et al.*, 2015; Liu *et al.*, 2017). There is a strong association between MB and hereditary cancer predisposition syndromes with germline mutations such as Turcot syndrome, Gorlin syndrome, Fanconi anaemia, Li Fraumeni syndrome and Rubinstein Taybi syndrome that account for 6% of medulloblastoma diagnoses (Waszak *et al.*, 2018). MB patients are usually diagnosed by a non-contrast head CT scan confirmed by magnetic resonance imaging (MRI). The current treatment plan for all MB patients involves a maximal safe resection of the tumour limiting the amount of damage caused to the neural architecture and brain function. This is followed by external beam radiotherapy for patients over the age of 3 and adjuvant chemotherapy. Radiotherapy is restricted for infants as it can have a detrimental impact on the developing brain.

MB has four molecularly distinct subgroups: wingless activated (WNT), sonic hedgehog activated (SHH), Group 3 and Group 4 (Pomeroy *et al.*, 2002; Taylor *et al.*, 2012; Cavalli *et al.*, 2017). WNT is the least common subgroup accounting for 10% of all MB cases with 90% of those displaying classic histology with minimal to no differentiation (Ellison *et al.*, 2011;

Taylor *et al.*, 2012; Gajjar and Robinson, 2014; Louis *et al.*, 2016; Cavalli *et al.*, 2017). Tumours grouped with WNT-MB are often located in the midline of the fourth ventricle with WNT – MB tumour cells suspected to originate from the lower rhombic lip (Gibson *et al.*, 2010; Northcott, Shih, Peacock, *et al.*, 2012; Perreault *et al.*, 2014). The average age occurrence for WNT MB is between 10 – 12 years old displaying an equal ratio between male and female patients (Taylor *et al.*, 2012; Gajjar and Robinson, 2014; Cavalli *et al.*, 2017). Metastasis with WNT – MB patients is relatively rare only occurring in 5 – 10% of incidents, and an overall better prognosis is rather frequent, compared to other subgroups, with 90% of patients having 5 years of event-free survival (Clifford *et al.*, 2006; Remke *et al.*, 2011; Northcott, Shih, Peacock, *et al.*, 2012). The WNT/β-catenin pathway, which this subgroup was named has a vital role during embryonic development, regulating pluripotency, cell growth and proliferation (MacDonald, Tamai and He, 2009; Northcott, Jones, *et al.*, 2012; Northcott *et al.*, 2017). However, between 85 – 90% of WNT MB patients harbour mutations within exon 3 of the Catenin Beta 1 (*CTNNB1*) gene (Gilbertson, 2004; Northcott, Jones, *et al.*, 2012; Pugh *et al.*, 2012; Robinson *et al.*, 2012; Northcott *et al.*, 2017). This caused β-catenin to become resistant to cytoplasmic degradation, leading to accumulation within the nucleus and upregulation of the WNT pathway (Gilbertson, 2004; Northcott, Jones, *et al.*, 2012; Pugh *et al.*, 2012; Robinson *et al.*, 2012; Northcott *et al.*, 2017). Another genetic alteration that occurs in between 70 – 80% of WNT – MB cases is the monosomy and diploidy of chromosome 6 along with the overexpression of MYC Proto-Oncogene (c-MYC) and MYCN proto-oncogene (MYCN) proteins (Park *et al.*, 1983; de Haas *et al.*, 2008). Overexpression of MYC and MYCN leads to activation of WNT signalling and, therefore, both proteins are regarded as indicators for a worse prognosis in MB patients (Park *et al.*, 1983; de Haas *et al.*, 2008). Other notable genetic alterations found within the WNT subgroup include mutations of DEAD-Box Helicase 3 X-Linked (*DDX3X*) in 50% of cases, SWI/SNF Related Matrix Associated Actin Dependent Regulator of Chromatin Subfamily A Member 4 (*SMARCA4*) in 26% of cases and Tumour protein p53 (*TP53*) in 13% of cases (Gajjar and Robinson, 2014).

The SHH subgroup of MB primarily occurs within the cerebellar hemisphere/vermis and accounts for 25 – 30% of all MB cases, with metastasis uncommon among patients (Northcott *et al.*, 2011; Taylor *et al.*, 2012; Perreault *et al.*, 2014). The SHH subgroup can display a

desmoplastic/nodular histology or a large cell/anaplastic MB histology and is proposed to derive from cerebellar granule neuron progenitors (Kool *et al.*, 2008; Gibson *et al.*, 2010; Louis *et al.*, 2016). SHH – MB has a similar ratio of male to female patients, with cases observed in infants aged between 0 – 3 years and adults older than 16 years (Taylor *et al.*, 2012). The SHH signalling pathway has key involvement in regulating the proliferation of neuronal precursor cells, cellular differentiation, tissue regeneration and maintenance (Choudhry *et al.*, 2014). The SHH pathway involves the SHH ligand to bind to the receptor protein Patched 1 (PTCH1) which activates the intracellular cascade of Smoothened (SMO) proteins. This activates forkhead box protein M1 (FOXM1) as well as triggers the dissociation of GLI transcription factors, GLI Family Zinc Finger 1 and 2 (GLI1/GLI2), from SUFU Negative Regulator of Hedgehog Signalling (SUFU) leading to the activation of Polo Like Kinase 1 (PLK1), MYCN and Telomerase Reverse Transcriptase (TERT) (Mazumdar *et al.*, 2013; Choudhry *et al.*, 2014; Pietrobono, Gagliardi and Stecca, 2019). Abnormal upregulation of the SHH signalling pathway is primarily observed in SHH – MB tumours with genetic mutations found in genes involved in this pathway such as *TERT* in 83%, *PTCH1* in 43%, *SUFU* in 10% and *SMO* in 9% of SHH – MB patients (Hallahan *et al.*, 2004; Thompson *et al.*, 2006; Ayrault *et al.*, 2010; Northcott *et al.*, 2011, 2017; Kool *et al.*, 2012, 2014; Northcott, Jones, *et al.*, 2012). Like in the tumours of the WNT subgroup, *DDX3X* is also mutated in 21% of patients (Robinson *et al.*, 2012; Northcott *et al.*, 2019). Amplification of *FOXM1*, *PLK1*, *MYCN*, *GLI1* and *GLI2*, the deletion of chromosome 9q, the deregulation of *TP53* and the PI3K/ Akt pathway have all been observed in SHH – MB tumours (Ellison *et al.*, 2011; Rausch *et al.*, 2012; Robinson *et al.*, 2012; Northcott *et al.*, 2017).

Group 3 accounts for 25% of all MB cases with a higher occurrence seen in male patients compared to female patients (Northcott, Jones, *et al.*, 2012; Taylor *et al.*, 2012). This subgroup is predominantly seen in infants and older children with both a classic and large cell/anaplastic histology (Eberhart *et al.*, 2002; Garrè *et al.*, 2009; Gibson *et al.*, 2010; Ellison *et al.*, 2011; Kool *et al.*, 2012; Louis *et al.*, 2016; Cavalli *et al.*, 2017). Group 3 MB has the worst prognosis with a 45 – 60% 5-year survival rate and metastasis present in over 45% of Group 3 MB cases (Taylor *et al.*, 2012). Group 3 MB patients can develop leptomeningeal dissemination, which entails the spreading of MB tumours cells to the leptomeningeal spaces of the brain and spinal

cord by disseminating into the cerebrospinal fluid (Dufour *et al.*, 2012; Kool *et al.*, 2012; Northcott, Shih, Peacock, *et al.*, 2012; Taylor *et al.*, 2012; Menyhárt, Giangaspero and Győrffy, 2019). Molecular characteristics of this subgroup include genetic mutations observed in CTD Nuclear Envelope Phosphatase 1 (*CTDNEP1*), Kelch Repeat and BTB Domain Containing 4 (*KBTBD4*), Lysine Methyltransferase 2D (*KMT2D*) and *SMARCA4*, the gain of chromosome 8q and formation of isochromosome 17q (Cavalli *et al.*, 2017; Northcott *et al.*, 2017). Furthermore, amplification of Growth Factor Independent 1 Transcriptional Repressor/ Growth Factor Independent 1B Transcriptional Repressor (*GFI1*/*GFI1B*), Pvt1 Oncogene (*PVT1*), *MYC*, *SMARCA4* and Orthodenticle Homeobox 2 (*OTX2*) has been observed in Group 3 MB patients (Northcott, Jones, *et al.*, 2012). Recent publications have identified an epigenetic process known as enhancer hijacking, where regulatory elements are translocated near coding regions within the genome resulting in overexpression and tumour formation (Northcott *et al.*, 2014, 2019). This phenomenon has been observed with *GFI1*/*GFI1B* oncogene activation in over 30% of Group 3 MB patients (Northcott *et al.*, 2014, 2019).

Group 4 is the most common MB subgroup accounting for 35% of cases with classic histology (Taylor *et al.*, 2012; Louis *et al.*, 2016). This subgroup has a high prevalence in males compared to females but with no specific age incidence (Kool *et al.*, 2012; Northcott, Jones, *et al.*, 2012; Taylor *et al.*, 2012; Cavalli *et al.*, 2017). Amplification of *MYCN*, *CDK6*, Notch receptor 1 (*NOTCH1*), Notch receptor 2 (*NOTCH2*) and Notch receptor 3 (*NOTCH3*) have been observed in Group 4 – MB patients with expression of the NOTCH network-related proteins associated with therapy resistance (Northcott, Shih, Peacock, *et al.*, 2012; Skowron, Ramaswamy and Taylor, 2015; Northcott *et al.*, 2019). Enhancer hijacking is also observed in Group 4 MB tumours, in particular, it causes the overexpression of *GFI1*/*GFI1B* and PR/SET Domain 6 (*PRDM6*) genes (Northcott *et al.*, 2014, 2017, 2019). Mutations observed in Group 4 MB tumours are found predominantly within histone-modifying genes such as Lysine Demethylase 6A (*KDM6A*), Zinc Finger MYM-Type Containing 3 (*ZMYM3*), Lysine Methyltransferase 2C (*KMT2C*) and *KBTBD4* (Northcott *et al.*, 2017). Cytogenetic abnormalities are common within Group 4 MB patients with a gain of chromosome 7 observed in 40% and chromosome 17q in 80% of tumours, deletion of chromosome 8 in 40%, chromosome 11 in 30%, and chromosome 17p in 75% of tumours (Northcott, Shih, Peacock,

et al., 2012; Skowron, Ramaswamy and Taylor, 2015). Formation of isochromosome 17q is observed in over 80% of Group 4 – MB patients (Northcott, Shih, Peacock, *et al.*, 2012; Skowron, Ramaswamy and Taylor, 2015). Loss of chromosome 11 and the gain of chromosome 17 have both been associated with a good outcome for Group 4 MB patients (Shih *et al.*, 2014).

Current publications have yet to investigate the presence and possible involvement of m^6A or DNA:RNA hybrids within MB. However, previous studies have examined the m^6A reader HNRNPA2B1 and other HNRNP family members in association with the c-MYC (Azizi *et al.*, 2012; Staal *et al.*, 2015). It was found that within Group 3 MB tumour cells, HNRNPs are associated with spliceosome activity and *HNRNPA2B1* had an elevated expression that was amplified by the transient knockdown of *MYC* (Azizi *et al.*, 2012; Staal *et al.*, 2015). *HNRNPA2B1* transcription has previously been found to be upregulated by c-MYC resulting in high levels of PKM2 compared to PKM1, although this was not studied in the context of MB (Clower *et al.*, 2010; David *et al.*, 2010). These publications may provide an insight into HNRNPA2B1's role in MB by its contribution to enhanced survival of tumour cells under hypoxic and nutrient-poor conditions (Staal *et al.*, 2015; Staal, Pei and Rood, 2016).

Presently, there are no publications that explore the presence and role of m^6A or DNA:RNA hybrids in MB. *HNRNPA2B1* expression has been observed to be elevated in MB cell lines previously (Azizi *et al.*, 2012; Staal *et al.*, 2015) but not in association with other m^6A readers or m^6A marked DNA:RNA hybrids. In this chapter, I examined whether m^6A-marked DNA:RNA hybrids are present in MB and if the transient knockdown of *HNRNPA2B1* impacts DNA:RNA hybrid levels in MB.

5.2 Aims

The aim of this chapter was to examine the potential presence of m^6A-marked DNA:RNA hybrids and m^6A reader HNRNPA2B1 in MB cells. Currently, there are limited studies that investigate m^6A and its related genes such as HNRNPA2B1 in MB (Azizi *et al.*, 2012; Staal *et*

al., 2015). Therefore, we first aimed to examine the expression and nuclear localisation of m^{6}A and DNA:RNA hybrid-related genes in the MB cell line, UW228-3. Following this, we utilised m^{6}A and DNA:RNA hybrid immunoprecipitation, mass spectrometry and immunocytochemistry, we sought to quantify the levels of m^{6}A-marked DNA:RNA hybrids within repetitive and intronic sequences in MB genomic DNA. Finally, we employed HNRNPA2B1 siRNA mediated knockdown and examined how the loss of *HNRNPA2B1* affected gene expression of apoptotic markers and DNA:RNA hybrid immunostaining signal in MB cells.

5.3 Results

5.3.1 Elevated levels of *HNRNPA2B1* are found in MB cells.

Our first aim was to determine whether m^{6}A-related genes and DNA:RNA hybrid-related genes are expressed in the MB, using the MB public expression datasets and the MB cell line, UW228-3. This was accomplished by evaluating Cavalli's public expression dataset of MB patients (Cavalli *et al.*, 2017), followed by gene expression analysis of UW228-3 cells.

5.3.1.1 MB patients samples are characterised by high levels of *HNRNPA2B1* expression.

Currently, there are no publications that examine the presence of m^{6}A in MB. However, the expression of *HNRNPA2B1* is elevated in Group 3 MB (Azizi *et al.*, 2012; Staal *et al.*, 2015) but is not attributed to m^{6}A, m^{6}A related genes or DNA:RNA hybrids.

Therefore, we initially wanted to explore whether m^{6}A and DNA:RNA hybrid-related genes are expressed in MB by utilising the Cavalli public microarray expression dataset available on R2: Genomics Analysis and Visualization Platform (http://r2.amc.nl) (Cavalli *et al.*, 2017). We focussed on the expression of four m^{6}A-related genes (*METTL3*, *METTL14*, *YTHDF2* and *HNRNPA2B1*) and two DNA:RNA hybrid-related helicases (*DHX9* and *DDX3X*). In the Cavalli dataset, *HNRNPA2B1* appears to have the highest expression of m^{6}A and DNA:RNA hybrid-related genes across the four MB subgroups with an average sqrt of expression of 41.43 in Group 3 MB, 40.87 in Group 4 MB, 41.03 in SHH MB and 38.90 in WNT MB (Fig. 5.1). Whereas *METTL3* and *YTHDF2* had a similar expression pattern with *METTL3* average sqrt

expression ranging from 21.82 in Group 4 MB to 22.76 in SHH MB and *YTHDF2* average sqrt expression ranging from 17.69 in Group 4 MB to 20.74 in WNT MB. DNA:RNA hybrid-related genes, *DHX9* and *DDX3X* displayed similar levels of expression within MB subgroups with *DHX9* average sqrt expression ranging from 19.44 in Group 4 MB to 21.71 in Group 3 MB and *DDX3X* average sqrt expression ranging from 25.15 in Group 4 MB to 27.27 in WNT MB.

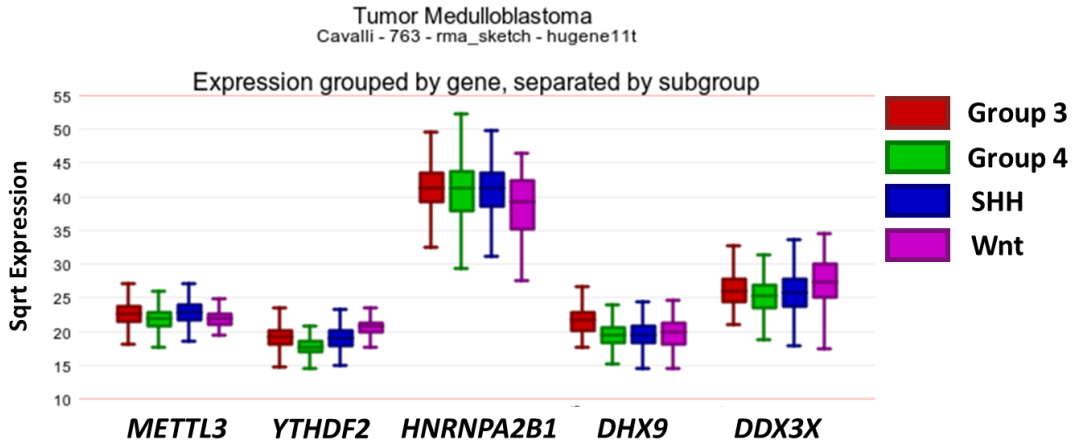


Figure 5.1: Elevated expression of HNRNPA2B1 in the subgroup of MB.

Microarray expression dataset from Cavalli (763 total samples) displaying the square root (sqrt) of expression for METTL3, YTHDF2, HNRNPA2B1, DHX9 and DDX3X. MB subgroups were: Group 3 (144 samples), Group 4 (326 samples), SHH (223 samples) and WNT (70 samples). The dataset was analysed by MAS5.0, available on R2: Genomics Analysis and Visualization Platform (http://r2.amc.nl).

The Cavalli patient dataset indicated that *HNRNPA2B1* displayed a high expression in all the MB subgroups. We next wanted to examine whether the high expression of *HNRNPA2B1* is linked to MB prognosis.

Using the R2: Genomic Analysis and Visualisation Platform (http://r2.amc.nl) to visualise the Cavalli 763 patient samples dataset for MB as Kaplan curves, we can observe the overall survival probability depending upon high or low expression of a candidate protein (Fig. 5.2). In Group 3 MB (Fig. 5.2 A, Supplementary figure 4 B), 25 patients had low *HNRNPA2B1* expression, and 88 patients had high expression of *HNRNPA2B1* that correlated with a worse overall survival probability ($p = 0.131$). In Group 4 MB (Fig. 5.2 B, Supplementary figure 5), high expression of *HNRNPA2B1* was detected in 74 patients and low *HNRNPA2B1*

expression was found in 190 patients with low expression associated with a worse overall survival probability (p = 0.084). In WNT MB patients (Fig. 5.2 C, Supplementary figure 4 A), high *HNRNPA2B1* expression was observed in 52 patients with no negative impact on survival probability, while low *HNRNPA2B1* expression was found in 11 patients and led to a worse overall survival probability ($p = 1.5 \times 10^{-3}$). Finally, in SHH MB patients (Fig. 5.2 D, Supplementary figure 6), 159 patients had a high expression of *HNRNPA2B1* and low expression of *HNRNPA2B1* in only 11 patients (p = 0.027). Low *HNRNPA2B1* expression reduced the SHH patient's overall survival probability to 58% within 30 months compared to an overall survival probability of 63% within 113 months in high *HNRNPA2B1* expression SHH patients.

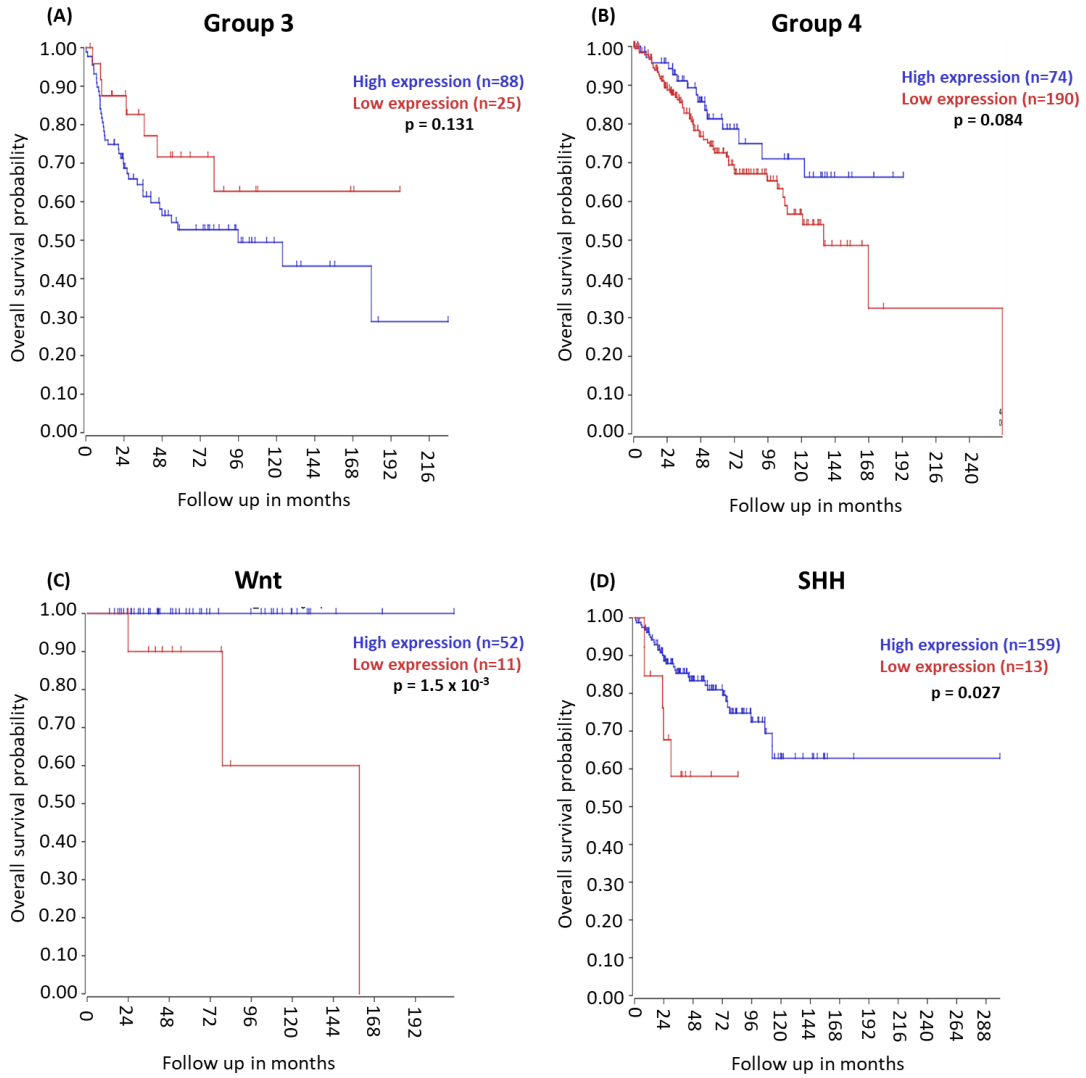


Figure 5.2: HNRNPA2B1 expression and impact on overall survival probability varies upon subgroup.

Kaplan curves on HNRNPA2B1 expression were generated on Cavalli (763) MB dataset available on R2: Genomics Analysis and Visualization Platform (http://r2.amc.nl), separated by subgroup: ***(A)*** *Group 3,* ***(B)*** *Group 4,* ***(C)*** *WNT, and* ***(D)*** *SHH.*

5.3.1.2 Elevated levels of m^{6}A writers, readers, and erasers in UW228-3 cells.

MB patient datasets published by Cavalli (Cavalli *et al.*, 2017) suggested that HNRNPA2B1 is expressed in all MB subgroups (Fig. 5.3). Therefore, we wanted to evaluate the mRNA expression of m^{6}A writers, readers and erasers within the MB cell line, UW228-3, which has been proposed to belong to the SHH-MB subgroup (Triscott *et al.*, 2013). We compared

UW228-3 expression to hiPSCs as the expression of the m^{6}A-related gene has been reported in pluripotent stem cells (Batista *et al.*, 2014; Geula *et al.*, 2015) and hiPSCs used in Chapter 4 as an m^{6}A control for GBM mRNA expression (4.3.1.3). We started by evaluating the expression of genes that belong to the m^{6}A writer complex, *METTL3*, *METTL14* and *WTAP* (Fig. 5.3 A). All these writers exhibited elevated gene expression with *METTL3* averaging 35.49 – fold ($p = 0.00010$), *METTL14* averaging 11.49 – fold ($p = 0.00026$) and *WTAP* averaging 1.63 – fold ($p = 0.00407$) in UW228-3 compared to hiPSCs. We next studied the gene expression of m^{6}A readers, *HNRNPA2B1*, *YTHDF2* and *YTHDC1* (Fig. 5.3 B-C). Both *HNRNPA2B1* and *YTHDF2* had elevated mRNA levels within UW228-3 cells of 113.36 – fold ($p = 0.00015$) and 146.90 – fold ($p = 0.00016$) respectively, compared to hiPSCs. Whereas the m^{6}A reader *YTHDC1* mRNA exhibited no change in expression in UW228-3 (1.03 – fold, $p = 0.725$) compared to hiPSCs. Then we examined the expression of m^{6}A erasers *FTO* and *ALKBH5* in UW228-3 compared to hiPSCs (Fig. 5.3 D). The m^{6}A erasers are both elevated in UW228-3 with *FTO* averaging 2.76 – fold ($p = 0.0362$) and *ALKBH5* averaging 10.48 – fold ($p = 0.0293$) compared to hiPSCs. These results suggested that the expression of most m^{6}A writers, readers and erasers are elevated in UW228-3 compared to hiPSCs.

Based on this, we next wanted to compare the mRNA expression levels of these m^{6}A-related genes between MB, GBM, other brain tissues and hiPSCs. By creating a heatmap visualising the median of side-by-side replicates, we compared the gene expression of m^{6}A writers, readers, and erasers in human astrocytes cell line SVGA, human foetal brain cell line FB83, GBM cell lines (LN18, LN229, U251, U87MG) and MB cell line UW228-3 (Fig. 5.4). The heatmap suggested that *YTHDF2* had the overall highest mRNA expression in FB83, GBM cell lines and UW228-3, but not in SVGA. *METTL3* also had mRNA expression across FB83, GBM cell lines and UW228-3 although it was not as highly expressed as *YTHDF2*. Elevated expression of *HNRNPA2B1* appeared to be unique to UW228-3 with SVGA, FB83 and GBM cell lines appearing to have comparatively low *HNRNPA2B1* expression.

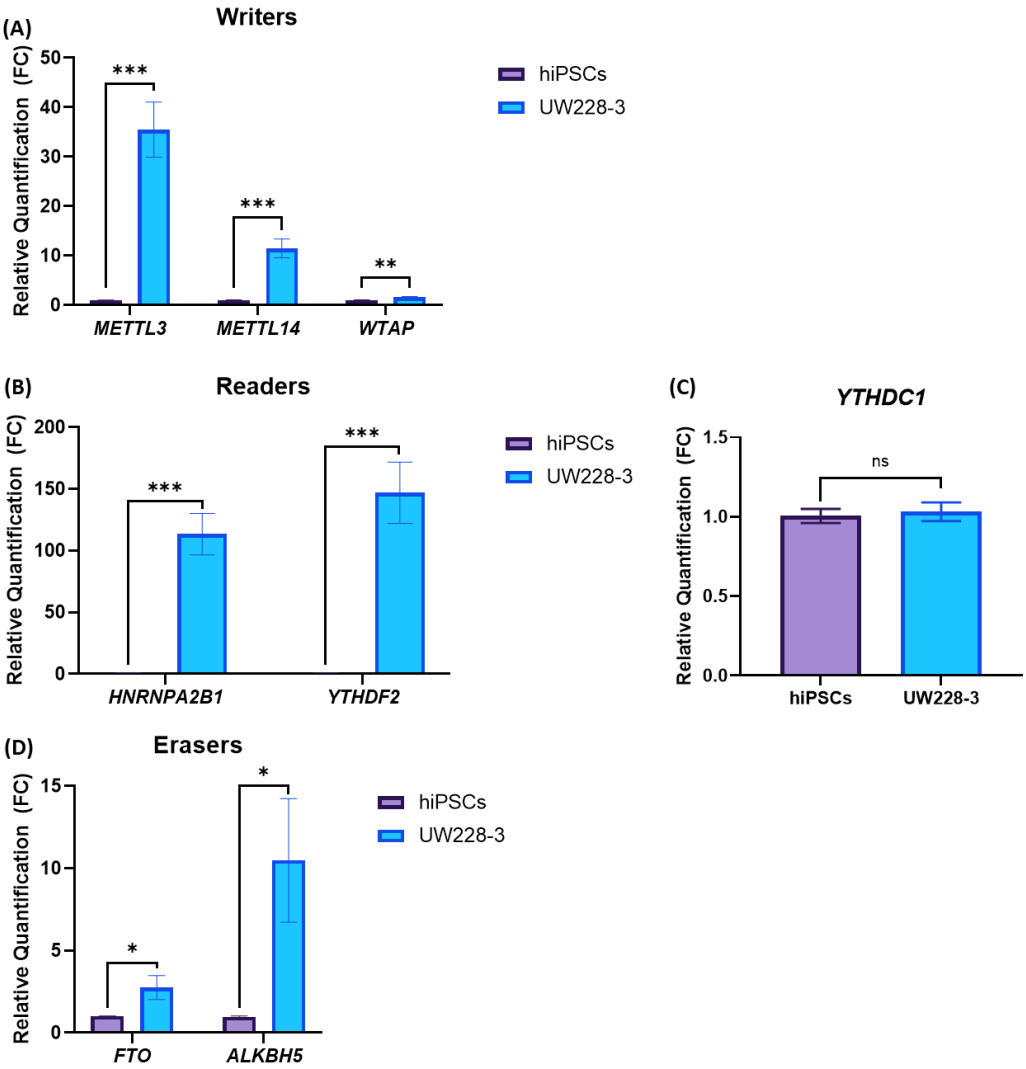


Figure 5.3: Gene expression of m^{6}A writers, readers and erasers are elevated in UW228-3 cells.

Gene expression qPCR results of m^{6}A writers ***(A)*** *METTL3, METTL14, WTAP; m^{6}A readers* ***(B)*** HNRNPA2B1, *YTHDF2,* ***(C)*** *YTHDC1; and m^{6}A erasers* ***(D)*** *FTO and ALKBH5 in MB cell line UW228-3 compared to hiPSCs. Mean ± SEM, 2 biological replicates each with 3 technical replicates. Unpaired t-test, ns = p ≥ 0.05,* = p < 0.05, ** = p < 0.01, *** = p < 0.001.*

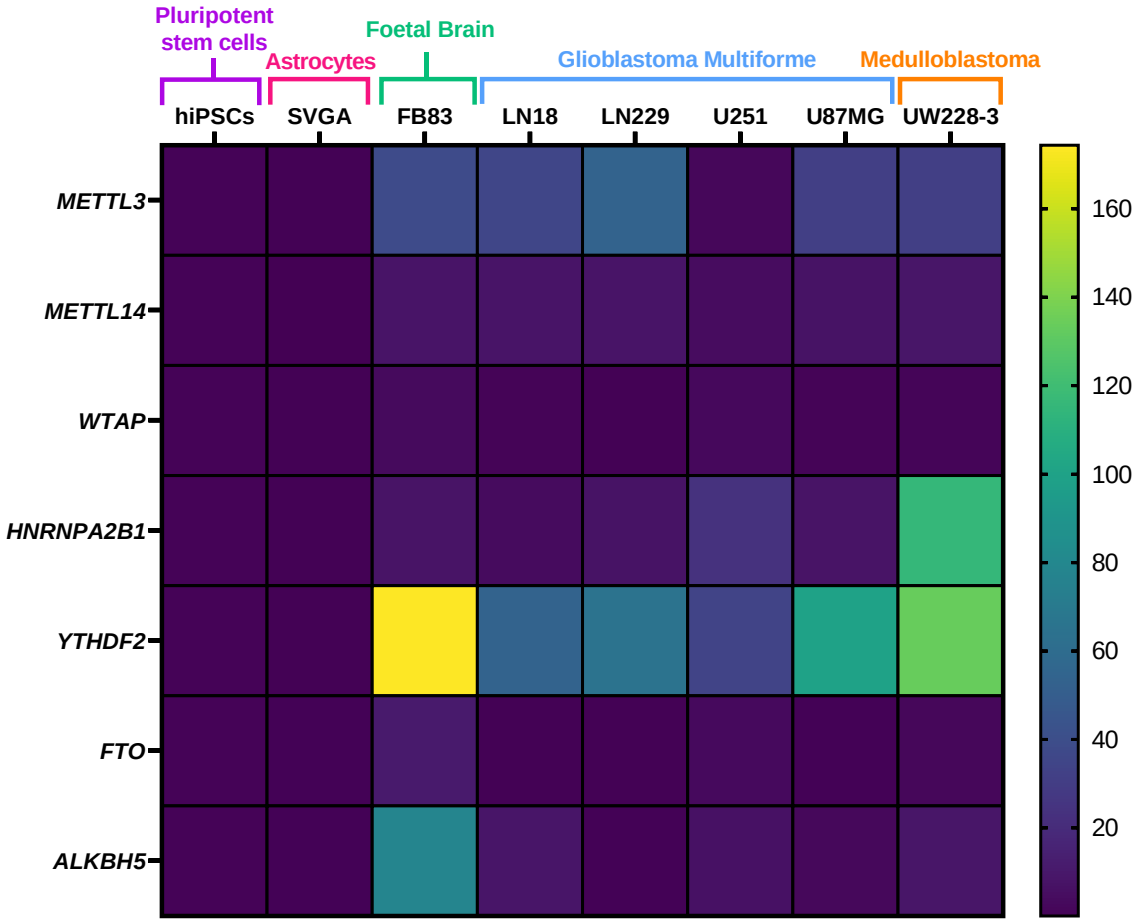


Figure 5.4: *HNRNPA2B1* and *YTHDF2* gene expression have higher expression in UW228-3 compared to GBM cell lines.

Heat Map comparison between Pluripotent stem cells, hiPSCs, Astrocytes, SVGA, Foetal Brain tissue, FB83, Glioblastoma cell lines: LN18, LN229, U251, and U87MG and Medulloblastoma cell line: UW228-3 in the gene expression of m^{6}A genes: METTL3, METTL14, WTAP, YTHDF2, HNRNPA2B1, FTO and ALKBH5. Map of the median side-by-side replicates. All cell lines had 2 biological replicates each with 3 technical replicates.

5.3.1.3 Elevated mRNA expression of DNA:RNA hybrid related genes within UW228-3 cells.

DDX3 has been previously reported to have high levels of protein expression in both paediatric and adult MB (Tantravedi *et al.*, 2019). *DDX3X* and *DHX9* have also been described as DNA:RNA hybrid helicases (Cristini *et al.*, 2018), therefore we wanted to examine whether their gene expression increases similarly to *HNRNPA2B1* and *YTHDF2* in UW228-3 cells (Fig.

5.5). Upon examination, we observed elevated gene expression of *DHX9* by 224.38 – fold (p = 0.0022, Fig. 5.5 A) and *DDX3X* by 17.99 – fold in UW228-3 (p = 0.0007, Fig. 5.5 B) when compared to hiPSCs.

Overall, we observed an increased gene expression of m^{6}A writers, readers, and DNA:RNA hybrid helicases in MB cells.

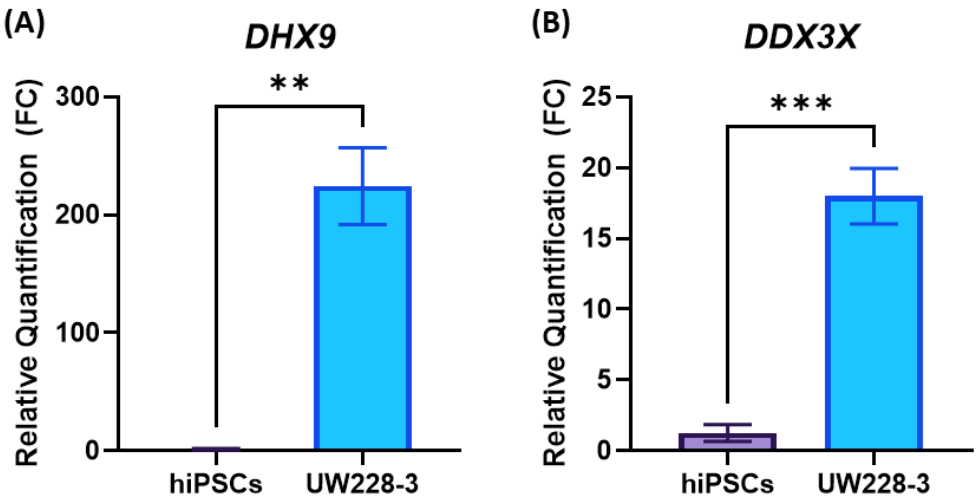


Figure 5.5: Increased expression of DNA:RNA hybrid related genes within UW228-3.

Gene expression qPCR results of DNA:RNA hybrid related genes, ***(A)*** *DHX9 and* ***(B)*** *DDX3X in MB UW228-3 cells compared to hiPSCs. Mean ± SEM, 2 biological replicates each with 3 technical replicates. Unpaired t-test, ** = p < 0.01, *** = p < 0.001.*

5.3.2 m^{6}A-marked DNA:RNA hybrids are present in UW228-3 cells.

Gene expression analysis has alluded to the presence of m^{6}A interacting genes as well as DNA:RNA hybrid genes within MB cells, with *METTL3*, *METTL14*, *YTHDF2*, *HNRNPA2B1*, *DHX9* and *DDX3X* all presenting elevated gene expression. We next aimed to examine whether m^{6}A marked DNA:RNA hybrids are present within MB cells by m^{6}A DRIP, S9.6 DRIP and SID–UPLC–MS/MS.

5.3.2.1 m^{6}A-DNA:RNA hybrids levels in repetitive sequences are lower in UW228-3 compared to hiPSCs.

As with previous chapters, we primarily wanted to examine whether m^{6}A-marked DNA:RNA hybrids residing in repetitive sequences are enriched with MB genomic DNA, compared to hiPSCs genomic DNA (Fig. 5.6 A – D). The m^{6}A-DRIP qPCR results suggested that m^{6}A on DNA:RNA hybrids residing in repetitive elements are present in UW228-3, but with lower enrichment compared to hiPSCs. In *α-satellites* (Fig. 5.6 A), we observed a decreased enrichment of m^{6}A on DNA:RNA hybrids by 15.72 – fold in UW228-3 cells compared to hiPSCs. In *LINE1* (Fig. 5.6 B), we observed a decrease in m^{6}A levels on DNA:RNA hybrids by 3.29 x10^3 – fold between UW228-3 cells and hiPSCs. In *Alu-Y* (Fig. 5.6 C) and *Alu-S* (Fig. 5.6 D), we detected a decrease in m^{6}A on DNA:RNA hybrids by 15.35 – fold and 14.65 – fold in UW228-3 cells, respectively compared to hiPSCs. In summary, m^{6}A-marked DNA:RNA hybrids are present at the repetitive elements including *α-satellites*, *LINE1*, *Alu-Y* and *Alu-S* elements within UW228-3.

On the other hand, when examining the levels of DNA:RNA hybrids by the S9.6 D-RIP approach (Fig. 5.7 A – D), we observed no enrichment of DNA:RNA hybrids within UW228-3 as all UW228-3 values were below their matched no antibody control (α-satellites = 0.067, LINE1/L1 = 0.527, Alu-Y = 0.608, Alu-S = 0.479), yet was present in hiPSCs (Alpha-Satellites = 47.32 – fold, LINE1/L1 = 586.4 – fold, Alu-Y = 988.1 – fold, Alu-S = 394.6 – fold) within the same experiment. As this is one biological replicate, it is difficult to decipher whether this is a true representation of the DNA:RNA hybrid levels within repetitive sequences in UW228-3 or an experimental error.

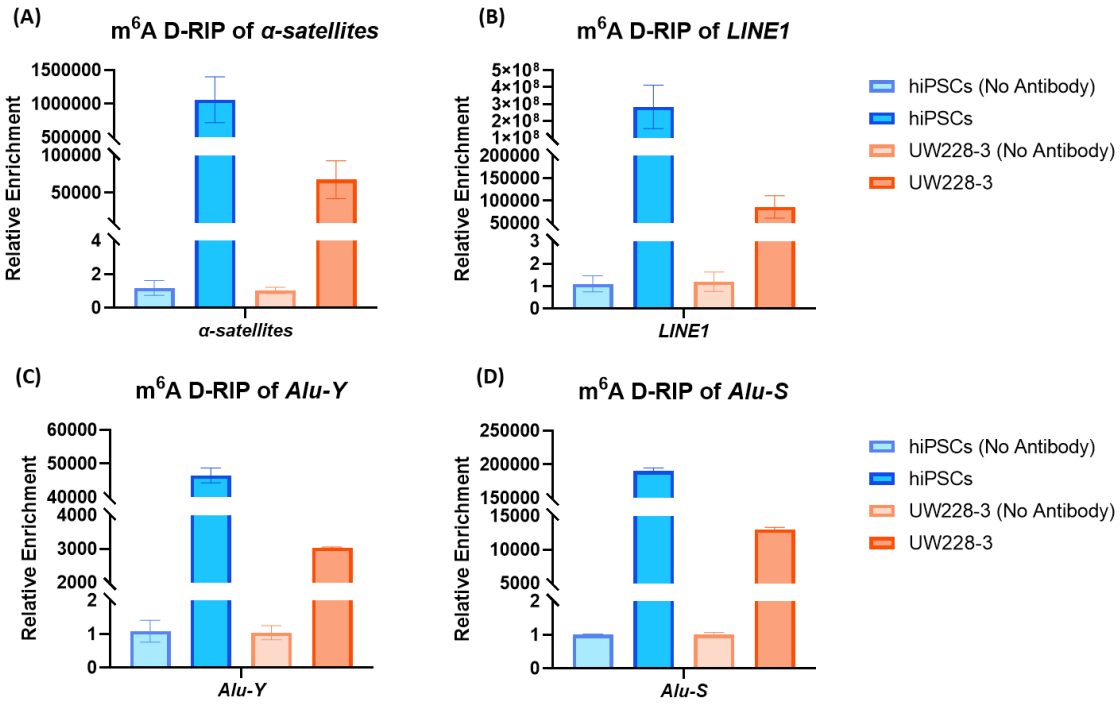


Figure 5.6: Levels of m^{6}A-marked DNA:RNA hybrids within repetitive elements are lower in UW228-3 compared to hiPSCs.

m^{6}A-DRIP qPCR comparison of repetitive elements: ***(A)*** *α-satellites,* ***(B)*** *LINE1, and SINE elements* ***(C)*** *Alu-Y and* ***(D)*** *Alu-S between hiPSCs and UW228-3 accompanied by their no antibody controls. Mean ± SEM, 1 biological replicate with 3 technical replicates.*

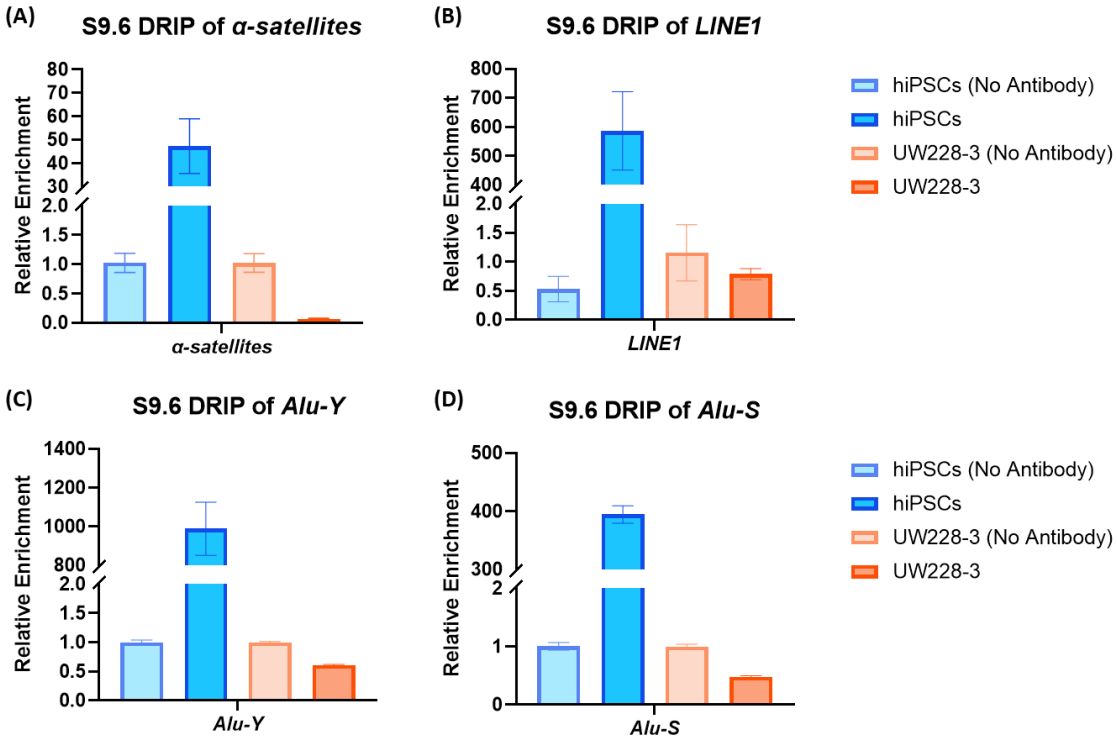


Figure 5.7: Levels of DNA:RNA hybrids within repetitive elements are lower in UW228-3 compared to hiPSCs.

S9.6-DRIP qPCR comparison of repetitive elements: ***(A)*** *α-satellites,* ***(B)*** *LINE1, and SINE elements* ***(C)*** *Alu-Y and* ***(D)*** *Alu-S between hiPSCs and UW228-3 accompanied by their no antibody controls. Mean ± SEM, 1 biological replicate with 3 technical replicates.*

5.3.2.2 Intronic loci in *GLI2*, *CDK6*, *RB1* and *NF1* have lower m^{6}A-marked DNA:RNA hybrid enrichment in UW228-3 compared to hiPSCs.

The presence of m^{6}A marked DNA:RNA hybrids have also been found to reside within intronic regions of the genome (Abakir *et al.*, 2020). Using bioinformatics data from next-generation sequencing of m^{6}A DRIP and S9.6 DRIP hiPSCs datasets (Abakir *et al.*, 2020), a list of possible gene locations of overlapping peaks in hiPSCs was formed. With this list, we focussed on intronic regions within MB-related genes that have been reported in publications such as GLI Family Zinc Finger 2 (*GLI2*; Fig. 5.8 A) and Cyclin-dependent kinase 6 (*CDK6*; Fig. 5.9 A).

GLI2 has mainly been associated with the SHH subgroup of MB, with focal amplification of *GLI2* found in 9% of SHH tumours (Cho *et al.*, 2011; Northcott *et al.*, 2011, 2017; Kool *et al.*, 2012, 2014; Skowron *et al.*, 2021). Excessive activation of the SHH pathway amplifies the expression of *GLI2* inducing uncontrolled proliferation of granule cells and tumour formation (Marino, 2005; Hatten and Roussel, 2011). Using IGV software, we visualised the overlapping m^6A DRIP and S9.6 DRIP peaks in hiPSCs and found a large m^6A-marked DNA:RNA hybrid-containing region in Intron 2 of *GLI2* (Fig. 5.8 A). We made a set of primers to cover the first half of the m^6A-marked DNA:RNA hybrid in *GLI2* to keep the size of the fragment to around 200bp for use in the m^6A DRIP qPCR of hiPSCs and UW228-3 genomic DNA. In *GLI2* (Fig. 5.8 B), we observed decreased enrichment m^6A levels on DNA:RNA hybrids by 4.62 $x10^3$ – fold in UW228-3 compared to hiPSCs.

CDK6 and CDK4 are involved in driving the G_1-S transition during the cell cycle (Sherr, Beach and Shapiro, 2016; Tigan *et al.*, 2016). Within MB, *CDK6* is amplified by 5-10% of Group 4 MB tumours (Cho *et al.*, 2011; Northcott, Shih, Remke, *et al.*, 2012; Menyhárt, Giangaspero and Győrffy, 2019) and preclinical trials of CDK6/CDK4 inhibitors within MB models have shown encouraging results (Faria *et al.*, 2015; Hanaford *et al.*, 2016; Cook Sangar *et al.*, 2017). Using IGV software, we found overlapping m^6A DRIP and S9.6 DRIP peaks within Intron 4 of *CDK6* (Fig. 5.9 A). After creating primers to span the intronic region where the m^6A marked DNA:RNA hybrid resides in *CDK6*, we performed m^6A DRIP qPCR on hiPSCs and UW228-3 genomic DNA (Fig 5.9 B). In *CDK6*, we detected decreased enrichment of m^6A levels on DNA:RNA hybrids by 2.29 – fold in UW228-3 compared to hiPSCs.

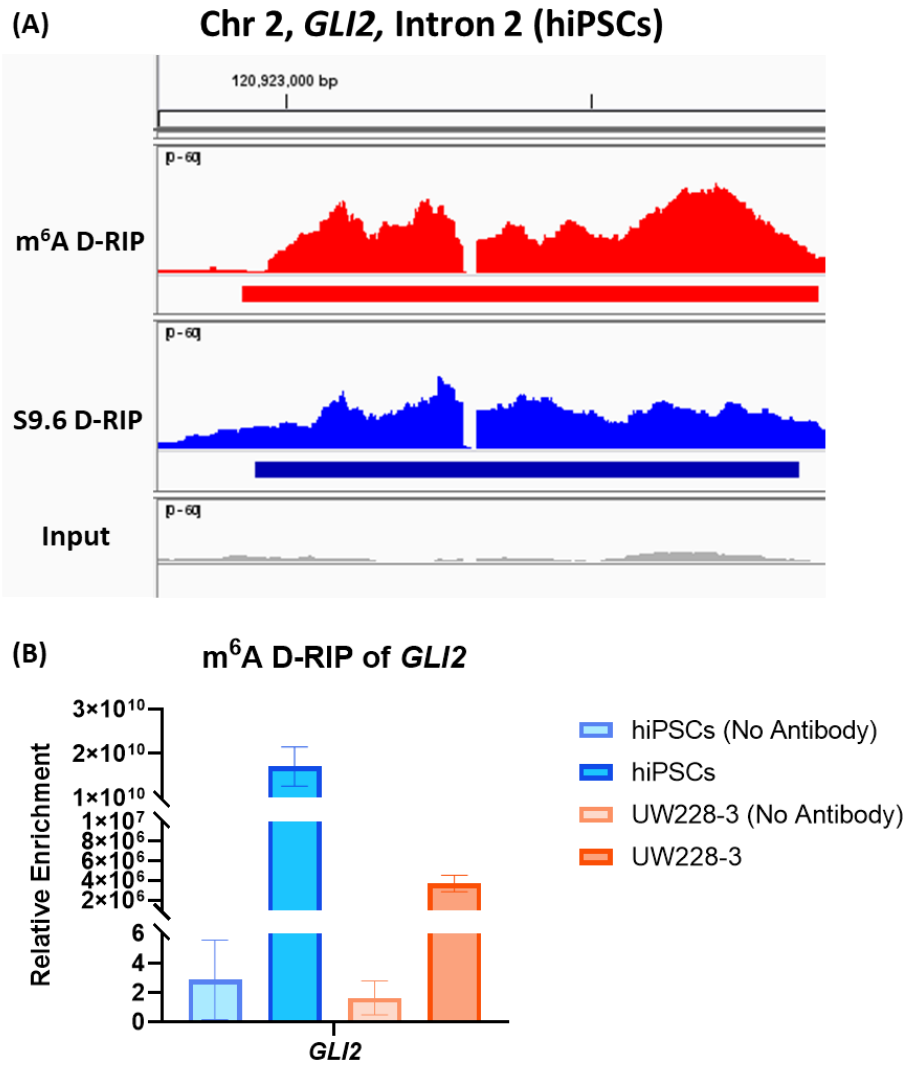


Figure 5.8: Enrichment levels of m^{6}A marked DNA:RNA hybrids within intronic sequences of *GLI2* are lower in UW228-3 compared to hiPSCs.

(A) *GLI2 IGV coverage plot of m^{6}A DRIP and S9.6 DRIP next-generation sequencing within hiPSCs. IGV coverage plots were compared to hiPSCs input with the data range set at 60 for GLI2.* ***(B)*** *m^{6}A DRIP qPCR comparison between hiPSCs and UW228-3 for GLI2 with matched no antibody controls. Mean ± SEM, 1 biological replicate with 3 technical replicates.*

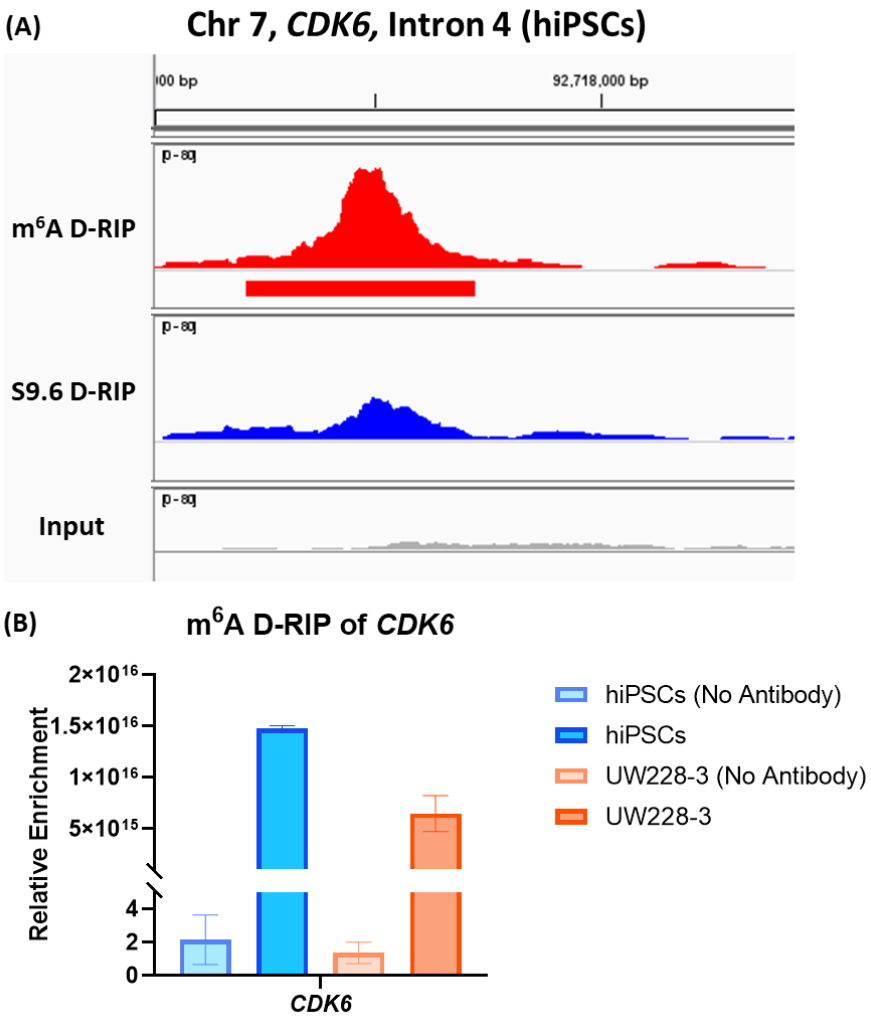


Figure 5.9: Enrichment levels of m^{6}A marked DNA:RNA hybrids within intronic sequences of *CDK6* are lower in UW228-3 compared to hiPSCs.

(A) *CDK6 IGV coverage plot of m^{6}A DRIP and S9.6 DRIP next-generation sequencing within hiPSCs. IGV coverage plots were compared to hiPSCs input with the data range set at 80 for CDK6.* ***(B)*** *m^{6}A DRIP qPCR comparison between hiPSCs and UW228-3 for CDK6 with matched no antibody controls. Mean ± SEM, 1 biological replicate with 3 technical replicates.*

5.3.2.3 SID-UPLC-MS/MS identified the presence of m^{6}A-marked DNA:RNA hybrids in UW228-3 cells.

Previously, our group used SID-UPLC-MS/MS to evaluate the overall levels of m^{6}A marked DNA:RNA hybrids within the genome (Abakir *et al.*, 2020). With this technique, we aimed to examine the overall levels of m^{6}A marked DNA:RNA hybrids in a UW228-3 cell line (Fig. 5.10),

in comparison to hiPSCs where m^{6}A marked DNA:RNA hybrids have been previously detected (Abakir *et al.*, 2020). Using SID-UPLC-MS/MS method previously described in Chapter 3, we observed that RNase H treated UW228-3 cells had a lower amount of m^{6}A present on DNA:RNA hybrids (18.065 fmol/µg of input DNA) compared to RNase H treated hiPSCs (56.774 fmol/µg of input DNA). This would further suggest that m^{6}A marked DNA:RNA hybrids are present within UW228-3 cells but at a lower level in comparison to hiPSCs.

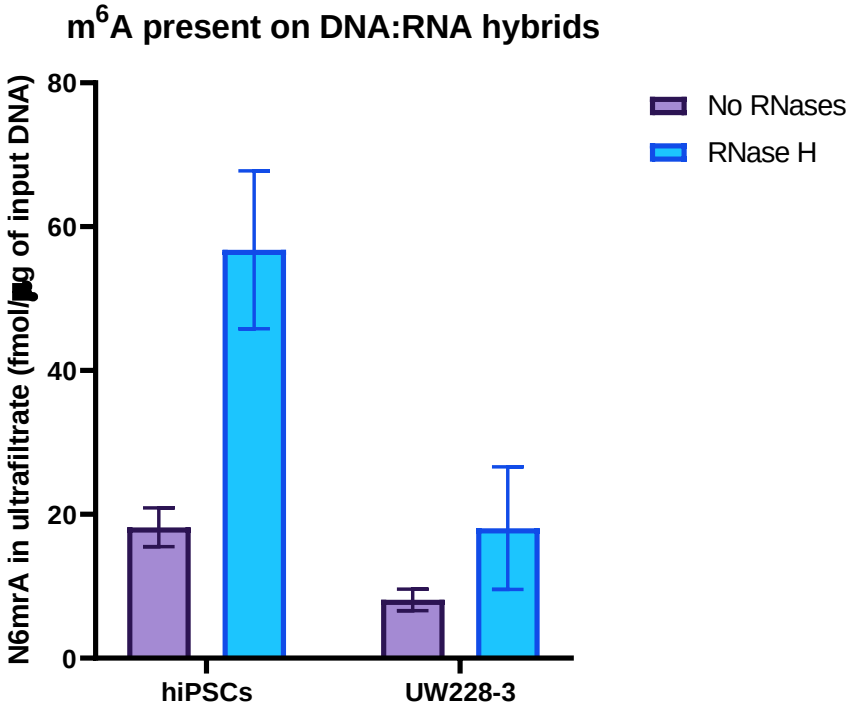


Figure 5.10: UW228-3 cells have lower levels of m^{6}A present on DNA:RNA hybrids compared to hiPSCs.

SID–UPLC–MS/MS quantification of m^{6}A present on adenosine (N6mrA) within the fractions of hiPSCs-derived, UW228-3 nucleic acids released following RNase H treatment. Mean ± SEM, 2 biological replicates.

5.3.3 siRNA mediated knockdown of HNRNPA2B1 within UW228-3 leads to elevated DNA:RNA hybrid presence.

Within this chapter, we found by gene expression analysis of UW228-3 that *HNRNPA2B1* expression was higher in UW228-3 compared to SVGA cells, FB83 cells, and GBM cell lines

(Fig. 5.4). Moreover, m^{6}A DRIP qPCR and SID-UPLC-MS/MS both suggested that m^{6}A marked DNA:RNA hybrids are present in UW228-3 cells (Fig. 5.6 – 5.10). Our next aim was to examine whether the levels of DNA:RNA hybrids are altered upon the loss of *HNRNPA2B1.*

5.3.3.1 Validation HNRNPA2B1 knockdown in UW228-3 cells.

Initially, we needed to optimise the concentration of HNRNPA2B1 siRNA and chemical transfection reagent, DharmaFECT, to have the strongest knockout efficiency on UW228-3 cells without detrimentally impacting cell viability. From three biological replicates, we observed that 50 nM siHNRNPA2B1 siRNA combined with 4 µL of DharmaFECT produced a consistent knockdown efficiency without affecting cell viability (Fig. 5.11 A). To verify that gene expression of *HNRNPA2B1* has been impacted by transfection of HNRNPA2B1 siRNA, we performed qPCR comparing mRNA expression between UW228-3 cells in reduced serum OptiMEM media and siHNRNPA2B1 treated UW228-3 cells (Fig. 5.11 B). Knockdown of *HNRNPA2B1* was shown to have a 90.68% knockdown efficiency ($p = 0.0011$) compared to UW228-3 cells in OptiMEM media.

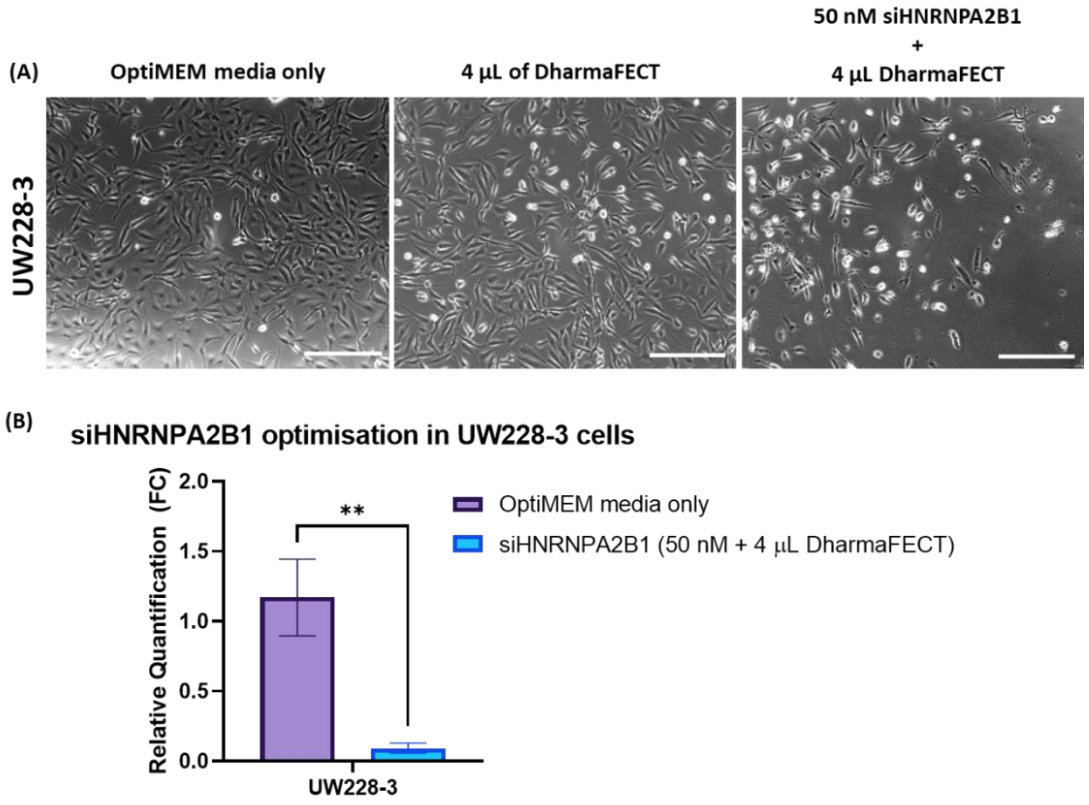


Figure 5.11: Optimisation of HNRNPA2B1 siRNA within UW228-3 cells.

(A) *Brightfield light microscope images of optimised siRNA treatment of siHNRNPA2B1 in UW228-3 cells 24 hours post-transfection compared to UW228-3 cells in reduced serum OptiMEM media and DharmaFECT treated UW228-3 cells. Transfection of HNRNPA2B1 siRNA was optimised to 50 nM siHNRNPA2B1 with 4 µL per well of DharmaFECT. Scale bar represents 250 µM.* ***(B)*** *RT-qPCR testing of HNRNPA2B1 siRNA knockdown efficiency at 50 nM siHNRNPA2B1 with 4 µL per well of DharmaFECT compared to OptiMEM only media cells. Mean ± SEM, 3 biological replicates shown in different bars each with 3 technical replicates. Unpaired t-test, ** = p < 0.01.*

5.3.3.2 Attachment to growth surface is impaired after knockdown of *HNRNPA2B1* in UW228-3 cells and is restored with the use of a commercial attachment factor.

The brightfield light microscope images suggest that UW228-3 cells transfected with siHNRNPA2B1 for 24 hours exhibited cell lifting from the growth surface with some of the remaining attached cells displaying a rounded morphology (Fig. 5.11). To see if the detachment from the growth surface could be limited, we coated the growth surface with an attachment factor containing 0.01% gelatin (Gibco, ThermoFisher Scientific – #S006100) (Fig.

5.12). Using the same seeding density as well as the same concentration of siHNRNPA2B1 and DharmaFECT optimised, we found more cells remaining attached to the surface.

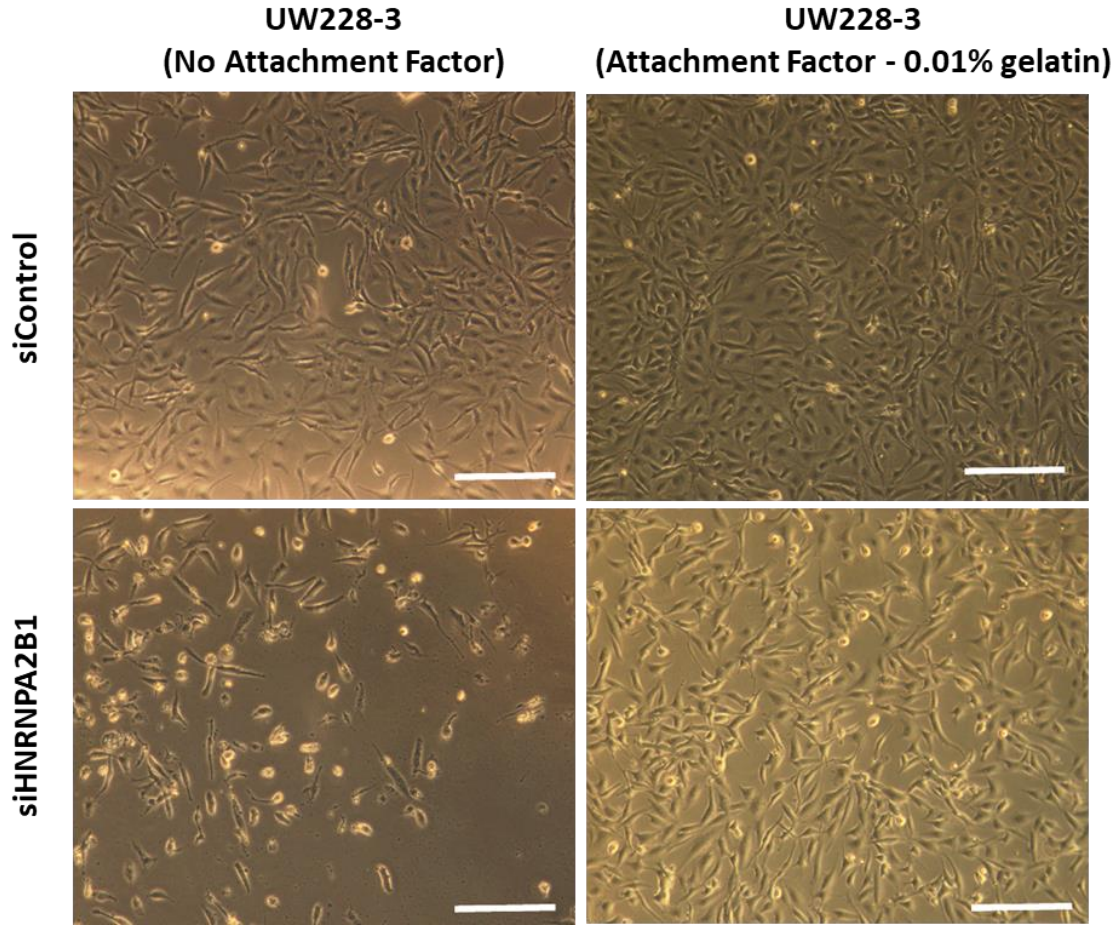


Figure 5.12: Increased level of cell attachment to growth surface with commercial attachment factor in UW228-3 siHNRNPA2B1 knockdown cells compared to untreated UW228-3 siHNRNPA2B1 knockdown cells.

Brightfield light microscope images of OptiMEM media only and siHNRNPA2B1 transfected UW228-3 cells at same seeding density and imaged 24 hours post-transfection. Wells were either left untreated in normal growing conditions and other coated first with ThermoFisher attachment factor (0.01% gelatin) (Gibco, ThermoFisher Scientific – #S006100) before seeding. Scale bar represents 250 µM.

5.3.3.3 Knockdown of HNRNPA2B1 significantly increases the levels of DNA:RNA hybrids in UW228-3 cells.

We have previously found that DNA:RNA hybrid helicases *DHX9* and *DDX3X* have elevated expression in UW228-3 cells (Fig. 5.5). We next tested whether the loss of *HNRNPA2B1* impacted the gene expression of DNA:RNA hybrid helicases (Fig. 5.13). Both *DHX9* and *DDX3X* expression was increased by 10.58 – fold (p = 0.0246) and 11.07 – fold (p = 0.0044), respectively after transfection with HNRNPA2B1 siRNA in UW228-3 cells compared to siControl UW228-3 cells.

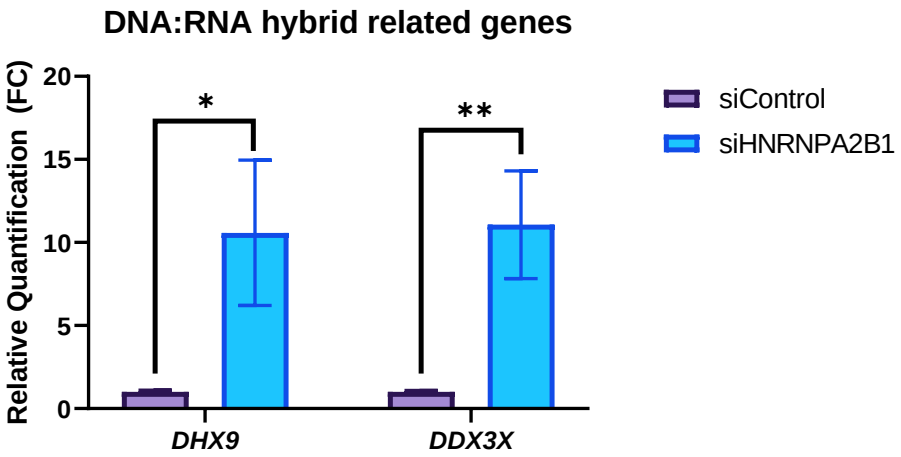


Figure 5.13: Knockdown of HNRNPA2B1 in UW228-3 increases expression of DNA:RNA hybrid related genes.

*Gene expression qPCR results showing DNA:RNA hybrid related genes: DHX9 and DDX3X comparison between siControl and siHNRNPA2B1 UW228-3 cells. Mean ± SEM, 2 biological replicates each with 3 technical replicates. Unpaired t-test, * = p< 0.05, ** = p < 0.01.*

The qPCR analysis of DNA:RNA hybrid helicases *DHX9* and *DDX3X* indicated that mRNA expression is increased in siHNRNPA2B1 UW228-3 cells. We next wanted to observe whether the presence of DNA:RNA hybrids were affected by the knockdown of *HNRNPA2B1*. Using a DNA:RNA hybrid (clone S9.6) antibody and DAPI nuclear staining, we compared the presence and spatial distribution of DNA:RNA hybrids in siControl and siHNRNPA2B1 UW228-3 cells (Fig. 5.14). Focussing on the immunostaining within the nucleus, there was an increased presence of DNA:RNA hybrids in the siHNRNPA2B1 UW228-3 cells compared to siControl

UW228-3 cells (Fig. 5.14 A). This increased DNA:RNA hybrid presence was corroborated by single-cell comparison (Fig. 5.14 B) and pixel intensity quantification analysis of 19 nuclei (Fig. 5.14 C, $p < 0.0001$). Thus, using immunocytochemistry, we observed that the loss of *HNRNPA2B1* in UW228-3 cells appears to increase the presence of both DNA:RNA hybrids and DNA:RNA hybrid helicases. These results together are rather unexpected, as we would expect DNA:RNA hybrid levels to be reduced if DNA:RNA hybrid helicase expression was elevated.

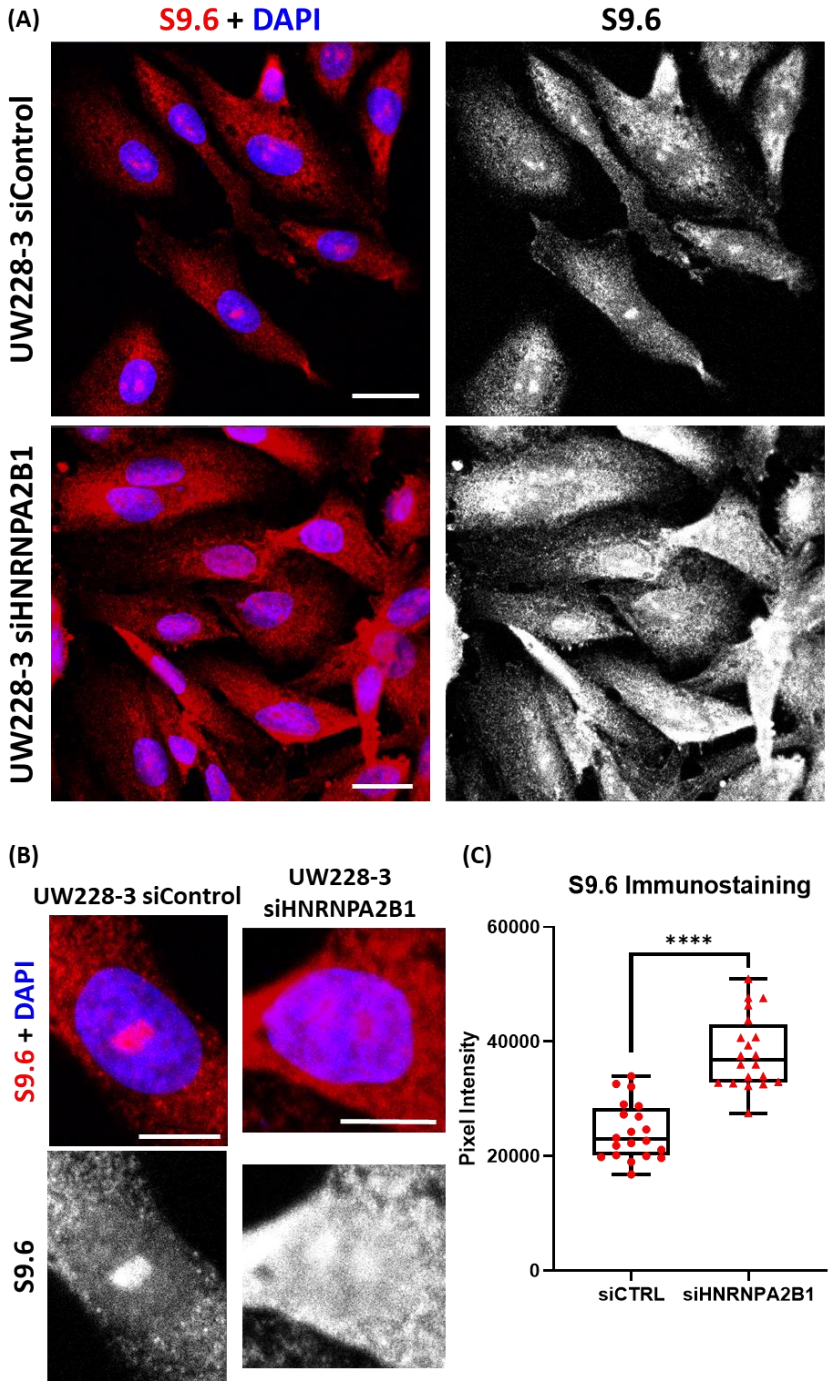


Figure 5.14: DNA:RNA hybrids presence increased in UW228-3 siHNRNPA2B1 cells.

(A) *Immunostaining with DNA:RNA hybrid antibody (S9.6 clone) and DAPI nuclear staining in siControl and siHNRNPA2B1 UW228-3 cells. Representative image shown from 4 technical replicates. Scale bar represents 20 μM.* ***(B)*** *Single cell comparison of S9.6 and DAPI nuclear immunostaining within siControl and siHNRNPA2B1 UW228-3 cells. Scale bar represents 10 μM.* ***(C)*** *Quantification boxplot of S9.6 pixel intensity between siControl and siHNRNPA2B1 UW228-3 cells in 19 nuclei. Values had normal distribution and evaluated by Unpaired t-test, **** = $p < 0.0001$.*

5.4 Technical Discussion

In this chapter, we started with evaluating the expression levels of m^{6}A-related genes in MB, as currently, no publications have investigated m^{6}A presence or their roles in MB. However, recent publications have alluded to m^{6}A methylation levels to be highest in brain tissues and proposed functions for m^{6}A in embryonic stem cell differentiation, brain development, neurodevelopmental disorders and brain tumours such as GBM (Batista et al., 2014; Y. Wang et al., 2014; Cui et al., 2017; Yoon et al., 2017; Ma et al., 2018; Yen and Chen, 2021). By performing gene expression analysis of MB cell line UW228-3 and identified that *YTHDF2* had the highest gene expression, followed by *HNRNPA2B1* expression and *METTL3* gene expression compared to hiPSCs (Fig. 5.3). The elevated HNRNPA2B1 expression we observed in MB (Fig. 5.3 B), is comparable to previous publications (Azizi *et al.*, 2012; Staal *et al.*, 2015). When we compared the gene expression to astrocyte cells, foetal brain tissue and GBM, we identified that the high HNRNPA2B1 expression was unique to UW228-3 cells (Fig. 5.4). Although there are no publications currently to compare the expression of other m^{6}A related genes in MB, other studies than high m^{6}A methylation levels are a common trait of brain tissues (J. Liu et al., 2020; Yen and Chen, 2021). This is noticeable when looking at the heatmap (Fig. 5.4) with the increased *METTL3* and *YTHDF2* expression in FB83, 4 GBM cell lines and MB cells. However, this observation is only considering continuous cell lines whereas we have previously shown that primary GBM cell lines have a lower expression level of m^{6}A-related genes (Fig 4.5) (Robertson *et al.*, 2019). Moreover, in this experiment, we only consider one cell line of MB, UW228-3. We could have strengthened these results by including another SHH MB subgroup cell line such as DAOY that has been used by other researchers (Tantravedi *et al.*, 2019). Furthermore, utilising other MB cell lines from different MB subgroups could provide insight into whether the expression of m^{6}A-related genes is detected similarly across MB subgroups as our Cavalli dataset analysis suggested (Fig. 5.1). Recent publications studying MB have used patient-derived MB cells as it provided a closer representation to the expression observed in MB patients (Delyan P. Ivanov et al., 2016; Nasir et al., 2021).

We also observed the mRNA expression for DNA:RNA hybrid-related genes *DHX9* and *DDX3X* and found they are both elevated in UW228-3 cells (Fig. 5.5). Although DNA:RNA hybrids have not been studied in MB, *DDX3X* has shown to be recurrently mutated within WNT MB subgroup with associations with the WNT/β-catenin signalling pathway (Tantravedi *et al.*, 2019) as well as genomic instability has been observed in Group 3 and Group 4 MB subgroups (Kool *et al.*, 2012).

In this chapter, we wanted to study whether m^6A-marked DNA:RNA hybrids are present in MB cells by using m^6A DRIP qPCR. We identified that m^6A-marked DNA:RNA hybrids are present within repetitive elements such as LINE1/L1 and SINE elements Alu-Y and Alu-S (Fig. 5.6 A – D) as well as intronic regions within *GLI2* and *CDK6* in UW228-3 cells (Fig. 5.8 – 5.9). More potential MB gene candidates that were brain cancer-specific could have been identified if m^6A DRIP next-generation sequencing was carried out rather than using filtering through the positive candidates with m^6A DNA:RNA hybrids found in the hiPSCs peak list.

Since the original S9.6 DRIP protocol was published in 2006 (Hu *et al.*, 2006), variations and adaptations have since been made to optimise the mapping of DNA:RNA hybrids within the genome (Ginno et al., 2012; Chan et al., 2014; el Hage et al., 2014; Nadel et al., 2015; Wahba et al., 2016). A publication that evaluated these variations suggested the best protocol involved purified nucleic acids by solid-phase purification kit and fragmentation by sonication with formaldehyde (HCHO) fixation and RNase A treatment excluded (Halász *et al.*, 2017). However, our protocol performs RNase A treatment after cell lysing before the genomic DNA is extracted (Methods and Materials – 2.3.6). RNase A has been observed to digest DNA:RNA hybrids at low salt concentrations, therefore, removing DNA:RNA hybrids before we can perform S9.6 immunoprecipitation (Benore-Parsons and Ayoub, 1997; Donà and Houseley, 2014; Halász *et al.*, 2017). Our reasoning for using RNase A was to degrade ssRNA as this genomic DNA would be used for both the S9.6 DRIP and the m^6A DRIP and prevent m^6A binding to modified RNA found within the samples. As previously mentioned, the S9.6 antibody has its limitations such as the specificity of the antibody to DNA:RNA hybrids and a low affinity for dsRNA (Phillips *et al.*, 2013; König, Schubert and Längst, 2017; Hartono *et al.*, 2018) as well as cell cycle stage in which the cells are at the point of collection (Hamperl *et al.*, 2017;

Lang *et al.*, 2017; Abakir *et al.*, 2020). DNA:RNA hybrids accumulate during S-phase and mitosis, therefore comparing the DNA:RNA hybrid levels between a pluripotent stem cell line with a high mitosis level and a UW228-3 MB cell line that is differentiated therefore a much lower dividing time will influence our observation in the S9.6 DRIP qPCR (Supplementary figure 1). One way to overcome this would have been to perform live cell sorting by flow cytometry of the cell cycle stage, selecting for cells within the $G_0/G_1/G_2$ cell cycle phases. Another alternative would have been to use a neural tissue-specific comparison such as FB83 instead of hiPSCs reducing the large disparity observed. A recent publication has described an alternative methodology to map native DNA:RNA hybrids referred to as the R-loop CUT&Tag (Wang *et al.*, 2021). By constructing 2 tagged glutathione S-transferases (GST), a tagged hexahistidine (His_6) artificial sensor proteins and tandem repeats of the N-terminal hybrid binding domain (HBD) (GST-His_6-2xHSD) and combining with the previously published CUT&Tag method (Kaya-Okur *et al.*, 2019; Di *et al.*, 2020), it produced a reproducible method to map DNA:RNA hybrids at promoters as well as transient DNA:RNA hybrids within gene bodies (Wang *et al.*, 2021). The R-loop CUT&Tag was proposed to provide a highly specific method for identifying DNA:RNA hybrids, that did not require fixation, sonication, restriction digestion or the use of stable transgenic cell lines (Wang *et al.*, 2021). Since our focus is examining m^6A marked DNA:RNA hybrids, adaptions would need to be made before it could be utilized for our work, nevertheless, this is a promising step away from depending upon the S9.6 antibody.

Our gene expression analysis (Fig. 5.3 – Fig. 5.4) suggested that *HNRNPA2B1* had elevated expression that was specific to MB UW22-3 cells. Therefore, we wanted to examine whether the loss of *HNRNPA2B1* in UW228-3 cells influenced the cell morphology, gene expression and immunocytochemical presence of DNA:RNA hybrids. We found that transient knockdown of *HNRNPA2B1* caused similar lifting and rounded MB cells (Fig. 5.11 – 5.12) as previously seen with both LN18 and U251 GBM cells with HNRNPA2B1 siRNA transfections (Fig. 4.11, 4.15 – 4.16). However, with the results produced in this chapter, we were unable to determine the reason for the cell lifting of MB cells after the siRNA knockdown of HNRNPA2B1. One possibility for the lifted and rounded morphology after transfection of HNRNPA2B1 siRNA could enhance apoptosis. To explore whether apoptosis is responsible for the rounded

morphology and lifting techniques such as flow cytometry analysis of apoptotic cells by using Annexin V and propidium iodide (PI) staining could have been utilized (Vermes *et al.*, 1995; Vermes, Haanen and Reutelingsperger, 2000). Annexin V is conjugated to a FITC green-fluorescent dye that detects the translocation of phosphatidylserine to the outer plasma membrane, a key feature of apoptosis, whereas PI with red fluorescence stains for necrotic or late apoptotic cells and dead cells exhibiting both red and green fluorescence (Fried, Perez and Clarkson, 1976; Darzynkiewicz *et al.*, 1992; Vermes *et al.*, 1995; Bacsó, Everson and Eliason, 2000; Vermes, Haanen and Reutelingsperger, 2000). However, this methodology has its drawbacks with Annexin V/PI protocols vulnerable to up to 40% false positives due to PI's capability to stain RNA within the cytoplasm (Rieger *et al.*, 2010). A suggested modification to this protocol could be to treat the samples with RNase A before staining, as during this flow cytometry method the cells are fixed allowing permeation of RNase A into the cytoplasmic compartment to degrade the ssRNA (Rieger *et al.*, 2011).

The lifting and rounded morphology of MB cells after transfection of HNRNPA2B1 siRNA could be related to other pathways and processes that were not analysed in this chapter. For example, silencing of HNRNPA2B1 has been shown to suppress proliferation, migration and invasion as well as induce cell cycle arrest triggering apoptosis in cervical, oesophagal, prostate and pancreatic cancer (Stockley *et al.*, 2014; Dai *et al.*, 2017; Shi *et al.*, 2017; Guo *et al.*, 2020). Moreover, HNRNPA2B1 has also been associated with the promotion of the epithelial-to-mesenchymal transition (EMT) via the Extracellular signal-regulated kinases (ERK)/ Zinc finger protein SNAI1 (Snail) signalling pathway within pancreatic cancer as well as within head and neck cancer (Dai *et al.*, 2017; Gupta *et al.*, 2020). Therefore, further assays would need to be performed to clarify the pathway that silencing HNRNPA2B1 has an impact on. That would include a wound-healing assay to assess cell mobility, a Transwell chamber assay to observe cell invasion, 3-(4, 5-dimethylthiazolyl-2)-2, 5-diphenyltetrazolium bromide (MTT) assay to assess cell viability as well as further qPCR gene expression analysis of proliferation, migration, and EMT related genes.

Chapter 6: Main Discussion

6.1 Potential role of HNRNPA2B1 in the metabolism of R-loops.

6.1.1 The impact of HNRNPA2B1 depletion on DNA:RNA hybrids is dependent upon their genomic location.

HNRNPA2B1 is primarily known for its role in RNA metabolism, alternative splicing and as an m^6A reader (Mayeda et al., 1994; Hoek et al., 1998; Kwon, Barbarese and Carson, 1999; Fähling et al., 2006; Goodarzi et al., 2012; C. Alarcón et al., 2015; Wu et al., 2018) but our group and others have recently reported HNRNPA2B1 capable of interacting with DNA:RNA hybrids (Cristini *et al.*, 2018; Abakir *et al.*, 2020). Thus, Cristini et al., using DRIP followed by mass spectrometry, reported that RBPs such as HNRNP proteins constitute over 38% of DNA:RNA hybrid's interactome in HeLa cells, followed by DNA binding proteins (15%), mRNA processing factors (12%), miscellaneous (11%), helicases (8%) and rRNA processing factors (6%) (Cristini *et al.*, 2018). HNRNPA2B1 was then reported to interact with m^6A marked DNA:RNA hybrids during interphase (G_0/G_1/S) phase compared to YTHDF2 preferential interaction with m^6A-DNA:RNA hybrids in G_2 and mitotic cell cycle phases (Abakir *et al.*, 2020). Furthermore, using HNRNPA2B1 ChIP, our group found that HNRNPA2B1 had a high binding enrichment with m^6A marked DNA:RNA hybrids found in intronic regions compared to repetitive sequences such as *α-satellites* and *LINE1* (Abakir *et al.*, 2020). Additional HNRNPA2B1 ChIP experiments on these intronic regions showed that HNRNPA2B1 binding was impacted by the loss of *METTL3* which reflected previous publication findings (C. Alarcón et al., 2015), as well as HNRNPA2B1 binding to intronic sequences slightly increased after siRNA mediated knockdown of *RNASEH1* but at a lesser extent compared to YTHDF2 ChIP (Abakir *et al.*, 2020). Transient knockdown of *HNRNPA2B1* was observed to only have a small increase in the presence of DNA DSBs marker, γ-H2AX, compared to the knockdown of *YTHDF2* or *METTL3* (Abakir *et al.*, 2020). This initial work by our group has led to more questions about the role of HNRNPA2B1 with m^6A-marked DNA:RNA hybrids. Therefore, one

of the aims of the first chapter was to examine the effect that the loss of HNRNPA2B1 has on m^{6}A-marked DNA:RNA hybrids in human cells.

Intronic sequences were found to fluctuate in DNA:RNA hybrid enrichment levels depending on the gene of interest (Fig. 3.13) but m^{6}A marked DNA:RNA hybrid enrichment levels were both increased upon loss of HNRNPA2B1 (Fig. 3.15). Contrastingly our group has previously found elevated enrichment for DNA:RNA hybrid intronic sequences in YTHDF2 KO cells (Abakir *et al.*, 2020). This could suggest the loss of HNRNPA2B1 is more complex in terms of the many roles (Mayeda et al., 1994; Hoek et al., 1998; Kwon, Barbarese and Carson, 1999; Fähling et al., 2006; Goodarzi et al., 2012; C. Alarcón et al., 2015; Wu et al., 2018) it has as well as its specificity for intronic loci. For example, *MYH16* has elevated enrichment in both m^{6}A- (Fig. 3.15) and S9.6 DRIP (Fig. 3.13) in HAP1 cells producing a similar response to HNRNPA2B1 loss as when YTHDF2 is depleted (Abakir *et al.*, 2020). Whereas *HECW1* was found to have increased enrichment of m^{6}A on DNA:RNA hybrids paralleled by a large reduction of DNA:RNA hybrid levels in HNRNPA2B1 KO cells (Fig. 3.13; Fig. 3.15). These results would suggest that HNRNPA2B1 in the case of *HECW1* promoted the presence of m^{6}A on DNA:RNA hybrids within this intronic region. This is also observed in *WWOX-specific* loci presenting different impacts on DNA:RNA hybrids, yet we have limited information and therefore it is difficult to grasp the meaning of these differences or whether these are outliers. Another observation we made in this thesis, is that m^{6}A-marked DNA:RNA hybrids are found in a large variety of cell types but the levels of these are cell-type specific (Fig. 3.14 – 3.15; Fig. 4.7 – 4.12; Fig. 5.6 – 5.10). Thus, no enrichment in m^{6}A DRIP was detected in several intronic loci such as *RANBP17*, *MAN2B2*, *MAD1L1* and *LPA* either in WT or HNRNPA2B1 KO HAP1 cells.

Our group previously found that HNRNPA2B1 did not preferentially bind to *α-satellites* and *LINE1* sequences with m^{6}A marked DNA:RNA hybrids present (Abakir et al., 2020) and yet, contrastingly, our S9.6 and m^{6}A DRIP qPCR indicated that the loss of HNRNPA2B1 did impact the enrichment levels of DNA:RNA hybrids and m^{6}A-DNA:RNA hybrids in SINE *Alu-Y* and *Alu-S* the most dramatically with no significant effect on *α-satellites* and *LINE1* sequences (Fig. 3.12; Fig 3.14). This then bodes the question of why R-loop levels in *Alu* elements are

particularly affected by the loss of HNRNPA2B1. *Alu* sequences are the most prominent mobile elements that constitute 11% of the human genome with more than 1.1 million insertion copies (Batzer and Deininger, 2002). These sequences are approximately 300 base pairs in length and comprise of three subfamilies: *Alu-J* (oldest), *Alu-S* (intermediate) and *Alu-Y* (youngest) (Quentin, 1992; Kapitonov and Jurkal, 1996). Although abundant in the genome, *Alu* elements have the potential to become mutagenic to the host due to their roles in inhibiting translation, causing genomic instability, and acting as a splice acceptor (Elbarbary, Lucas and Maquat, 2016). *Alu* elements were found to be the main targets of RNA editing enzymes ADARs and actively suppressed the formation of *Alu* exons by HNRNPC (Kim *et al.*, 2004; Zarnack *et al.*, 2013). Furthermore, DHX9 was identified to act as a nuclear RNA resolvase which neutralises *Alu* and other SINE insertions (Aktaş *et al.*, 2017). Therefore, it is plausible that HNRNPA2B1 could interact with *Alu* elements to suppress the formation of *Alu* exons in a similar manner to HNRNPC, with targeting and binding capability has been suggested to be shared between HNRNP protein family members (Mayeda *et al.*, 1994; Liu *et al.*, 2015; Wu *et al.*, 2018). We have also identified a potential interaction between HNRNPA2B1 and DHX9 (Fig. 3.16 – 3.17), therefore one possibility could suggest HNRNPA2B1 involvement to prevent the reinsertion of *Alu* sequences after DHX9 revolves the threat of SINE elements insertion.

A recent publication has proposed that *Alu* sequences are strongly associated with enhancer-promoter interactions (EPIs) and that enhancer-associated RNAs (eRNAs) may be responsible for directly interacting with their targeted promoter to form R-loops unrelated to replication (trans-acting R-loops) at *Alu* sequences (Bai, Li and Zhang, 2021). Other studies have also associated the presence of eRNAs with R-loop formation (Pefanis *et al.*, 2015; Nojima *et al.*, 2018; Tan-Wong, Dhir and Proudfoot, 2019). Tan-Wong et al. performed chromatin associated RNA sequencing (ChrRNA-seq) on HeLa cells (Nojima *et al.*, 2015) and RNase H1 overexpressed HeLa cells (Cerritelli *et al.*, 2003) as well as RNA-specific RNase H1 ChIP sequencing (RR-ChIP seq) (L. Chen et al., 2017), instead of using the hybrid-specific antibody which is known to have low affinity for dsRNA structures as well as DNA:RNA hybrids (Hartono *et al.*, 2018). Comparing the ChrRNA-seq and RR-ChIP seq datasets produced, 26% of eRNA peaks were found to overlap with R-loop peaks with 44% of those overlapping peaks sensitive to RNase H1 overexpression (Tan-Wong, Dhir and Proudfoot, 2019). Moreover,

recent publications have observed m^{6}A to be present on eRNAs and suggest that the presence of m^{6}A on eRNAs indicates a highly active enhancer (Lee *et al.*, 2021). Lee et al., used a highly sensitive method known as methylation-inscribed nascent transcript sequencing (MINT-seq) to characterise m^{6}A presence on eRNAs as these nascent RNAs have a half-life of approximately 10 minutes the half-life of eRNAs is approximately 10 minutes (Schwalb *et al.*, 2016; Lee *et al.*, 2021). MINT-seq identified that eRNA exhibit the same canonical RRACH motif for m^{6}A as found on mRNA (Dominissini *et al.*, 2012) as well as m^{6}A modified eRNAs were longer and more stable than eRNAs without m^{6}A (Lee *et al.*, 2021). On the contrary, a preliminary examination by Bai, Le and Zhang in 2021 implies that m^{6}A was depleted on the R-loop loci of EPIs which correlates with another publication which describes m^{6}A to be negatively correlated with adenine-to-inosine editing that is commonly found in *Alu* sequences (Xiang *et al.*, 2018; Bai, Li and Zhang, 2021). Publications have also suggested that DRBPs such as members of the HNRNP protein family are inclined to bind and/or flank these EPI sites on *Alu* sequences (Bai, Li and Zhang, 2021). Tsai et al., 2018 also suggested HNRNPA2B1 to be a potential interactor with distal regulator region eRNAs within undifferentiated skeletal muscle cells but this was not the focus of the publication (Tsai *et al.*, 2018). However, several publications have identified that eRNAs are cell-type specific (Koch *et al.*, 2011; Andersson *et al.*, 2014; Tsai *et al.*, 2018; Nott *et al.*, 2019; Lee *et al.*, 2021). Consequently, if eRNAs are cell-type specific, further testing would be required to corroborate whether eRNAs are involved and responsible for the increases and decreases in enrichment observed in DNA:RNA hybrid and m^{6}A present on these structures (Fig. 3.12; Fig. 3.14) particularly in *Alu* sequences as well as what HNRNPA2B1 contribution in this process is, if at all.

In repetitive elements such as *α-satellites*, *LINE1*, *Alu-Y* and *Alu-S*, the presence of m^{6}A-on DNA:RNA hybrids decreased upon the depletion of HNRNPA2B1 (Fig. 3.14) whereas DNA:RNA hybrid levels were found to be enriched in these repetitive sequences (Fig. 3.12). The DRIP followed by qPCR results would suggest that increased levels of DNA:RNA hybrids without the m^{6}A modification present and therefore genomic instability within those cells. However, when we look globally at the presence of m^{6}A marked DNA:RNA hybrids by SID-UPLC-MS/MS (Fig. 3.11), DNA:RNA hybrids and a DNA DSBs marker (γ-H2AX) by

immunostaining (Fig. 3.9 – 3.10), it reflected that although m^{6}A marked DNA:RNA hybrids were lower, this did not lead to increased DNA:RNA hybrids or increased γ-H2AX immunostaining in HNRNPA2B1 KO cells. Therefore, this could indicate that HNRNPA2B1 loss could be counteracted to not disrupt the R-loop equilibrium on which genomic stability depends. Balancing the levels of R-loops is crucial for cells since it can have both positive and negative repercussions on CSR, telomere dynamics, DNA repair, DNA damage and genomic stability (Yu *et al.*, 2003; Li and Manley, 2005; Ginno *et al.*, 2012; Balk *et al.*, 2013; Hamperl *et al.*, 2017; Yasuhara *et al.*, 2018). In 2018, Cristini et al., studied the DNA helicase, DHX9, involvement in R-loop metabolism and proposed that the cell is constantly trying to maintain a condition of equilibrium with R-loop levels (Cristini *et al.*, 2018). Disruption of DHX9 and other R-loop interacting proteins can lead to transcription termination defects, R-loop accumulation, and R-loop dependent genomic instability (Cristini *et al.*, 2018). Therefore, it is plausible that other protein/s could act to prevent the accumulation of R-loop and possible genomic instability. However, the extent and manner in which these proteins act still need examination.

6.1.2 HNRNPA2B1 depends on YTHDF2 in its binding to m^{6}A-marked DNA:RNA hybrids.

Our next aim was to test if there is a functional interplay in the regulation of dynamics of DNA:RNA hybrids between HNRNPA2B1 and another m^{6}A reader, YTHDF2. YTHDF2 has been previously implicated in the regulation of both m^{6}A marked DNA:RNA hybrids and genomic stability (X. Wang et al., 2014; Du et al., 2016; Abakir et al., 2020). Moreover, during the cell cycle, YTHDF2 was found to interact with m^{6}A DNA:RNA hybrids within mitotic chromatin during G_2/M phases whereas in other cell cycle phases remained predominantly cytoplasmic (Abakir *et al.*, 2020), whereas HNRNPA2B1 as nucleus-based protein was assumed to interact with m^{6}A marked DNA:RNA hybrids during G_0/G_1 and S phases of the cell cycle known as interphase (Abakir *et al.*, 2020). Moreover, according to unpublished data of our collaborators, HNRNPA2B1 was identified as one of the proteins interacting with YTHDF2 (Miaomiao Lee, Oslo University, private communication).

Although YTHDF2 is primarily located within the cytoplasm, the depletion of HNRNPA2B1 increased the presence of YTHDF2 within the nucleus regardless of whether the HAP1 cells were in the mitosis or interphase cell cycle stage (Fig. 3.19). This was corroborated by YTHDF2 ChIP qPCR, as YTHDF2 binding increased to m^{6}A marked DNA:RNA hybrid-prone loci in both repetitive and intronic sequences in HNRNPA2B1 depleted cells (Fig. 3.21). However, this was not reciprocated in YTHDF2 depleted cells as immunostaining displayed that HNRNPA2B1 did not change its localisation but decreased its nuclear presence upon YTHDF2 depletion (Fig. 3.20). The immunostaining was strengthened by HNRNPA2B1 ChIP, where HNRNPA2B1 binding to m^{6}A marked DNA:RNA hybrids were reduced in both repetitive and intronic sequences in YTHDF2 depleted cells (Fig. 3.22). These results suggested that HNRNPA2B1 depends on YTHDF2 to interact with m^{6}A-DNA:RNA hybrids. There is currently no other literature that describes this novel interaction between YTHDF2 and HNRNPA2B1, yet preliminary transcriptome profiles of m^{6}A methylation regulators in prostate adenocarcinoma suggested a close protein network between HNRNPA2B1 and most of the other m^{6}A regulators (J. Xu *et al.*, 2020) which agrees with our observations made using the STRING database (Fig. 3.16). Yet, we can explore the possible mechanisms in which this interplay between HNRNPA2B1 and YTHDF2 may function.

Our immunostaining, m^{6}A-, S9.6-DRIP qPCR and ChIP qPCR of HAP1 WT, HNRNPA2B1 KO and YTHDF2 KO cells could suggest a role for HNRNPA2B1 in preventing the reannealing of RNA transcripts to the template after R-loop resolution by YTHDF2 and DHX9/DDX3X (Fig. 6.1). In WT cells, YTHDF2 binds to m^{6}A on DNA:RNA hybrids as shown previously (Abakir *et al.*, 2020) and could introduce HNRNPA2B1 and possibly DNA:RNA hybrid helicases DHX9/DDX3X to these structures. After resolution of the R-loop either by YTHDF2 or by DNA:RNA hybrid helicases DHX9/DDX3X, HNRNPA2B1 could bind to the RNA transcript to prevent reannealing to the template as well as the potential to carry other functions such as mRNA processing (Hoek et al., 1998; Fähling et al., 2006; Listerman, Sapra and Neugebauer, 2006; C. Alarcón et al., 2015). In HNRNPA2B1 KO cells, loss of HNRNPA2B1 presence could hinder DHX9/DDX3X capability to detect these DNA:RNA hybrids. Our ChIP results suggested enriched YTHDF2 binding to these structures, and hence would be able to resolve R-loops at these specific loci, with the RNA either degraded or possibly re-annealed to the DNA template

without HNRNPA2B1 presence. Finally, in the YTHDF2 KO cells, the loss of YTHDF2 disrupts HNRNPA2B1 ability to interact with m^6A on DNA:RNA hybrids and therefore could impede DHX9/DDX3X unwinding of these R-loops. This lack of either DHX9 or YTHDF2 neutralising and resolving the R-loops could lead to the accumulation of R-loops, transcript-replication conflicts and genetic instability, which has been previously demonstrated by our group (Abakir *et al.*, 2020). However, to further confirm or refute this model, additional experiments are needed.

6.1.3 Is the DNA:RNA hybrid presence in WWOX linked to alternative splicing or common fragile sites?

HNRNPA2B1 has been implicated in AS before being described as an m^6A reader (Mayeda and Krainer, 1992; Bilodeau et al., 2001; Zhu, Mayeda and Krainer, 2001; C. Alarcón et al., 2015). HNRNPA2B1 promotes exon exclusion by binding to the ESS or ISS on RNA strands to inhibit 5' or 3' splice site recognition, inhibit proximal splicing sites, disrupt the effects of SR proteins and promote distal 5' splice site selection (Mayeda and Krainer, 1992; Caceres *et al.*, 1994; Mayeda *et al.*, 1994; Caputi *et al.*, 1999; Zhu, Mayeda and Krainer, 2001; Olsen *et al.*, 2014; Bruun *et al.*, 2016). Previous studies have found that HNRNPA2B1 is involved in the alternative splicing of *SMN*, *PKM*, *RON* and *WWOX* (Hua *et al.*, 2008; Clower *et al.*, 2010; David *et al.*, 2010; Golan-Gerstl *et al.*, 2011; Singh and Singh, 2011; Singh *et al.*, 2011). WWOX has a key role in maintaining the integrity of the genome and resides within the CFS known as *FRA16D* (Ried et al., 2000; Abu-Odeh, Salah, et al., 2014; Aqeilan, Abu-Remaileh and Abu-Odeh, 2014). As a splicing target of HNRNPA2B1, *WWOX* AS isoforms normally result in the exclusions of exons 7-8, exons 6-8 or exons 5-8 (Driouch *et al.*, 2002; Kuroki *et al.*, 2002; Golan-Gerstl *et al.*, 2011). R-loops have also been associated with AS with SRSF1 found to interconnect pre-mRNA processing and genomic instability in chicken and HeLa cells (Li and Manley, 2005). Other splicing factors and RBPs have also been linked to DNA:RNA hybrids to prevent genomic instability but the mechanisms in which it occurs are yet to be fully identified (Moreira *et al.*, 2004). We aimed to explore whether DNA:RNA hybrids or m^6A marked DNA:RNA hybrids are present in the HNRNPA2B1 splicing target and then understand whether the binding changed upon depletion of HNRNPA2B1 or YTHDF2.

We identified m^{6}A marked DNA:RNA hybrids peaks within introns 4, 5 and 8 of *WWOX* by looking at previous next-generation sequencing performed on hiPSCs (Fig. 3.23). Yet, when we wanted to quantify these levels in HAP1 cells, m^{6}A marked DNA:RNA hybrid presence was only observed at low levels in intron 5 of *WWOX* (Fig. 3.26), whereas DNA:RNA hybrids presence was found in introns 4, 5 and 8 (Fig. 3.25). These results would suggest that the presence of m^{6}A on DNA:RNA hybrids could be cell type-specific since the peaks identified within hiPSCs were not possible to quantify such as the m^{6}A DNA:RNA hybrids that residing in the intronic regions of *RANBP17*, *MAN2B2*, *MAD1L1* and *LPA* (Abakir *et al.*, 2020). The presence of m^{6}A has been reported to vary amongst different cell lines (stem cells, somatic and cancer cell lines) (Batista *et al.*, 2014; An *et al.*, 2020; Jiang *et al.*, 2021; Shen *et al.*, 2021). One publication has suggested that m^{6}A flanking stop codons were the most consistent among multiple cell lines and could be considered 'structural m^{6}A sites' (An *et al.*, 2020). These m^{6}A sites could therefore be important for basic cellular functions as well as the biogenesis of mRNAs (Wen *et al.*, 2018; Yue *et al.*, 2018; An *et al.*, 2020). Whereas m^{6}A found within coding regions were found to exhibit cell-specificities which are considered as 'dynamic m^{6}A sites' (An *et al.*, 2020). These m^{6}A sites are dynamically regulated by several m^{6}A writers, readers and erasers that exhibit spatial and temporal specificities that then play diverse roles in different cell types (Barbieri *et al.*, 2017; An *et al.*, 2020).

Like previous YTHDF2 and HNRNPA2B1 ChIP experiments in specific intronic loci (Fig. 3.21 B; Fig. 3.22 B), we wanted to quantify whether HNRNPA2B1 or YTHDF2 binding was changed upon loss of the other, but in the context of DNA:RNA hybrid regions in *WWOX* introns (Fig. 3.27 – 3.28). Enriched YTHDF2 binding to *WWOX* intron 4 and 8 after depletion of HNRNPA2B1 (Fig 3.27 A; Fig. 3.27 C), was found to be consistent with our previous ChIP results (Fig. 3.21 B). Intriguingly, YTHDF2 was bound to the DNA:RNA hybrid in intron 5 after the removal of HNRNPA2B1 whereas in WT, YTHDF2 binding had a lower enrichment than the WT IgG control suggested no binding before HNRNPA2B1 removal (Fig. 3.27 B). The loss of YTHDF2 affected the binding of HNRNPA2B1 to *WWOX* intron 4 and 8 (Fig. 3.28 A; Fig. 3.28 C), which appears consistent with YTHDF2 enriched binding to repetitive and intronic specific loci after depletion of HNRNPA2B1 (Fig. 3.22 B). In contrast to the other DNA:RNA hybrids within the introns of WWOX, intron 5 displayed comparatively low HNRNPA2B1

binding in WT cells but HNRNPA2B1 binding was unexpectedly increased upon the loss of YTHDF2 (Fig. 3.28), contrasting with our previous ChIP qPCR results (Fig. 3.22 B). Yet, without evaluating the levels of DNA:RNA hybrids in *WWOX* intron 5 in YTHDF2 KO cells, we cannot establish the impact on R-loops levels in this region. The question is now, why is the binding dynamic of HNRNPA2B1 and YTHDF2 different within intron 5 of *WWOX*? Time constraints prevent us from exploring further, yet studies could illuminate two possibilities: AS-related or CFS-related.

Our initial hypothesis was that the HNRNPA2B1 binding to different *WWOX* intronic sequences may depend on the presence of DNA:RNA hybrids in these loci affecting the repertoire of splicing isoforms produced of *WWOX*. R-loops have been reported to be involved in AS with SR proteins particularly (Aguilera, 2005; Li and Manley, 2005; Li, Niu and Manley, 2007; Chakraborty, Huang and Hiom, 2018). Looking at the positioning of the DNA:RNA hybrids present in the introns of *WWOX* (Fig. 3.24), there appear to be 3 main alternative splicing isoforms that have been found to occur in oesophagal squamous cell carcinoma, GBM and breast cancer (Driouch *et al.*, 2002; Kuroki *et al.*, 2002; Golan-Gerstl *et al.*, 2011). HNRNPA2B1 has been previously demonstrated to promote exon exclusion in AS (Mayeda and Krainer, 1992; Caceres *et al.*, 1994; Mayeda *et al.*, 1994; Caputi *et al.*, 1999; Zhu, Mayeda and Krainer, 2001; Olsen *et al.*, 2014; Bruun *et al.*, 2016), therefore increased binding within intron 5 would suggest the exclusion of exon 5 in *WWOX* transcripts. Yet, if this was the case, intron 8 would also display a similar HNRNPA2B1 binding pattern. Contrastively, the HNRNPA2B1 binding pattern observed at intron 8 is identical to intron 4 which is included in all *WWOX* isoforms described (Fig. 3.24). Considering this, RNA and ChIP sequencing over WWOX splice isoforms as well as other candidates is needed to fully accept or reject this hypothesis.

An alternate hypothesis concerns *WWOX* positioning in the CFS *FRA16D* (Ried *et al.*, 2000; Abu-Odeh, Salah, *et al.*, 2014; Aqeilan, Abu-Remaileh and Abu-Odeh, 2014). In the human genome, there are around 90 CFSs with *FRA3B* (3p14.2) and *FRA16D* (16q23) being the most susceptible to breakage (Durkin and Glover, 2007). CFSs are known to present cell-type specific expression with chromosomal breakages in *FRA16D* expressed at various

frequencies in fibroblasts, epithelial and erythroid cell lines (Letessier *et al.*, 2011; Hosseini *et al.*, 2013; Le Tallec *et al.*, 2013). Within the core regions of CFSs replication initiation events rarely occur, this, therefore, forces the replicant forks (RFs) to advance from flanking regions to cover long distances (Letessier *et al.*, 2011). Intron 8 of *WWOX* is the fifth largest intron in the human genome spanning 778,856 base pairs (Bednarek *et al.*, 2000; Ried *et al.*, 2000), therefore the transcription of these long CFS-associated genes such as *WWOX* usually traverses a complete round of the cell cycle or in some cases into the following G_1/early S phases (Helmrich, Ballarino and Tora, 2011). These longer genes normally are replicated at the end of the cell cycle leading to the potential colliding of the transcription machinery and RF in S phases inducing the formation of DNA:RNA hybrids (Helmrich, Ballarino and Tora, 2011). This impeding of the progression of the RF form and/or exposure of non-template DNA to cleavage or recombination makes long genes such as *WWOX* vulnerable to R-loops and hotspots for chromosomal fragility (Helmrich, Ballarino and Tora, 2011). Hussain and their colleagues used an R-loop prediction tool and database, described by (Jenjaroenpun *et al.*, 2017), and found R-loop forming sequences (RLFPs) along the entire *WWOX* but particularly intensive presence within intron 5 and intron 8, known areas of high fragility (Hussain *et al.*, 2019). They found that the 5' edge of *FRA16D* extends to intron 5 of *WWOX* whereas intron 8 is the core of *FRA16D* (Hussain *et al.*, 2018). Moreover, the clustering of breakpoints that extend from intron 5 to intron 6 was found to overlap with the 5' end of *FRA16D* (Hussain *et al.*, 2019). Collectively, these publications would suggest that the accumulation of DNA:RNA hybrids could promote genomic instability in intron 5 and 8 of WWOX/FRA16D. Concerning our results, we identified that the loss of HNRNPA2B1 within intron 5 of WWOX increased the binding of YTHDF2 to a region where WT did not preferentially bind to that specific region. This could suggest that the loss of HNRNPA2B1 did promote the accumulation of DNA:RNA hybrids within intron 5 but was rescued by YTHDF2 binding and promoting decay of this area. The loss of YTHDF2 is already known to cause a large accumulation of DNA:RNA hybrids (Abakir *et al.*, 2020). Consequently, the removal of YTHDF2 at the edge of this fragile site could lead to HNRNPA2B1 recruiting deadenylases, helicases and other proteins to reduce the presence of DNA:RNA hybrids within intron 5 of WWOX. However, at this point, we can only make a conjecture about the mechanism and the reasoning for the elevations and

reductions in HNRNPA2B1 binding and the varying levels for DNA:RNA hybrids. Overall, this research is in the initial stages and further examination is needed to clarify which hypothesis is true.

6.2 Presence of m^{6}A marked DNA:RNA hybrids are markedly lower in brain tumours compared to hiPSCs, yet gene expression of m^{6}A related genes were elevated in brain tumours.

In GBM, the presence of m^{6}A and expression of m^{6}A-related genes are strongly associated with their proposed involvement in GBM progression, tumorigenesis, as well as GSCs, enhanced growth and sphere formation (Cui et al., 2017; Zhang et al., 2017; C. Xu et al., 2020; W. Wang et al., 2020; Dixit et al., 2021). Yet within MB, only a few studies have mentioned m^{6}A readers such as HNRNPA2B1 but not in the context of m^{6}A (Azizi *et al.*, 2012; Staal *et al.*, 2015). Although m^{6}A marked DNA:RNA hybrids are yet to be investigated in relation to brain tumours, DNA:RNA hybrids are known to accumulate in neurological pathologies such as Friedreich's ataxia, fragile X syndrome, ALS/frontotemporal dementia (Grabczyk, Mancuso and Sammarco, 2007; Colak *et al.*, 2014; Groh and Gromak, 2014; Haeusler *et al.*, 2014; Loomis *et al.*, 2014) and carcinomas such as breast cancer, ovarian cancer, eosinophilic leukaemia and mixed lineage leukaemia (Stirling *et al.*, 2012; Hamperl *et al.*, 2017; Gorthi *et al.*, 2018; Shivji *et al.*, 2018). Therefore, our next aim was to assess the presence of m^{6}A-related genes and m^{6}A-marked DNA:RNA hybrids in adult and paediatric brain tumour cell lines.

We examined the gene expression of m^{6}A-related genes in 4 GBM cell lines (LN18, LN229, U251 and U87MG), an MB cell line (UW228-3), a foetal brain cell line (FB83) and a human astrocyte cell line (SVGA) (Fig. 5.4). *HNRNPA2B1* gene expression levels were consistent between the GBM cell lines and FB83 (Fig. 4.3 F; Fig. 5.4) but were dramatically increased in MB compared to GBM and FB83 (Fig. 5.3 B; Fig. 5.4). *HNRNPA2B1* has been previously reported to have elevated mRNA levels in the MB cell line D245Med as well as upregulated

mRNA transcripts and protein levels in primary Group 3 MB cells, which would corroborate our gene expression findings and suggest that this elevated expression is common in other MB cell lines (Azizi *et al.*, 2012; Staal *et al.*, 2015). *METTL3* appeared to have a comparable gene expression level between LN18, LN229, U87MG, UW228-3 and FB83 (Fig. 4.3 A; Fig. 5.3 A; Fig. 5.4). *YTHDF2* transcripts were present in all GBM, MB and FB83 cell lines but levels appeared dependent upon the cell line (Fig. 4.3 E; Fig. 5.3 B; Fig. 5.4). As mentioned previously, m^6A methylome has been established to be cell type specific (Batista *et al.*, 2014; An *et al.*, 2020; Jiang *et al.*, 2021; Shen *et al.*, 2021). To elaborate on this, m^6A RNA immunoprecipitation sequencing (m^6A RIP-seq) identified that m^6A epitranscriptome signals were highly specific to brain tissues compared to non-brain tissues in humans and mice (J. Liu *et al.*, 2020). When comparing the m^6A methylome of 43 human tissues and 16 mouse tissues, the authors of this study identified that the m^6A signal was highly conserved in brain tissues (J. Liu *et al.*, 2020). Furthermore, the presence of m^6A has been attributed to neural development (Meyer *et al.*, 2012; Chang *et al.*, 2017; Yoon *et al.*, 2017; Livneh *et al.*, 2020), adult brain development (Chang *et al.*, 2017; Merkurjev *et al.*, 2018), neurogenesis (Yoon et al., 2017; Y. Wang et al., 2018), oligodendrocytes (R. Wu et al., 2019; H. Xu et al., 2020), neurological disorders (Choudhry *et al.*, 2013; Du *et al.*, 2015; Han *et al.*, 2020) as well as brain tumours (Golan-Gerstl *et al.*, 2011; Deng *et al.*, 2016; Cui *et al.*, 2017; Zhang *et al.*, 2017; Visvanathan *et al.*, 2018).

The presence of m^6A marked DNA:RNA hybrids in GBM and MB were both comparably lower than hiPSCs (Fig. 4.7 – 4.12; Fig. 5.6 – Fig. 5.10). Yet in comparison to the m^6A DNA:RNA hybrid levels observed in HAP1 (Fig. 3.11), GBM and MB were relatively higher than these semi-haploid human cells. This could suggest that hiPSCs have the highest m^6A marked DNA:RNA hybrids levels due to the high division rate of hiPSCs allowing more cells to be within the S and G_2/M phases of the cell cycles where modified DNA:RNA hybrids are known to accumulate (Abakir *et al.*, 2020). However, HAP1 WT cells have been observed to have a high proliferation rate (Abakir *et al.*, 2020) therefore this would not explain why HAP1 has lower levels of m^6A marked DNA:RNA hybrids compared to hiPSCs. An alternative suggestion could relate again to the influence of m^6A on pluripotency potential (Batista *et al.*, 2014; Cui *et al.*, 2017). This would explain why hiPSCs have a high presence of m^6A marked DNA:RNA

hybrids, whereas GBM and MB have a moderate presence with the somatic HAP1 cell line presenting the lowest levels of m^6A marked DNA:RNA hybrids.

6.3 Depletion of HNRNPA2B1 resulted in increased levels of DNA:RNA hybrids and m^6A in brain tumours.

Reduced HNRNPA2B1 expression has been reported to promote apoptosis, EMT and reduced proliferation in GBM and other tumours (Golan-Gerstl *et al.*, 2011; Stockley *et al.*, 2014; Deng *et al.*, 2016; Dai *et al.*, 2017; Shi *et al.*, 2018; Guo *et al.*, 2020; Gupta *et al.*, 2020). Therefore, we wanted to examine if the loss of *HNRNPA2B1* led to similar results in our brain tumour cell lines and if the presence of DNA:RNA hybrids and m^6A associated with them were affected by the siRNA-mediated knockdown of this protein.

Loss of *HNRNPA2B1* in LN18 and UW228-3 cells caused an increase in DNA:RNA hybrid levels (Fig. 4.23; Fig. 5.14). Contrastingly, the transcript levels of *DHX9* and *DDX3X* also increased in LN18 and UW228-3 cells compared to hiPSCs (Fig. 4.22; Fig. 5.13). Whether the loss of *HNRNPA2B1* affects the levels of DNA:RNA hybrids directly or indirectly is still yet to be elucidated. The correlation of *HNRNPA2B1* loss to DNA:RNA hybrids could just be correlating two events rather than the causation of the event. However, previously mentioned work does suggest that *HNRNPA2B1* loss could reduce the recruitment of deadenylases and decay proteins to specific loci (Collart, 2016; Du *et al.*, 2016; Geissler *et al.*, 2016). In breast cancer cells, it was identified that the loss of the tumour suppressors and DNA DSB repair factors *BRCA1* or *BRCA2* would trigger the accumulation of DNA:RNA hybrids (Bhatia *et al.*, 2014; Hill *et al.*, 2014; Savage *et al.*, 2014; Hatchi *et al.*, 2015; Gorthi *et al.*, 2018; Shivji *et al.*, 2018). Yet further experiments are needed to fully understand what is occurring in GBM and MB cells and whether these brain tumours behave similarly to HAP1 cells, where our observations proposed HNRNPA2B1 involvement in the resolution of R-loops depending on YTHDF2.

In both GBM and MB, the loss of HNRNPA2B1 caused cell lifting from the growth surface that was partially recovered by the use of an attachment factor (Fig. 4.19; Fig. 5.12). However, the

cause of the cell lifting after *HNRNPA2B1* siRNA treatment was not yet determined. A plausible reason for the cell lifting after the loss of HNRNPA2B1 could be the initiation of apoptosis. Publications previously have attributed HNRNPA2B1 depletion to apoptosis in GBM cells (Deng *et al.*, 2016) but also in cervical cancer (Shi *et al.*, 2018). In cervical cancer, HNRNPA2B1 was reported to be inhibited by lobaplatin resulting in the induction of apoptosis and cell cycle arrest (Li *et al.*, 2014). Moreover, knockdown of HNRNPA2B1 in cervical cancer cells increased the number of cells within the G_1 phase of the cell cycle, inducing G_1/S phase arrest as well as promoting apoptosis (Shi *et al.*, 2018). The depletion of HNRNPA2B1 has also been observed to inhibit proliferation and colony formation in cervical cancer (Shi *et al.*, 2018), GBM (Golan-Gerstl *et al.*, 2011; Deng *et al.*, 2016), prostate cancer (Stockley *et al.*, 2014) and oesophageal squamous cell carcinoma (OSCC) (Guo *et al.*, 2020), all examined by siRNA mediated knockdown of HNRNPA2B1. In cervical cancer and OSCC, transient knockdown of HNRNPA2B1 was found to significantly reduce the migration ability and invasion capability of these cancer cells tested by wound healing assay and Transwell chamber assay (Shi *et al.*, 2018; Guo *et al.*, 2020). On the other hand, a reduction of HNRNPA2B1 has also been accredited to promote EMT within pancreatic cancer and head and neck cancer (HNC) (Dai *et al.*, 2017; Gupta *et al.*, 2020). In HNC, using CRISPR-cas9 HNRNPA2B1 knockout cells and HNRNPA2B1 overexpression HNC cells, they suggested that HNRNPA2B1 mediates AS via exclusion of exon 11 from MST1R which encodes a RON isoform, RONΔ165 (Gupta *et al.*, 2020). The RONΔ165 isoform then activates the Akt/PKB signalling pathway which, in turn, induces EMT in HNC cells (Gupta *et al.*, 2020). Yet in pancreatic cancer, HNRNPA2B1 expression was associated with the mesenchymal phenotype, with depletion of HNRNPA2B1 leading to the reduction of invasion by elevated E-cadherin levels and overexpression of HNRNPA2B1 promoting invasion by high levels of N-cadherin/vimentin and low levels of E-cadherin (Dai *et al.*, 2017). When we compared these publications to our findings, if HNRNPA2B1 loss reduces invasion and increases levels of E-cadherin, an epithelial cell-cell adhesion marker, we should have observed no change in the attachment level due to the siRNA-mediated knockdown (Fig. 4.19; Fig. 5.12). Levels of HNRNPA2B1 and other m^6A interactors have been previously noted to vary depending upon the disease or tumour type (Jiang *et al.*, 2021; Shen *et al.*, 2021) so examining all the

possibilities is key to build a complete picture of HNRNPA2B1 role in GBM and MB. Therefore, from the results we have, the loss of HNRNPA2B1 in GBM and MB is likely to promote apoptosis.

6.4 Could HNRNPA2B1 be a potential targeted cancer therapy for brain tumours?

One of the main aims of this thesis was to comprehend whether HNRNPA2B1 could be considered as an oncogene or as a potential therapy in brain tumours. Our results have yet to indicate the exact impact that the loss of HNRNPA2B1 has on GBM and MB cells, but in our results, we have observed a lifting of the cells away from the cell surface (Fig 4.14; Fig 4.18 – 4.19; Fig 5.11 – 5.12) that could be related to either apoptosis, proliferation or EMT. Previous publications have considered HNRNPA2B1 as a target for cancers such as BC and GBM. In BC, HNRNPA2B1 was considered a negative regulator of BC and was found to inhibit EMT and metastasis (Y. Liu *et al.*, 2020). In GBM, HNRNPA2B1's loss was suggested to have a role in tumour cell invasion (Deng *et al.*, 2016).

However, HNRNPA2B1 is a member of the HNRNP A/B protein family with a 70% homology with HNRNPA1 (Mayeda *et al.*, 1994). Furthermore, HNRNPA1 and HNRNPA2B1 have been suggested to have similar functions in relation to splicing as well as capable of binding to the same motif (Mayeda *et al.*, 1994; Caputi *et al.*, 1999; Bilodeau *et al.*, 2001; Zhu, Mayeda and Krainer, 2001; Hutchison *et al.*, 2002; Wu *et al.*, 2018). It has also been suggested that HNRNPA1 and HNRNPA2 compensate for the loss of expression at both the RNA and protein levels (Chang, Lu and Qiu, 2021). In terms of HNRNPA2B1 as a possible target for brain tumours, if HNRNPA1 can compensate for the expression of loss of HNRNPA2B1, targeting HNRNPA2B1 may be more challenging. One possibility could be to not inhibit HNRNPA2B1 as a monotherapy but target both HNRNPA1 and HNRNPA2B1 due to the shared functions and targeting motifs. However, more research is needed to further investigate these questions and HNRNPA2B1's potential as a brain tumour-targeted therapy.

6.5 Concluding remarks and future work

In conclusion, the data generated in this thesis by the implementation of immunostaining, confocal microscopy, SID-UPLC-MS/MS and m^6A DRIP followed by qPCR showed that HNRNPA2B1 is dependent on YTHDF2 to interact with m^6A marked DNA:RNA hybrids in loci specific sequences. While in adult and paediatric brain tumours, m^6A marked DNA:RNA hybrids were found at moderate levels in both GBM and MB. High *HNRNPA2B1* transcript levels were observed in MB with depletion of *HNRNPA2B1* resulting in cell lifting in both adult and paediatric brain tumours.

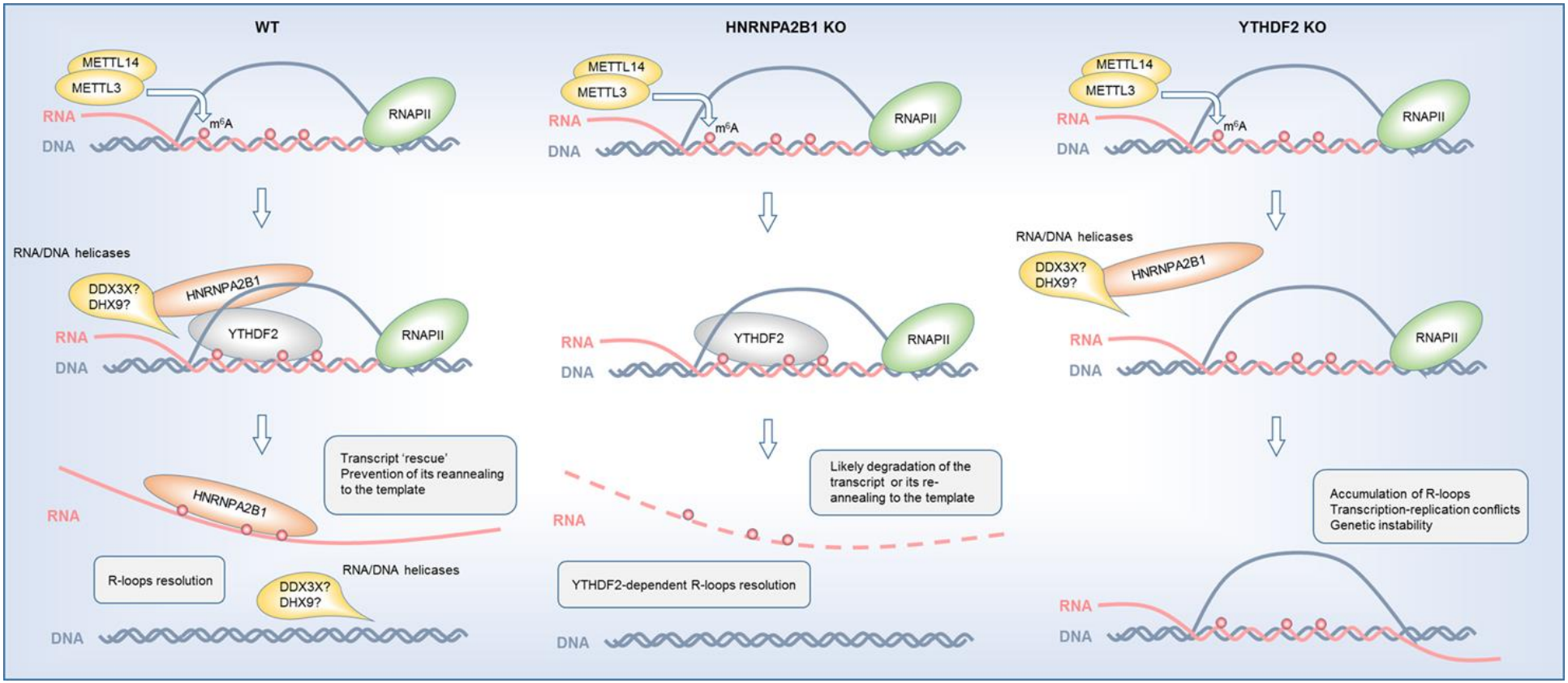


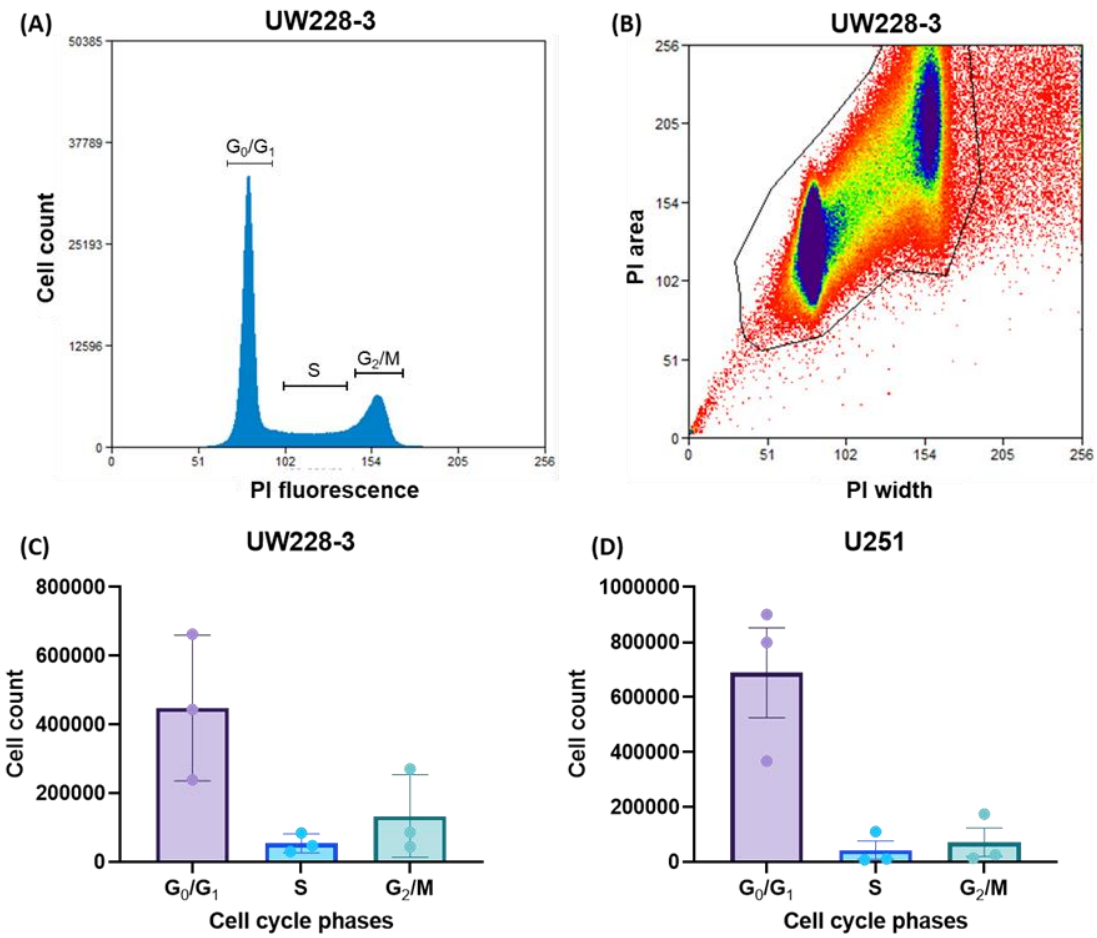
Figure 6.1: Proposed model of YTHDF2 and HNRNPA2B1 interplay in regulation of DNA:RNA hybrid dynamics in WT, HNRNPA2B1 KO and YTHDF2 KO HAP1 cells.

Nevertheless, to complete this work and consolidate our hypothesis, several experiments need to be conducted. For our work looking at m^{6}A marked DNA:RNA hybrids in HAP1 WT and HNRNPA2B1 KO cells, it was evident that next-generation sequencing of these cells was required due to the fluctuations observed in m^{6}A marked DNA:RNA hybrid between cell types, tumours, or diseases, comparable to m^{6}A variable levels (Jiang *et al.*, 2021; Shen *et al.*, 2021). Therefore, m^{6}A DRIP and S9.6 DRIP would be required in both HAP1 WT and HNRNPA2B1 KO to evaluate any different m^{6}A marked DNA:RNA hybrid locations, particularly in intronic sequences. Due to the preliminary work to examine HNRNPA2B1 and YTHDF2 binding, this could be expanded by carrying out HNRNPA2B1 ChIP sequencing on HAP1 WT and YTHDF2 KO cells and YTHDF2 ChIP sequencing on HAP1 WT and HNRNPA2B1 KO cells. To answer whether m^{6}A marked DNA:RNA hybrid overlap with AS sites, high-depth RNA next-generation sequencing of HAP1 WT and HNRNPA2B1 KO cells would provide information on whether particular isoforms are preferentially selected as well as compare to m^{6}A DRIP sequencing to provide insight to whether m^{6}A marked DNA:RNA hybrid are associated.

Although our GBM gene expression dataset presented a similar pattern of m^{6}A interactor expression, the use of primary GBM cell lines provides a closer representation of the epitranscriptome of GBM patients (Lee et al., 2006; Hughes et al., 2007; Robertson et al., 2019). Immunostaining, SID-UPLC-MS/MS and m^{6}A DRIP qPCR of these primary GBM cells would allow us to compare our cell lines results to examine whether the levels of m^{6}A marked DNA:RNA hybrids have a lower presence similar to m^{6}A interactors. Again, since the levels of m^{6}A and m^{6}A marked DNA:RNA hybrids have been observed to vary between tumours (Jiang *et al.*, 2021; Shen *et al.*, 2021), m^{6}A DRIP next-generation sequencing on LN18 and UW228-3 could provide an understanding into any different m^{6}A marked DNA:RNA hybrid locations particularly within intronic sequences of apoptotic, proliferation, invasion, migration, or GBM/MB subgroup related genes. Within our gene expression analysis of MB, we only observed our results in one MB cell line, UW228-3. Future work would need to evaluate cell lines or primary MB cells from more subgroups, to perform gene expression analysis of the m^{6}A interactors as well as SID-UPLC-MS/MS to evaluate if m^{6}A marked DNA:RNA hybrids levels are a marker of a particular subgroup.

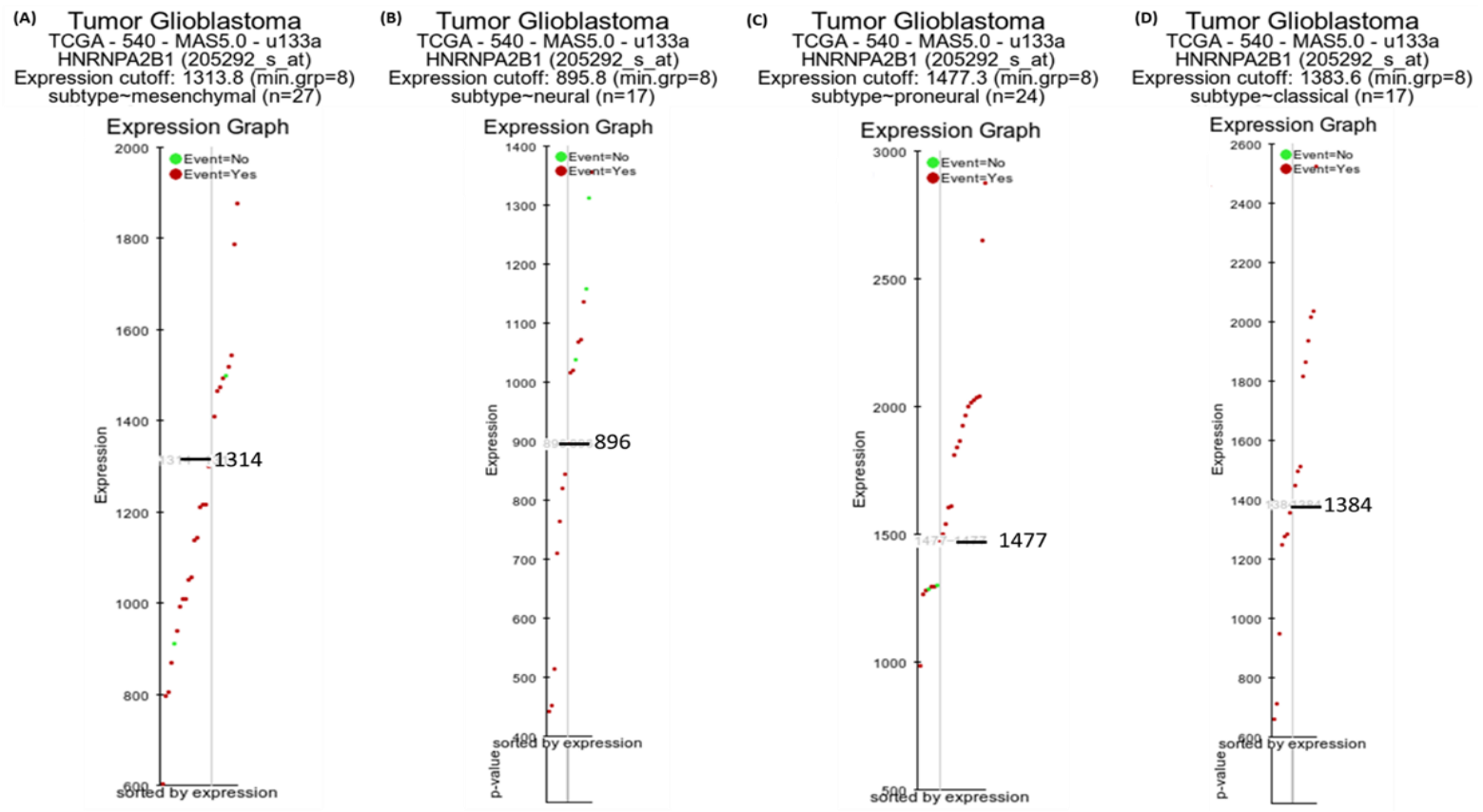
To further evaluate HNRNPA2B1 function in GBM and MB, *HNRNPA2B1* overexpression via PiggyBac transposon transfection can be employed to determine if high levels of HNRNPA2B1 reduces the levels of m^6A marked DNA:RNA hybrids as well as if we can reverse the effects HNRNPA2B1 loss has on GBM and MB cells. Finally, more experiments are required to fully comprehend the effect of the HNRNPA2B1 knockdown on GBM and MB. To determine whether HNRNPA2B1 knockdown initiates apoptosis, we would perform apoptotic cell analysis by collecting both the supernatant and cell pellet for flow cytometry analysis using Annexin V and PI staining would be important to corroborate our apoptotic marker gene expression in siRNA knockdown compared to a siRNA control. For analysis of HNRNPA2B1 knockdown on proliferation, cell counting kit 8 (CCK8) assay and EdU assay may be employed to detect and quantify cell proliferation. To examine the impact of HNRNPA2B1 knockdown on invasion and migration in GBM and MB, wound healing and transwell invasion assays would need to be performed. And lastly, to determine whether HNRNPA2B1 knockdown in GBM and MB impacts EMT, gene expression analysis of E-cadherin (*CDH1*), N-cadherin (*CDH2*), Vimentin (*VIM*), Snail1/2 (*SNAI1*/*SNAI2*) and Twist family BHLH transcription factor 1 (*TWIST1)*.

Appendix – Supplementary figures



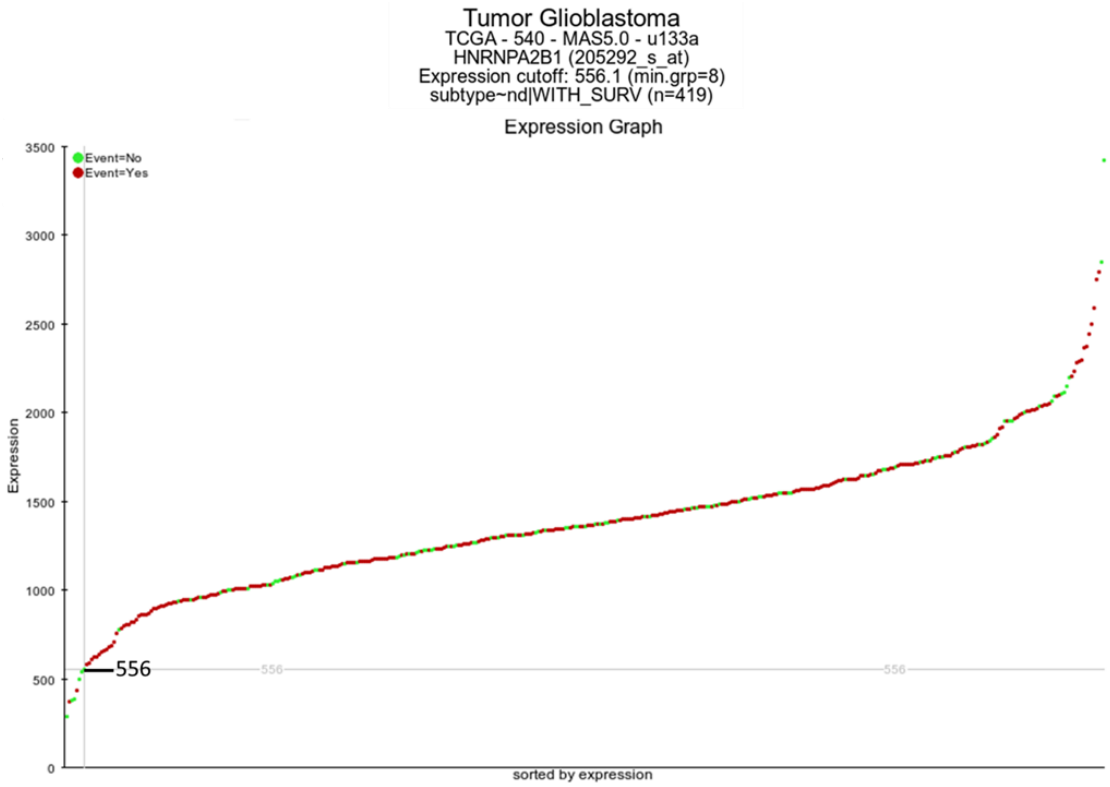
Supplementary figure 1: U251 and UW228-3 have similar cell population counts in the cell cycle phases.

(A) *DNA content frequency histogram of a representative UW228-3 cell population used for cell cycle analysis.* ***(B)*** *Gating of single UW228-3 sample using PI-area and PI-width signals. Average cell count for* ***(C)*** *UW228-3 and* ***(D)*** *U251 cells in G_0/G_1, S and G_2/M cell cycle phases. Collated data from 3 technical replicates.*



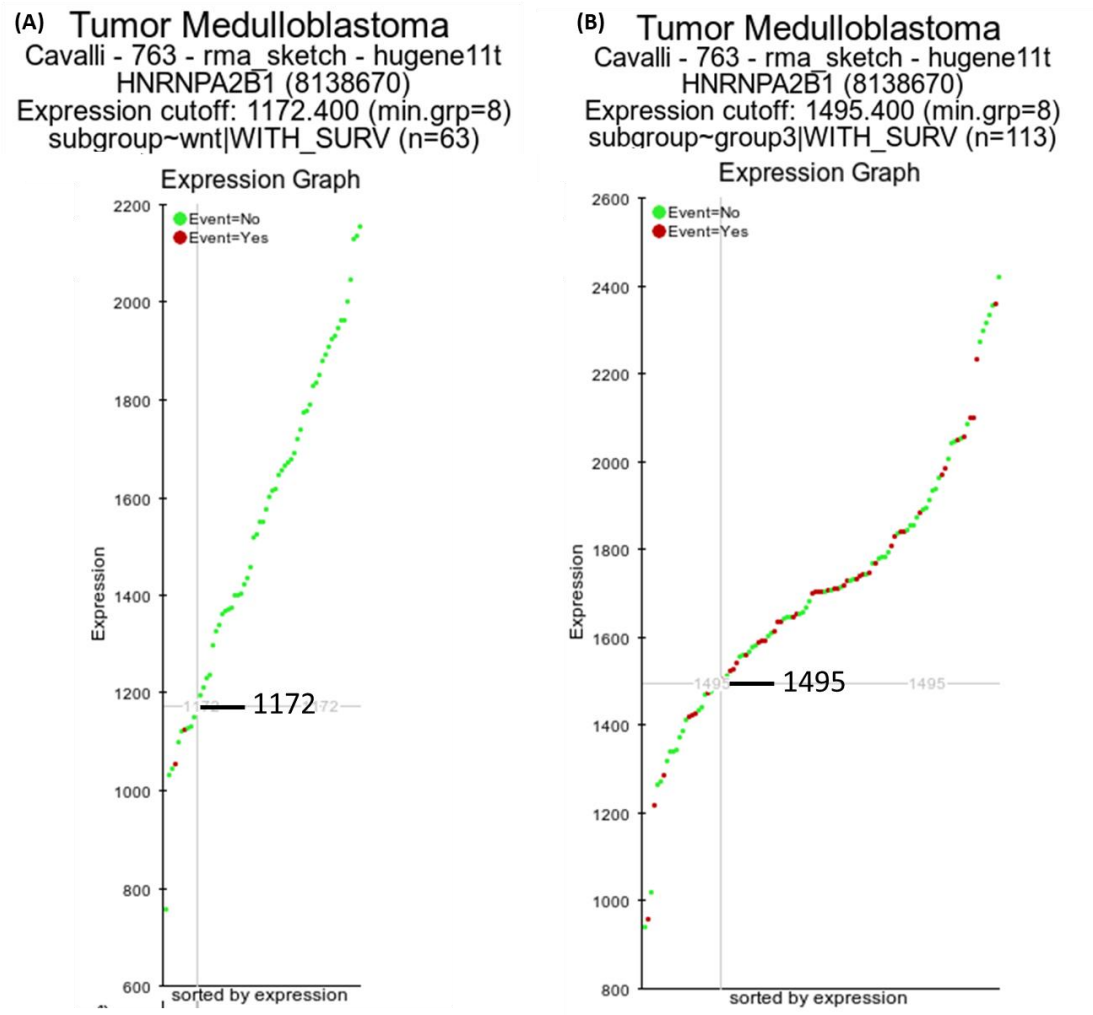
Supplementary figure 2: Expression cut off for high and low expression of HNRNPA2B1 in GBM subgroups.

Generated on TCGA (540) GBM dataset available on R2: Genomics Analysis and Visualization Platform (http://r2.amc.nl), separated by subgroup: ***(A)*** *Mesenchymal,* ***(B)*** *Neural,* ***(C)*** *Pro-neural,* ***(D)*** *Classical.*



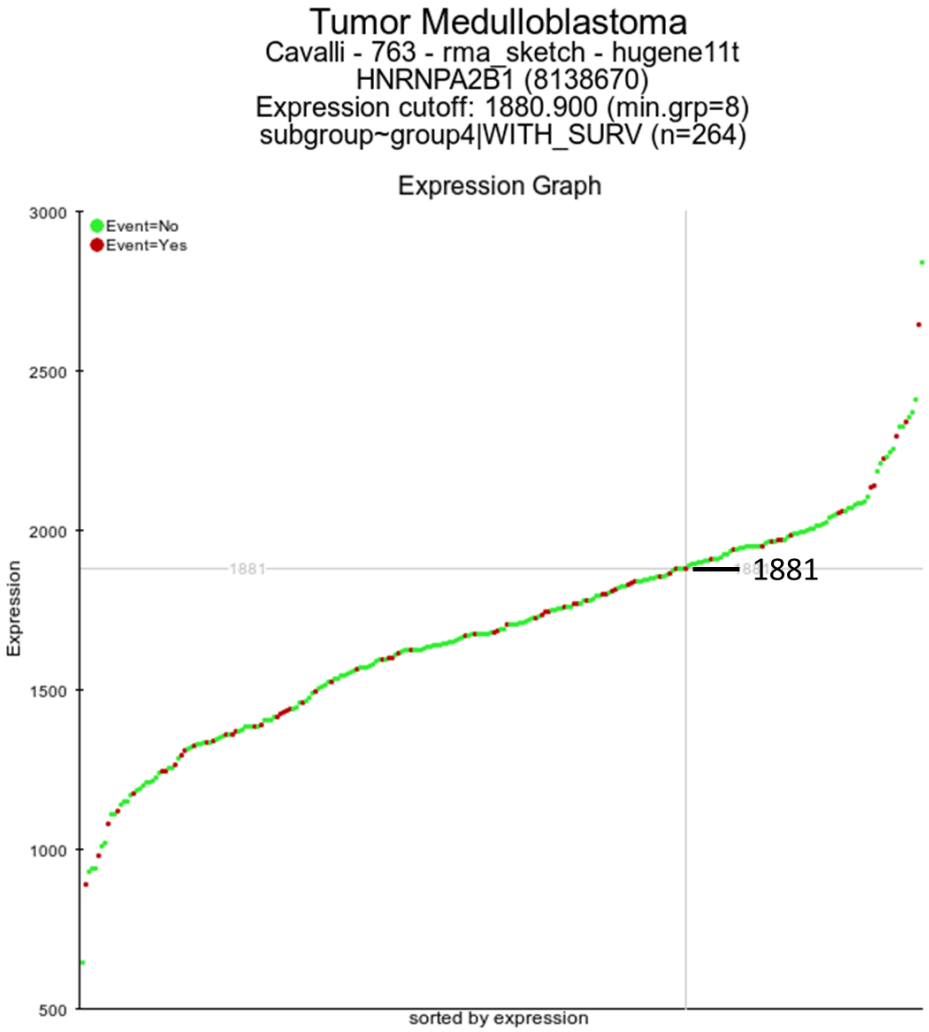
Supplementary figure 3: Expression cut off for high and low expression of HNRNPA2B1 in GBM non-disclosed subgroups.

Generated on TCGA (540) GBM dataset available on R2: Genomics Analysis and Visualization Platform (http://r2.amc.nl).



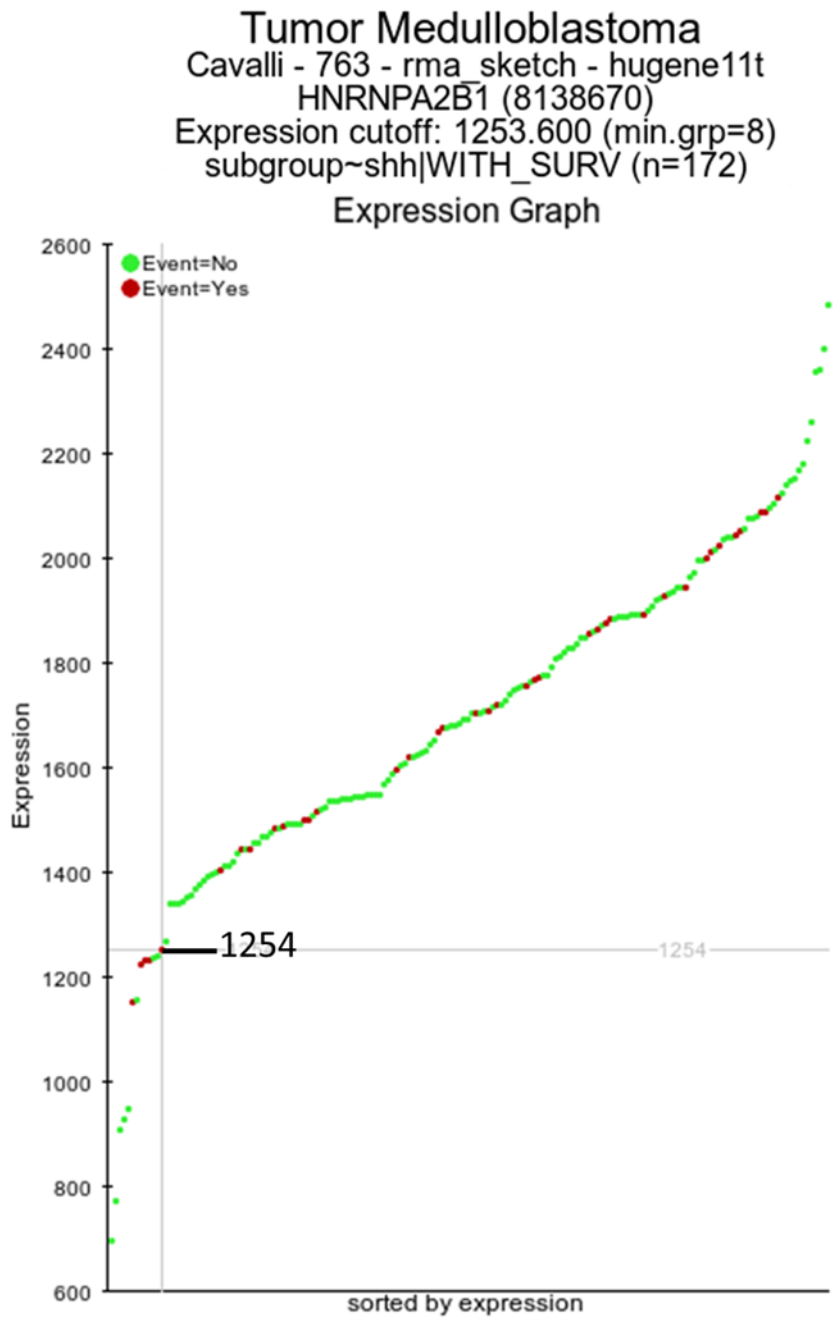
Supplementary figure 4: Expression cut off for high and low expression of HNRNPA2B1 in MB subgroups.

Generated on Cavalli (763) MB dataset available on R2: Genomics Analysis and Visualization Platform (http://r2.amc.nl), separated by subgroups: ***(A)*** *WNT and* ***(B)*** *Group 3.*



Supplementary figure 5: Expression cut off for high and low expression of HNRNPA2B1 in MB Group 3 subgroup.

Generated on Cavalli (763) MB dataset available on R2: Genomics Analysis and Visualization Platform (http://r2.amc.nl).



Supplementary figure 6: Expression cut off for high and low expression of HNRNPA2B1 in MB SHH subgroup.

Generated on Cavalli (763) MB dataset available on R2: Genomics Analysis and Visualization Platform (http://r2.amc.nl).

References

Abakir, A. *et al.* (2020) “N6-methyladenosine regulates the stability of RNA:DNA hybrids in human cells,” *Nature Genetics*, 52(1), pp. 48–55. Available at: https://doi.org/10.1038/s41588-019-0549-x.

Abbassi, R.H. *et al.* (2019) “Lower Tubulin Expression in Glioblastoma Stem Cells Attenuates Efficacy of Microtubule-Targeting Agents,” *ACS Pharmacology & Translational Science*, 2(6), pp. 402–413. Available at: https://doi.org/10.1021/acsptsci.9b00045.

Abu-Odeh, M., Bar-Mag, T., *et al.* (2014) “Characterizing WW Domain Interactions of Tumor Suppressor WWOX Reveals Its Association with Multiprotein Networks,” *Journal of Biological Chemistry*, 289(13). Available at: https://doi.org/10.1074/jbc.M113.506790.

Abu-Odeh, M., Salah, Z., *et al.* (2014) “WWOX, the common fragile site FRA16D gene product, regulates ATM activation and the DNA damage response,” *Proceedings of the National Academy of Sciences of the United States of America*, 111(44). Available at: https://doi.org/10.1073/pnas.1409252111.

Adams, H. *et al.* (2013) “Adult Cerebellar Glioblastoma: Understanding Survival and Prognostic Factors Using a Population-Based Database from 1973 to 2009,” *World Neurosurgery*, 80(6). Available at: https://doi.org/10.1016/j.wneu.2013.02.010.

Aguilera, A. (2002) “The connection between transcription and genomic instability,” *The EMBO Journal*, 21(3). Available at: https://doi.org/10.1093/emboj/21.3.195.

Aguilera, A. (2005) “mRNA processing and genomic instability,” *Nature Structural & Molecular Biology*, 12(9). Available at: https://doi.org/10.1038/nsmb0905-737.

Aguilera, A. and García-Muse, T. (2012) “R loops: from transcription byproducts to threats to genome stability,” *Molecular Cell*, 46(2), pp. 115–124.

Aktaş, T. *et al.* (2017) “DHX9 suppresses RNA processing defects originating from the Alu invasion of the human genome,” *Nature*, 544(7648). Available at: https://doi.org/10.1038/nature21715.

Alarcón, C. *et al.* (2015) “HNRNPA2B1 Is a Mediator of m(6)A-Dependent Nuclear RNA Processing Events,” *Cell*, 162(6), pp. 1299–1308.

Alarcón, C.R. *et al.* (2015) “N6-methyladenosine marks primary microRNAs for processing,” *Nature*, 519(7544). Available at: https://doi.org/10.1038/nature14281.

An, S. *et al.* (2020) “Integrative network analysis identifies cell-specific trans regulators of m6A,” *Nucleic Acids Research*, 48(4). Available at: https://doi.org/10.1093/nar/gkz1206.

Andersson, R. *et al.* (2014) “An atlas of active enhancers across human cell types and tissues,” *Nature*, 507(7493). Available at: https://doi.org/10.1038/nature12787.

Aqeilan, R.I. *et al.* (2005) “WW Domain–Containing Proteins, WWOX and YAP, Compete for Interaction with ErbB-4 and Modulate Its Transcriptional Function,” *Cancer Research*, 65(15). Available at: https://doi.org/10.1158/0008-5472.CAN-05-1150.

Aqeilan, R.I. *et al.* (2009) “Targeted Ablation of the WW Domain-Containing Oxidoreductase Tumor Suppressor Leads to Impaired Steroidogenesis,” *Endocrinology*, 150(3). Available at: https://doi.org/10.1210/en.2008-1087.

Aqeilan, R.I., Abu-Remaileh, M. and Abu-Odeh, M. (2014) “The common fragile site FRA16D gene product WWOX: Roles in tumor suppression and genomic stability,” *Cellular and Molecular Life Sciences*. Available at: https://doi.org/10.1007/s00018-014-1724-y.

Arora, R. *et al.* (2014) “RNaseH1 regulates TERRA-telomeric DNA hybrids and telomere maintenance in ALT tumour cells,” *Nature Communications*, 5(1). Available at: https://doi.org/10.1038/ncomms6220.

Ayrault, O. *et al.* (2010) “Atoh1 Inhibits Neuronal Differentiation and Collaborates with Gli1 to Generate Medulloblastoma-Initiating Cells,” *Cancer Research*, 70(13). Available at: https://doi.org/10.1158/0008-5472.CAN-09-3740.

Azizi, A.A. *et al.* (2012) “Identification of c-myc-dependent proteins in the medulloblastoma cell line D425Med,” *Amino Acids*, 42(6). Available at: https://doi.org/10.1007/s00726-011-0953-8.

Bacsó, Z., Everson, R.B. and Eliason, J.F. (2000) “The DNA of annexin V-binding apoptotic cells is highly fragmented.,” *Cancer research*, 60(16).

Bai, X., Li, F. and Zhang, Z. (2021) “A hypothetical model of trans-acting R-loops-mediated promoter-enhancer interactions by Alu elements,” *Journal of Genetics and Genomics* [Preprint]. Available at: https://doi.org/10.1016/j.jgg.2021.07.005.

Bailey, P. (1925) “Medulloblastoma cerebelli,” *Archives of Neurology & Psychiatry*, 14(2). Available at: https://doi.org/10.1001/archneurpsyc.1925.02200140055002.

Balk, B. *et al.* (2013) “Telomeric RNA-DNA hybrids affect telomere-length dynamics and senescence,” *Nature Structural & Molecular Biology*, 20(10). Available at: https://doi.org/10.1038/nsmb.2662.

Bansal, H. *et al.* (2014) “WTAP is a novel oncogenic protein in acute myeloid leukemia,” *Leukemia*, 28(5), pp. 1171–1174.

Barbieri, I. *et al.* (2017) “Promoter-bound METTL3 maintains myeloid leukaemia by m6A-dependent translation control,” *Nature*, 552(7683), pp. 126–131.

Barbieri, I. and Kouzarides, T. (2020) “Role of RNA modifications in cancer,” *Nature Reviews Cancer*, 20(6). Available at: https://doi.org/10.1038/s41568-020-0253-2.

Bartek, J., Bartkova, J. and Lukas, J. (1997) “The Retinoblastoma Protein Pathway in Cell Cycle Control and Cancer,” *Experimental Cell Research*, 237, pp. 1–6.

Bartek, J. and Lukas, J. (2007) “DNA damage checkpoints: from initiation to recovery or adaptation,” *Current Opinion in Cell Biology*, 19(2). Available at: https://doi.org/10.1016/j.ceb.2007.02.009.

Bass, B. and Weintraub, H. (1987) “A developmentally regulated activity that unwinds RNA duplexes,” *Cell*, 48(4). Available at: https://doi.org/10.1016/0092-8674(87)90239-X.

Bass, B.L. and Weintraub, H. (1988) “An unwinding activity that covalently modifies its double-stranded RNA substrate,” *Cell*, 55(6). Available at: https://doi.org/10.1016/0092-8674(88)90253-X.

Batista, P.J. *et al.* (2014) “m6A RNA modification controls cell fate transition in mammalian embryonic stem cells,” *Cell Stem Cell*, 15(6), pp. 707–719. Available at: https://doi.org/10.1016/j.stem.2014.09.019.m.

Batzer, M.A. and Deininger, P.L. (2002) “Alu repeats and human genomic diversity,” *Nature Reviews Genetics*, 3(5). Available at: https://doi.org/10.1038/nrg798.

Baudin-Baillieu, A. *et al.* (2009) “Nucleotide modifications in three functionally important regions of the Saccharomyces cerevisiae ribosome affect translation accuracy,” *Nucleic Acids Research*, 37(22). Available at: https://doi.org/10.1093/nar/gkp816.

Bednarek, A.K. *et al.* (2000) “WWOX, a novel WW domain-containing protein mapping to human chromosome 16q23.3-24.1, a region frequently affected in breast cancer,” *Cancer Res*, 60(8), pp. 2140–2145.

Behm-Ansmant, I., Helm, M. and Motorin, Y. (2011) “Use of Specific Chemical Reagents for Detection of Modified Nucleotides in RNA,” *Journal of Nucleic Acids*, 2011. Available at: https://doi.org/10.4061/2011/408053.

Beiko, J. *et al.* (2014) “IDH1 mutant malignant astrocytomas are more amenable to surgical resection and have a survival benefit associated with maximal surgical resection,” *Neuro-Oncology*, 16(1). Available at: https://doi.org/10.1093/neuonc/not159.

Bell, E.H. *et al.* (2018) “Association of MGMT Promoter Methylation Status With Survival Outcomes in Patients With High-Risk Glioma Treated With Radiotherapy and Temozolomide,” *JAMA Oncology*, 4(10). Available at: https://doi.org/10.1001/jamaoncol.2018.1977.

Bell, J.L. *et al.* (2013) “Insulin-like growth factor 2 mRNA-binding proteins (IGF2BPs): post-transcriptional drivers of cancer progression?,” *Cellular and Molecular Life Sciences*, 70(15). Available at: https://doi.org/10.1007/s00018-012-1186-z.

Benore-Parsons, M. and Ayoub, M.A. (1997) “Presence of RNase A Causes Aberrant DNA Band Shifts,” *BioTechniques*, 23(1). Available at: https://doi.org/10.2144/97231st04.

Bestor, T.H. and Ingram, V.M. (1983) “Two DNA methyltransferases from murine erythroleukemia cells : Purification , sequence specificity , and mode of interaction with DNA,” *PNAS*, 80(September), pp. 5559–5563.

Bhatia, V. *et al.* (2014) “BRCA2 prevents R-loop accumulation and associates with TREX-2 mRNA export factor PCID2,” *Nature*, 511(7509). Available at: https://doi.org/10.1038/nature13374.

Biernat, W. *et al.* (1997) “Alterations of cell cycle regulatory genes in primary (de novo) and secondary glioblastomas,” *Acta Neuropathologica*, 94(4). Available at: https://doi.org/10.1007/s004010050711.

Bilodeau, P.S. *et al.* (2001) “RNA Splicing at Human Immunodeficiency Virus Type 1 3′ Splice Site A2 Is Regulated by Binding of hnRNP A/B Proteins to an Exonic Splicing Silencer Element,” *Journal of Virology*, 75(18). Available at: https://doi.org/10.1128/jvi.75.18.8487-8497.2001.

Black, D.L. (2003) “Mechanisms of Alternative Pre-Messenger RNA Splicing,” *Annual Review of Biochemistry*, 72(1). Available at: https://doi.org/10.1146/annurev.biochem.72.121801.161720.

Blencowe, B.J. (2006) “Alternative Splicing: New Insights from Global Analyses,” *Cell*, 126(1). Available at: https://doi.org/10.1016/j.cell.2006.06.023.

Boccaletto, P. *et al.* (2018) “MODOMICS: a database of RNA modification pathways. 2017 update,” *Nucleic Acids Research*, 46(D1). Available at: https://doi.org/10.1093/nar/gkx1030.

Boguslawski, S.J. *et al.* (1986) “Characterization of monoclonal antibody to DNA · RNA and its application to immunodetection of hybrids,” *Journal of Immunological Methods*, 89(1). Available at: https://doi.org/10.1016/0022-1759(86)90040-2.

Bohnsack, K., Höbartner, C. and Bohnsack, M. (2019) “Eukaryotic 5-methylcytosine (m5C) RNA Methyltransferases: Mechanisms, Cellular Functions, and Links to Disease,” *Genes*, 10(2). Available at: https://doi.org/10.3390/genes10020102.

Bokar, J.A. *et al.* (1997) “Purification and cDNA cloning of the AdoMet-binding subunit of the human mRNA (N6-adenosine)-methyltransferase.,” *RNA (New York, N.Y.)*, 3(11).

Bonnet, A. *et al.* (2017) “Introns Protect Eukaryotic Genomes from Transcription-Associated Genetic Instability Article Introns Protect Eukaryotic Genomes from Transcription-Associated Genetic Instability,” *Molecular Cell*, 67, pp. 608–621. Available at: https://doi.org/10.1016/j.molcel.2017.07.002.

Boque-Sastre, R. *et al.* (2015) “Head-to-head antisense transcription and R-loop formation promotes transcriptional activation,” *Proceedings of the National Academy of Sciences*, 112(18). Available at: https://doi.org/10.1073/pnas.1421197112.

Breitbart, R.E., Andreadis, A. and Nadal-Ginard, B. (1987) “Alternative Splicing: A Ubiquitous Mechanism for the Generation of Multiple Protein Isoforms from Single Genes,” *Annual Review of Biochemistry*, 56(1). Available at: https://doi.org/10.1146/annurev.bi.56.070187.002343.

Brennan, C.W. *et al.* (2013) “The Somatic Genomic Landscape of Glioblastoma,” *Cell*, 155(2). Available at: https://doi.org/10.1016/j.cell.2013.09.034.

Brown, J.A. *et al.* (2016) “Methyltransferase-like protein 16 binds the 3′-terminal triple helix of MALAT1 long noncoding RNA,” *Proceedings of the National Academy of Sciences*, 113(49). Available at: https://doi.org/10.1073/pnas.1614759113.

Bruun, G.H. *et al.* (2016) “Global identification of hnRNP A1 binding sites for SSO-based splicing modulation,” *BMC Biology*, 14(1). Available at: https://doi.org/10.1186/s12915-016-0279-9.

Burd, C.G. *et al.* (1989) “Primary structures of the heterogeneous nuclear ribonucleoprotein A2, B1, and C2 proteins: A diversity of RNA binding proteins is generated by small peptide inserts,” *Proceedings of the National Academy of Sciences of the United States of America*, 86(24). Available at: https://doi.org/10.1073/pnas.86.24.9788.

Busch, A. and Hertel, K.J. (2012) “Evolution of SR protein and hnRNP splicing regulatory factors,” *Wiley Interdisciplinary Reviews: RNA*, 3(1). Available at: https://doi.org/10.1002/wrna.100.

Caceres, J. *et al.* (1994) “Regulation of alternative splicing in vivo by overexpression of antagonistic splicing factors,” *Science*, 265(5179). Available at: https://doi.org/10.1126/science.8085156.

Cai, X. *et al.* (2018) “HBXIP-elevated methyltransferase METTL3 promotes the progression of breast cancer via inhibiting tumor suppressor let-7g,” *Cancer Letters*, 415. Available at: https://doi.org/10.1016/j.canlet.2017.11.018.

Caputi, M. *et al.* (1999) “hnRNP A/B proteins are required for inhibition of HIV-1 pre-mRNA splicing,” *EMBO Journal*, 18(14). Available at: https://doi.org/10.1093/emboj/18.14.4060.

Carette, J.E. *et al.* (2011) “Ebola virus entry requires the cholesterol transporter Niemann–Pick C1,” *Nature*, 477(7364). Available at: https://doi.org/10.1038/nature10348.

Carter, B.Z. *et al.* (2019) “An ARC-Regulated IL1β/Cox-2/PGE2/β-Catenin/ARC Circuit Controls Leukemia–Microenvironment Interactions and Confers Drug Resistance in AML,” *Cancer Research*, 79(6). Available at: https://doi.org/10.1158/0008-5472.CAN-18-0921.

Cavalli, F.M.G. *et al.* (2017) “Intertumoral Heterogeneity within Medulloblastoma Subgroups,” *Cancer Cell*, 31(6). Available at: https://doi.org/10.1016/j.ccell.2017.05.005.

Cerritelli, S.M. *et al.* (2003) “Failure to Produce Mitochondrial DNA Results in Embryonic Lethality in Rnaseh1 Null Mice,” *Molecular Cell*, 11(3). Available at: https://doi.org/10.1016/S1097-2765(03)00088-1.

Cerritelli, S.M. and Crouch, R.J. (2009) “Ribonuclease H: the enzymes in eukaryotes,” *FEBS Journal*, 276(6). Available at: https://doi.org/10.1111/j.1742-4658.2009.06908.x.

Chakrabarti, I. *et al.* (2005) “A population-based description of glioblastoma multiforme in Los Angeles County, 1974-1999,” *Cancer*, 104(12). Available at: https://doi.org/10.1002/cncr.21539.

Chakraborty, P. and Grosse, F. (2011) “Human DHX9 helicase preferentially unwinds RNA-containing displacement loops (R-loops) and G-quadruplexes.,” *DNA repair*, 10(6). Available at: https://doi.org/10.1016/j.dnarep.2011.04.013.

Chakraborty, P., Huang, J.T.J. and Hiom, K. (2018) “DHX9 helicase promotes R-loop formation in cells with impaired RNA splicing,” *Nature Communications*, 9(1). Available at: https://doi.org/10.1038/s41467-018-06677-1.

Chan, Y.A. *et al.* (2014) “Genome-Wide Profiling of Yeast DNA:RNA Hybrid Prone Sites with DRIP-Chip,” *PLoS Genetics*, 10(4). Available at: https://doi.org/10.1371/journal.pgen.1004288.

Chang, M. *et al.* (2017) “Region-specific RNA m 6 A methylation represents a new layer of control in the gene regulatory network in the mouse brain,” *Open Biology*, 7.

Chang, Y., Lu, X. and Qiu, J. (2021) “Compensatory expression regulation of highly homologous proteins HNRNPA1 and HNRNPA2,” *Turkish Journal of Biology*, 45(2), pp. 187–195. Available at: https://doi.org/10.3906/biy-2010-29.

Chen, J. *et al.* (2017) “YTH domain family 2 orchestrates epithelial-mesenchymal transition/proliferation dichotomy in pancreatic cancer cells,” *Cell Cycle*, 16(23). Available at: https://doi.org/10.1080/15384101.2017.1380125.

Chen, J. and Du, B. (2019) “Novel positioning from obesity to cancer: FTO, an m6A RNA demethylase, regulates tumour progression.,” *Journal of cancer research and clinical oncology*, 145(1). Available at: https://doi.org/10.1007/s00432-018-2796-0.

Chen, L. *et al.* (2017) “R-ChIP Using Inactive RNase H Reveals Dynamic Coupling of R-loops with Transcriptional Pausing at Gene Promoters,” *Molecular Cell*, 68(4). Available at: https://doi.org/10.1016/j.molcel.2017.10.008.

Chen, L. and Pan, J. (2017) “Dual cyclin-dependent kinase 4/6 inhibition by PD-0332991 induces apoptosis and senescence in oesophageal squamous cell carcinoma cells,” *British Journal of Pharmacology*, 174(15). Available at: https://doi.org/10.1111/bph.13836.

Chen, M. *et al.* (2017) “RNA N6-methyladenosine methyltransferase METTL3 promotes liver cancer progression through YTHDF2 dependent post-transcriptional silencing of SOCS2,” *Hepatology* [Preprint], (81572446). Available at: https://doi.org/10.1002/hep.

Chen, M. and Manley, J.L. (2009) “Mechanisms of alternative splicing regulation: insights from molecular and genomics approaches,” *Nature Reviews Molecular Cell Biology*, 10(11). Available at: https://doi.org/10.1038/nrm2777.

Chen, Z. *et al.* (2019) “Transfer RNA demethylase ALKBH3 promotes cancer progression via induction of tRNA-derived small RNAs,” *Nucleic Acids Research*, 47(5). Available at: https://doi.org/10.1093/nar/gky1250.

Cho, Y.-J. *et al.* (2011) “Integrative Genomic Analysis of Medulloblastoma Identifies a Molecular Subgroup That Drives Poor Clinical Outcome,” *Journal of Clinical Oncology*, 29(11). Available at: https://doi.org/10.1200/JCO.2010.28.5148.

Choudhry, Z. *et al.* (2013) “Association between obesity-related gene FTO and ADHD,” *Obesity*, 21(12). Available at: https://doi.org/10.1002/oby.20444.

Choudhry, Z. *et al.* (2014) “Sonic hedgehog signalling pathway: a complex network,” *Annals of Neurosciences*, 21(1). Available at: https://doi.org/10.5214/ans.0972.7531.210109.

Chow, C.S., Lamichhane, T.N. and Mahto, S.K. (2007) “Expanding the Nucleotide Repertoire of the Ribosome with Post-Transcriptional Modifications,” *ACS Chemical Biology*, 2(9). Available at: https://doi.org/10.1021/cb7001494.

Chow, L.M.L. *et al.* (2011) “Cooperativity within and among Pten, p53, and Rb Pathways Induces High-Grade Astrocytoma in Adult Brain,” *Cancer Cell*, 19(3). Available at: https://doi.org/10.1016/j.ccr.2011.01.039.

Clifford, S.C. *et al.* (2006) “Wnt/Wingless Pathway Activation and Chromosome 6 Loss Characterise a Distinct Molecular Sub-Group of Medulloblastomas Associated with a Favourable Prognosis,” *Cell Cycle*, 5(22). Available at: https://doi.org/10.4161/cc.5.22.3446.

Clower, C. v. *et al.* (2010) “The alternative splicing repressors hnRNP A1/A2 and PTB influence pyruvate kinase isoform expression and cell metabolism,” *Proceedings of the National Academy of Sciences*, 107(5). Available at: https://doi.org/10.1073/pnas.0914845107.

Cohn, W.E. (1960) “Pseudouridine, a carbon-carbon linked ribonucleoside in ribonucleic acids: isolation, structure, and chemical characteristics.,” *The Journal of biological chemistry*, 235.

Colak, D. *et al.* (2014) “Promoter-bound trinucleotide repeat mRNA drives epigenetic silencing in fragile X syndrome,” *Science*, 343(6174), pp. 1002–1005.

Collart, M.A. (2016) “The Ccr4-Not complex is a key regulator of eukaryotic gene expression,” *Wiley Interdisciplinary Reviews: RNA*, 7(4). Available at: https://doi.org/10.1002/wrna.1332.

Colman, H. *et al.* (2010) “A multigene predictor of outcome in glioblastoma,” *Neuro-Oncology*, 12(1). Available at: https://doi.org/10.1093/neuonc/nop007.

Cook Sangar, M.L. *et al.* (2017) “Inhibition of CDK4/6 by Palbociclib Significantly Extends Survival in Medulloblastoma Patient-Derived Xenograft Mouse Models,” *Clinical Cancer Research*, 23(19). Available at: https://doi.org/10.1158/1078-0432.CCR-16-2943.

Coppin, L. *et al.* (2018) “Messenger RNA Life-Cycle in Cancer Cells: Emerging Role of Conventional and Non-Conventional RNA-Binding Proteins?,” *International Journal of Molecular Sciences*, 19(3). Available at: https://doi.org/10.3390/ijms19030650.

Costantino, L. and Koshland, D. (2018) “Genome-wide Map of R-Loop-Induced Damage Reveals How a Subset of R-Loops Contributes to Genomic Instability,” *Molecular Cell*, 71(4). Available at: https://doi.org/10.1016/j.molcel.2018.06.037.

Cristini, A. *et al.* (2018) “RNA / DNA Hybrid Interactome Identifies DHX9 as a Molecular Player in Transcriptional Termination and Resource RNA / DNA Hybrid Interactome Identifies DHX9 as a Molecular Player in Transcriptional Termination and R-Loop-Associated DNA Damage,” *CellReports*, 23(6), pp. 1891–1905. Available at: https://doi.org/10.1016/j.celrep.2018.04.025.

Crossley, M.P. *et al.* (2020) “qDRIP: a method to quantitatively assess RNA–DNA hybrid formation genome-wide,” *Nucleic Acids Research*, 48(14). Available at: https://doi.org/10.1093/nar/gkaa500.

Cui, Q. *et al.* (2017) “m 6 A RNA Methylation Regulates the Self-Renewal and Tumorigenesis of Glioblastoma Stem Cells Article m 6 A RNA Methylation Regulates the Self-Renewal and Tumorigenesis of Glioblastoma Stem Cells,” *Cell Reports*, 18, pp. 2622–2634. Available at: https://doi.org/10.1016/j.celrep.2017.02.059.

Dai, S. *et al.* (2017) “HNRNPA2B1 regulates the epithelial-mesenchymal transition in pancreatic cancer cells through the ERK/snail signalling pathway,” *Cancer Cell International*, 17(12).

Darzynkiewicz, Z. *et al.* (1992) “Features of apoptotic cells measured by flow cytometry,” *Cytometry*, 13(8). Available at: https://doi.org/10.1002/cyto.990130802.

Daubner, G.M., Cléry, A. and Allain, F.H.-T. (2013) “RRM–RNA recognition: NMR or crystallography…and new findings,” *Current Opinion in Structural Biology*, 23(1). Available at: https://doi.org/10.1016/j.sbi.2012.11.006.

David, C.J. *et al.* (2010) “HnRNP proteins controlled by c-Myc deregulate pyruvate kinase mRNA splicing in cancer,” *Nature*, 463(7279). Available at: https://doi.org/10.1038/nature08697.

Davis, F.F. and Allen, F.W. (1957) “Ribonucleic acids from yeast which contain a fifth nucleotide.,” *The Journal of biological chemistry*, 227(2).

Decatur, W.A. and Fournier, M.J. (2002) “rRNA modifications and ribosome function,” *Trends in Biochemical Sciences*, 27(7). Available at: https://doi.org/10.1016/S0968-0004(02)02109-6.

Delatte, B. *et al.* (2016) “RNA biochemistry. Transcriptome-wide distribution and function of RNA hydroxymethylcytosine.,” *Science (New York, N.Y.)*, 351(6270), pp. 282–5. Available at: https://doi.org/10.1126/science.aac5253.

Deng, J. *et al.* (2016) “Effects of hnRNP A2/B1 Knockdown on Inhibition of Glioblastoma Cell Invasion, Growth and Survival,” *Molecular Neurobiology*, 53(2). Available at: https://doi.org/10.1007/s12035-014-9080-3.

Deng, R. *et al.* (2019) “m6A methyltransferase METTL3 suppresses colorectal cancer proliferation and migration through p38/ERK pathways,” *OncoTargets and Therapy*, Volume 12. Available at: https://doi.org/10.2147/OTT.S201052.

Deng, X. *et al.* (2018) “Critical Enzymatic Functions of FTO in Obesity and Cancer.,” *Frontiers in endocrinology*, 9. Available at: https://doi.org/10.3389/fendo.2018.00396.

Desrosiers, R., Friderici, K. and Rottman, F. (1974) “Identification of Methylated Nucleosides in Messenger RNA from Novikoff Hepatoma Cells,” *Proceedings of the National Academy of Sciences*, 71(10). Available at: https://doi.org/10.1073/pnas.71.10.3971.

Di, L. *et al.* (2020) “RNA sequencing by direct tagmentation of RNA/DNA hybrids,” *Proceedings of the National Academy of Sciences*, 117(6). Available at: https://doi.org/10.1073/pnas.1919800117.

Dina, C. *et al.* (2007) “Variation in FTO contributes to childhood obesity and severe adult obesity,” *Nature Genetics*, 39(6), pp. 724–726.

Dixit, D. *et al.* (2021) “The RNA m6A Reader YTHDF2 Maintains Oncogene Expression and Is a Targetable Dependency in Glioblastoma Stem Cells,” *Cancer Discovery*, 11(2). Available at: https://doi.org/10.1158/2159-8290.CD-20-0331.

Dominissini, D. *et al.* (2012) “Topology of the human and mouse m6A RNA methylomes revealed by m6A-seq,” *Nature*, 485(7397). Available at: https://doi.org/10.1038/nature11112.

Dominissini, D. *et al.* (2016) “The dynamic N1-methyladenosine methylome in eukaryotic messenger RNA,” *Nature*, 530(7591). Available at: https://doi.org/10.1038/nature16998.

Domsic, J.K. *et al.* (2003) “Human Immunodeficiency Virus Type 1 hnRNP A/B-Dependent Exonic Splicing Silencer ESSV Antagonizes Binding of U2AF65 to Viral Polypyrimidine Tracts,” *Molecular and Cellular Biology*, 23(23). Available at: https://doi.org/10.1128/mcb.23.23.8762-8772.2003.

Donà, F. and Houseley, J. (2014) “Unexpected DNA Loss Mediated by the DNA Binding Activity of Ribonuclease A,” *PLoS ONE*, 9(12). Available at: https://doi.org/10.1371/journal.pone.0115008.

Doxtader, K.A. *et al.* (2018) “Structural Basis for Regulation of METTL16, an S-Adenosylmethionine Homeostasis Factor,” *Molecular Cell*, 71(6). Available at: https://doi.org/10.1016/j.molcel.2018.07.025.

Dreyfuss, G. *et al.* (1993) “hnRNP proteins and the biogenesis of mRNA,” *Annual Review of Biochemistry*. Available at: https://doi.org/10.1146/annurev.bi.62.070193.001445.

Driouch, K. *et al.* (2002) “Alternative transcripts of the candidate tumor suppressor gene, WWOX, are expressed at high levels in human breast tumors,” *Oncogene*, 21(12). Available at: https://doi.org/10.1038/sj.onc.1205273.

Du, H. *et al.* (2016) “YTHDF2 destabilizes m6A-containing RNA through direct recruitment of the CCR4–NOT deadenylase complex,” *Nature Communications*, 7(1). Available at: https://doi.org/10.1038/ncomms12626.

Du, T. *et al.* (2015) “An association study of the m6A genes with major depressive disorder in Chinese Han population,” *Journal of Affective Disorders*, 183. Available at: https://doi.org/10.1016/j.jad.2015.05.025.

Dubin, D.T. and Taylor, R.H. (1975) “The methylation state of poly A-containing-messenger RNA from cultured hamster cells,” *Nucleic Acids Research*, 2(10). Available at: https://doi.org/10.1093/nar/2.10.1653.

Dufour, C. *et al.* (2012) “Metastatic Medulloblastoma in Childhood: Chang’s Classification Revisited,” *International Journal of Surgical Oncology*, 2012. Available at: https://doi.org/10.1155/2012/245385.

Dumelie, J.G. and Jaffrey, S.R. (2017) “Defining the location of promoter-associated R-loops at near-nucleotide resolution using bisDRIP-seq,” *eLife*, 6. Available at: https://doi.org/10.7554/eLife.28306.

Durkin, S.G. and Glover, T.W. (2007) “Chromosome Fragile Sites,” *Annual Review of Genetics*, 41(1). Available at: https://doi.org/10.1146/annurev.genet.41.042007.165900.

Eberhart, C.G. *et al.* (2002) “Histopathologic grading of medulloblastomas,” *Cancer*, 94(2). Available at: https://doi.org/10.1002/cncr.10189.

Elbarbary, R.A., Lucas, B.A. and Maquat, L.E. (2016) “Retrotransposons as regulators of gene expression,” *Science*, 351(6274). Available at: https://doi.org/10.1126/science.aac7247.

Elcheva, I.A. *et al.* (2020) “RNA-binding protein IGF2BP1 maintains leukemia stem cell properties by regulating HOXB4, MYB, and ALDH1A1,” *Leukemia*, 34(5). Available at: https://doi.org/10.1038/s41375-019-0656-9.

Ellison, D.W. *et al.* (2011) “Medulloblastoma: clinicopathological correlates of SHH, WNT, and non-SHH/WNT molecular subgroups,” *Acta Neuropathologica*, 121(3). Available at: https://doi.org/10.1007/s00401-011-0800-8.

Engelhard, H.H. *et al.* (2010) “Clinical presentation, histology, and treatment in 430 patients with primary tumors of the spinal cord, spinal meninges, or cauda equina,” *Journal of Neurosurgery: Spine*, 13(1). Available at: https://doi.org/10.3171/2010.3.SPINE09430.

Essletzbichler, P. *et al.* (2014) “Megabase-scale deletion using CRISPR/Cas9 to generate a fully haploid human cell line,” *Genome Research*, 24(12). Available at: https://doi.org/10.1101/gr.177220.114.

Fähling, M. *et al.* (2006) “Heterogeneous nuclear ribonucleoprotein-A2/B1 modulate collagen prolyl 4-hydroxylase, α (I) mRNA stability,” *Journal of Biological Chemistry*, 281(14). Available at: https://doi.org/10.1074/jbc.M510925200.

Faria, C.C. *et al.* (2015) “Identification of alsterpaullone as a novel small molecule inhibitor to target group 3 medulloblastoma,” *Oncotarget*, 6(25). Available at: https://doi.org/10.18632/oncotarget.4304.

Fazi, F. and Fatica, A. (2019) “Interplay Between N6-Methyladenosine (m6A) and Non-coding RNAs in Cell Development and Cancer,” *Frontiers in Cell and Developmental Biology*, 7. Available at: https://doi.org/10.3389/fcell.2019.00116.

Ford, D. *et al.* (1998) “Genetic heterogeneity and penetrance analysis of the BRCA1 and BRCA2 genes in breast cancer families. The Breast Cancer Linkage Consortium.,” *American journal of human genetics*, 62(3). Available at: https://doi.org/10.1086/301749.

Frayling, T. *et al.* (2007) “A common variant in the FTO gene is associated with body mass index and predisposes to childhood and adult obesity,” *Science*, 316(5826), pp. 889–894.

Fried, J., Perez, A.G. and Clarkson, B.D. (1976) “Flow cytofluorometric analysis of cell cycle distributions using propidium iodide. Properties of the method and mathematical analysis of the data.,” *Journal of Cell Biology*, 71(1). Available at: https://doi.org/10.1083/jcb.71.1.172.

Friend, L.R. *et al.* (2013) “Arginine Methylation of hnRNP A2 Does Not Directly Govern Its Subcellular Localization,” *PLoS ONE*, 8(9). Available at: https://doi.org/10.1371/journal.pone.0075669.

Fu, L. *et al.* (2014) “Tet-Mediated Formation of 5-Hydroxymethylcytosine in RNA,” *Journal of the American Chemical Society*, 136(33). Available at: https://doi.org/10.1021/ja505305z.

Fu, X.D. (1995) “The superfamily of arginine/serine-rich splicing factors,” *RNA*, 1(7), pp. 663–680.

Fu, Y. *et al.* (2013) “FTO-mediated formation of N6-hydroxymethyladenosine and N6-formyladenosine in mammalian RNA,” *Nature Communications*, 4(1798).

Fu, Y. *et al.* (2014) “Gene expression regulation mediated through reversible m6A RNA methylation,” *Nature Reviews Genetics*, 15(5). Available at: https://doi.org/10.1038/nrg3724.

Gajjar, A.J. and Robinson, G.W. (2014) “Medulloblastoma—translating discoveries from the bench to the bedside,” *Nature Reviews Clinical Oncology*, 11(12). Available at: https://doi.org/10.1038/nrclinonc.2014.181.

Galante, P.A.F. *et al.* (2004) “Detection and evaluation of intron retention events in the human transcriptome,” *RNA*, 10(5). Available at: https://doi.org/10.1261/rna.5123504.

Gan, W. *et al.* (2011) “R-loop-mediated genomic instability is caused by impairment of replication fork progression,” *Genes & Development*, 25(19). Available at: https://doi.org/10.1101/gad.17010011.

García-Mauriño, S.M. *et al.* (2017) “RNA Binding Protein Regulation and Cross-Talk in the Control of AU-rich mRNA Fate,” *Frontiers in Molecular Biosciences*, 4. Available at: https://doi.org/10.3389/fmolb.2017.00071.

García-Muse, T. and Aguilera, A. (2019) “R Loops: From Physiological to Pathological Roles,” *Cell*, 179(3). Available at: https://doi.org/10.1016/j.cell.2019.08.055.

Garcia-Pichardo, D. *et al.* (2017) “Histone Mutants Separate R Loop Formation from Histone Mutants Separate R Loop,” *Molecular Cell*, 66, pp. 597–609. Available at: https://doi.org/10.1016/j.molcel.2017.05.014.

Garrè, M.L. *et al.* (2009) “Medulloblastoma Variants: Age-Dependent Occurrence and Relation to Gorlin Syndrome—A New Clinical Perspective,” *Clinical Cancer Research*, 15(7). Available at: https://doi.org/10.1158/1078-0432.CCR-08-2023.

del Gatto-Konczak, F. *et al.* (1999) “hnRNP A1 Recruited to an Exon In Vivo Can Function as an Exon Splicing Silencer,” *Molecular and Cellular Biology*, 19(1). Available at: https://doi.org/10.1128/mcb.19.1.251.

Gebert, L.F.R. and MacRae, I.J. (2019) “Regulation of microRNA function in animals,” *Nature Reviews Molecular Cell Biology*, 20(1). Available at: https://doi.org/10.1038/s41580-018-0045-7.

Geissler, R. *et al.* (2016) “A widespread sequence-specific mRNA decay pathway mediated by hnRNPs A1 and A2/B1,” *Genes & Development*, 30(9). Available at: https://doi.org/10.1101/gad.277392.116.

Gerber, N.U. *et al.* (2014) “Recent developments and current concepts in medulloblastoma,” *Cancer Treatment Reviews*, 40(3). Available at: https://doi.org/10.1016/j.ctrv.2013.11.010.

Gerstberger, S., Hafner, M. and Tuschl, T. (2014) “A census of human RNA-binding proteins,” *Nature Reviews Genetics*, 15(12). Available at: https://doi.org/10.1038/nrg3813.

Geuens, T., Bouhy, D. and Timmerman, V. (2016) “The hnRNP family: insights into their role in health and disease,” *Human Genetics*. Available at: https://doi.org/10.1007/s00439-016-1683-5.

Geula, S. *et al.* (2015) “Stem cells. m6A mRNA methylation facilitates resolution of naïve pluripotency toward differentiation,” *Science*, 347(6225), pp. 1002–1006.

Gibson, P. *et al.* (2010) “Subtypes of medulloblastoma have distinct developmental origins,” *Nature*, 468(7327). Available at: https://doi.org/10.1038/nature09587.

Gil, J. and Peters, G. (2006) “Regulation of the INK4b–ARF–INK4a tumour suppressor locus: all for one or one for all,” *Nature Reviews Molecular Cell Biology*, 7(9). Available at: https://doi.org/10.1038/nrm1987.

Gilbertson, R.J. (2004) “Medulloblastoma: signalling a change in treatment,” *The Lancet Oncology*, 5(4). Available at: https://doi.org/10.1016/S1470-2045(04)01424-X.

Ginno, P. *et al.* (2012) “R-Loop Formation Is a Distinctive Characteristic of Unmethylated Human CpG Island Promoters,” *Molecular Cell*, 45, pp. 814–825. Available at: https://doi.org/10.1016/j.molcel.2012.01.017.

Glover, T.W. (2006) “Common fragile sites,” *Cancer Letters*, 232(1). Available at: https://doi.org/10.1016/j.canlet.2005.08.032.

Golan-Gerstl, R. *et al.* (2011) “Splicing factor hnRNP A2/B1 regulates tumor suppressor gene splicing and is an oncogenic driver in glioblastoma,” *Cancer Research*, 71(13), pp. 4464–4472. Available at: https://doi.org/10.1158/0008-5472.CAN-10-4410.

Goll, M. and Bestor, T.H. (2005) “Eukaryotic cytosine methyltransferases.,” *Annual Review of Biochemistry*, 74, pp. 481–514.

Gomez-Gonzalez, B. and Aguilera, A. (2007) “Activation-induced cytidine deaminase action is strongly stimulated by mutations of the THO complex,” *Proceedings of the National Academy of Sciences*, 104(20). Available at: https://doi.org/10.1073/pnas.0702836104.

Goodarzi, H. *et al.* (2012) “Systematic discovery of structural elements governing stability of mammalian messenger RNAs,” *Nature*, 485(7397). Available at: https://doi.org/10.1038/nature11013.

Gorthi, A. *et al.* (2018) “EWS–FLI1 increases transcription to cause R-loops and block BRCA1 repair in Ewing sarcoma,” *Nature*, 555(7696). Available at: https://doi.org/10.1038/nature25748.

Grabczyk, E., Mancuso, M. and Sammarco, M.C. (2007) “A persistent RNA:DNA hybrid formed by transcription of the Friedreich ataxia triplet repeat in live bacteria, and by T7

RNAP in vitro," *Nucleic Acids Research*, 35(16). Available at: https://doi.org/10.1093/nar/gkm589.

Groh, M. *et al.* (2014) "R-loops associated with triplet repeat expansions promote gene silencing in Friedreich ataxia and fragile X syndrome," *PLoS Genetics*, 10(5).

Groh, M. and Gromak, N. (2014) "Out of balance: R-loops in human disease," *PLoS Genetics*, 10(9).

Grunseich, C. *et al.* (2018) "Senataxin Mutation Reveals How R-Loops Promote Transcription by Blocking DNA Methylation at Gene Promoters," *Molecular Cell*, 69(3). Available at: https://doi.org/10.1016/j.molcel.2017.12.030.

Guo, H. *et al.* (2020) "m6A Reader HNRNPA2B1 Promotes Esophageal Cancer Progression via Up-Regulation of ACLY and ACC1," *Frontiers in Oncology*, 10. Available at: https://doi.org/10.3389/fonc.2020.553045.

Gupta, A. *et al.* (2020) "The HNRNPA2B1–MST1R–Akt axis contributes to epithelial-to-mesenchymal transition in head and neck cancer," *Laboratory Investigation*, 100(12). Available at: https://doi.org/10.1038/s41374-020-0466-8.

de Haas, T. *et al.* (2008) "Molecular Risk Stratification of Medulloblastoma Patients Based on Immunohistochemical Analysis of MYC, LDHB, and CCNB1 Expression," *Clinical Cancer Research*, 14(13). Available at: https://doi.org/10.1158/1078-0432.CCR-07-4159.

Haeusler, A. *et al.* (2014) "C9orf72 nucleotide repeat structures initiate molecular cascades of disease," *Nature*, 507(7491), pp. 195–200.

el Hage, A. *et al.* (2014) "Genome-Wide Distribution of RNA-DNA Hybrids Identifies RNase H Targets in tRNA Genes, Retrotransposons and Mitochondria," *PLoS Genetics*, 10(10). Available at: https://doi.org/10.1371/journal.pgen.1004716.

Halász, L. *et al.* (2017) "RNA-DNA hybrid (R-loop) immunoprecipitation mapping: an analytical workflow to evaluate inherent biases," *Genome Research*, 27(6). Available at: https://doi.org/10.1101/gr.219394.116.

Hallahan, A.R. *et al.* (2004) “The SmoA1 Mouse Model Reveals That Notch Signaling Is Critical for the Growth and Survival of Sonic Hedgehog-Induced Medulloblastomas,” *Cancer Research*, 64(21). Available at: https://doi.org/10.1158/0008-5472.CAN-04-1813.

Halperin, R.F. *et al.* (2021) “Improved methods for RNAseq-based alternative splicing analysis,” *Scientific Reports*, 11(1). Available at: https://doi.org/10.1038/s41598-021-89938-2.

Hamma, T. and Ferré-D’Amaré, A.R. (2006) “Pseudouridine Synthases,” *Chemistry & Biology*, 13(11). Available at: https://doi.org/10.1016/j.chembiol.2006.09.009.

Hamperl, S. *et al.* (2017) “Transcription-Replication Conflict Orientation Modulates R-Loop Levels and Activates Distinct DNA Damage Responses Article Transcription-Replication Conflict Orientation Modulates R-Loop Levels and Activates Distinct DNA Damage Responses,” *Cell*, 170(4), pp. 774-774.e19. Available at: https://doi.org/10.1016/j.cell.2017.07.043.

Han, M. *et al.* (2020) “Abnormality of m6A mRNA Methylation Is Involved in Alzheimer’s Disease,” *Frontiers in Neuroscience*, 14. Available at: https://doi.org/10.3389/fnins.2020.00098.

Hanaford, A.R. *et al.* (2016) “DiSCoVERing Innovative Therapies for Rare Tumors: Combining Genetically Accurate Disease Models with *In Silico* Analysis to Identify Novel Therapeutic Targets,” *Clinical Cancer Research*, 22(15). Available at: https://doi.org/10.1158/1078-0432.CCR-15-3011.

Hanahan, D. and Weinberg, R. (2011) “Hallmarks of cancer: the next generation,” *Cell*, 144(5), pp. 646–674.

Hanahan, D. and Weinberg, R.A. (2000) “The Hallmarks of Cancer,” *Cell*, 100(1). Available at: https://doi.org/10.1016/S0092-8674(00)81683-9.

Harper, J.W. and Elledge, S.J. (2007) “The DNA Damage Response: Ten Years After,” *Molecular Cell*, 28(5). Available at: https://doi.org/10.1016/j.molcel.2007.11.015.

Harrison, A.F. and Shorter, J. (2017) “RNA-binding proteins with prion-like domains in health and disease,” *Biochemical Journal*. Available at: https://doi.org/10.1042/BCJ20160499.

Hartono, S.R. *et al.* (2018) “The Affinity of the S9.6 Antibody for Double-Stranded RNAs Impacts the Accurate Mapping of R-Loops in Fission Yeast,” *Journal of Molecular Biology*, 430(3), pp. 272–284. Available at: https://doi.org/10.1016/j.jmb.2017.12.016.

Harvey, S.E. and Cheng, C. (2016) “Methods for Characterization of Alternative RNA Splicing,” in. Available at: https://doi.org/10.1007/978-1-4939-3378-5_18.

Hatchi, E. *et al.* (2015) “BRCA1 recruitment to transcriptional pause sites is required for R-loop-driven DNA damage repair.,” *Molecular cell*, 57(4). Available at: https://doi.org/10.1016/j.molcel.2015.01.011.

Hatten, M.E. and Roussel, M.F. (2011) “Development and cancer of the cerebellum,” *Trends in Neurosciences*, 34(3). Available at: https://doi.org/10.1016/j.tins.2011.01.002.

Hauenschild, R. *et al.* (2015) “The reverse transcription signature of N-1-methyladenosine in RNA-Seq is sequence dependent,” *Nucleic Acids Research* [Preprint]. Available at: https://doi.org/10.1093/nar/gkv895.

He, C. (2010) “Grand Challenge Commentary: RNA epigenetics?,” *Nature Chemical Biology*, 6(12). Available at: https://doi.org/10.1038/nchembio.482.

He, L. *et al.* (2019) “Functions of N6-methyladenosine and its role in cancer,” *Molecular Cancer*, 18(1). Available at: https://doi.org/10.1186/s12943-019-1109-9.

He, X. *et al.* (2018) “IGF2BP2 Overexpression Indicates Poor Survival in Patients with Acute Myelocytic Leukemia,” *Cellular Physiology and Biochemistry*, 51(4). Available at: https://doi.org/10.1159/000495719.

He, Y. *et al.* (2018) “ALKBH5 Inhibits Pancreatic Cancer Motility by Decreasing Long Non-Coding RNA KCNK15-AS1 Methylation,” *Cellular Physiology and Biochemistry*, 48(2). Available at: https://doi.org/10.1159/000491915.

Heiss, N.S. *et al.* (1998) “X-linked dyskeratosis congenita is caused by mutations in a highly conserved gene with putative nucleolar functions,” *Nature Genetics*, 19(1). Available at: https://doi.org/10.1038/ng0598-32.

Helmrich, A., Ballarino, M. and Tora, L. (2011) “Collisions between Replication and Transcription Complexes Cause Common Fragile Site Instability at the Longest Human Genes,” *Molecular Cell*, 44(6). Available at: https://doi.org/10.1016/j.molcel.2011.10.013.

Hill, S.J. *et al.* (2014) “Systematic screening reveals a role for BRCA1 in the response to transcription-associated DNA damage.,” *Genes & development*, 28(17). Available at: https://doi.org/10.1101/gad.241620.114.

Hoek, K.S. *et al.* (1998) “hnRNP A2 selectively binds the cytoplasmic transport sequence of myelin basic protein mRNA,” *Biochemistry*, 37(19). Available at: https://doi.org/10.1021/bi9800247.

Hofweber, M. and Dormann, D. (2019) “Friend or foe—Post-translational modifications as regulators of phase separation and RNP granule dynamics,” *Journal of Biological Chemistry*, 294(18). Available at: https://doi.org/10.1074/jbc.TM118.001189.

Homma, T. *et al.* (2006) “Correlation Among Pathology, Genotype, and Patient Outcomes in Glioblastoma,” *Journal of Neuropathology and Experimental Neurology*, 65(9). Available at: https://doi.org/10.1097/01.jnen.0000235118.75182.94.

Horiuchi, K. *et al.* (2006) “Wilms’ tumor 1-associating protein regulates G2/M transition through stabilization of cyclin A2 mRNA,” *PNAS*, 103(46), pp. 17278–17283.

Horiuchi, K. *et al.* (2013) “Identification of Wilms’ tumor 1-associating protein complex and its role in alternative splicing and the cell cycle,” *Journal of Biological Chemistry*, 288(46), pp. 33292–22302.

Hosseini, S.A. *et al.* (2013) “Common chromosome fragile sites in human and murine epithelial cells and *FHIT/FRA3B* loss-induced global genome instability,” *Genes, Chromosomes and Cancer*, 52(11). Available at: https://doi.org/10.1002/gcc.22097.

Hsieh, J.-Y. *et al.* (2013) “miR-146a-5p circuitry uncouples cell proliferation and migration, but not differentiation, in human mesenchymal stem cells,” *Nucleic Acids Research*, 41(21). Available at: https://doi.org/10.1093/nar/gkt666.

Hsu, P.J. *et al.* (2017) “Ythdc2 is an N6-methyladenosine binding protein that regulates mammalian spermatogenesis,” *Cell Research*, 27(9). Available at: https://doi.org/10.1038/cr.2017.99.

Hu, Y. *et al.* (2017) “Splicing factor hnRNPA2B1 contributes to tumorigenic potential of breast cancer cells through STAT3 and ERK1/2 signaling pathway,” *Tumour Biology*, 39(3).

Hu, Z. *et al.* (2006) “An antibody-based microarray assay for small RNA detection,” *Nucleic Acids Research*, 34(7). Available at: https://doi.org/10.1093/nar/gkl142.

Hua, Y. *et al.* (2008) “Antisense Masking of an hnRNP A1/A2 Intronic Splicing Silencer Corrects SMN2 Splicing in Transgenic Mice,” *The American Journal of Human Genetics*, 82(4). Available at: https://doi.org/10.1016/j.ajhg.2008.01.014.

Huang, F.-T. *et al.* (2006) “Downstream boundary of chromosomal R-loops at murine switch regions: Implications for the mechanism of class switch recombination,” *Proceedings of the National Academy of Sciences*, 103(13). Available at: https://doi.org/10.1073/pnas.0506548103.

Huang, F.-T. *et al.* (2007) “Sequence Dependence of Chromosomal R-Loops at the Immunoglobulin Heavy-Chain Sμ Class Switch Region,” *Molecular and Cellular Biology*, 27(16). Available at: https://doi.org/10.1128/MCB.00702-07.

Huang, H. *et al.* (2018) “Recognition of RNA N6-methyladenosine by IGF2BP proteins enhances mRNA stability and translation,” *Nature Cell Biology*, 20(3). Available at: https://doi.org/10.1038/s41556-018-0045-z.

Huang, T. *et al.* (2019) “Genome-wide identification of mRNA 5-methylcytosine in mammals,” *Nature Structural & Molecular Biology*, 26(5). Available at: https://doi.org/10.1038/s41594-019-0218-x.

Hudson, W.H. and Ortlund, E.A. (2014) “The structure, function and evolution of proteins that bind DNA and RNA,” *Nature Reviews Molecular Cell Biology*, 15(11). Available at: https://doi.org/10.1038/nrm3884.

Huelga, S.C. *et al.* (2012) “Integrative Genome-wide Analysis Reveals Cooperative Regulation of Alternative Splicing by hnRNP Proteins,” *Cell Reports*, 1(2). Available at: https://doi.org/10.1016/j.celrep.2012.02.001.

Huertas, P. and Aguilera, A. (2003) “Cotranscriptionally Formed DNA:RNA Hybrids Mediate Transcription Elongation Impairment and Transcription-Associated Recombination,” *Molecular Cell*, 12(3). Available at: https://doi.org/10.1016/j.molcel.2003.08.010.

Hughes, P. *et al.* (2007) “The costs of using unauthenticated, over-passaged cell lines: how much more data do we need?,” *BioTechniques*, 43(5). Available at: https://doi.org/10.2144/000112598.

Hussain, T. *et al.* (2018) “Delineating WWOX Protein Interactome by Tandem Affinity Purification-Mass Spectrometry: Identification of Top Interactors and Key Metabolic Pathways Involved,” *Frontiers in Oncology*, 8. Available at: https://doi.org/10.3389/fonc.2018.00591.

Hussain, T. *et al.* (2019) “WWOX, the FRA16D gene: A target of and a contributor to genomic instability,” *Genes Chromosomes and Cancer*. Available at: https://doi.org/10.1002/gcc.22693.

Hutchison, S. *et al.* (2002) “Distinct Sets of Adjacent Heterogeneous Nuclear Ribonucleoprotein (hnRNP) A1/A2 Binding Sites Control 5′ Splice Site Selection in the hnRNP A1 mRNA Precursor,” *Journal of Biological Chemistry*, 277(33). Available at: https://doi.org/10.1074/jbc.M203633200.

Ivanov, Delyan P. *et al.* (2016) “In vitro models of medulloblastoma: Choosing the right tool for the job,” *Journal of Biotechnology*, 236. Available at: https://doi.org/10.1016/j.jbiotec.2016.07.028.

Ivanov, Delyan P *et al.* (2016) “Separating chemotherapy-related developmental neurotoxicity from cytotoxicity in monolayer and neurosphere cultures of human fetal brain cells.,” *Toxicology in vitro : an international journal published in association with BIBRA*, 37, pp. 88–96. Available at: https://doi.org/10.1016/j.tiv.2016.09.007.

Jack, K. *et al.* (2011) “rRNA Pseudouridylation Defects Affect Ribosomal Ligand Binding and Translational Fidelity from Yeast to Human Cells,” *Molecular Cell*, 44(4). Available at: https://doi.org/10.1016/j.molcel.2011.09.017.

Jackson, M., Hassiotou, F. and Nowak, A. (2015) “Glioblastoma stem-like cells: at the root of tumor recurrence and a therapeutic target,” *Carcinogenesis*, 36(2). Available at: https://doi.org/10.1093/carcin/bgu243.

Jahner, D. *et al.* (1982) “De novo Methylation and Expression of Retroviral Genomes during Mouse Embryogenesis,” *Nature*, 298(5875), pp. 623–8.

Jen, J. *et al.* (1994) “Deletion of p16 and p15 Genes in Brain Tumors,” *Cancer research*, 54(24), pp. 6353–6358.

Jenjaroenpun, P. *et al.* (2017) “R-loopDB: a database for R-loop forming sequences (RLFS) and R-loops,” *Nucleic Acids Research*, 45(D1). Available at: https://doi.org/10.1093/nar/gkw1054.

Jia, G. *et al.* (2011) “N6-methyladenosine in nuclear RNA is a major substrate of the obesity-associated FTO,” *Nature Chemical Biology*, 7(12), pp. 885–887.

Jiang, X. *et al.* (2021) “The role of m6A modification in the biological functions and diseases,” *Signal Transduction and Targeted Therapy*, 6(1). Available at: https://doi.org/10.1038/s41392-020-00450-x.

Johannessen, L.E. *et al.* (2018) “MGMT Gene Promoter Methylation Status – Assessment of Two Pyrosequencing Kits and Three Methylation-specific PCR Methods for their Predictive Capacity in Glioblastomas,” *Cancer Genomics - Proteomics*, 15(6). Available at: https://doi.org/10.21873/cgp.20102.

Kao, Y.-P. *et al.* (2013) “Detection and characterization of R-loops at the murine immunoglobulin Sα region,” *Molecular Immunology*, 54(2). Available at: https://doi.org/10.1016/j.molimm.2012.11.009.

Kapitonov, V. and Jurkal, J. (1996) “The age of Alu subfamilies,” *Journal of Molecular Evolution*, 42(1). Available at: https://doi.org/10.1007/BF00163212.

Karijolich, J., Yi, C. and Yu, Y.-T. (2015) “Transcriptome-wide dynamics of RNA pseudouridylation,” *Nature Reviews Molecular Cell Biology*, 16(10). Available at: https://doi.org/10.1038/nrm4040.

Kaya-Okur, H.S. *et al.* (2019) “CUT&Tag for efficient epigenomic profiling of small samples and single cells,” *Nature Communications*, 10(1). Available at: https://doi.org/10.1038/s41467-019-09982-5.

Keskin, H. *et al.* (2014) “Transcript-RNA-templated DNA recombination and repair,” *Nature*, 515(7527). Available at: https://doi.org/10.1038/nature13682.

Kim, D.D.Y. *et al.* (2004) “Widespread RNA Editing of Embedded Alu Elements in the Human Transcriptome,” *Genome Research*, 14(9). Available at: https://doi.org/10.1101/gr.2855504.

Kim, E., Magen, A. and Ast, G. (2007) “Different levels of alternative splicing among eukaryotes,” *Nucleic Acids Research*, 35(1). Available at: https://doi.org/10.1093/nar/gkl924.

Kim, H.J. *et al.* (2013) “Mutations in prion-like domains in hnRNPA2B1 and hnRNPA1 cause multisystem proteinopathy and ALS,” *Nature*, 495(7442). Available at: https://doi.org/10.1038/nature11922.

Kiss, T., Fayet-Lebaron, E. and Jády, B.E. (2010) “Box H/ACA Small Ribonucleoproteins,” *Molecular Cell*, 37(5). Available at: https://doi.org/10.1016/j.molcel.2010.01.032.

Knuckles, P. *et al.* (2018) “Zc3h13/Flacc is required for adenosine methylation by bridging the mRNA-binding factor Rbm15/Spenito to the m6A machinery component Wtap/Fl(2)d,” *Genes & Development*, 32(5–6). Available at: https://doi.org/10.1101/gad.309146.117.

Ko, C.-Y. *et al.* (2016) “IL-18-induced interaction between IMP3 and HuR contributes to COX-2 mRNA stabilization in acute myeloid leukemia.,” *Journal of leukocyte biology*, 99(1). Available at: https://doi.org/10.1189/jlb.2A0414-228RR.

Koch, F. *et al.* (2011) “Transcription initiation platforms and GTF recruitment at tissue-specific enhancers and promoters,” *Nature Structural & Molecular Biology*, 18(8). Available at: https://doi.org/10.1038/nsmb.2085.

Kohli, R.M. and Zhang, Y. (2013) “TET enzymes, TDG and the dynamics of DNA demethylation,” *Nature*, 502(7472), pp. 472–479.

Kong, F. *et al.* (2020) “Downregulation of METTL14 increases apoptosis and autophagy induced by cisplatin in pancreatic cancer cells,” *The International Journal of Biochemistry & Cell Biology*, 122. Available at: https://doi.org/10.1016/j.biocel.2020.105731.

König, F., Schubert, T. and Längst, G. (2017) “The monoclonal S9.6 antibody exhibits highly variable binding affinities towards different R-loop sequences,” *PLOS ONE*, 12(6). Available at: https://doi.org/10.1371/journal.pone.0178875.

Kool, M. *et al.* (2008) “Integrated Genomics Identifies Five Medulloblastoma Subtypes with Distinct Genetic Profiles, Pathway Signatures and Clinicopathological Features,” *PLoS ONE*, 3(8). Available at: https://doi.org/10.1371/journal.pone.0003088.

Kool, M. *et al.* (2012) “Molecular subgroups of medulloblastoma: an international meta-analysis of transcriptome, genetic aberrations, and clinical data of WNT, SHH, Group 3, and Group 4 medulloblastomas,” *Acta Neuropathologica*, 123(4). Available at: https://doi.org/10.1007/s00401-012-0958-8.

Kool, M. *et al.* (2014) “Genome Sequencing of SHH Medulloblastoma Predicts Genotype-Related Response to Smoothened Inhibition,” *Cancer Cell*, 25(3). Available at: https://doi.org/10.1016/j.ccr.2014.02.004.

Kotecki, M. (1999) “Isolation and Characterization of a Near-Haploid Human Cell Line,” *Experimental Cell Research*, 252(2). Available at: https://doi.org/10.1006/excr.1999.4656.

Kouzine, F. *et al.* (2017) “Permanganate/S1 Nuclease Footprinting Reveals Non-B DNA Structures with Regulatory Potential across a Mammalian Genome,” *Cell Systems*, 4(3). Available at: https://doi.org/10.1016/j.cels.2017.01.013.

Kozu, T., Henrich, B. and Schäfer, K.P. (1995) “Structure and expression of the gene (HNRPA2B1) encoding the human hnRNP protein A2/B1,” *Genomics*, 25(2). Available at: https://doi.org/10.1016/0888-7543(95)80035-K.

Kriaucionis, S. and Heintz, N. (2009) “The Nuclear DNA Base 5-Hydroxymethylcytosine Is Present in Purkinje Neurons and the Brain,” *Science*, 324(5929), pp. 929–930. Available at: https://doi.org/10.1126/science.1169786.

Kumar, L. *et al.* (2015) “Medulloblastoma: A common pediatric tumor: Prognostic factors and predictors of outcome,” *Asian Journal of Neurosurgery*, 10(1). Available at: https://doi.org/10.4103/1793-5482.151516.

Kuroki, T. *et al.* (2002) “Genetic alterations of the tumor suppressor gene WWOX in esophageal squamous cell carcinoma,” *Cancer Res*, 62(8), pp. 2258–2260.

Kwon, S., Barbarese, E. and Carson, J.H. (1999) “The cis-acting RNA trafficking signal from myelin basic protein mRNA and its cognate trans-acting ligand hnRNP A2 enhance cap-dependent translation,” *Journal of Cell Biology*, 147(2). Available at: https://doi.org/10.1083/jcb.147.2.247.

Lang, K.S. *et al.* (2017) “Replication-Transcription Conflicts Generate R-Loops that Orchestrate Bacterial Stress Survival and Pathogenesis,” *Cell*, 170(4). Available at: https://doi.org/10.1016/j.cell.2017.07.044.

Lee, J. *et al.* (2006) “Tumor stem cells derived from glioblastomas cultured in bFGF and EGF more closely mirror the phenotype and genotype of primary tumors than do serum-cultured cell lines,” *Cancer Cell*, 9(5). Available at: https://doi.org/10.1016/j.ccr.2006.03.030.

Lee, J.-H. *et al.* (2021) “Enhancer RNA m6A methylation facilitates transcriptional condensate formation and gene activation.,” *Molecular cell*, 81(16). Available at: https://doi.org/10.1016/j.molcel.2021.07.024.

Lee, Y. *et al.* (2020) “Molecular Mechanisms Driving mRNA Degradation by m6A Modification,” *Trends in Genetics*, 36(3). Available at: https://doi.org/10.1016/j.tig.2019.12.007.

Legrand, C. *et al.* (2017) “Statistically robust methylation calling for whole-transcriptome bisulfite sequencing reveals distinct methylation patterns for mouse RNAs,” *Genome Research*, 27(9). Available at: https://doi.org/10.1101/gr.210666.116.

Le Tallec, B. *et al.* (2013) “Common Fragile Site Profiling in Epithelial and Erythroid Cells Reveals that Most Recurrent Cancer Deletions Lie in Fragile Sites Hosting Large Genes,” *Cell Reports*, 4(3). Available at: https://doi.org/10.1016/j.celrep.2013.07.003.

Letessier, A. *et al.* (2011) “Cell-type-specific replication initiation programs set fragility of the FRA3B fragile site,” *Nature*, 470(7332). Available at: https://doi.org/10.1038/nature09745.

Li, A. *et al.* (2017) “Cytoplasmic m6A reader YTHDF3 promotes mRNA translation,” *Cell Research*, 27(3). Available at: https://doi.org/10.1038/cr.2017.10.

Li, J. *et al.* (2019) “The m6A demethylase FTO promotes the growth of lung cancer cells by regulating the m6A level of USP7 mRNA,” *Biochemical and Biophysical Research Communications*, 512(3). Available at: https://doi.org/10.1016/j.bbrc.2019.03.093.

Li, S. and Mason, C.E. (2014) “The Pivotal Regulatory Landscape of RNA Modifications,” *Annual Review of Genomics and Human Genetics*, 15(1). Available at: https://doi.org/10.1146/annurev-genom-090413-025405.

Li, T. *et al.* (2019) “METTL3 facilitates tumor progression via an m6A-IGF2BP2-dependent mechanism in colorectal carcinoma,” *Molecular Cancer*, 18(1). Available at: https://doi.org/10.1186/s12943-019-1038-7.

Li, X. *et al.* (2014) “Lobaplatin arrests cell cycle progression, induces apoptosis and alters the proteome in human cervical cancer cell Line CaSki,” *Biomedicine & Pharmacotherapy*, 68(3). Available at: https://doi.org/10.1016/j.biopha.2013.10.004.

Li, X. *et al.* (2015) “Chemical pulldown reveals dynamic pseudouridylation of the mammalian transcriptome,” *Nature Chemical Biology*, 11(8). Available at: https://doi.org/10.1038/nchembio.1836.

Li, X. *et al.* (2016) “Transcriptome-wide mapping reveals reversible and dynamic N1-methyladenosine methylome,” *Nature Chemical Biology*, 12(5). Available at: https://doi.org/10.1038/nchembio.2040.

Li, X. *et al.* (2017) “The M6A methyltransferase METTL3: acting as a tumor suppressor in renal cell carcinoma,” *Oncotarget*, 8(56). Available at: https://doi.org/10.18632/oncotarget.21726.

Li, X., Ma, S. and Yi, C. (2016) “Pseudouridine: the fifth RNA nucleotide with renewed interests,” *Current Opinion in Chemical Biology*, 33. Available at: https://doi.org/10.1016/j.cbpa.2016.06.014.

Li, X. and Manley, J. (2005) “Inactivation of the SR protein splicing factor ASF/SF2 results in genomic instability,” *Cell*, 122(3), pp. 365–378.

Li, X., Niu, T. and Manley, J.L. (2007) “The RNA binding protein RNPS1 alleviates ASF/SF2 depletion-induced genomic instability,” *RNA*, 13(12). Available at: https://doi.org/10.1261/rna.734407.

Li, X., Xiong, X. and Yi, C. (2017) “Epitranscriptome sequencing technologies: decoding RNA modifications,” *Nature Methods*, 14(1). Available at: https://doi.org/10.1038/nmeth.4110.

Li, Y. *et al.* (2018) “Novel long noncoding RNA NMR promotes tumor progression via NSUN2 and BPTF in esophageal squamous cell carcinoma,” *Cancer Letters*, 430. Available at: https://doi.org/10.1016/j.canlet.2018.05.013.

Li, Y. *et al.* (2019) “Flexible Binding of m6A Reader Protein YTHDC1 to Its Preferred RNA Motif,” *Journal of Chemical Theory and Computation*, 15(12). Available at: https://doi.org/10.1021/acs.jctc.9b00987.

Li, Zejuan *et al.* (2017) “FTO Plays an Oncogenic Role in Acute Myeloid Leukemia as a N 6 -Methyladenosine RNA Demethylase,” *Cancer Cell*, 31(1). Available at: https://doi.org/10.1016/j.ccell.2016.11.017.

Li, Z *et al.* (2017) “FTO Plays an Oncogenic Role in Acute Myeloid Leukemia as a N6-Methyladenosine RNA Demethylase,” *Cancer Cell*, 31(1), pp. 127–141.

Linder, B. *et al.* (2015) “Single-nucleotide-resolution mapping of m6A and m6Am throughout the transcriptome,” *Nature Methods*, 12(8). Available at: https://doi.org/10.1038/nmeth.3453.

Listerman, I., Sapra, A.K. and Neugebauer, K.M. (2006) “Cotranscriptional coupling of splicing factor recruitment and precursor messenger RNA splicing in mammalian cells,” *Nature Structural and Molecular Biology*, 13(9). Available at: https://doi.org/10.1038/nsmb1135.

Little, N., Hastie, N. and Davies, R. (2000) “Identification of WTAP, a novel Wilms’ tumour 1-associating protein,” *Human Molecular Genetics*, 9(15), pp. 2231–2239.

Liu, F. *et al.* (2016) “ALKBH1-Mediated tRNA Demethylation Regulates Translation,” *Cell*, 167(3). Available at: https://doi.org/10.1016/j.cell.2016.09.038.

Liu, J. *et al.* (2020) “Landscape and Regulation of m6A and m6Am Methylome across Human and Mouse Tissues,” *Molecular Cell*, 77(2). Available at: https://doi.org/10.1016/j.molcel.2019.09.032.

Liu, K.-W. *et al.* (2017) “Molecular mechanisms and therapeutic targets in pediatric brain tumors,” *Science Signaling*, 10(470). Available at: https://doi.org/10.1126/scisignal.aaf7593.

Liu, N. *et al.* (2015) “N6-methyladenosine-dependent RNA structural switches regulate RNA–protein interactions,” *Nature*, 518(7540). Available at: https://doi.org/10.1038/nature14234.

Liu, N. and Pan, T. (2016) “N6-methyladenosine–encoded epitranscriptomics,” *Nature Structural & Molecular Biology*, 23(2), pp. 98–102. Available at: https://doi.org/10.1038/nsmb.3162.

Liu, Y. *et al.* (2020) “Heterogeneous nuclear ribonucleoprotein A2/B1 is a negative regulator of human breast cancer metastasis by maintaining the balance of multiple genes and pathways,” *EBioMedicine*, 51. Available at: https://doi.org/10.1016/j.ebiom.2019.11.044.

Livak, K.J. and Schmittgen, T.D. (2001) “Analysis of Relative Gene Expression Data Using Real-Time Quantitative PCR and the 2−ΔΔCT Method,” *Methods*, 25(4), pp. 402–408. Available at: https://doi.org/10.1006/METH.2001.1262.

Livneh, I. *et al.* (2020) “The m6A epitranscriptome: transcriptome plasticity in brain development and function,” *Nature Reviews Neuroscience*, 21(1). Available at: https://doi.org/10.1038/s41583-019-0244-z.

Long, J.C. and Caceres, J.F. (2009) “The SR protein family of splicing factors: master regulators of gene expression,” *Biochemical Journal*, 417(1). Available at: https://doi.org/10.1042/BJ20081501.

Loomis, E.W. *et al.* (2014) “Transcription-Associated R-Loop Formation across the Human FMR1 CGG-Repeat Region,” *PLoS Genetics*, 10(4). Available at: https://doi.org/10.1371/journal.pgen.1004294.

Louis, D.N. *et al.* (2016) “The 2016 World Health Organization Classification of Tumors of the Central Nervous System: a summary,” *Acta Neuropathologica*, 131(6). Available at: https://doi.org/10.1007/s00401-016-1545-1.

Lu, W.-T. *et al.* (2018) “Drosha drives the formation of DNA:RNA hybrids around DNA break sites to facilitate DNA repair,” *Nature Communications*, 9(1). Available at: https://doi.org/10.1038/s41467-018-02893-x.

Luke, B. *et al.* (2008) “The Rat1p 5’ to 3’ exonuclease degrades telomeric repeat-containing RNA and promotes telomere elongation in Saccharomyces cerevisiae.,” *Molecular cell*, 32(4). Available at: https://doi.org/10.1016/j.molcel.2008.10.019.

Ma, C. *et al.* (2018) “RNA m 6 A methylation participates in regulation of postnatal development of the mouse cerebellum,” pp. 1–18.

Ma, F. *et al.* (2019) “Long non-coding RNA FGF13-AS1 inhibits glycolysis and stemness properties of breast cancer cells through FGF13-AS1/IGF2BPs/Myc feedback loop,” *Cancer Letters*, 450. Available at: https://doi.org/10.1016/j.canlet.2019.02.008.

Ma, H. *et al.* (2020) “Specific glioblastoma multiforme prognostic-subtype distinctions based on DNA methylation patterns,” *Cancer Gene Therapy*, 27(9). Available at: https://doi.org/10.1038/s41417-019-0142-6.

MacDonald, B.T., Tamai, K. and He, X. (2009) “Wnt/β-Catenin Signaling: Components, Mechanisms, and Diseases,” *Developmental Cell*, 17(1). Available at: https://doi.org/10.1016/j.devcel.2009.06.016.

Maden, B.E.H. (1986) “Identification of the locations of the methyl groups in 18 S ribosomal RNA from Xenopus laevis and man,” *Journal of Molecular Biology*, 189(4). Available at: https://doi.org/10.1016/0022-2836(86)90498-5.

Maden, B.E.H. (1988) “Locations of methyl groups in 28 S rRNA of Xenopus laevis and man,” *Journal of Molecular Biology*, 201(2). Available at: https://doi.org/10.1016/0022-2836(88)90139-8.

Makhafola, T.J. *et al.* (2020) “Apoptosis in Cancer Cells Is Induced by Alternative Splicing of hnRNPA2/B1 Through Splicing of Bcl-x, a Mechanism that Can Be Stimulated by an Extract of the South African Medicinal Plant, Cotyledon orbiculata,” *Frontiers in Oncology*, 10. Available at: https://doi.org/10.3389/fonc.2020.547392.

Malig, M. *et al.* (2020) “Ultra-deep Coverage Single-molecule R-loop Footprinting Reveals Principles of R-loop Formation,” *Journal of Molecular Biology*, 432(7). Available at: https://doi.org/10.1016/j.jmb.2020.02.014.

Mamouni, K. *et al.* (2014) “RhoB Promotes γH2AX Dephosphorylation and DNA Double-Strand Break Repair,” *Molecular and Cellular Biology*, 34(16). Available at: https://doi.org/10.1128/MCB.01525-13.

Mao, Y. *et al.* (2019) “m6A in mRNA coding regions promotes translation via the RNA helicase-containing YTHDC2,” *Nature Communications*, 10(1). Available at: https://doi.org/10.1038/s41467-019-13317-9.

Marino, S. (2005) “Medulloblastoma: developmental mechanisms out of control,” *Trends in Molecular Medicine*, 11(1). Available at: https://doi.org/10.1016/j.molmed.2004.11.008.

Marusyk, A. and Polyak, K. (2010) “Tumor heterogeneity: Causes and consequences,” *Biochimica et Biophysica Acta (BBA) - Reviews on Cancer*, 1805(1). Available at: https://doi.org/10.1016/j.bbcan.2009.11.002.

Mauer, J. *et al.* (2017) “Reversible methylation of m6Am in the 5′ cap controls mRNA stability,” *Nature*, 541(7637). Available at: https://doi.org/10.1038/nature21022.

Mayeda, A. *et al.* (1994) “Function of conserved domains of hnRNP A1 and other hnRNP A/B proteins,” *EMBO J.*, 13(22), pp. 5483–5495.

Mayeda, A. and Krainer, A.R. (1992) “Regulation of alternative pre-mRNA splicing by hnRNP A1 and splicing factor SF2,” *Cell*, 68(2). Available at: https://doi.org/10.1016/0092-8674(92)90477-T.

Mazina, O.M. *et al.* (2017) “Rad52 Inverse Strand Exchange Drives RNA-Templated DNA Double-Strand Break Repair,” *Molecular Cell*, 67(1). Available at: https://doi.org/10.1016/j.molcel.2017.05.019.

Mazumdar, T. *et al.* (2013) “Hedgehog Signaling Regulates Telomerase Reverse Transcriptase in Human Cancer Cells,” *PLoS ONE*, 8(9). Available at: https://doi.org/10.1371/journal.pone.0075253.

McCloskey, A. *et al.* (2012) “hnRNP C Tetramer Measures RNA Length to Classify RNA Polymerase II Transcripts for Export,” *Science*, 335(6076). Available at: https://doi.org/10.1126/science.1218469.

Mears, W.E. and Rice, S.A. (1996) “The RGG box motif of the herpes simplex virus ICP27 protein mediates an RNA-binding activity and determines in vivo methylation.,” *Journal of virology*, 70(11). Available at: https://doi.org/10.1128/jvi.70.11.7445-7453.1996.

Menyhárt, O., Giangaspero, F. and Győrffy, B. (2019) “Molecular markers and potential therapeutic targets in non-WNT/non-SHH (group 3 and group 4) medulloblastomas,” *Journal of Hematology & Oncology*, 12(1). Available at: https://doi.org/10.1186/s13045-019-0712-y.

Merkurjev, D. *et al.* (2018) “Synaptic N6-methyladenosine (m6A) epitranscriptome reveals functional partitioning of localized transcripts,” *Nature Neuroscience*, 21(7). Available at: https://doi.org/10.1038/s41593-018-0173-6.

Meyer, K. *et al.* (2012) “Comprehensive Analysis of mRNA Methylation Reveals Enrichment in 3’ UTRs and Near Stop Codons,” *Cell*, 149(7), pp. 1635–1646. Available at: https://doi.org/10.1016/j.cell.2012.05.003.Comprehensive.

Meyer, K.D. and Jaffrey, S.R. (2014) “The dynamic epitranscriptome: N6-methyladenosine and gene expression control,” *Nature Reviews Molecular Cell Biology*, 15(5). Available at: https://doi.org/10.1038/nrm3785.

Miki, Y. *et al.* (1994) “A Strong Candidate for the Breast and Ovarian Cancer Susceptibility Gene BRCA1,” *Science*, 266(5182). Available at: https://doi.org/10.1126/science.7545954.

Mischo, H.E. *et al.* (2011) “Yeast Sen1 helicase protects the genome from transcription-associated instability.,” *Molecular cell*, 41(1). Available at: https://doi.org/10.1016/j.molcel.2010.12.007.

Montanaro, L. *et al.* (2010) “Novel Dyskerin-Mediated Mechanism of p53 Inactivation through Defective mRNA Translation,” *Cancer Research*, 70(11). Available at: https://doi.org/10.1158/0008-5472.CAN-09-4024.

Morales, J.C. *et al.* (2016) “XRN2 Links Transcription Termination to DNA Damage and Replication Stress,” *PLOS Genetics*, 12(7). Available at: https://doi.org/10.1371/journal.pgen.1006107.

Moreira, M.-C. *et al.* (2004) “Senataxin, the ortholog of a yeast RNA helicase, is mutant in ataxia-ocular apraxia 2,” *Nature Genetics*, 36(3). Available at: https://doi.org/10.1038/ng1303.

Motorin, Y. and Helm, M. (2010) “tRNA Stabilization by Modified Nucleotides,” *Biochemistry*, 49(24). Available at: https://doi.org/10.1021/bi100408z.

Mozaffari-Jovin, S. *et al.* (2014) “Novel regulatory principles of the spliceosomal Brr2 RNA helicase and links to retinal disease in humans,” *RNA Biology*, 11(4). Available at: https://doi.org/10.4161/rna.28353.

Muslimov, I.A. *et al.* (2014) “Interactions of noncanonical motifs with hnRNP A2 promote activity-dependent RNA transport in neurons,” *Journal of Cell Biology*, 205(4). Available at: https://doi.org/10.1083/jcb.201310045.

Nachtergaele, S. and He, C. (2017) “The emerging biology of RNA post-transcriptional modifications,” *RNA biology*, 14(2), pp. 156–163.

Nadel, J. *et al.* (2015) “RNA : DNA hybrids in the human genome have distinctive nucleotide characteristics , chromatin composition , and transcriptional relationships,” *Epigenetics & Chromatin*, pp. 1–19. Available at: https://doi.org/10.1186/s13072-015-0040-6.

Nasir, A. *et al.* (2021) “ABCB1 inhibition provides a novel therapeutic target to block TWIST1-induced migration in medulloblastoma,” *Neuro-Oncology Advances*, 3(1). Available at: https://doi.org/10.1093/noajnl/vdab030.

Nichols, R.C. *et al.* (2000) “The RGG Domain in hnRNP A2 Affects Subcellular Localization,” *Experimental Cell Research*, 256(2). Available at: https://doi.org/10.1006/excr.2000.4827.

Nishikura, K. (2010) “Functions and Regulation of RNA Editing by ADAR Deaminases,” *Annual Review of Biochemistry*, 79(1). Available at: https://doi.org/10.1146/annurev-biochem-060208-105251.

Nishikura, K. (2016) “A-to-I editing of coding and non-coding RNAs by ADARs,” *Nature Reviews Molecular Cell Biology*, 17(2). Available at: https://doi.org/10.1038/nrm.2015.4.

Niu, Y. *et al.* (2019) “RNA N6-methyladenosine demethylase FTO promotes breast tumor progression through inhibiting BNIP3,” *Molecular Cancer*, 18(1). Available at: https://doi.org/10.1186/s12943-019-1004-4.

Nojima, T. *et al.* (2015) “Mammalian NET-Seq Reveals Genome-wide Nascent Transcription Coupled to RNA Processing,” *Cell*, 161(3). Available at: https://doi.org/10.1016/j.cell.2015.03.027.

Nojima, T. *et al.* (2018) “Deregulated Expression of Mammalian lncRNA through Loss of SPT6 Induces R-Loop Formation, Replication Stress, and Cellular Senescence,” *Molecular Cell*, 72(6). Available at: https://doi.org/10.1016/j.molcel.2018.10.011.

Northcott, P.A. *et al.* (2011) “Pediatric and adult sonic hedgehog medulloblastomas are clinically and molecularly distinct,” *Acta Neuropathologica*, 122(2). Available at: https://doi.org/10.1007/s00401-011-0846-7.

Northcott, P.A., Jones, D.T.W., *et al.* (2012) “Medulloblastomics: the end of the beginning,” *Nature Reviews Cancer*, 12(12). Available at: https://doi.org/10.1038/nrc3410.

Northcott, P.A., Shih, D.J.H., Remke, M., *et al.* (2012) “Rapid, reliable, and reproducible molecular sub-grouping of clinical medulloblastoma samples,” *Acta Neuropathologica*, 123(4). Available at: https://doi.org/10.1007/s00401-011-0899-7.

Northcott, P.A., Shih, D.J.H., Peacock, J., *et al.* (2012) “Subgroup-specific structural variation across 1,000 medulloblastoma genomes,” *Nature*, 488(7409). Available at: https://doi.org/10.1038/nature11327.

Northcott, P.A. *et al.* (2014) “Enhancer hijacking activates GFI1 family oncogenes in medulloblastoma,” *Nature*, 511(7510). Available at: https://doi.org/10.1038/nature13379.

Northcott, P.A. *et al.* (2017) “The whole-genome landscape of medulloblastoma subtypes,” *Nature*, 547(7663). Available at: https://doi.org/10.1038/nature22973.

Northcott, P.A. *et al.* (2019) “Medulloblastoma,” *Nature Reviews Disease Primers*, 5(1). Available at: https://doi.org/10.1038/s41572-019-0063-6.

Nott, A. *et al.* (2019) “Brain cell type–specific enhancer–promoter interactome maps and disease ‐ risk association,” *Science*, 366(6469). Available at: https://doi.org/10.1126/science.aay0793.

Ohle, C. *et al.* (2016) “Transient RNA-DNA Hybrids Are Required for Efficient Double-Strand Break Repair.,” *Cell*, 167(4). Available at: https://doi.org/10.1016/j.cell.2016.10.001.

Olsen, R.K.J. *et al.* (2014) “The ETFDH c.158A>G Variation Disrupts the Balanced Interplay of ESE- and ESS-Binding Proteins thereby Causing Missplicing and Multiple Acyl-CoA Dehydrogenation Deficiency,” *Human Mutation*, 35(1). Available at: https://doi.org/10.1002/humu.22455.

Ostrom, Q.T. *et al.* (2013) “CBTRUS Statistical Report: Primary Brain and Central Nervous System Tumors Diagnosed in the United States in 2006-2010,” *Neuro-Oncology*, 15(suppl 2). Available at: https://doi.org/10.1093/neuonc/not151.

Paris, J. *et al.* (2019) “Targeting the RNA m6A Reader YTHDF2 Selectively Compromises Cancer Stem Cells in Acute Myeloid Leukemia,” *Cell Stem Cell*, 25(1). Available at: https://doi.org/10.1016/j.stem.2019.03.021.

Park, T.S. *et al.* (1983) “Medulloblastoma: clinical presentation and management,” *Journal of Neurosurgery*, 58(4). Available at: https://doi.org/10.3171/jns.1983.58.4.0543.

Parsons, D.W. *et al.* (2008) “An Integrated Genomic Analysis of Human Glioblastoma Multiforme,” *Science*, 321(5897). Available at: https://doi.org/10.1126/science.1164382.

Patil, D.P. *et al.* (2016) “m6A RNA methylation promotes XIST-mediated transcriptional repression,” *Nature*, 537(7620), pp. 369–373. Available at: https://doi.org/10.1038/nature19342.m.

Paulsen, R.D. *et al.* (2009) “A Genome-wide siRNA Screen Reveals Diverse Cellular Processes and Pathways that Mediate Genome Stability,” *Molecular Cell*, 35(2). Available at: https://doi.org/10.1016/j.molcel.2009.06.021.

Pefanis, E. *et al.* (2015) “RNA Exosome-Regulated Long Non-Coding RNA Transcription Controls Super-Enhancer Activity,” *Cell*, 161(4). Available at: https://doi.org/10.1016/j.cell.2015.04.034.

Pendleton, K.E. *et al.* (2017) “The U6 snRNA m 6 A Methyltransferase METTL16 Regulates SAM Synthetase Intron Retention,” *Cell*, 169(5). Available at: https://doi.org/10.1016/j.cell.2017.05.003.

Peng, W. *et al.* (2019) “Upregulated METTL3 promotes metastasis of colorectal Cancer via miR-1246/SPRED2/MAPK signaling pathway,” *Journal of Experimental & Clinical Cancer Research*, 38(1). Available at: https://doi.org/10.1186/s13046-019-1408-4.

Penzo, M. and Montanaro, L. (2018) “Turning Uridines around: Role of rRNA Pseudouridylation in Ribosome Biogenesis and Ribosomal Function,” *Biomolecules*, 8(2). Available at: https://doi.org/10.3390/biom8020038.

Perreault, S. *et al.* (2014) “MRI Surrogates for Molecular Subgroups of Medulloblastoma,” *American Journal of Neuroradiology*, 35(7). Available at: https://doi.org/10.3174/ajnr.A3990.

Perry, R.P. and Kelley, D.E. (1974) “Existence of methylated messenger RNA in mouse L cells,” *Cell*, 1(1). Available at: https://doi.org/10.1016/0092-8674(74)90153-6.

Phillips, D.D. *et al.* (2013) “The sub-nanomolar binding of DNA-RNA hybrids by the single-chain Fv fragment of antibody S9.6,” *Journal of Molecular Recognition*, 26(8). Available at: https://doi.org/10.1002/jmr.2284.

Phillips, H.S. *et al.* (2006) “Molecular subclasses of high-grade glioma predict prognosis, delineate a pattern of disease progression, and resemble stages in neurogenesis,” *Cancer Cell*, 9(3). Available at: https://doi.org/10.1016/j.ccr.2006.02.019.

Pietrobono, S., Gagliardi, S. and Stecca, B. (2019) “Non-canonical Hedgehog Signaling Pathway in Cancer: Activation of GLI Transcription Factors Beyond Smoothened,” *Frontiers in Genetics*, 10. Available at: https://doi.org/10.3389/fgene.2019.00556.

Ping, X. *et al.* (2014) “Mammalian WTAP is a regulatory subunit of the RNA N6-methyladenosine methyltransferase,” *Cell Research*, 24(2), pp. 177–189.

Pollard, S.M. *et al.* (2009) “Glioma Stem Cell Lines Expanded in Adherent Culture Have Tumor-Specific Phenotypes and Are Suitable for Chemical and Genetic Screens,” *Cell Stem Cell*, 4(6). Available at: https://doi.org/10.1016/j.stem.2009.03.014.

Pomeroy, S.L. *et al.* (2002) “Prediction of central nervous system embryonal tumour outcome based on gene expression,” *Nature*, 415(6870). Available at: https://doi.org/10.1038/415436a.

Pozarowski, P. and Darzynkiewicz, Z. (2004) “Analysis of Cell Cycle by Flow Cytometry,” in *Checkpoint Controls and Cancer*. New Jersey: Humana Press, pp. 301–311. Available at: https://doi.org/10.1385/1-59259-811-0:301.

Pugh, T.J. *et al.* (2012) “Medulloblastoma exome sequencing uncovers subtype-specific somatic mutations,” *Nature*, 488(7409). Available at: https://doi.org/10.1038/nature11329.

Pui, C.-H. *et al.* (2011) “Challenging issues in pediatric oncology,” *Nature Reviews Clinical Oncology*, 8(9). Available at: https://doi.org/10.1038/nrclinonc.2011.95.

Qian, J.-Y. *et al.* (2019) “KIAA1429 acts as an oncogenic factor in breast cancer by regulating CDK1 in an N6-methyladenosine-independent manner,” *Oncogene*, 38(33). Available at: https://doi.org/10.1038/s41388-019-0861-z.

Quentin, Y. (1992) “Fusion of a free left Alu monomer and a free right Alu monometer at the origin of the Alu family in the primate genomes,” *Nucleic Acids Research*, 20(3). Available at: https://doi.org/10.1093/nar/20.3.487.

Rácz, I., Király, I. and Lásztily, D. (1978) “Effect of light on the nucleotide composition of rRNA of wheat seedlings,” *Planta*, 142(3). Available at: https://doi.org/10.1007/BF00385075.

Ramsawhook, A.H. *et al.* (2017) “Immunostaining for DNA Modifications: Computational Analysis of Confocal Images,” *Journal of Visualized Experiments* [Preprint], (127). Available at: https://doi.org/10.3791/56318.

Rausch, T. *et al.* (2012) “Genome Sequencing of Pediatric Medulloblastoma Links Catastrophic DNA Rearrangements with TP53 Mutations,” *Cell*, 148(1–2). Available at: https://doi.org/10.1016/j.cell.2011.12.013.

Rebagliati, M.R. and Melton, D.A. (1987) “Antisense RNA injections in fertilized frog eggs reveal an RNA duplex unwinding activity,” *Cell*, 48(4). Available at: https://doi.org/10.1016/0092-8674(87)90238-8.

Reijns, M.A.M. *et al.* (2012) “Enzymatic Removal of Ribonucleotides from DNA Is Essential for Mammalian Genome Integrity and Development,” *Cell*, 149(5). Available at: https://doi.org/10.1016/j.cell.2012.04.011.

Remke, M. *et al.* (2011) “Adult Medulloblastoma Comprises Three Major Molecular Variants,” *Journal of Clinical Oncology*, 29(19). Available at: https://doi.org/10.1200/JCO.2011.34.9373.

Richardson, J.P. (2003) “Loading Rho to terminate transcription.,” *Cell*, 114(2). Available at: https://doi.org/10.1016/s0092-8674(03)00554-3.

Ried, K. *et al.* (2000) “Common chromosomal fragile site FRA16D sequence: identification of the FOR gene spanning FRA16D and homozygous deletions and translocation breakpoints in cancer cells,” *Human Molecular Genetics*, 9(11). Available at: https://doi.org/10.1093/hmg/9.11.1651.

Rieger, A.M. *et al.* (2010) “Conventional apoptosis assays using propidium iodide generate a significant number of false positives that prevent accurate assessment of cell death,” *Journal of Immunological Methods*, 358(1–2). Available at: https://doi.org/10.1016/j.jim.2010.03.019.

Rieger, A.M. *et al.* (2011) “Modified Annexin V/Propidium Iodide Apoptosis Assay For Accurate Assessment of Cell Death,” *Journal of Visualized Experiments* [Preprint], (50). Available at: https://doi.org/10.3791/2597.

Ries, R.J. *et al.* (2019) “m6A enhances the phase separation potential of mRNA,” *Nature*, 571(7765). Available at: https://doi.org/10.1038/s41586-019-1374-1.

Roberts, R.W. and Crothers, D.M. (1992) “Stability and properties of double and triple helices: dramatic effects of RNA or DNA backbone composition.,” *Science (New York, N.Y.)*, 258(5087). Available at: https://doi.org/10.1126/science.1279808.

Robertson, F.L. *et al.* (2019) “Experimental models and tools to tackle glioblastoma,” *Disease Models & Mechanisms*, 12(9). Available at: https://doi.org/10.1242/dmm.040386.

Robinson, G. *et al.* (2012) “Novel mutations target distinct subgroups of medulloblastoma,” *Nature*, 488(7409). Available at: https://doi.org/10.1038/nature11213.

Roost, C. *et al.* (2015) “Structure and Thermodynamics of N6-Methyladenosine in RNA: A Spring-Loaded Base Modification,” *Journal of the American Chemical Society*, 137(5). Available at: https://doi.org/10.1021/ja513080v.

Roundtree, I.A. *et al.* (2017) “Dynamic RNA modifications in gene expression regulation,” *Cell*, 169(7), pp. 1187–1200. Available at: https://doi.org/10.1016/j.cell.2017.05.045.Dynamic.

Roy, D. *et al.* (2010) “Competition between the RNA transcript and the nontemplate DNA strand during R-loop formation in vitro: a nick can serve as a strong R-loop initiation site.,” *Molecular and cellular biology*, 30(1). Available at: https://doi.org/10.1128/MCB.00897-09.

Roy, P.H. and Weissbach, A. (1975) “DNA methylase from HeLa cell nuclei,” *Nucleic Acids Research*, 2(10), pp. 1669–1684.

Ruggero, D. (2003) “Dyskeratosis Congenita and Cancer in Mice Deficient in Ribosomal RNA Modification,” *Science*, 299(5604). Available at: https://doi.org/10.1126/science.1079447.

Safa, A.R. *et al.* (2015) “Glioblastoma stem cells (GSCs) epigenetic plasticity and interconversion between differentiated non-GSCs and GSCs,” *Genes & Diseases*, 2(2). Available at: https://doi.org/10.1016/j.gendis.2015.02.001.

Safra, M. *et al.* (2017) “The m1A landscape on cytosolic and mitochondrial mRNA at single-base resolution,” *Nature*, 551(7679). Available at: https://doi.org/10.1038/nature24456.

Saikia, M. *et al.* (2010) “Genome-wide analysis of N1-methyl-adenosine modification in human tRNAs,” *RNA*, 16(7). Available at: https://doi.org/10.1261/rna.2057810.

Salas-Armenteros, I. *et al.* (2017) “Human THO–Sin3A interaction reveals new mechanisms to prevent R-loops that cause genome instability,” *The EMBO Journal*, 36(23). Available at: https://doi.org/10.15252/embj.201797208.

Saletore, Y. *et al.* (2012) “The birth of the Epitranscriptome: deciphering the function of RNA modifications,” *Genome Biology*, 13(10). Available at: https://doi.org/10.1186/gb-2012-13-10-175.

Sanz, L.A. *et al.* (2016) “Structures Associate with Specific Epigenomic Signatures in Mammals Prevalent , Dynamic , and Conserved R-Loop Structures Associate with Specific Epigenomic Signatures in Mammals,” *Molecular Cell*, 63, pp. 167–178. Available at: https://doi.org/10.1016/j.molcel.2016.05.032.

Savage, K.I. *et al.* (2014) “Identification of a BRCA1-mRNA splicing complex required for efficient DNA repair and maintenance of genomic stability.,” *Molecular cell*, 54(3). Available at: https://doi.org/10.1016/j.molcel.2014.03.021.

Schevitz, R.W. *et al.* (1979) “Crystal structure of a eukaryotic initiator tRNA,” *Nature*, 278(5700). Available at: https://doi.org/10.1038/278188a0.

Schibler, U. and Perry, R.P. (1977) “The 5′-termini of heterogeneous nuclear RNA: a comparison among molecules of different sizes and ages,” *Nucleic Acids Research*, 4(12). Available at: https://doi.org/10.1093/nar/4.12.4133.

Schlacher, K., Wu, H. and Jasin, M. (2012) “A distinct replication fork protection pathway connects Fanconi anemia tumor suppressors to RAD51-BRCA1/2.,” *Cancer cell*, 22(1). Available at: https://doi.org/10.1016/j.ccr.2012.05.015.

Schosserer, M. *et al.* (2015) “Methylation of ribosomal RNA by NSUN5 is a conserved mechanism modulating organismal lifespan,” *Nature Communications*, 6(1). Available at: https://doi.org/10.1038/ncomms7158.

Schwalb, B. *et al.* (2016) “TT-seq maps the human transient transcriptome,” *Science*, 352(6290). Available at: https://doi.org/10.1126/science.aad9841.

Schwartz, S. *et al.* (2014) “Perturbation of m6A writers reveals two distinct classes of mRNA methylation at internal and 5’ sites,” *Cell Reports*, 8(1), pp. 284–296.

Scuteri, A. *et al.* (2007) “Genome-wide association scan shows genetic variants in the FTO gene are associated with obesity-related traits,” *PLoS Genetics*, 3(7), p. e115.

Sharma, A. *et al.* (2017) “Angiogenic Gene Signature Derived from Subtype Specific Cell Models Segregate Proneural and Mesenchymal Glioblastoma,” *Frontiers in Oncology*, 7. Available at: https://doi.org/10.3389/fonc.2017.00146.

Shelton, S.B., Reinsborough, C. and Xhemalce, B. (2016) “Who Watches the Watchmen: Roles of RNA Modifications in the RNA Interference Pathway,” *PLOS Genetics*, 12(7). Available at: https://doi.org/10.1371/journal.pgen.1006139.

Shen, C. *et al.* (2020) “RNA Demethylase ALKBH5 Selectively Promotes Tumorigenesis and Cancer Stem Cell Self-Renewal in Acute Myeloid Leukemia,” *Cell Stem Cell*, 27(1). Available at: https://doi.org/10.1016/j.stem.2020.04.009.

Shen, S. *et al.* (2021) “Comprehensive analyses of m6A regulators and interactive coding and non-coding RNAs across 32 cancer types,” *Molecular Cancer*, 20(1). Available at: https://doi.org/10.1186/s12943-021-01362-2.

Sherr, C.J., Beach, D. and Shapiro, G.I. (2016) “Targeting CDK4 and CDK6: From Discovery to Therapy,” *Cancer Discovery*, 6(4). Available at: https://doi.org/10.1158/2159-8290.CD-15-0894.

Shi, H. *et al.* (2017) “YTHDF3 facilitates translation and decay of N6-methyladenosine-modified RNA,” *Cell Research*, 27(3), pp. 315–328.

Shi, X. *et al.* (2018) “Knockdown of hnRNP A2/B1 inhibits cell proliferation, invasion and cell cycle triggering apoptosis in cervical cancer via PI3K/AKT signaling pathway,” *Oncology Reports* [Preprint]. Available at: https://doi.org/10.3892/or.2018.6195.

Shih, D.J.H. *et al.* (2014) “Cytogenetic Prognostication Within Medulloblastoma Subgroups,” *Journal of Clinical Oncology*, 32(9). Available at: https://doi.org/10.1200/JCO.2013.50.9539.

Shima, H. *et al.* (2017) “S-Adenosylmethionine Synthesis Is Regulated by Selective N6-Adenosine Methylation and mRNA Degradation Involving METTL16 and YTHDC1,” *Cell Reports*, 21(12). Available at: https://doi.org/10.1016/j.celrep.2017.11.092.

Shivji, M. *et al.* (2018) “BRCA2 Regulates Transcription Elongation by RNA Polymerase II to Prevent R-Loop Accumulation Article BRCA2 Regulates Transcription Elongation by RNA Polymerase II to Prevent R-Loop Accumulation,” *Cell Reports*, 22, pp. 1031–1039. Available at: https://doi.org/10.1016/j.celrep.2017.12.086.

Singh, A.K. *et al.* (2015) “Tumor heterogeneity and cancer stem cell paradigm: Updates in concept, controversies and clinical relevance,” *International Journal of Cancer*, 136(9). Available at: https://doi.org/10.1002/ijc.28804.

Singh, G. *et al.* (2015) “The Clothes Make the mRNA: Past and Present Trends in mRNP Fashion,” *Annual Review of Biochemistry*, 84(1). Available at: https://doi.org/10.1146/annurev-biochem-080111-092106.

Singh, N.N. *et al.* (2011) “TIA1 Prevents Skipping of a Critical Exon Associated with Spinal Muscular Atrophy,” *Molecular and Cellular Biology*, 31(5). Available at: https://doi.org/10.1128/MCB.00945-10.

Singh, N.N. and Singh, R.N. (2011) “Alternative splicing in spinal muscular atrophy underscores the role of an intron definition model,” *RNA Biology*, 8(4). Available at: https://doi.org/10.4161/rna.8.4.16224.

Singh, S.K. *et al.* (2004) “Identification of human brain tumour initiating cells,” *Nature*, 432(7015). Available at: https://doi.org/10.1038/nature03128.

Skourti-Stathaki, K. and Proudfoot, N. (2014) “A double-edged sword: R loops as threats to genome integrity and powerful regulators of gene expression,” *Genes and Development*, 28(13), pp. 1384–1396.

Skourti-Stathaki, K., Proudfoot, N. and Gromak, N. (2011) “Human senataxin resolves RNA/DNA hybrids formed at transcriptional pause sites to promote Xrn2-dependent termination,” *Molecular Cell*, 42(6), pp. 794–805.

Skowron, P. *et al.* (2021) “The transcriptional landscape of Shh medulloblastoma,” *Nature Communications*, 12(1). Available at: https://doi.org/10.1038/s41467-021-21883-0.

Skowron, P., Ramaswamy, V. and Taylor, M.D. (2015) “Genetic and molecular alterations across medulloblastoma subgroups,” *Journal of Molecular Medicine*, 93(10). Available at: https://doi.org/10.1007/s00109-015-1333-8.

Śledź, P. and Jinek, M. (2016) “Structural insights into the molecular mechanism of the m6A writer complex,” *eLife*, 5. Available at: https://doi.org/10.7554/eLife.18434.

Sloan, K.E. *et al.* (2017) “Tuning the ribosome: The influence of rRNA modification on eukaryotic ribosome biogenesis and function,” *RNA Biology*, 14(9). Available at: https://doi.org/10.1080/15476286.2016.1259781.

Smolka, J.A. *et al.* (2021) “Recognition of RNA by the S9.6 antibody creates pervasive artifacts when imaging RNA:DNA hybrids,” *Journal of Cell Biology*, 220(6). Available at: https://doi.org/10.1083/jcb.202004079.

Solomon, M.J., Larsen, P.L. and Varshavsky, A. (1988) “Mapping proteinDNA interactions in vivo with formaldehyde: Evidence that histone H4 is retained on a highly transcribed gene,” *Cell*, 53(6). Available at: https://doi.org/10.1016/S0092-8674(88)90469-2.

Squires, J.E. and Preiss, T. (2010) “Function and detection of 5-methylcytosine in eukaryotic RNA,” *Epigenomics*, 2(5). Available at: https://doi.org/10.2217/epi.10.47.

Staal, J., Pei, Y. and Rood, B. (2016) “A Proteogenomic Approach to Understanding MYC Function in Metastatic Medulloblastoma Tumors,” *International Journal of Molecular Sciences*, 17(10). Available at: https://doi.org/10.3390/ijms17101744.

Staal, J.A. *et al.* (2015) “Proteomic profiling of high risk medulloblastoma reveals functional biology,” *Oncotarget*, 6(16). Available at: https://doi.org/10.18632/oncotarget.3927.

Stancheva, G. *et al.* (2014) “IDH1/IDH2 but Not TP53 Mutations Predict Prognosis in Bulgarian Glioblastoma Patients,” *BioMed Research International*, 2014. Available at: https://doi.org/10.1155/2014/654727.

Stavnezer, J., Guikema, J.E.J. and Schrader, C.E. (2008) “Mechanism and Regulation of Class Switch Recombination,” *Annual Review of Immunology*, 26(1). Available at: https://doi.org/10.1146/annurev.immunol.26.021607.090248.

Stirling, P.C. *et al.* (2012) “R-loop-mediated genome instability in mRNA cleavage and polyadenylation mutants,” *Genes & Development*, 26(2). Available at: https://doi.org/10.1101/gad.179721.111.

Stockley, J. *et al.* (2014) “The RNA-binding protein hnRNPA2 regulates β-catenin protein expression and is overexpressed in prostate cancer,” *RNA Biology*, 11(6). Available at: https://doi.org/10.4161/rna.28800.

Stork, C.T. *et al.* (2016) “Co-transcriptional R-loops are the main cause of estrogen-induced DNA damage,” pp. 1–21. Available at: https://doi.org/10.7554/eLife.17548.

Stupp, R. *et al.* (2005) “Radiotherapy plus Concomitant and Adjuvant Temozolomide for Glioblastoma,” *New England Journal of Medicine*, 352(10). Available at: https://doi.org/10.1056/NEJMoa043330.

Sugimoto, N. *et al.* (1995) “Thermodynamic parameters to predict stability of RNA/DNA hybrid duplexes.,” *Biochemistry*, 34(35). Available at: https://doi.org/10.1021/bi00035a029.

Sun, T. *et al.* (2015) “An integrative view on sex differences in brain tumors,” *Cellular and Molecular Life Sciences*, 72(17). Available at: https://doi.org/10.1007/s00018-015-1930-2.

Sun, T. *et al.* (2020) “LNC942 promoting METTL14-mediated m6A methylation in breast cancer cell proliferation and progression,” *Oncogene*, 39(31). Available at: https://doi.org/10.1038/s41388-020-1338-9.

Szerlip, N.J. *et al.* (2012) “Intratumoral heterogeneity of receptor tyrosine kinases EGFR and PDGFRA amplification in glioblastoma defines subpopulations with distinct growth factor response,” *Proceedings of the National Academy of Sciences*, 109(8). Available at: https://doi.org/10.1073/pnas.1114033109.

Taga, T. and Tabu, K. (2020) “Glioma progression and recurrence involving maintenance and expansion strategies of glioma stem cells by organizing self-advantageous niche microenvironments,” *Inflammation and Regeneration*, 40(1). Available at: https://doi.org/10.1186/s41232-020-00142-7.

Tahiliani, M. *et al.* (2009) “Conversion of 5-methylcytosine to 5-hydroxymethylcytosine in mammalian DNA by MLL partner TET1,” *Science*, 324(5929), pp. 930–935.

Taketo, K. *et al.* (2017) “The epitranscriptome m6A writer METTL3 promotes chemo- and radioresistance in pancreatic cancer cells,” *International Journal of Oncology* [Preprint]. Available at: https://doi.org/10.3892/ijo.2017.4219.

Tantravedi, S. *et al.* (2019) “Targeting DDX3 in Medulloblastoma Using the Small Molecule Inhibitor RK-33,” *Translational Oncology*, 12(1), pp. 96–105. Available at: https://doi.org/10.1016/j.tranon.2018.09.002.

Tan-Wong, S.M., Dhir, S. and Proudfoot, N.J. (2019) “R-Loops Promote Antisense Transcription across the Mammalian Genome,” *Molecular Cell*, 76(4). Available at: https://doi.org/10.1016/j.molcel.2019.10.002.

Taouis, K. *et al.* (2021) “Molecular Functions of WWOX Potentially Involved in Cancer Development,” *Cells*, 10(5). Available at: https://doi.org/10.3390/cells10051051.

Taylor, M.D. *et al.* (2012) “Molecular subgroups of medulloblastoma: the current consensus,” *Acta Neuropathologica*, 123(4). Available at: https://doi.org/10.1007/s00401-011-0922-z.

Teng, Y. *et al.* (2018) “ROS-induced R loops trigger a transcription-coupled but BRCA1/2-independent homologous recombination pathway through CSB,” *Nature Communications*, 9(1). Available at: https://doi.org/10.1038/s41467-018-06586-3.

Thomas, M., White, R.L. and Davis, R.W. (1976) “Hybridization of RNA to double-stranded DNA: formation of R-loops.,” *Proceedings of the National Academy of Sciences*, 73(7). Available at: https://doi.org/10.1073/pnas.73.7.2294.

Thompson, M.C. *et al.* (2006) “Genomics Identifies Medulloblastoma Subgroups That Are Enriched for Specific Genetic Alterations,” *Journal of Clinical Oncology*, 24(12). Available at: https://doi.org/10.1200/JCO.2005.04.4974.

Tigan, A.-S. *et al.* (2016) “CDK6—a review of the past and a glimpse into the future: from cell-cycle control to transcriptional regulation,” *Oncogene*, 35(24). Available at: https://doi.org/10.1038/onc.2015.407.

Triscott, J. *et al.* (2013) “Personalizing the Treatment of Pediatric Medulloblastoma: Polo-like Kinase 1 as a Molecular Target in High-Risk Children,” *Cancer Research*, 73(22). Available at: https://doi.org/10.1158/0008-5472.CAN-12-4331.

Trixl, L. and Lusser, A. (2019) “The dynamic RNA modification 5-methylcytosine and its emerging role as an epitranscriptomic mark,” *WIREs RNA*, 10(1). Available at: https://doi.org/10.1002/wrna.1510.

Tsai, P.-F. *et al.* (2018) “A Muscle-Specific Enhancer RNA Mediates Cohesin Recruitment and Regulates Transcription In trans,” *Molecular Cell*, 71(1). Available at: https://doi.org/10.1016/j.molcel.2018.06.008.

Tuduri, S. *et al.* (2009) “Topoisomerase I suppresses genomic instability by preventing interference between replication and transcription,” *Nature Cell Biology*, 11(11). Available at: https://doi.org/10.1038/ncb1984.

van Tran, N. *et al.* (2019) “The human 18S rRNA m6A methyltransferase METTL5 is stabilized by TRMT112,” *Nucleic Acids Research*, 47(15). Available at: https://doi.org/10.1093/nar/gkz619.

Verhaak, R.G.W. *et al.* (2010) “Integrated Genomic Analysis Identifies Clinically Relevant Subtypes of Glioblastoma Characterized by Abnormalities in PDGFRA, IDH1, EGFR, and NF1,” *Cancer Cell*, 17(1), pp. 98–110. Available at: https://doi.org/10.1016/j.ccr.2009.12.020.

Vermes, I. *et al.* (1995) “A novel assay for apoptosis Flow cytometric detection of phosphatidylserine expression on early apoptotic cells using fluorescein labelled Annexin V,” *Journal of Immunological Methods*, 184(1). Available at: https://doi.org/10.1016/0022-1759(95)00072-I.

Vermes, I., Haanen, C. and Reutelingsperger, C. (2000) “Flow cytometry of apoptotic cell death,” *Journal of Immunological Methods*, 243(1–2). Available at: https://doi.org/10.1016/S0022-1759(00)00233-7.

Vieira de Castro, J. *et al.* (2020) “Exploiting the Complexities of Glioblastoma Stem Cells: Insights for Cancer Initiation and Therapeutic Targeting,” *International Journal of Molecular Sciences*, 21(15). Available at: https://doi.org/10.3390/ijms21155278.

Vilardo, E. *et al.* (2012) “A subcomplex of human mitochondrial RNase P is a bifunctional methyltransferase—extensive moonlighting in mitochondrial tRNA biogenesis,” *Nucleic Acids Research*, 40(22). Available at: https://doi.org/10.1093/nar/gks910.

Visvanathan, A. *et al.* (2018) “Essential role of METTL3-mediated m6A modification in glioma stem-like cells maintenance and radioresistance,” *Oncogene*, 37(4). Available at: https://doi.org/10.1038/onc.2017.351.

Vu, L. *et al.* (2017) “The N6-methyladenosine (m6A)-forming enzyme METTL3 controls myeloid differentiation of normal hematopoietic and leukemia cells,” *Nature Medicine*, 23(11), pp. 1369–1376.

Wahba, L. *et al.* (2011) “RNase H and multiple RNA biogenesis factors cooperate to prevent RNA-DNA hybrids from generating genome instability,” *Molecular Cell*, 44(6), pp. 978–988.

Wahba, L. *et al.* (2016) “S1-DRIP-seq identifies high expression and polyA tracts as major contributors to R-loop formation,” *Genes & Development*, 30(11). Available at: https://doi.org/10.1101/gad.280834.116.

Wahl, M.C., Will, C.L. and Lührmann, R. (2009) “The Spliceosome: Design Principles of a Dynamic RNP Machine,” *Cell*, 136(4). Available at: https://doi.org/10.1016/j.cell.2009.02.009.

Waku, T. *et al.* (2016) “NML-mediated rRNA base methylation links ribosomal subunit formation to cell proliferation in a p53-dependent manner,” *Journal of Cell Science* [Preprint]. Available at: https://doi.org/10.1242/jcs.183723.

Wang, C. *et al.* (2018) “miR-146a-5p mediates epithelial–mesenchymal transition of oesophageal squamous cell carcinoma via targeting Notch2,” *British Journal of Cancer*, 118(6). Available at: https://doi.org/10.1038/bjc.2017.471.

Wang, H., Xu, B. and Shi, J. (2020) “N6-methyladenosine METTL3 promotes the breast cancer progression via targeting Bcl-2,” *Gene*, 722. Available at: https://doi.org/10.1016/j.gene.2019.144076.

Wang, J. *et al.* (2020) “Leukemogenic Chromatin Alterations Promote AML Leukemia Stem Cells via a KDM4C-ALKBH5-AXL Signaling Axis.,” *Cell stem cell*, 27(1). Available at: https://doi.org/10.1016/j.stem.2020.04.001.

Wang, K. *et al.* (2021) “Genomic profiling of native R loops with a DNA-RNA hybrid recognition sensor,” *Science Advances*, 7(8). Available at: https://doi.org/10.1126/sciadv.abe3516.

Wang, L. *et al.* (2020) “M6A RNA Methylation Regulator HNRNPC Contributes to Tumorigenesis and Predicts Prognosis in Glioblastoma Multiforme,” *Frontiers in Oncology*, 10. Available at: https://doi.org/10.3389/fonc.2020.536875.

Wang, L., Wen, M. and Cao, X. (2019) “Nuclear hnRNPA2B1 initiates and amplifies the innate immune response to DNA viruses,” *Science*, 365(6454). Available at: https://doi.org/10.1126/science.aav0758.

Wang, P., Doxtader, K. and Nam, Y. (2016) “Structural Basis for Cooperative Function of Mettl3 and Mettl14 Methyltransferases,” *Molecular Cell*, 63(2), pp. 306–317.

Wang, W. *et al.* (2020) “Identification of N6-methyladenosine-related lncRNAs for patients with primary glioblastoma,” *Neurosurgical Review* [Preprint]. Available at: https://doi.org/10.1007/s10143-020-01238-x.

Wang, X. *et al.* (2014) “N6-methyladenosine-dependent regulation of messenger RNA stability,” *Nature*, 505(7481), pp. 117–120.

Wang, X. *et al.* (2015) “N(6)-methyladenosine Modulates Messenger RNA Translation Efficiency,” *Cell*, 161(6), pp. 1388–1399.

Wang, X. *et al.* (2016) “Structural basis of N6-adenosine methylation by the METTL3–METTL14 complex,” *Nature*, 534(7608). Available at: https://doi.org/10.1038/nature18298.

Wang, Y. *et al.* (2014) “N6-methyladenosine modification destabilizes developmental regulators in embryonic stem cells,” *Nature Cell Biology*, 16(2), pp. 191–198.

Wang, Y. *et al.* (2015) “Mechanism of alternative splicing and its regulation,” *Biomedical Reports*, 3(2). Available at: https://doi.org/10.3892/br.2014.407.

Wang, Y. *et al.* (2018) “N6-methyladenosine RNA modification regulates embryonic neural stem cell self-renewal through histone modifications,” *Nature Neuroscience*, 21(2). Available at: https://doi.org/10.1038/s41593-017-0057-1.

Wang, Y. *et al.* (2020) “Emerging roles of N6-methyladenosine (m6A) modification in breast cancer,” *Cell & Bioscience*, 10(1). Available at: https://doi.org/10.1186/s13578-020-00502-3.

Wang, Z. and Burge, C.B. (2008) “Splicing regulation: From a parts list of regulatory elements to an integrated splicing code,” *RNA*, 14(5). Available at: https://doi.org/10.1261/rna.876308.

Warda, A.S. *et al.* (2017) “Human METTL16 is a N6-methyladenosine (m6A) methyltransferase that targets pre-mRNAs and various non-coding RNAs,” *EMBO reports*, 18(11). Available at: https://doi.org/10.15252/embr.201744940.

Waszak, S.M. *et al.* (2018) “Spectrum and prevalence of genetic predisposition in medulloblastoma: a retrospective genetic study and prospective validation in a clinical trial cohort,” *The Lancet Oncology*, 19(6). Available at: https://doi.org/10.1016/S1470-2045(18)30242-0.

Wei, G. *et al.* (2018) “Expression of miR-146a-5p in breast cancer and its role in proliferation of breast cancer cells,” *Oncology Letters* [Preprint]. Available at: https://doi.org/10.3892/ol.2018.8589.

Wei, J. *et al.* (2018) “Differential m6A, m6Am, and m1A Demethylation Mediated by FTO in the Cell Nucleus and Cytoplasm,” *Molecular Cell*, 71(6). Available at: https://doi.org/10.1016/j.molcel.2018.08.011.

Wellinger, R.E., Prado, F. and Aguilera, A. (2006) “Replication Fork Progression Is Impaired by Transcription in Hyperrecombinant Yeast Cells Lacking a Functional THO Complex,” *Molecular and Cellular Biology*, 26(8). Available at: https://doi.org/10.1128/MCB.26.8.3327-3334.2006.

Wemmert, S. *et al.* (2009) “p15 promoter methylation - A novel prognostic marker in glioblastoma patients,” *International Journal of Oncology*, 34(6). Available at: https://doi.org/10.3892/ijo_00000305.

Wen, J. *et al.* (2018) “Zc3h13 Regulates Nuclear RNA m6A Methylation and Mouse Embryonic Stem Cell Self-Renewal,” *Molecular Cell*, 69(6). Available at: https://doi.org/10.1016/j.molcel.2018.02.015.

Weng, H. *et al.* (2018) “METTL14 Inhibits Hematopoietic Stem/Progenitor Differentiation and Promotes Leukemogenesis via mRNA m6A Modification,” *Cell Stem Cell*, 22(2). Available at: https://doi.org/10.1016/j.stem.2017.11.016.

Wiedemann, E.-M., Peycheva, M. and Pavri, R. (2016) “DNA Replication Origins in Immunoglobulin Switch Regions Regulate Class Switch Recombination in an R-Loop-Dependent Manner,” *Cell Reports*, 17(11). Available at: https://doi.org/10.1016/j.celrep.2016.11.041.

Wiseman, D.H., Bonney, D.K. and Wynn, R.F. (2012) “Hemophagocytosis by leukemic megakaryoblasts in acute myeloid leukemia (megakaryoblastic) with t(1;22)(p13;q13);RBM15-MKL1.,” *Journal of pediatric hematology/oncology*, 34(7). Available at: https://doi.org/10.1097/MPH.0b013e318245a027.

Woo, H.-H. and Chambers, S.K. (2019) “Human ALKBH3-induced m1A demethylation increases the CSF-1 mRNA stability in breast and ovarian cancer cells,” *Biochimica et Biophysica Acta (BBA) - Gene Regulatory Mechanisms*, 1862(1). Available at: https://doi.org/10.1016/j.bbagrm.2018.10.008.

Wu, B. *et al.* (2018) “Molecular basis for the specific and multivariant recognitions of RNA substrates by human hnRNP A2/B1,” *Nature Communications*, 9(1). Available at: https://doi.org/10.1038/s41467-017-02770-z.

Wu, L. *et al.* (2019) “Changes of N6-methyladenosine modulators promote breast cancer progression,” *BMC Cancer*, 19(1). Available at: https://doi.org/10.1186/s12885-019-5538-z.

Wu, R. *et al.* (2019) “A novel m6A reader Prrc2a controls oligodendroglial specification and myelination,” *Cell Research*, 29(1). Available at: https://doi.org/10.1038/s41422-018-0113-8.

Wulff, B.-E., Sakurai, M. and Nishikura, K. (2011) “Elucidating the inosinome: global approaches to adenosine-to-inosine RNA editing,” *Nature Reviews Genetics*, 12(2). Available at: https://doi.org/10.1038/nrg2915.

Wyatt, G. (1950) “Recognition and Estimation of 5-Methylcytosine in Nucleic Acids Eii,” *Biochemistry*, 48, pp. 581–584.

Xiang, J.-F. *et al.* (2018) “N6-Methyladenosines Modulate A-to-I RNA Editing,” *Molecular Cell*, 69(1). Available at: https://doi.org/10.1016/j.molcel.2017.12.006.

Xiao, W. *et al.* (2016) “Nuclear m(6)A Reader YTHDC1 Regulates mRNA Splicing,” *Molecular Cell*, 61(4), pp. 507–519.

Xu, C. *et al.* (2014) “Structural basis for selective binding of m6A RNA by the YTHDC1 YTH domain,” *Nature Chemical Biology*, 10(11), pp. 927–929.

Xu, C. *et al.* (2020) “Prognostic values of YTHDF1 regulated negatively by mir-3436 in Glioma,” *Journal of Cellular and Molecular Medicine*, 24(13). Available at: https://doi.org/10.1111/jcmm.15382.

Xu, H. *et al.* (2020) “m6A mRNA Methylation Is Essential for Oligodendrocyte Maturation and CNS Myelination,” *Neuron*, 105(2). Available at: https://doi.org/10.1016/j.neuron.2019.12.013.

Xu, J. *et al.* (2020) “The Identification of Critical m6A RNA Methylation Regulators as Malignant Prognosis Factors in Prostate Adenocarcinoma,” *Frontiers in Genetics*, 11. Available at: https://doi.org/10.3389/fgene.2020.602485.

Yan, H. *et al.* (2009) “IDH1 and IDH2 Mutations in Gliomas,” *New England Journal of Medicine*, 360(8). Available at: https://doi.org/10.1056/NEJMoa0808710.

Yan, K., Yang, K. and Rich, J.N. (2013) “The evolving landscape of glioblastoma stem cells,” *Current Opinion in Neurology*, 26(6). Available at: https://doi.org/10.1097/WCO.0000000000000032.

Yang, G., Sun, Z. and Zhang, N. (2020) “Reshaping the role of m6A modification in cancer transcriptome: a review,” *Cancer Cell International*, 20(1). Available at: https://doi.org/10.1186/s12935-020-01445-y.

Yang, J. *et al.* (2020) “Guidelines and definitions for research on epithelial–mesenchymal transition,” *Nature Reviews Molecular Cell Biology*, 21(6). Available at: https://doi.org/10.1038/s41580-020-0237-9.

Yang, X. *et al.* (2017) “5-methylcytosine promotes mRNA export — NSUN2 as the methyltransferase and ALYREF as an m5C reader,” *Cell Research*, 27(5). Available at: https://doi.org/10.1038/cr.2017.55.

Yang, X. *et al.* (2019) “m6A promotes R-loop formation to facilitate transcription termination,” *Cell Research*, 29(12). Available at: https://doi.org/10.1038/s41422-019-0235-7.

Yankova, E. *et al.* (2021) “Small-molecule inhibition of METTL3 as a strategy against myeloid leukaemia,” *Nature*, 593(7860). Available at: https://doi.org/10.1038/s41586-021-03536-w.

Yanling Zhao, D. *et al.* (2016) “SMN and symmetric arginine dimethylation of RNA polymerase II C-terminal domain control termination,” *Nature*, 529(7584). Available at: https://doi.org/10.1038/nature16469.

Yao, Q.J. *et al.* (2018) “Mettl3–Mettl14 methyltransferase complex regulates the quiescence of adult hematopoietic stem cells,” *Cell Research*, 28(9). Available at: https://doi.org/10.1038/s41422-018-0062-2.

Yao, R.-W., Wang, Y. and Chen, L.-L. (2019) “Cellular functions of long noncoding RNAs,” *Nature Cell Biology*, 21(5). Available at: https://doi.org/10.1038/s41556-019-0311-8.

Yasuhara, T. *et al.* (2018) “Human Rad52 Promotes XPG-Mediated R-loop Processing to Initiate Transcription-Associated Homologous Recombination Repair.,” *Cell*, 175(2). Available at: https://doi.org/10.1016/j.cell.2018.08.056.

Yen, Y.-P. and Chen, J.-A. (2021) “The m6A epitranscriptome on neural development and degeneration,” *Journal of Biomedical Science*, 28(1). Available at: https://doi.org/10.1186/s12929-021-00734-6.

Yi, D. *et al.* (2020) “METTL14 promotes the migration and invasion of breast cancer cells by modulating N6-methyladenosine and hsa-miR-146a-5p expression,” *Oncology Reports* [Preprint]. Available at: https://doi.org/10.3892/or.2020.7515.

Yoon, K. *et al.* (2017) “Temporal Control of Mammalian Cortical Neurogenesis by m 6 A Methylation Article Temporal Control of Mammalian Cortical Neurogenesis by m 6 A Methylation,” pp. 877–889. Available at: https://doi.org/10.1016/j.cell.2017.09.003.

You, C., Dai, X. and Wang, Y. (2017) “Position-dependent effects of regioisomeric methylated adenine and guanine ribonucleosides on translation,” *Nucleic Acids Research*, 45(15). Available at: https://doi.org/10.1093/nar/gkx515.

Yu, K. *et al.* (2003) “R-loops at immunoglobulin class switch regions in the chromosomes of stimulated B cells,” *Nature Immunology*, 4(5). Available at: https://doi.org/10.1038/ni919.

Yue, Y. *et al.* (2018) “VIRMA mediates preferential m6A mRNA methylation in 3’UTR and near stop codon and associates with alternative polyadenylation,” *Cell Discovery*, 4(10).

Zaccara, S. and Jaffrey, S.R. (2020) “A Unified Model for the Function of YTHDF Proteins in Regulating m6A-Modified mRNA,” *Cell*, 181(7). Available at: https://doi.org/10.1016/j.cell.2020.05.012.

Zanzoni, A. *et al.* (2019) “Post-transcriptional regulatory patterns revealed by protein-RNA interactions,” *Scientific Reports*, 9(1). Available at: https://doi.org/10.1038/s41598-019-40939-2.

Zarnack, K. *et al.* (2013) “Direct Competition between hnRNP C and U2AF65 Protects the Transcriptome from the Exonization of Alu Elements,” *Cell*, 152(3). Available at: https://doi.org/10.1016/j.cell.2012.12.023.

Zhang, Chuanzhao *et al.* (2016) “Hypoxia induces the breast cancer stem cell phenotype by HIF-dependent and ALKBH5-mediated m ^{6} A-demethylation of NANOG mRNA,” *Proceedings of the National Academy of Sciences*, 113(14). Available at: https://doi.org/10.1073/pnas.1602883113.

Zhang, C *et al.* (2016) “Hypoxia-inducible factors regulate pluripotency factor expression by ZNF217- and ALKBH5-mediated modulation of RNA methylation in breast cancer cells,” *Oncotarget*, 7(40), pp. 64527–64542.

Zhang, C. *et al.* (2020) “METTL3 and N6-Methyladenosine Promote Homologous Recombination-Mediated Repair of DSBs by Modulating DNA-RNA Hybrid Accumulation,” *Molecular Cell*, 79(3). Available at: https://doi.org/10.1016/j.molcel.2020.06.017.

Zhang, S. *et al.* (2017) “m 6 A Demethylase ALKBH5 Maintains Tumorigenicity of Glioblastoma Stem-like Cells by Sustaining FOXM1 Expression and Cell Proliferation Program Article m 6 A Demethylase ALKBH5 Maintains Tumorigenicity of Glioblastoma Stem-like Cells by Sustaining FOXM1 E,” pp. 591–606. Available at: https://doi.org/10.1016/j.ccell.2017.02.013.

Zhao, B.S. *et al.* (2017) “Post-transcriptional gene regulation by mRNA modifications,” *Nature Reviews Molecular Cell Biology*, 18(1), pp. 31–42. Available at: https://doi.org/10.1038/nrm.2016.132.Post-transcriptional.

Zhao, X. *et al.* (2004) “Regulation of Nuclear Receptor Activity by a Pseudouridine Synthase through Posttranscriptional Modification of Steroid Receptor RNA Activator,” *Molecular Cell*, 15(4). Available at: https://doi.org/10.1016/j.molcel.2004.06.044.

Zhao, X. *et al.* (2014) “FTO-dependent demethylation of N6-methyladenosine regulates mRNA splicing and is required for adipogenesis,” *Cell Research*, 24(12), pp. 1403–1419.

Zheng, C.L., Fu, X.-D. and Gribskov, M. (2005) “Characteristics and regulatory elements defining constitutive splicing and different modes of alternative splicing in human and mouse,” *RNA*, 11(12). Available at: https://doi.org/10.1261/rna.2660805.

Zheng, G. *et al.* (2013) “Sprouts of RNA epigenetics: the discovery of mammalian RNA demethylases,” *RNA biology*, 10(6), pp. 915–918.

Zheng, Q. *et al.* (2016) “Nuclear distribution of eIF3g and its interacting nuclear proteins in breast cancer cells,” *Molecular Medicine Reports*, 13(4). Available at: https://doi.org/10.3892/mmr.2016.4935.

Zhong, L. *et al.* (2019) “YTHDF2 suppresses cell proliferation and growth via destabilizing the EGFR mRNA in hepatocellular carcinoma,” *Cancer Letters*, 442. Available at: https://doi.org/10.1016/j.canlet.2018.11.006.

Zhou, H. *et al.* (2016) “m1A and m1G disrupt A-RNA structure through the intrinsic instability of Hoogsteen base pairs,” *Nature Structural & Molecular Biology*, 23(9). Available at: https://doi.org/10.1038/nsmb.3270.

Zhou, H. *et al.* (2019) “Evolution of a reverse transcriptase to map N1-methyladenosine in human messenger RNA,” *Nature Methods*, 16(12). Available at: https://doi.org/10.1038/s41592-019-0550-4.

Zhou, J. *et al.* (2015) “Dynamic m6A mRNA methylation directs translational control of heat shock response,” *Nature*, 526(7574). Available at: https://doi.org/10.1038/nature15377.

Zhou, J. *et al.* (2017) “Inhibition of LIN28B impairs leukemia cell growth and metabolism in acute myeloid leukemia.,” *Journal of hematology & oncology*, 10(1). Available at: https://doi.org/10.1186/s13045-017-0507-y.

Zhou, Z. and Fu, X.-D. (2013) “Regulation of splicing by SR proteins and SR protein-specific kinases,” *Chromosoma*, 122(3). Available at: https://doi.org/10.1007/s00412-013-0407-z.

Zhu, J., Mayeda, A. and Krainer, A.R. (2001) “Exon Identity Established through Differential Antagonism between Exonic Splicing Silencer-Bound hnRNP A1 and Enhancer-Bound SR Proteins,” *Molecular Cell*, 8(6). Available at: https://doi.org/10.1016/S1097-2765(01)00409-9.

Zhuang, Changshui *et al.* (2019) “N6-methyladenosine demethylase FTO suppresses clear cell renal cell carcinoma through a novel FTO-PGC-1α signalling axis,” *Journal of Cellular and Molecular Medicine*, 23(3). Available at: https://doi.org/10.1111/jcmm.14128.